Maciej
Misiorny

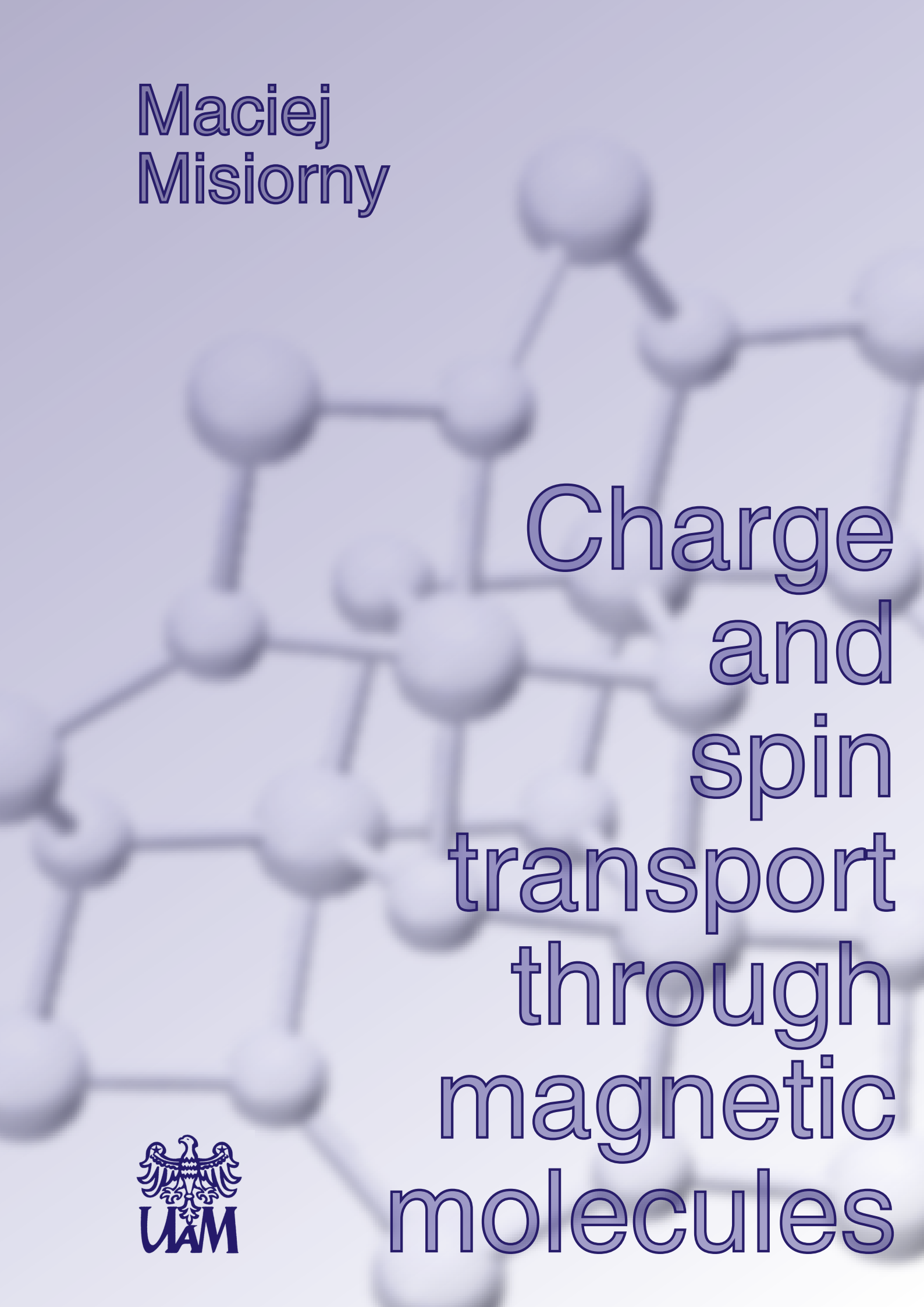

Charge and spin transport through magnetic molecules

UAM

Uniwersytet im. Adama Mickiewicza
w Poznaniu

Charge and spin transport through magnetic molecules

Transport ładunku i spinu przez magnetyczne molekuły

Maciej Misiorny

Rozprawa doktorska

Promotor: prof. dr hab. Józef Barnaś

Zakład Fizyki Mezoskopowej
Wydział Fizyki

Poznań 2010

Abstract

Among different types of molecular systems, there is one specific class of molecules which exhibit an intrinsic magnetic moment, i.e. the so-called *single-molecule magnets* (SMMs). Due to their peculiar physical properties such as an energy barrier for the spin reversal or long spin relaxation times, SMMs are inherently predestined for applications in novel molecular electronic and spintronic devices. The following thesis is therefore devoted to studying transport properties of such molecules, with the main emphasis laid on discussing how the flow of spin-polarized current through a SMM can affect the magnetic state of the molecule.

The system under investigation consists of a SMM bridged between two metallic, ferromagnetic electrodes with collinear magnetic moments. Furthermore, electronic transport is assumed to take place *via* the lowest unoccupied molecular orbital (LUMO) level of the molecule. Within the thesis I consider transport in both the limits of *weak* and *strong* coupling between the molecule and electrodes, using for this purpose different perturbation approaches, such as Fermi golden rule or the real-time diagrammatic technique, as well as the Willson's numerical renormalization group method, which is nonperturbative.

I show that due to exchange interaction between an electron occupying the LUMO level and the SMM's core spin, during tunneling of spin-polarized electrons through a molecule one can observe an effect analogous to the current-induced magnetic switching (CIMS) phenomenon, known from other magnetic systems, for instance, nanowires or spin valves. The origin of the CIMS mechanism in SMMs stems from angular momentum transfer between a spin-polarized current and the molecule, and it allows for manipulating the SMM's spin state without application of an external magnetic field. I also focus on studying dynamical aspects of the magnetic switching mechanism, together with other spin effects that can arise in the situation under consideration. Finally, I analyze the possibility of employing a pulse of circularly polarized electromagnetic radiation for stimulating the mechanism of CIMS.

Contents

Acknowledgments

Above all, the first person to whom I owe sincere gratitude is my supervisor, Prof. Józef Barnaś, without whose guidance, support and enthusiasm, I would most probably not have got to where I am today. Thank you for enabling me to learn so much from you over the past years.

Next, I would like to express my personal appreciation to Dr. Ireneusz Weymann for a very professional and fruitful collaboration, and especially for enlightening discussions, which allowed me to spare a lot of time. I really enjoy working with you.

Heartfelt thanks to all colleagues from Mesoscopic Physics Division for fostering an environment in which our creativity and scientific curiosity can thrive unhindered.

An ocean of thanks would scarcely suffice to express all of my gratitude to my friends for their company, encouragement and faith in me. You always know how to brighten up my day.

Last, but by no means least, I would like to thank my parents and family for their unconditional love and support which always motivates me and fuels my actions.

The research included in the following thesis, as part of the European Science Foundation EUROCORES Programme SPINTRA, was supported by funds from the Ministry of Science and Higher Education as a research project in years 2006-2009 and the EC Sixth Framework Programme, under Contract N. ERAS-CT-2003-980409. Financial suport from the Ministry of Science and Higher Education in the form of the PhD thesis supervisor's grant (Polish. *'grant promotorski'*) entitled *'Transport elektronowy i zjawiska magnetycznego przełączania w molekularnych magnetykach'* (N N202 173135) is also acknowledged. Finally, the author was the beneficiary of a scientific scholarship from the Adam Mickiewicz University Foundation in the calendar year 2009.

CHAPTER 1

Introduction and motivation

When at the beginning of the eighteenth century, Stephen Gray was carrying out his experiments on electricity, which eventually led him to the discovery that *'the Electick Vertue passes by the Line of Communication'* [1–3] (or that some materials conduct current, as it would be said nowadays), nobody would have expected that, within next three hundred years, people would be able to control motion of single electrons.

In traditional electronic devices, the mechanism of information processing exploits usually electronic *charge*. However, it should be noted that the charge is not the only degree of freedom that electrons possess, as they are also characterized by *spin*, which in principle might be utilized in transport processes. It was just the discovery of the *giant magnetoresistance* (GMR) effect in artificially layered magnetic structures [4, 5] that gave the first practical realization of a simple spin-based device, a *spin valve*. Its functionality relied on the interplay of these two degrees of freedom, and its behavior could not be fully understood without taking into account the electron spin [6–8]. The GMR discovery originated a new area of electronics, called *spintronics* (sometimes also referred to as *magnetolectronics* or *spin-based electronics*), which aims at developing a future generation of devices operating on the basis of spin-dependent effects [9, 10]. Making use of the spin degree of freedom raises hopes for a new class of integrated circuits for commercial use, which due to their nonvolatility, higher data processing speed, and smaller size compared with conventional electronic devices [10–12] would be a great technological leap forward

An ever-increasing demand for faster and more efficient information processing technologies fuels the downsizing trend in building smaller and smaller electronic devices, with the ultimate goal of reaching a *molecular level*, where a single molecule can be functioning as a fully operating part of a bigger spintronic system. In recent years, with the advent of technological advances in experimental techniques, it has actually become

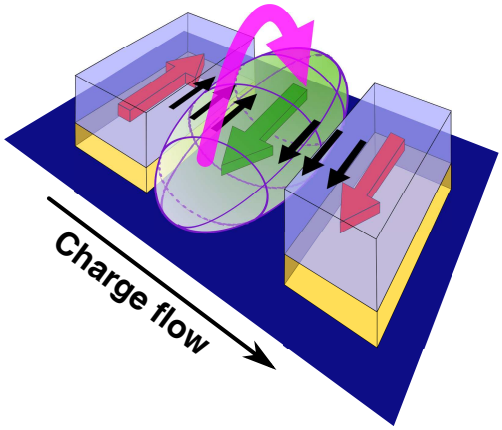

Figure 1.1: Schematic visualization of spin-dependent transport through a *single-molecule magnet* (SMM). Exchange interaction between tunneling electrons and the molecule's spin can effectively lead to the reversal of the latter.

possible to study transport properties of nanoscale objects, like quantum dots [13], nanotubes [14–17] and other molecules [18–23]. The main interest in investigating transport properties of single molecules stems from the fact that – owing to their unique optical, magnetic and/or mechanical properties – molecules are suitable for building hybrid devices of features which would be rather hardly accessible for conventional silicon-based electronic systems [9, 24–28]. For instance, one interesting feature of nanomolecular systems, which does not have counterpart in the case of bulk materials, concerns the interplay between the quantized electronic and mechanical degrees of freedom [18].

Furthermore, since molecules are the result of chemical synthesis, specific functions can be imposed on them during their preparation [26]. Among many different classes of molecules through which electronic and spin transport can be considered, particularly interesting seem to be the ones exhibiting intrinsic magnetic moment [29], as they are promising for potential applications in information storage and processing technologies [9, 30, 31]. A molecule to be considered as a candidate for a molecular memory cell has to satisfy two main requirements. First, it has to be magnetically bistable; and second, its state should persist for a sufficiently long time [32]. It turned out that systems which meet the above prerequisites, offering additionally some unique features, are *single-molecule magnets* (SMMs) [33–38]. Interestingly enough, it has also been suggested that SMMs can be a suitable base for implementation of quantum computing operations [39–43].

Despite the fact that SMMs have attracted much attention, especially among chemists, and a great deal of effort was put into experimental measurements of electronic transport through these molecules [44–49],[1] the research concerning transport properties of individual SMMs is still on its early stage. It means that many questions haven't been addressed, or even brought up yet. In particular, since it has been demonstrated that transport through a SMM is technologically feasible, at least in the case of nonmagnetic

[1] It should be noted that all these experiments employed metallic, but *nonmagnetic* electrodes.

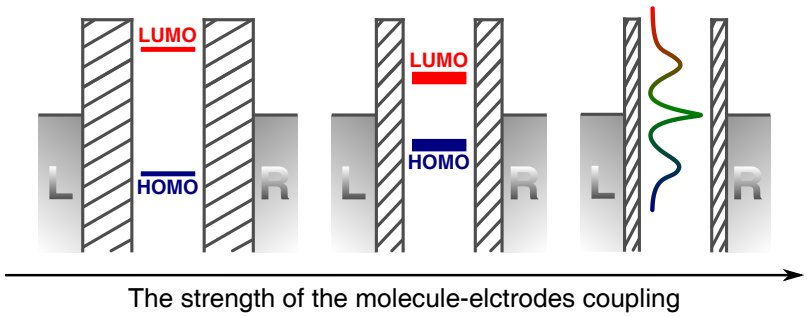

Figure 1.2: As the strength of the molecule-electrodes coupling increases, the character of electronic transport through a SMM changes. In the *weak* coupling regime (the left-hand side), tunneling of electrons can be assumed to occur *via* molecular many-body states. In the opposite limit of the *strong* coupling (the right-hand side), however, the molecular states are no longer a good approximation for describing transport of electrons. One should replace them by new hybrid states taking into account partial delocalization of electrons between electrodes and the molecule. Furthermore, spin exchange processes may in such a case result in formation of an additional resonance in the density of states near the Fermi level of electrodes – the *Kondo resonance* (for further details see Chapter 6). The idea adopted from Ref. [28].

electrodes, it would be interesting to go one step further, and ask what new effects could arise owing to the replacement of nonmagnetic electrodes by magnetic ones.

The objective of this thesis is therefore to analyze theoretically spin-polarized transport through individual SMMs. To be more precise, I am interested in investigating the interplay between spin-polarized currents and the magnetic state of the molecule, because, similarly as for other magnetic systems of nanoscopic size, one can expect here the *current-induced magnetic switching* to take place,[2] Fig. 1.1. In addition to this, I also discuss the influence of spin-polarized reservoirs on the *quantum tunneling of magnetization* mechanism (Chapter 3), which is a phenomenon typical of many SMMs.

Another important problem to be considered in the following thesis is related to the complex nature of the binding of a SMM to a substrate or electrode surface (Section 2.2), which may affect transport processes as well. By changing, for example, the type or length of the linker molecule, the strength of the SMM-electrode coupling can be modified. Consequently, one can generally identify two different transport regimes through a SMM, depending on the coupling strength between the molecule and external leads, Fig. 1.2. In the *weak* coupling regime, the Coulomb correlations and the discreteness of energy spectrum lead to blockade phenomena, so that some external bias has to be applied to electrodes in order to force conduction electrons to traverse the molecule. This regime is analyzed in Chapters 4 and 5. On the other hand, in the *strong* coupling regime, i.e. when resistance of the contact between the molecule and electrodes becomes smaller than the quantum resistance, the electronic correlations may lead to formation of the *Kondo effect* [50–54]. These correlations result in a screening of the SMM's spin by conduction

[2]The general idea of the *current-induced magnetic switching* mechanism in the case of a single ferromagnetic layer is presented at the beginning of Chapter 4.

electrons of the leads, giving rise to a peak in the density of states and full transparency through the molecule, Fig. 1.2. Problems related to transport processes in the strong coupling regime are addressed in Chapters 6.

Moreover, it is worth mentioning that in the *weak* coupling regime one can distinguish two regimes of electronic transport through the molecule with respect to bias voltage applied to the system. For voltages lower than a certain threshold value, sequential tunneling processes through the molecule are exponentially suppressed as electrons lack energy to overcome the energy barrier due to Coulomb correlations and/or size quantization. However, once the bias voltage exceeds the threshold value, the electrons are energetically allowed to tunnel one-by-one through the molecule. The latter regime is known as the *sequential tunneling* regime, and it is discussed in Section 4.2, whereas the former one is often referred to as the *Coulomb blockade* or *cotunneling* regime [55, 56], and it is the subject of Section 4.3. It should be noted, however, that although the sequential processes are suppressed in the Coulomb blockade regime, current still can flow due to second- and higher-order tunneling processes, which involve correlated tunneling through virtual states of the molecule. Additional spin-effects stemming from coexistence of sequential tunneling and cotunneling processes are considered in Chapter 5.

Finally, as the mechanism of the SMM's current-induced magnetic switching relies on the exchange of angular momentum between the molecule and tunneling current, thus the general mechanism of the magnetic switching should also be valid for other sources of angular momentum, e.g. a *circularly polarized* light. For this reason, in the last chapter of this dissertation (Chapter 7) I investigate the possibility of using a pulse of circularly polarized, monochromatic electromagnetic radiation for stimulating the current-induced magnetic switching of a SMM in the Coulomb blockade regime.

CHAPTER 2

Preliminary concepts and description of the system

Single-molecule magnets (SMMs) are systems in which permanent magnetization and consequently also magnetic hysteresis have a pure molecular origin [37, 38, 57, 58] – some examples of most popular SMMs are presented in Fig. 2.1. The key feature which allows one to distinguish a molecular magnet as a SMM is extremely slow relaxation of the magnetization observed at low temperatures. The energy barrier ΔE, which the molecule has to overcome to reverse its spin, arises as the combined effect of a high spin S ground state and a large Ising type magnetic anisotropy, described by the parameter D. Molecular magnets form usually a crystal lattice of large molecules coupled *via* weak interactions. Very often they appear in the powder form. However, recent achievements of nanotechnology allow to manipulate and control a single molecule. This, in turn, has opened a fascinating area of research – not only for experimentalists, but also for theoreticians.

2.1 Single-molecule magnets – general properties

The studies of SMMs at low temperatures revealed that their behavior resembles much that of superparamagnets [34, 59], i.e. single-domain nanometric particles of bulk magnets, whose magnetization can be flipped due to thermal activation [60, 61]. Such particles can be viewed as systems with extremely high spins of the order of 10^3 or even larger. This, in turn, leads to the most fundamental difference between energy spectra of SMMs and superparamagnetic nanoparticles, i.e. the energy levels of a superparamagnet form a quasicontinuum, whereas in the case of SMMs a discrete spectrum is observed [62]. A limited number of states to be considered together with a relatively large size are the

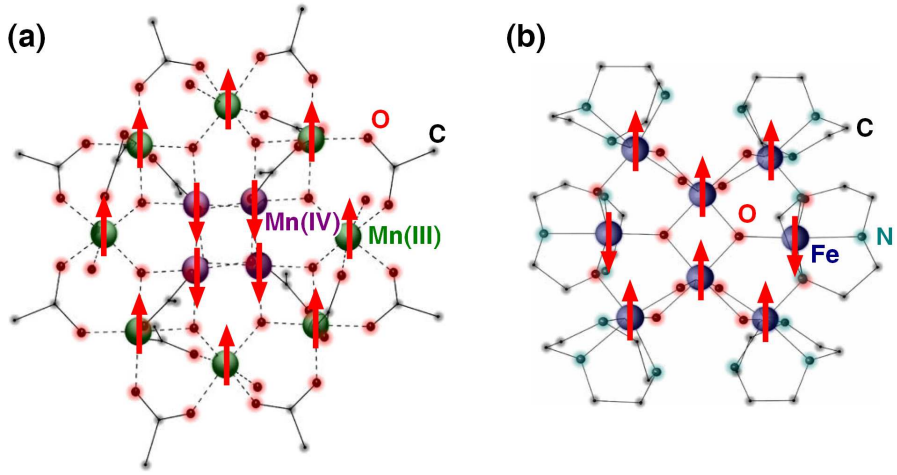

Figure 2.1: Two example structures of the most intensively studied single-molecule magnets: (a) $[Mn_{12}O_{12}(RCOO)_{16}(H_2O)_4]$ (shortly called Mn_{12}) and (b) $[Fe_8O_2(OH)_{12}(tacn)_6]^{8+}$ (shortly Fe_8). Both the molecules are characterized by the ground state spin $S = 10$, and arrows denote here corresponding spin orientations of relevant magnetic ions. In order to keep the illustration clear, hydrogen atoms are omitted. Modified from Ref. [58].

main reason why SMMs are favored as systems suitable for testing quantum phenomena at the mesoscopic scale, e.g. tunneling [63] or interference effects [57].

At higher temperatures the SMM's spin can freely rotate, and the molecule behaves like a paramagnet with a giant magnetic moment. On the other hand, when temperature is lowered, the thermal energy is not sufficient to reverse spin orientation of the molecule. As a consequence, below a certain *blocking temperature* T_B, which is related to ΔE, the spin gets trapped in one of two allowed orientations [37]. Thermostimulated processes of magnetic relaxation are then extremely slow, so that a time delay between the change of an external magnetic field and the system response occurs, leading to magnetic hysteresis.

As the property of magnetic bistability is of immense significance for future applications of SMMs in information storage, much scientific efforts are currently devoted to synthesizing SMMs with higher and higher anisotropy barriers and consequently higher blocking temperatures [58, 64, 65], and thus to increasing functional temperatures of the molecules. The immediate goal is to increase T_B at least above liquid helium temperature, which would allow to relax (to some extent) rigorous conditions of low temperature experiments. Furthermore, in the most general case, apart from the longitudinal component of magnetic anisotropy, a molecule can also possess a transversal one [37]. As it will be discussed later, the presence of transverse magnetic anisotropy is responsible for the phenomenon of quantum tunneling of magnetization in SMMs, which effectively reduces the height of the anisotropy barrier [38, 66]. Therefore, when designing new SMMs, one should try to eliminate the transverse anisotropy from the system as far as possible. The good example of molecules which can be approximately considered as of uniaxial anisotropy are molecules belonging to the most studied family of the dode-

canuclear manganese complexes of the general formula $[Mn_{12}O_{12}(RCOO)_{16}(H_2O)_x] \cdot Y$ (usually called shortly Mn_{12} molecules) with $x = 3, 4$, R = a chemical functional group, and Y = solvent molecules [37, 58, 67], Fig. 2.1(a). For a long time, molecules from this group were also the SMMs with the highest known blocking temperatures $T_B \approx 3.5$ K (currently the record is held by a hexamanganese(III) complex with $T_B \approx 4.5$ K [65]). Since the energy barrier ΔE is proportional to DS^2 (for integer spin) or $D(S^2 - 1/4)$ (for half-integer spin), one could naturally think that its height should be easily enhanced by increasing both D and S. However, it transpires that ΔE is almost independent of S and it scales linearly with D, which basically depends on the number of metal centers constituting a molecule [68].

Another issue important from the point of view of potential applications is related to intrinsic spin relaxation and coherence loss due to interaction of SMMs with the environment. Even at low temperatures the dephasing effect of the environment cannot be neglected, as nuclear spins of SMMs still remain in thermal contact with the lattice vibrations [69]. Hence, a SMM in an excited molecular spin level can undergo transitions to neighboring states of lower energy, which is accompanied by emission of a phonon. In consequence, excited molecular spin states have a finite lifetime, which has been shown to be of the order of 10^{-9}–10^{-6} s [70–73]. Due to the lack of results for single molecules, the results cited above concern either crystal or powder samples of SMM, which automatically implies the presence of magnetic interactions with the environment. It has been shown that the coupling with nuclear moments of protons and other magnetic nuclei in the vicinity of the molecule can be considered as an important source of relaxation [42, 69, 74]. Hyperfine and dipolar interactions between neighboring molecules also can have a notable dephasing effect on the magnetic state of molecules [37, 75]. Furthermore, it turns out that in a time-dependent magnetic field such interactions are responsible for modification of local magnetic fields in the sample, leading to enhanced tunneling of molecules' spins [76–79]. More recently, the influence of intermolecular magnetic interactions on phase coherence of single molecules has been studied in the $[Mn_4]_2$ dimmer [80–82], where it has been proven that even weak interaction can have a significant effect on the quantum behavior of SMMs.

2.2 Coupling of a single-molecule magnet to magnetic metallic leads

A few different geometric schemes how to attached a SMM to metallic, or magnetic in particular, electrodes have been proposed up to now [28]. Four alternative ways for realization of the transport through a single molecule are shown in Fig. 2.2(a)-(d). The first one, Fig. 2.2(a), assumes that a molecule deposited on a metallic substrate is pinned from the top by a scanning tunneling microscope (STM) tip, which serves then as an electrode [83]. The experimental system of such a geometry, where a functionalized gold surface was used, has by now been proven to be suitable for investigating transport properties of individual Mn_{12} molecules at room temperature [48, 49]. Another possibil-

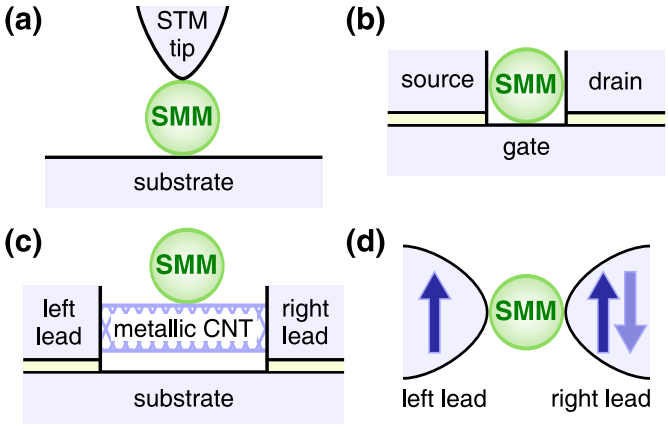

Figure 2.2: Different geometric schemes proposed for realization of spin and charge transport through a single-molecule magnet (SMM): (a) a molecule pinned by a STM tip, (b) a molecule captured in a break-junction device, (c) a molecule grafted on a suspended metallic carbon nanotube (CNT) [28], (d) an individual molecule attached chemically to metallic (ferromagnetic in this case) electrodes.

ity, Fig. 2.2(b), which has already been employed to study electron transport through a single Mn_{12} molecule below the blocking temperature [44, 46, 47], involves a break-junction geometry [84], whose main advantage is the presence of a gate electrode. The serious problem that can be encountered when applying devices of this type concerns the fact that they fail to provide a definitive evidence that transport really takes place through an individual molecule. Moreover, the exact number of molecules interconnecting the junction is still beyond control [9, 22]. Recently, the idea has been put forward that a molecule could be grafted on a metallic carbon nanotube (CNT) [16, 17, 85, 86], Fig. 2.2(c). The appealing feature of such a device would be the possibility of tuning the coupling between the molecule and CNT. Conceptually the simplest way seems to be a SMM connected chemically to two electrodes, Fig. 2.2(d).

It should be noted that even in the case of metallic electrodes attached to a SMM, investigation of individual SMM's transport properties requires a lot of technical efforts. It becomes even more challenging if one wants to use magnetic electrodes. In general, not only does one have to deal with low efficiency of spin injection from the electrode to a molecule, but also the overall performance of the device is strongly sensitive to the molecule-electrode contact geometry, the molecular end-groups, and intrinsic properties of the molecule [25, 26]. It's worth emphasizing that experimental techniques available at present offer only limited control of the relative orientation of the molecule's easy axis and leads' magnetizations. Additionally, an external magnetic field applied to a molecule is characterized by a finite directional resolution, i.e. it is virtually impossible to align the filed ideally parallel to the easy axis of the molecule. As a result, the longitudinal field usually gives also rise to a small transverse component.

In view of aforementioned technical obstacles to be surmounted in order to perform spin-dependent transport measurements of SMMs, it seems that the first step towards

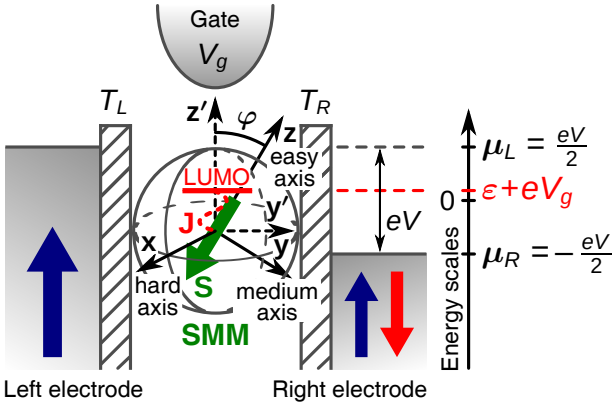

Figure 2.3: Schematic representation of the system under consideration. The system consists of a SMM weakly coupled to two ferromagnetic electrodes with the collinear configuration of their magnetic moments, i.e. either *parallel* or *antiparallel*. Due to symmetrical application of a finite bias voltage $V = (\mu_L - \mu_R)/e$, where $\mu_{L(R)}$ denotes the electrochemical potential of the left (right) lead, the system is in a nonequilibrium state. Position of the LUMO level can be tuned by the gate voltage V_g. Note that the axis x (x') is normal to the yz ($y'z'$) plane.

building a device with two magnetic electrodes could be the system involving the STM with a magnetic tip suspended above a molecule resting on a metallic but nonmagnetic substrate. One of the reasons is that by choosing an appropriate ligand shell for the molecule one can in such a case obtain the specific orientation (e.g. perpendicular) of the molecule's easy axis with respect to the surface [87]. Furthermore, different experimental approaches allowing for deposition of a film of well-dispersed SMMs on a substrate, so that addressing individual molecules by means of a STM tip is possible, have been developed [88–92].

In order to understand the influence of the interface between a SMM and electrodes or the surface on the electronic and magnetic properties of the molecule density-functional theory was also applied for studying the Mn_{12} molecule [93–97]. First of all, it has been shown that the deposition on a surface leads to breaking the fourfold symmetry of the molecule, and the broadening of molecular orbitals due to interaction with the metallic electrodes strongly depends on the orientation of the molecule's easy axis with respect to the electronic transport direction. Since the Mn_{12} molecule is characterized by a planar shape with the anisotropy easy axis approximately perpendicular to the plane, it means that for the perpendicular orientation molecular orbitals are only slightly broadened as a result of large separation from electrodes. In the parallel configuration, on the other hand, the distance is reduced due to the presence of shorter linker molecule, whose consequence is the significant broadening of molecular orbitals so that individual orbitals become indistinguishable. Additionally, it has been concluded that the *spin-filter effect* stemming from the energy gap between the spin-majority and spin-minority lowest unoccupied molecular orbitals can occur [95, 96].

In the following I consider the model tunnel junction, Fig. 2.3, consisting of a SMM

embedded between two ferromagnetic metallic electrodes whose magnetizations are in the collinear configuration, either *parallel* or *antiparallel*. Throughout this thesis a model situation is assumed that electronic transport through the molecule takes place *via* the *lowest unoccupied molecular orbital* (LUMO) of the SMM. Such an assumption may be justified when the following conditions are obeyed. First, the higher unoccupied levels are sufficiently far from the LUMO level, so they can be neglected for voltages of interest. Second, the occupied orbitals, including those responsible for magnetic moment of SMMs are sufficiently far below the Fermi level, so their influence can be taken into account effectively *via* exchange coupling J between electrons in the LUMO level and internal magnetic core. The latter assumption also means that the molecule charged with one electron in the LUMO level corresponds to the total spin number equal either $S + 1/2$ or $S - 1/2$. In a general case, however, the situation may be more complex and the total spin number of the charged molecule in equilibrium can differ from $S \pm 1/2$. Transport through such states is suppressed due to the phenomenon of spin blockade. However, they may have significant impact on transport characteristics and should be taken into account. This problem is not addressed in this thesis. It is worth noting that the discussed problem does not occur in the cotunneling regime, where electrons only virtually enter the LUMO level and the charge state of the molecule remains unchanged.

A SMM coupled to external leads can be modelled by Hamiltonian of the general form

$$\mathcal{H} = \mathcal{H}_{\mathrm{SMM}} + \mathcal{H}_{\mathrm{el}} + \mathcal{H}_{\mathrm{tun}}, \tag{2.1}$$

where the first term on the right hand side describes a SMM and will be described in the following section of the present chapter. The next term describes ferromagnetic (in general) electrodes, and the qth electrode is characterized by *noninteracting* itinerant electrons with the dispersion relation $\varepsilon^q_{\mathbf{k}\sigma}$, where $\mathbf{k}$ denotes a wave vector and σ a spin index of an electron. The Hamiltonian describing the electrodes therefore takes the form

$$\mathcal{H}_{\mathrm{el}} = \sum_q \sum_{\mathbf{k}\sigma} \varepsilon^q_{\mathbf{k}\sigma} a^{q\dagger}_{\mathbf{k}\sigma} a^q_{\mathbf{k}\sigma}, \tag{2.2}$$

where $a^{q\dagger}_{\mathbf{k}\sigma}$ and $a^q_{\mathbf{k}\sigma}$ are the relevant creation and annihilation operators for the qth electrode, respectively. Since the problem under consideration requires application of magnetic leads, it is convenient to describe each of them by the polarization parameter $P_q = (D^q_+ - D^q_-)/(D^q_+ + D^q_-)$, where $D^q_\pm$ denotes the density of states (DOS) for majority (upper sign) and minority (lower sign) electrons at the Fermi level in the lead q.

The last term, $\mathcal{H}_{\mathrm{tun}}$, of Hamiltonian (2.1) corresponds to tunneling processes between the electrodes and molecule. As it has been discussed above, from a technical point of view, the problem of attaching a molecule to magnetic electrodes is highly nontrivial, as the overall performance of such a device is sensitive to many factors. Since on the formal level it is rather complicated to take into account separately all possible factors that may influence the transport through the junction, I simplify the situation by introducing one parameter T_q, i.e. the tunnel matrix element between the molecule and the qth

lead, which incorporates the combined effects of all processes that can affect tunneling of electrons in the system. Furthermore, I assume that the molecule's anisotropy easy axis can be tilted away in the $y'z'$ plane, forming an arbitrary angle φ with the direction collinear with spin moments of the electrodes, as shown in Fig. 2.3. Consequently, the tunneling Hamiltonian is given by

$$\mathcal{H}_{\rm tun} = \sum_q \sum_{\mathbf{k}\sigma} T_q a^{q\dagger}_{\mathbf{k}\sigma} \left[\cos\frac{\varphi}{2}\, c_\sigma - \eta_q \sin\frac{\varphi}{2}\, c_{\bar\sigma} \right] + \text{H.c.}, \tag{2.3}$$

where $\eta_{L(R)} = \pm 1$ and $\bar\sigma = -\sigma$. In addition, due to tunneling processes, the LUMO level acquires a finite spin-dependent width $\Gamma_\sigma = \sum_q \Gamma^q_\sigma$, where $\Gamma^q_\sigma = 2\pi |T_q|^2 D^q_\sigma$. The parameters $\Gamma^q_\pm$ can be presented as $\Gamma^q_\pm = \Gamma_q(1 \pm P_q)$ for spin-majority (upper sign) and spin-minority (lower sign) electrons. In the following these parameters will be used to describe the strength of the coupling between the LUMO level and leads. Here, $\Gamma_q = (\Gamma^q_+ + \Gamma^q_-)/2$, and P_q is the spin polarization of the qth lead. For simplicity the coupling is assumed to be symmetric, $\Gamma_{\rm L} = \Gamma_{\rm R} = \Gamma/2$. It should be noted that the form of $\Gamma_{\rm L}$ and $\Gamma_{\rm R}$ assumed here is the simplest one, which allows for capturing basic features of spin dependent transport, and generally these parameters can be more complex.

2.3 The model Hamiltonian of a single-molecule magnet

The most general Hamiltonian, which captures all characteristic features of SMMs, such as the Ising-type uniaxial magnetic anisotropy (including the influence of the molecule's oxidation state on the anisotropy [98–100]), transverse anisotropy, and intrinsic magnetic relaxation, can be written as follows [37, 101]

$$\mathcal{H}_{\rm SMM} = \mathcal{H}_0 + \mathcal{H}_{\rm rel}. \tag{2.4}$$

Here, $\mathcal{H}_0$ describes the uniaxial magnetic anisotropy of a SMM, hence defining the easy axis of the molecule, and also includes a term that describes the LUMO level and its coupling to the SMM's spin. In turn, $\mathcal{H}_{\rm rel}$ represents all terms responsible for magnetic relaxation of the SMM's spin (including the quantum tunneling of magnetization). I point that relaxation due to coupling with electrons in the leads is not included in $\mathcal{H}_{\rm rel}$, and is taken into account *via* other terms of the Hamiltonian (2.1). Finally, it should be emphasized that the Hamiltonian (2.4), sometimes referred to as the *giant spin Hamiltonian*, has also one serious drawback. As it will be seen below, it fails to include the orbital degrees of freedom for the extra electrons in the LUMO level, while it has been shown that the orbital effects arising as a result of excess charge on the molecule can influence its symmetry and magnetic anisotropy [99, 102].

For molecules with *integer* spin S, the first term, $\mathcal{H}_0$, of the Hamiltonian (2.4) can be

written explicitly as

$$\begin{aligned}\mathcal{H}_0 = &-\big(D + \sum_\sigma D_1\, c_\sigma^\dagger c_\sigma + D_2\, c_\uparrow^\dagger c_\uparrow c_\downarrow^\dagger c_\downarrow\big) S_z^2 \\ &+ \sum_\sigma \varepsilon c_\sigma^\dagger c_\sigma + U c_\uparrow^\dagger c_\uparrow c_\downarrow^\dagger c_\downarrow - J\mathbf{s}\cdot\mathbf{S} \\ &+ g\mu_{\mathrm{B}}(S_z + s_z)H_z, \end{aligned} \tag{2.5}$$

where S_z is the zth component of the internal (core) molecule's spin operator $\mathbf{S}$, $c_\sigma^\dagger$ (c_σ) creates (annihilates) an electron in the LUMO level, and D is the uniaxial anisotropy constant of a free-standing (uncharged) molecule. When, however, a bias voltage is applied between the leads, some additional charge (up to two electrons) can accumulate in the LUMO level. This, in turn, can affect the magnitude of uniaxial anisotropy, and the relevant corrections are taken into account by the terms including D_1 and D_2.

The second line of Eq. (2.5) accounts for the LUMO level of energy ε, with U denoting the Coulomb energy of two electrons of opposite spins occupying this level. Although the position of the LUMO level can be modified by the gate voltage V_g, it remains independent of the symmetrically applied bias voltage V. The most interesting term for the effects being the subject of this dissertation is the last term, given explicitly by

$$J\mathbf{s}\cdot\mathbf{S} = \frac{J}{2}c_\uparrow^\dagger c_\downarrow S_- + \frac{J}{2}c_\downarrow^\dagger c_\uparrow S_+ + \frac{J}{2}\Big[c_\uparrow^\dagger c_\uparrow - c_\downarrow^\dagger c_\downarrow\Big]S_z\,, \tag{2.6}$$

which stands for exchange coupling between the magnetic core of a SMM, represented by the spin $\mathbf{S}$, and electrons in the LUMO level, described by the local spin operator $\mathbf{s} = \frac{1}{2}\sum_{\sigma\sigma'} c_\sigma^\dagger \boldsymbol{\sigma}_{\sigma\sigma'} c_{\sigma'}$, where $\boldsymbol{\sigma} \equiv (\sigma^x, \sigma^y, \sigma^z)$ is the Pauli spin operator for conduction electrons. This interaction can be either of *ferromagnetic* ($J > 0$) or *antiferromagnetic* ($J < 0$) type. Finally, the last term of $\mathcal{H}_{\mathrm{SMM}}$ describes the Zeeman splitting associated with the magnetic field applied along the easy axis of the molecule, where g stands for the Landé factor, and μ_{B} is the Bohr magneton.

When the molecule is detached from the external reservoirs, it is electrically neutral and its charge state cannot change. Consequently, the Hamiltonian (2.5) becomes reduced to a much simpler form,

$$\mathcal{H}_0 = -DS_z^2 + g\mu_{\mathrm{B}}H_zS_z. \tag{2.7}$$

To complete description of the model Hamiltonian (2.4), I need to specify the second term, $\mathcal{H}_{\mathrm{rel}}$. This term is usually written in the form

$$\mathcal{H}_{\mathrm{rel}} = E(S_x^2 - S_y^2) + C(S_+^4 + S_-^4) + g\mu_{\mathrm{B}}[(S_x + s_x)H_x + (S_y + s_y)H_y] + \mathcal{H}'. \tag{2.8}$$

Here S_x and S_y are the transverse (to the easy axis) components of the molecule's spin operator $\mathbf{S}$, $S_\pm = S_x \pm iS_y$, whereas E and C are the transverse magnetic anisotropy constants (here any correction to the transverse anisotropy constant due to molecules oxidation are neglected). The penultimate term of Eq. (2.8) contains the Zeeman energy associated with the transverse components of magnetic field, whreas the term $\mathcal{H}'$

takes into account all other interactions which lead to SMM's spin relaxation (intrinsic relaxation).

2.4 Energy states of a single-molecule magnet

For molecules with a negligible transverse anisotropy and weak transverse magnetic field, the term $\mathcal{H}_{\rm rel}$ may be considered as a perturbation, while the energy spectrum of the molecule is then determined mainly by the term $\mathcal{H}_0$. The unperturbed part $\mathcal{H}_0$ of the Hamiltonian $\mathcal{H}_{\rm SMM}$ is then sufficient to model some physical processes, e.g. the current-induced magnetic switching. It can be easily shown that $\mathcal{H}_0$ commutes with the zth component S_t^z of the total spin operator $\mathbf{S}_t \equiv \mathbf{S} + \mathbf{s}$ [103, 104]. Consequently, one can enumerate the eigenstates of $\mathcal{H}_0$ with the eigenvalues m of S_t^z and the corresponding occupation number n of the LUMO level. Thus, the eigenstates of the SMM in the case considered are given by the formulas,

$$|S_t = S; 0, m\rangle \equiv |0\rangle_{\rm orb} \otimes |m\rangle_{\rm mol}, \tag{2.9}$$

$$|S_t = S{-}1/2; 1, m\rangle \equiv \mathbb{A}_m^{\mp}|{\downarrow}\rangle_{\rm orb} \otimes |m{+}1/2\rangle_{\rm mol} + \mathbb{B}_m^{\mp}|{\uparrow}\rangle_{\rm orb} \otimes |m{-}1/2\rangle_{\rm mol}, \tag{2.10}$$

$$|S_t = S{+}1/2; 1, m\rangle \equiv \mathbb{A}_m^{\pm}|{\downarrow}\rangle_{\rm orb} \otimes |m{+}1/2\rangle_{\rm mol} + \mathbb{B}_m^{\pm}|{\uparrow}\rangle_{\rm orb} \otimes |m{-}1/2\rangle_{\rm mol}, \tag{2.11}$$

$$|S_t = S; 2, m\rangle \equiv |{\uparrow}{\downarrow}\rangle_{\rm orb} \otimes |m\rangle_{\rm mol}, \tag{2.12}$$

for intermediate states $m = -S_t^z + 1, -S_t^z + 2, \ldots, S_t^z - 2, S_t^z - 1$, with upper (lower) sign referring to the case when $2(D + D_1) - J$ is positive (negative), and

$$|S_t = S; 0, \pm S\rangle \equiv |0\rangle_{\rm orb} \otimes |\pm\, S\rangle_{\rm mol}, \tag{2.13}$$

$$\begin{aligned} |S_t = S{-}1/2; 1, \pm S{\mp}1/2\rangle \equiv{}& \mathbb{A}^{\mp}_{\pm S\mp 1/2}|{\downarrow}\rangle_{\rm orb} \otimes |\pm\, S{+}0(1)\rangle_{\rm mol} \\ &+ \mathbb{B}^{\mp}_{\pm S\mp 1/2}|{\uparrow}\rangle_{\rm orb} \otimes |\pm\, S{-}1(0)\rangle_{\rm mol}, \end{aligned} \tag{2.14}$$

$$|S_t = S{+}1/2; 1, \pm S{\pm}1/2\rangle \equiv |{\uparrow}({\downarrow})\rangle_{\rm orb} \otimes |\pm\, S\rangle_{\rm mol}, \tag{2.15}$$

$$|S_t = S; 2, \pm S\rangle \equiv |{\uparrow}{\downarrow}\rangle_{\rm orb} \otimes |\pm\, S\rangle_{\rm mol}, \tag{2.16}$$

for the fully polarized states. According to the used notation $|\bullet\rangle_{\rm orb(mol)}$ denotes the spin state of the orbital (SMM). The coefficients $\mathbb{A}_m^{\pm}$ and $\mathbb{B}_m^{\pm}$ play here the role of effective Clebsch-Gordan coefficients which depend on the system's parameters and have the form

$$\mathbb{A}_m^{\pm} = \mp \frac{\sqrt{2\Delta\epsilon(m) \mp (2D^{(1)} - J)m}}{2\sqrt{\Delta\epsilon(m)}}, \tag{2.17}$$

$$\mathbb{B}_m^{\pm} = \frac{J\sqrt{S(S+1) - m^2 + 1/4}}{2\sqrt{\Delta\epsilon(m)}\sqrt{2\Delta\epsilon(m) \mp (2D^{(1)} - J)m}}, \tag{2.18}$$

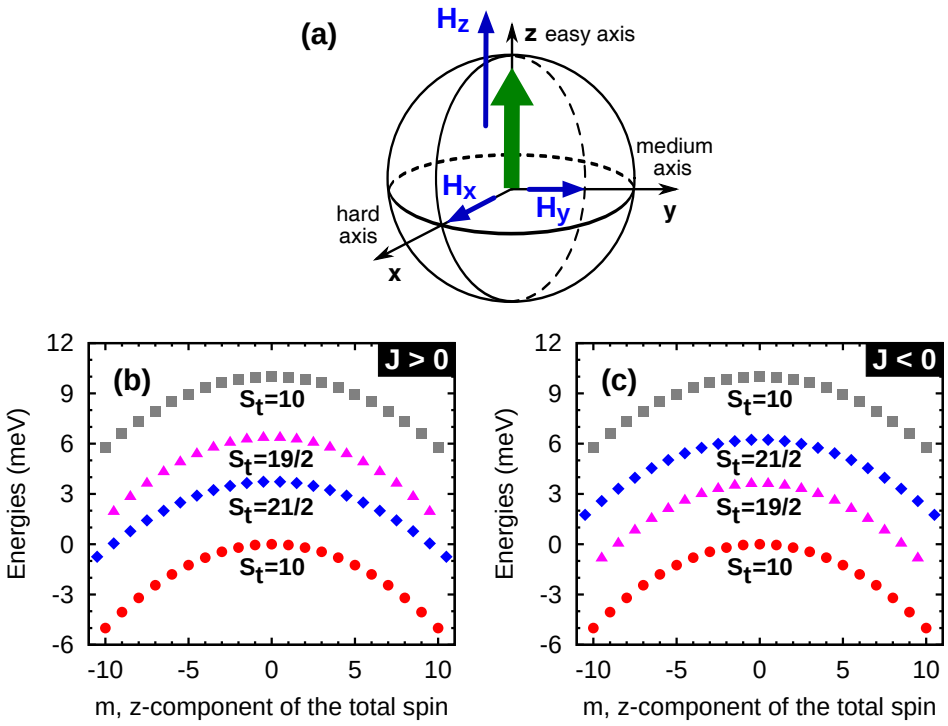

Figure 2.4: (a) Spatial orientation of the system's principle axes with respect to the longitudinal H_z and transversal H_x, H_y magnetic fields. The solid arrow represents the SMM's spin in the state $|S_t = S; 0, S\rangle$. In the bottom panel energy spectra of a hypothetical Mn_{12}-like molecule in the absence of an external magnetic field ($H_z = H_x = H_y = 0$) are shown for the following parameters: $D = 0.05$ meV, $D_1 = -0.005$ meV, $D_2 = 0.002$ meV, $|J| = 0.25$ meV, $\varepsilon = 5$ meV, and $U = 0$ in the case of *ferromagnetic* (b) and *antiferromagnetic* (c) exchange coupling between the electron spin in the LUMO level and the molecule's core spin. Different parabolas correspond to indicated values of the SMM's total spin, S_t, and occupation states of the LUMO level: $|10; 0, m\rangle$ (●), $|19/2; 1, m\rangle$ (▲), $|21/2; 1, m\rangle$ (♦), and $|10; 2, m\rangle$ (■).

with $\Delta\epsilon(m) = \sqrt{D^{(1)}(D^{(1)} - J)m^2 + (J/4)^2(2S+1)^2}$ and $D^{(1)} = D + D_1$. The corresponding eigenenergies of the Hamiltonian $\mathcal{H}_0$ are

$$\epsilon(S_t = S; 0, m) = -Dm^2 + g\mu_B m H_z, \tag{2.19}$$

$$\epsilon(S_t = S - 1/2; 1, m) = -D^{(1)}(m^2 + 1/4) + \varepsilon + J/4 \mp \Delta\epsilon(m) + g\mu_B m H_z, \tag{2.20}$$

$$\epsilon(S_t = S + 1/2; 1, m) = -D^{(1)}(m^2 + 1/4) + \varepsilon + J/4 \pm \Delta\epsilon(m) + g\mu_B m H_z, \tag{2.21}$$

$$\epsilon(S_t = S; 2, m) = -(D + 2D_1 + D_2)m^2 + 2\varepsilon + U + g\mu_B m H_z. \tag{2.22}$$

The energy spectrum of the molecule corresponding to the Hamiltonian $\mathcal{H}_0$, Eq. (2.5), and defined by Eqs. (2.19)-(2.22), has the form of four parabolas, Fig. 2.4(b)-(c), where

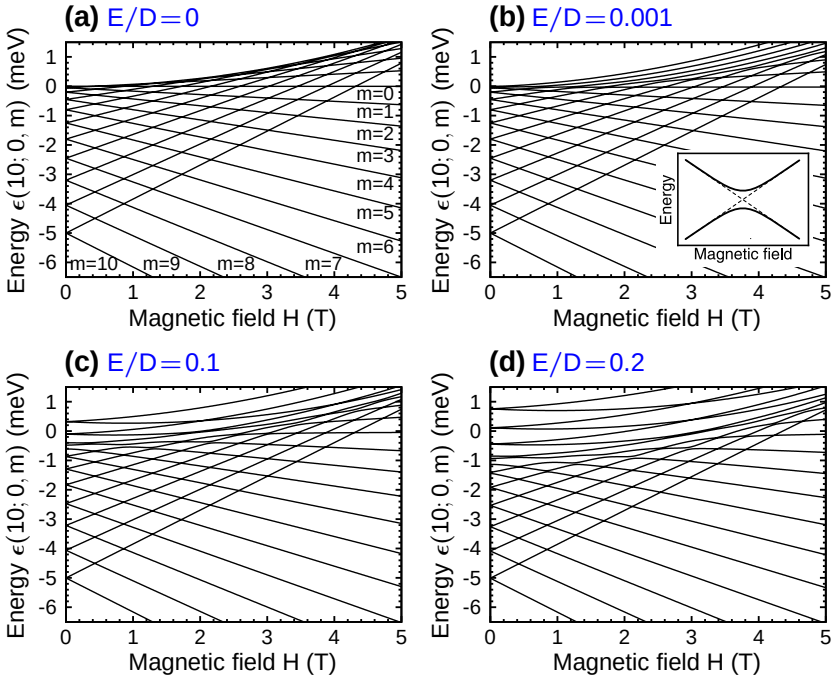

Figure 2.5: Zeeman plots for a hypothetical free-standing SMM of $S = 10$ and $D = 0.05$ meV in the case of different values of the second order transverse anisotropy constant E (the fourth order anisotropy term is neglected, i.e. $C = 0$), with the notation $H_z = -H$ ($H > 0$) used. Moreover, a misalignment of the magnetic field and molecule's easy axis is assumed so that the transverse component of the magnetic field is present, $H_x = 0.1H$ and $H_y = 0$. The inset in (b) is the magnification of the avoiding level crossing, which arises in the system owing to the presence of the transverse anisotropy and transverse magnetic field, and which is too small to be resolved in the energy plot.

each state is labeled by the corresponding spin number S_t, the occupation number n of the LUMO level, and the eigenvalue m of the z component of the molecule's total spin, $S_t^z \equiv S_z + \frac{1}{2}(c_\uparrow^\dagger c_\uparrow - c_\downarrow^\dagger c_\downarrow)$, with the second term representing the contribution from electrons in the LUMO level. The two situations shown in Fig. 2.4(b) and Fig. 2.4(c) correspond to $2(D + D_1) - J$ negative and positive, respectively.

Let's assume temporarily a free-standing hypothetical Mn_{12}-like molecule (empty LUMO level) of spin $S = 10$. In such a case, the energy spectrum of the Hamiltonian $\mathcal{H}_0$, corresponding to a molecule in zero magnetic field is described by the dotted parabola in Fig. 2.4(b)-(c). Thus, in the absence of external longitudinal magnetic field H_z, the SMM has two equivalent energy minima for the states $|S_t = S; 0, \pm S\rangle$, which correspond to either parallel (+) or antiparallel (−) alignment of the spin with respect to the axis z (easy axis). The energy barrier ΔE for switching the SMM's spin between these two minima is thus, as expected, $\Delta E = DS^2$. It should be noted, however, that when the magnitude of magnetic field along the easy axis increases (but e.g. $H_z \equiv -H < 0$), the energies of molecular spin states $|S_t = S; 0, m\rangle$ for $-S < m < 0$ increase, while for $0 < m < S$ they decrease, Fig. 2.5. As a result, the field effectively reduces height of

the energy barrier the SMM has to overcome to flip its spin orientation from $m = -S$ to $m = S$. Furthermore, for certain values of the field the energy levels on both sides of the barrier become pairwise degenerate, Fig. 3.3. If wave functions describing such two resonant states overlap, then one can expect tunneling processes between the states. The mechanism of the SMM's spin reversal based on quantum tunneling in a time dependent magnetic field is one of alternative ways how to magnetically switch a SMM, and it will be discussed in Chapter 3.

The uniaxial symmetry of the unperturbed Hamiltonian $\mathcal{H}_0$ can be broken by introducing the transverse anisotropy into the system (and the Zeeman energy associated with the transverse magnetic field), which hence is an important part of the relaxation term [105, 106]. As a consequence, $\mathcal{H}_{\text{rel}}$ (assuming $\mathcal{H}' = 0$) is responsible for coupling between the states of the Hamiltonian $\mathcal{H}_0$. The eigenstates of $\mathcal{H}_{\text{SMM}}$ contain then admixture of the unperturbed states $|S_t = S; 0, m\rangle$ corresponding to different m. Since there is no general analytic expression for the energy spectrum of the system in the general case, thus when the transverse anisotropy cannot be neglected, the problem can only be dealt with numerically by performing a unitary transformation $U^\dagger \mathcal{H}_{\text{SMM}} U = \widetilde{\mathcal{H}}_{\text{SMM}}$ to a new basis in which $\widetilde{\mathcal{H}}_{\text{SMM}}$ is diagonal. Consequently, one obtains the set of relevant eigenvectors $|\chi\rangle$ and corresponding eigenvalues ε_χ satisfying $\widetilde{\mathcal{H}}_{\text{SMM}}|\chi\rangle = \varepsilon_\chi|\chi\rangle$, where $|\chi\rangle$ denotes a many-body state of SMM and ε_χ its energy. Nonetheless, it is worth emphasizing at this point that, in general, numerical derivation of the energy spectrum, as well as further computation of thermodynamical quantities, such as specific heat or magnetization, in the case of many SMMs belong to highly nontrivial tasks [107–109]. The problem concerns especially molecules comprising of a large number of magnetic centers, the interactions among which can sometimes take a quite complicated form.

Before proceeding further, I should comment on the influence of the transverse anisotropy on the height of the energy barrier. It turns out that as the transverse anisotropy gets stronger, i.e. $0 \ll |E/D| \leqslant 1/3$ [37], the already introduced expression for the energy barrier ΔE becomes inadequate [38, 66], Fig. 2.5(d). In the present situation, $S_z = m$ is no longer a good quantum number for all the states. When approaching the top of the barrier, an extensive admixture of different states is encountered so that such a way of labelling losses any physical significance. However, if $|E|$ is appreciably smaller than $|D|$, it is physically justifiable to assume the parabolic form of the energy barrier described by $\mathcal{H}_0$, Eq. (2.5), and still use $S_z = m$ for labelling the magnetic molecular states, such as in Ref. [110].

Finally, it should be pointed out that although the transverse anisotropy is indispensable for quantum tunneling of the SMM's spin to occur, it is not the only mechanism which may lead to the magnetic switching. In general, all kinds of magnetic interactions between the spin and its environment may possibly result in the reversal of the former, and they can be formally included in the term $\mathcal{H}'$. In this thesis, however, the main emphasis is put on switching due to interaction of a SMM with spin-polarized currents.

CHAPTER 3

Quantum tunneling of magnetization (QTM) in single-molecule magnets

The principle of *tunneling effect* is conventionally formulated in terms of a particle whose energy is insufficient to cross a potential barrier, and which instead of climbing over the barrier can tunnel through it. Tunneling phenomenon is the most prominent manifestation of quantum mechanics, and its source lies in the overlap of wave functions corresponding to a particle on both sides of the barrier. This may be formulated in terms of an effective interaction between the states corresponding to these two wave functions. If the particle can tunnel back and forth between two states of the same energy, this interaction may lift the degeneracy. As a consequence, an energy gap may arise between the two levels [62].

Although tunneling processes are typically associated with single particles, e.g. electrons, they can actually also occur for much larger systems, taking then a much more complex form. An interesting example of such *macroscopic* quantum tunneling manifests in some nanometer-sized magnets where due to quantum tunneling the magnetic poles can suffer a sudden interchange [111–114]. The behavior of the particle's magnetic moment is then characteristic to a quantum object, and the only difference between the picture presented above and the tunneling of a magnetic moment (or spin) is that the latter takes place in angular momentum space between two potential energy minima [115–117], and more than a single electron are involved in a single tunneling event. Therefore such a tunneling is called *macroscopic quantum tunneling of magnetization* (QTM).

The first suggestion for the occurrence of the QTM was put forward by Bean and Livingstone in 1959 [60], who in this way tried to explain why the magnetization of superparamagnetic nickel particles appeared to stay unblocked even at very low temperatures. The problem of the QTM again received great attention at the end of the 1980s

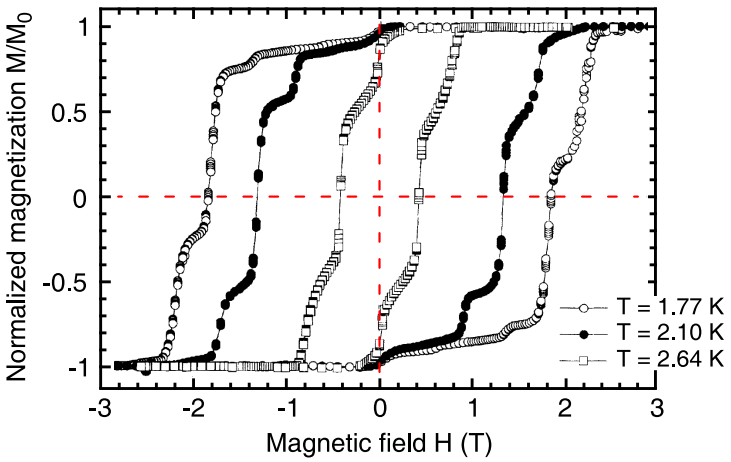

Figure 3.1: One of the first experimental results obtained for a crystal sample of Mn_{12} molecules exhibiting the magnetic hysteresis loop with a succession of flat regions and characteristic steps due to the QTM. Modified from Ref. [63], where also further details about how the data was obtained can be found.

after a series of rather fundamental theoretical papers had been published [118–123]. Within the next couple of years, the QTM was confirmed to be active in many magnetic systems, to mention only a few, ferrofluids containing small particles of FeC, Fe_3O_4; magnetic grains of Fe and Dy; amorphous alloys based on rare-earth and transition metals; as well as a ferritin protein [113, 124, 125]. One of the main obstacles encountered in experiments involving aforementioned materials concerns the fact that the number of constituent spins and the magnetic anisotropy, the two factors that determine the energy barrier and hance they affect the QTM, can widely differ from sample to sample. As a result, because of the statistical nature of these experiments, one can compare their results with theory only qualitatively [113]. In this context the discovery of the QTM in SMMs was a real breakthrough [33, 59, 63], as under the same conditions crystal samples formed by molecules of a specific type with well-defined anisotropy and a spin number yield reproducible results.

For a crystal sample of molecular magnets subject to a varying in time external magnetic field, the under-barrier transitions due to QTM reveal themselves as characteristic steps in magnetization hysteresis loops[1] [63, 126], Fig. 3.1. It would be instructive to briefly analyze the origin of the tunneling mechanism at this point. From the physical point of view, the QTM in SMMs arises due to the presence of transverse anisotropy and/or a small transverse magnetic field (*via* the Zeeman term in Eq. 2.8). The anisotropy is mainly induced by electrostatic crystal-field interaction and the spin-orbit coupling [127, 128], which consequently means the vital role of the molecule's symmetry [37, 129], whereas the field can basically come from three inherent sources [62, 66, 117, 130]. First, it can be the dipolar field resulting from the neighbor-

[1]It should be noted that all available experimental results indicating the presence of QTM concern crystal samples, whereas in the present case I focus on QTM in single molecules.

hood of other SMMs (if one considers a crystal or powder sample of SMMs), second, the hyperfine field owing to the presence of magnetic nuclei, and finally, it can simply be some external magnetic field. On the other hand, in the experimental setup aligning an external longitudinal field exactly parallel to the sample's easy axis poses a serious problem, and consequently one should expect the small transverse component to be usually present. Nonetheless, this argument doesn't apply once there is no external field.

The presence of an external transverse magnetic field in the case of SMMs has also another very interesting implication, namely, the field can be used to tune the tunnel splitting between two states on opposite sides of the energy barrier [57, 131, 132]. Furthermore, it has been demonstrated that for small angles between the hard axis and the direction of the field the tunnel splitting oscillates as a function of the field amplitude, and the oscillations gradually decay with increasing the angle. Such a periodic behavior is a consequence of the *geometric-phase* (or *Berry-phase*) oscillations attributed to topological quantum interference of two tunneling paths between the lowest-energy states on the opposite sides of the anisotropy energy barrier [133, 134]. Using the Stokes' theorem, one can prove that the path integrals can be converted to an area integral, and consequently that the tunnel splitting oscillations are suppressed owing to destructive interference whenever the area delimited by the tunnel paths equates to $k\pi/S$, where k is an odd integer and S denotes the value of the SMM's spin. Thus one may notice that the nature of the oscillations in the tunnel splitting is actually analogous to the Aharonov-Bohm oscillations of the conductivity in mesoscopic rings [38, 135].

Since the QTM phenomenon has become one of the hallmark feature of SMMs, it seems worth considering how the QTM processes are modified in the case when the molecule is attached to spin-polarized electronic reservoirs. It should be expected that interaction of the SMM's spin with the spins of tunneling electrons will introduce an additional relaxation path, and therefore it will enhance the effect of magnetic switching due to the QTM. For this reason, first I will analyze the QTM mechanism in the absence of any further relaxation processes using the Landau-Zener model for this purpose, and afterwards I will include the relaxation processes of interest to discuss their significance for the QTM.

3.1 QTM in an isolated single-molecule magnet

At the beginning, let's assume an isolated SMM whose interaction with the environment can be neglected. Such a simplification allows me to switch off the relaxation process due to coupling of the SMM to external electrodes and to study the spin reversal due to QTM only. Moreover, I also omit here other spin relaxation (intrinsic) processes which may occur in the molecule. The omitted relaxation processes will be taken under consideration in Section 3.2.

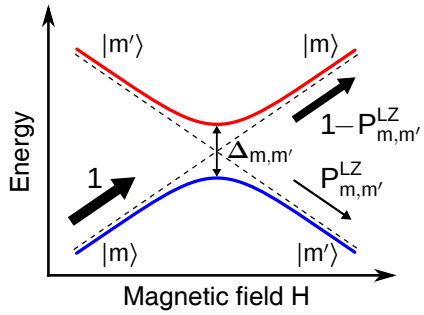

Figure 3.2: Energy diagram of the avoided level crossing region for the states $|m\rangle$ and $|m'\rangle$ with $\Delta_{m,m'}$ denoting the *tunnel splitting*. The size of black arrows corresponds to the probability of finding the system in a certain state, and $P^{\mathrm{LZ}}_{m,m'}$ describes the Landau-Zener probability, Eq. (3.3), that the SMM's spin tunnels from $|m\rangle$ to $|m'\rangle$.

3.1.1 The Landau-Zener mechanism of QTM

As discussed in Chapter 2 and in the introduction above, the degeneracy of energy levels on the opposite sides of the barrier is lifted due to the presence of the transverse anisotropy terms and/or a small transverse magnetic field, Eq. (2.8) (for $\mathcal{H}' = 0$). Consequently, at the resonant magnetic fields one observes energy gaps instead of level crossings, Fig. 2.5(b) and Fig. 3.2. The tunneling process appears when the system follows the same energy curve after leaving the region of the gap, whereas jump across the gap corresponds to staying in the initial state. The key idea of a SMM tunneling between molecular spin states on the opposite sides of the anisotropy energy barrier is schematically illustrated in Fig. 3.3.

The time evolution of the system can be obtained by solving the time-dependent Schrödinger equation (TDSE), where the time dependence enters the Hamiltonian $\mathcal{H}_{\mathrm{SMM}}$, Eq. (2.4), through the Zeeman term (the magnetic field depends on time). It has been shown, however, that in the vicinity of each avoided crossing the behavior of the system can be described by the two-level Landau-Zener (LZ) model [70, 101, 136–144]. Instead of solving TDSE to describe dynamics of the system, it is therefore sufficient to consider a sequence of two-level tunneling problems.

In the following discussion I assume the abbreviation $|S_t = S; 0, m\rangle \equiv |m\rangle$. Let's consider what happens when the region of the avoided energy level crossing between the two states $|m\rangle$ and $|m'\rangle$ is swept with an external magnetic field, $H = ct$, with c being the speed at which H changes, Fig. 3.2. It is assumed that initially ($t << 0$) the probability of finding the molecule in each of these two states is $P_m = 1$ and $P_{m'} = 0$, respectively. It turns out that the tunneling between the states $|m\rangle$ and $|m'\rangle$ can be successfully accounted for by an effective Hamiltonian [136, 137]

$$\mathcal{H}_{\mathrm{eff}}(t) = \begin{pmatrix} E_m(t) & \Delta_{m,m'}/2 \\ \Delta_{m,m'}/2 & E_{m'}(t) \end{pmatrix}, \tag{3.1}$$

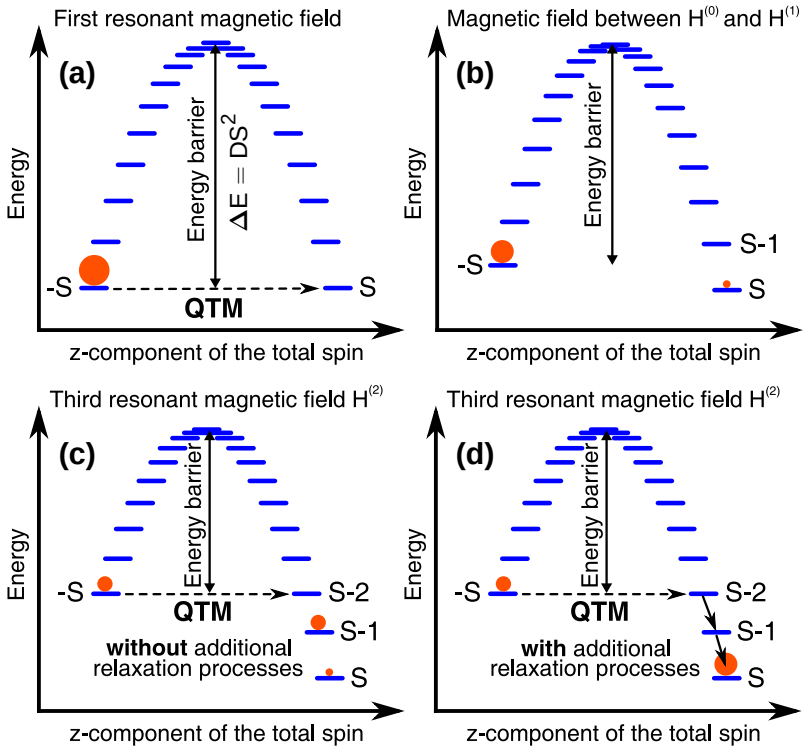

Figure 3.3: Schematic depiction of the QTM mechanism in a SMM occurring in a time-dependent magnetic field. The dot's size represents probability of a particular spin state at the corresponding stage of the reversal process.

with $E_k(t) = -g\mu_B kct$ ($k = m, m'$) and $\Delta_{m,m'}$ denoting the *tunnel splitting* (barrier) between the states $|m\rangle$ and $|m'\rangle$, Fig. 3.2. By solving the Schrödinger equation $i\hbar|\dot{\Psi}_{\rm ad}(t)\rangle = \mathcal{H}_{\rm eff}(t)|\Psi_{\rm ad}(t)\rangle$ for the wave function in the *adiabatic approximation* [145]

$$|\Psi_{\rm ad}(t)\rangle = a_m(t)\exp\left[-\frac{i}{\hbar}\int_0^t dt' E_m(t')\right]|m\rangle + a_{m'}(t)\exp\left[-\frac{i}{\hbar}\int_0^t dt' E_{m'}(t')\right]|m'\rangle, \tag{3.2}$$

where $a_k(t)$ ($k = m, m'$) is the probability amplitude, one finds that the system tunnels from the state $|m\rangle$ to the state $|m'\rangle$ with the probability [136]

$$P^{\rm LZ}_{m,m'} = \lim_{t\to\infty}\left|\langle m'|\Psi_{\rm ad}(t)\rangle\right|^2 = 1 - \exp\left[-2\pi\lambda_{m,m'}\right], \tag{3.3}$$

where $\lambda_{m,m'} = \Delta^2_{m,m'}/(4\hbar|m-m'|g\mu_B c)$.

The mechanism introduced above can be extended to the case when a series of successive avoided level crossings is encountered. For this purpose, it is assumed that a SMM of spin S is initially saturated in the state $|-S\rangle$ with a magnetic field. Moreover, one makes also an assumption that H ($H = -H_z$) grows linearly in time at a constant speed c, $H = ct$. At relevant resonant fields for $H \geq 0$ (that is $t \geq 0$), the

SMM's spin undergoes transitions from the state $|-S\rangle$ to states $|S-n\rangle$ (consecutively for $n = 0, 1, 2, \ldots$) on the opposite side of the energy barrier. The probabilities of all other states $|-S+1\rangle, \ldots, |S-n-1\rangle$ for each n are then equal to zero. The repetitive use of the two-level LZ model yields the formula for the probability with which the spin tunnels between the states $|-S\rangle$ and $|S-n\rangle$ [83, 146],

$$P^{\mathrm{LZ}}_{-S,S-n} = \Big(1 - \exp\big[-2\pi\lambda_n\big]\Big) \prod_{l=0}^{n-1} \exp\big[-2\pi\lambda_l\big], \tag{3.4}$$

where $\lambda_n \equiv \lambda_{-S,S-n}$. Within such a simplified model, the average value of the SMM's spin, $\langle S_z(H)\rangle$, changes stepwise and for the Mth resonant magnetic field $H_z^{(M)}$ its value can be found from the formula

$$\langle S_z(H^{(M)})\rangle = -S + \sum_{n=0}^{M} (2S-n) P^{\mathrm{LZ}}_{-S,S-n}. \tag{3.5}$$

To conclude the discussion of the LZ model, the question of its applicability for explaining the QTM should also be addressed. It has been proven experimentally that the LZ model provides the correct description of the QTM relaxation mechanism in SMMs within the range of the field sweeping speeds 0.001–1 T/s [70, 142]. At the lower speeds, there appear some deviations owing to so-called *hole-digging mechanism* [147, 148], which effectively slows down the relaxation. The mechanism can be understood on the basis of the theoretical concept put forward by Prokof'ev and Stamp [76, 77, 149], according to which the dipolar and hyperfine fields dynamically change the distribution of the local field at each molecular site, so that the QTM processes are possible only when the externally applied field and the internal field satisfy the resonance conditions. In consequence, a hole appears in the field distribution of the tunneling probability, and the approach using the LZ model breaks down.

3.1.2 Application of the Landau-Zener QTM model to a Fe_8 molecule

Now I present numerical results obtained for the Fe_8 molecule of $S = 10$. Although the Fe_8 molecule is characterized by a much smaller energy barrier than the Mn_{12} molecule (~ 25 K for Fe_8 compared with ~ 67 K for Mn_{12} [57]), it seems more suitable for investigating the switching due to QTM, because it posses reasonably large transverse anisotropy terms. The anisotropy constants $D = 0.292$ K, $E = 0.046$ K and $C = -2.9 \times 10^{-5}$ K together with the tunnel splittings $\Delta_{-S,S-n}$ are adopted from Refs. [57, 144]. Finally, it is assumed that the temperature of the system is low enough so that thermally activated QTM processes [150–152] are suppressed.

The average value of the zth component of the SMM's spin, $\langle S_z\rangle$, in an external magnetic field increasing linearly in time is depicted in Fig. 3.4. The reversal of the molecule's spin due to the QTM can be observed as a characteristic sequence of steps occurring at the resonant fields where the tunneling processes are allowed, Fig. 3.3. The height of each step is determined by the field sweeping speed c, as well as by parameters

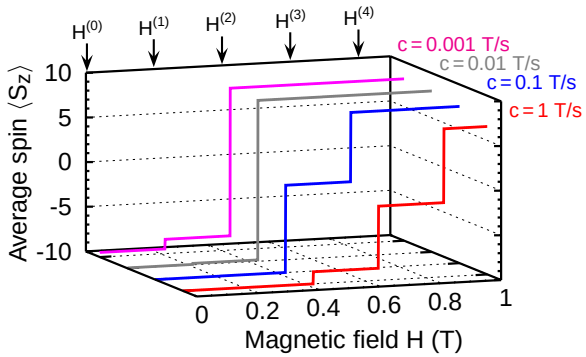

Figure 3.4: The average value of the SMM's spin, $\langle S_z \rangle$, as a function of an external magnetic field $H = -H_z$ (for $H > 0$) for various field sweeping speeds c in the absence of any other relaxation processes. Here, $H^{(n)} = Dn/(g\mu_B)$ for $n = 0, 1, 2, \ldots$ denotes resonant magnetic fields at which the QTM takes place. The parameters assumed for numerical calculations are typical of the Fe_8 molecule as described in the main text.

of $\mathcal{H}_{\rm rel}$, which influence the value of the tunnel splitting $\Delta_{m,m'}$. For small values of c the reversal begins at lower magnetic fields, and the depletion of the initial state $|-S\rangle$ takes place already after passing the third avoided level crossing region, Fig. 3.4. However, it should be noted that due to lack of any additional relaxation processes, deliberately excluded from the present discussion, the complete reversal of the SMM's spin is not possible, Fig. 3.3(c). For the complete reversal one needs any relaxation processes, either intrinsic ones or due to coupling to external leads, as wit will be discussed below.

3.2 QTM in a single-molecule magnet coupled to ferromagnetic reservoirs

As mentioned already in Section 2.1, SMMs are susceptible to interaction with their environment, which may result in additional spin relaxation effects. In the present section I consider how relaxation processes in SMMs modify the picture of the SMM's magnetic switching due to the QTM introduced in the previous subsection. More specifically, I focus primarily on the spin relaxation owing to coupling of a molecule with two reservoirs of spin polarized electrons, whereas the overall effect of other relaxation mechanisms is taken into account on a phenomenological level *via* an appropriate relaxation time.

3.2.1 Scattering of tunneling electrons on a single-molecule magnet's spin

Considered now a SMM inserted in an unbiased magnetic tunnel junction, Fig. 3.5(a). For simplicity, I restrict the considerations to the case of collinear (parallel or antiparallel) configurations of the leads' magnetic moments, with the magnetic easy axis of the molecule aligned with magnetic moments of the leads. Furthermore, it is assumed that an

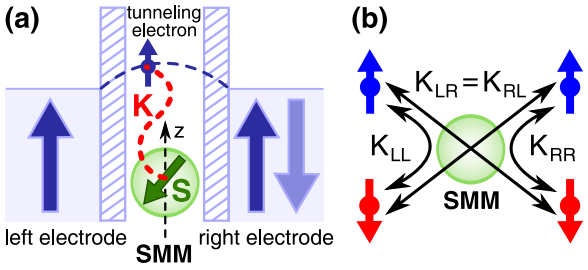

Figure 3.5: (a) Schema of a SMM embedded in a tunnel barrier for collinear (parallel or antiparallel) magnetic configuration of the leads' magnetizations. (b) Possible scattering paths due to exchange interaction of an electron with the SMM's spin with corresponding interaction constants indicated.

external time-dependent magnetic field is oriented in such a way that it provides a large longitudinal component along the magnetic easy axis of the molecule, and a significantly weaker transverse one. Finally, two additional assumption are made. First, the molecule stays electrically neutral, with the LUMO level unoccupied during the entire switching process. Second, the field does not affect the magnetic configuration of the leads.

Exchange interaction between electrons of both leads and the SMM can be conveniently described by means of the Appelbaum Hamiltonian [83, 146, 153, 154],

$$\begin{aligned}\mathcal{H}_{\mathrm{I}} &= \frac{1}{2}\sum_{qq'}\sum_{\mathbf{k}\mathbf{k}'\alpha\beta}\frac{K_{qq'}}{\sqrt{N_q N_{q'}}}\,\sigma_{\alpha\beta}\cdot\mathbf{S}\,a^{q\dagger}_{\mathbf{k}\alpha}a^{q'}_{\mathbf{k}'\beta} + \mathrm{H.c.}\\ &= \frac{1}{2}\sum_{qq'}\sum_{\mathbf{k}\mathbf{k}'}\frac{K_{qq'}}{\sqrt{N_q N_{q'}}}\left\{a^{q\dagger}_{\mathbf{k}\uparrow}a^{q'}_{\mathbf{k}'\downarrow}S_- + a^{q\dagger}_{\mathbf{k}\downarrow}a^{q'}_{\mathbf{k}'\uparrow}S_+ + \left[a^{q\dagger}_{\mathbf{k}\uparrow}a^{q'}_{\mathbf{k}'\uparrow} - a^{q\dagger}_{\mathbf{k}\downarrow}a^{q'}_{\mathbf{k}'\downarrow}\right]S_z\right\} + \mathrm{H.c.}\end{aligned} \tag{3.6}$$

As within the scope of interest is only the unbiased situation, the direct tunneling between the electrodes (without interaction with the SMM) has been omitted. The exchange interaction is characterized by the parameters $K_{qq'}$, which are assumed to be independent of energy and polarization of the leads. Although in a general case it is possible that $K_{LL} \neq K_{RR} \neq K_{LR} = K_{RL}$, Fig. 3.5(b), in the following only the symmetrical situation ($K_{LL} = K_{RR} = K_{LR} = K_{RL} \equiv K$) is taken under consideration. Finally, owing to proper normalization with respect to the number of elementary cells N_q in the qth electrode, K is also independent of the electrodes' size.

According to the Hamiltonian (3.6), tunneling electrons can flip their spins and hence add/subtract some amount of angular momentum to/from the molecule. As a consequence, transitions between neighboring molecular magnetic states become allowed. The total transition rate,

$$\gamma^{\pm}_m = \sum_{qq'=\mathrm{L,R}}\gamma^{qq'\pm}_m, \tag{3.7}$$

at which the molecule's spin is changed from the state $|m\rangle$ to the nearest adjacent upper (lower) state $|m \pm 1\rangle$, is the sum of all possible rates $\gamma^{qq'\pm}_m$ that correspond to transition

of electrons between the leads q and q'. Such transition rates can be obtained from the Fermi golden rule [146],

$$\gamma_m^{qq'\pm} = \sum_{\mathbf{k}\alpha\in q}\sum_{\mathbf{k}'\beta\in q'} W_{|q'\mathbf{k}'\beta,m\pm1\rangle}^{|q\mathbf{k}\alpha,m\rangle} f_{\mathrm{FD}}(\varepsilon_{\mathbf{k}\alpha}^{q})\Big[1-f_{\mathrm{FD}}(\varepsilon_{\mathbf{k}'\beta}^{q'})\Big], \tag{3.8}$$

where $f_{\mathrm{FD}}(x)$ is the Fermi-Dirac distribution function. The probability of transition from the initial state $|q\mathbf{k}\alpha,m\rangle \equiv |i\rangle$ of the whole system to the final one $|q'\mathbf{k}'\beta,m\pm1\rangle \equiv |j\rangle$ is given by

$$W_{|j\rangle}^{|i\rangle} = \frac{2\pi}{\hbar}\big|\langle j|\mathcal{H}_{\mathrm{I}}|i\rangle\big|^2\delta(E_j-E_i), \tag{3.9}$$

with $E_i = \varepsilon_{\mathbf{k}\alpha}^{q} + \epsilon_m$ and $\epsilon_m \equiv \epsilon(S_t^z = S;0,m)$ [see Eq. (2.19)]. Energy E_j of the final state has a similar form.

The final expression for the transition rates $\gamma_m^{\pm}$ takes the following form

$$\gamma_m^{\pm} = \frac{2\pi}{\hbar}|K|^2 A_{\pm}(m)\Delta E_{\pm} f_{\mathrm{BE}}(\Delta E_{\pm})\sum_{qq'} D_{\downarrow}^{q} D_{\uparrow}^{q'}. \tag{3.10}$$

Here, D_σ^q is the DOS at the Fermi level in the qth electrode for spin σ, and $A_\pm = S(S+1)-m(m\pm1)$. Moreover, $\Delta E_\pm = \epsilon_{m\pm1}-\epsilon_m = (\mp2m-1)D \mp g\mu_{\mathrm{B}}H$, whereas $f_{\mathrm{BE}}(x)$ denotes the Bose-Einstein distribution function.

One should note that Eq. (3.10) is generally applicable to systems with electrodes made out of different ferromagnetic materials. For simplicity reasons, I assume that both the leads have the same average density of states per spin, $(D_+^L+D_-^L)/2 = (D_+^R+D_-^R)/2 = \widetilde{D}$, although they may differ in spin polarizations. This allows us to rewrite Eq. (3.10) into a more compact form,

$$\gamma_m^{\pm} = \frac{2\pi}{\hbar}|K|^2\widetilde{D}^2\mathcal{C}_{\mathrm{P(AP)}}A_{\pm}(m)\Delta E_{\pm} f_{\mathrm{BE}}(\Delta E_{\pm}). \tag{3.11}$$

The parameter $\mathcal{C}_{\mathrm{P(AP)}} = 4-(P_L \pm P_R)^2$ represents the influence of the magnetic configuration of the leads, either *parallel* (P) or *antiparallel* (AP).

In addition to the relaxation processes stemming from coupling of the molecule to metallic leads, there are also *intrinsic spin-relaxation processes* that influence QTM as well. It is assumed that the resultant effect of all intrinsic processes is fully described by a single phenomenological relaxation time τ_{rel}. Furthermore, allowing only transitions from a given state $|m\rangle$ to its nearest neighbor states $|m\pm1\rangle$ to occur, the relaxation rate $\gamma_m^{R\pm}$ can be written as follows

$$\gamma_m^{R\pm} = \frac{1}{\tau_{\mathrm{rel}}} \times \frac{\exp\left[\frac{1}{2}(\epsilon_m-\epsilon_{m\pm1})\beta\right]}{2\cosh\left[\frac{1}{2}(\epsilon_m-\epsilon_{m\pm1})\beta\right]}, \tag{3.12}$$

where $\beta = (k_{\mathrm{B}}T)^{-1}$, k_{B} is the Boltzmann constant and T denotes the temperature of the system. The Boltzmann factor in Eq. (3.12) assures that the additional spin relaxation

processes drive the molecule's spin to a state of lower energy.

The presence of additional relaxation processes in the system means that now all molecular spin states $|m\rangle$ can be involved in the reversal of the SMM's spin, in contrast to the pure-QTM switching where only the states between which tunneling takes place can be realized. Moreover, transitions between neighboring molecular spin states due to the exchange interaction with the leads depend on an external magnetic field H, Eq. (3.10). As a result, the average value of the zth component of the SMM's spin $\langle S_z\rangle$ changes not only at the resonant magnetic fields, where the QTM is observed, Fig. 3.4, but also for intermediate values of the field. To calculate the average

$$\langle S_z\rangle = \sum_m m P_m, \tag{3.13}$$

one has to determine the probabilities P_m of finding the SMM in all possible spin states $|m\rangle$. These probabilities can be found from the relevant set of rate equations, solved separately for each range of magnetic fields between two consecutive resonant fields $H^{(M)}$ and $H^{(M+1)}$ $(M = 0, 1, 2, \ldots)$,

$$\begin{cases} c\dot{P}^{(M)}_{-S} = -\left[\gamma^{+}_{-S} + \gamma^{R+}_{-S}\right] P^{(M)}_{-S} + \left[\gamma^{-}_{-S+1} + \gamma^{R-}_{-S+1}\right] P^{(M)}_{-S+1}, \\ c\dot{P}^{(M)}_{m} = -\left[\gamma^{-}_{m} + \gamma^{+}_{m} + \gamma^{R-}_{m} + \gamma^{R+}_{m}\right] P^{(M)}_{m} \\ \qquad\qquad + \left[\gamma^{+}_{m-1} + \gamma^{R+}_{m-1}\right] P^{(M)}_{m-1} + \left[\gamma^{-}_{m+1} + \gamma^{R-}_{m+1}\right] P^{(M)}_{m+1}, \\ c\dot{P}^{(M)}_{S} = -\left[\gamma^{-}_{S} + \gamma^{R-}_{S}\right] P^{(M)}_{S} + \left[\gamma^{+}_{S-1} + \gamma^{R+}_{S-1}\right] P^{(M)}_{S-1}, \end{cases} \tag{3.14}$$

for $-S+1 \leqslant m \leqslant S-1$, and $\dot{P}$ defined as $\dot{P} \equiv \mathrm{d}P/\mathrm{d}H$. The superscript '$(M)$' means that the probabilities P_m are calculated for the field range $H^{(M)} \leqslant H \leqslant H^{(M+1)}$.

Equations (3.14) can be substantially simplified for $k_B T \ll D$, when the molecule spin is trapped in the spin state of the lowest energy and no thermal excitations to higher energy states are allowed. Furthermore, there are several different time scales present in the system. These are set by the speed c at which the magnetic field is increased, the relaxation rates due to interaction with the electrodes, and the transition rates due to intrinsic-spin relaxation, with the first scale being significantly longer than the other two. One should also bear in mind that the transition rates $\gamma^{\pm}_m$ depend on magnetic field and for the left branch of the parabolic energy spectrum, Fig. 3.3, $\gamma^{+}_m \approx 0$, whereas for the right one $\gamma^{-}_m \approx 0$. In consequence, if initially only the state $|-S\rangle$ is populated, the only possible way the molecule can escape from it is by means of the QTM, and Eqs. (3.14) can be therefore effectively reduced to

$$\begin{cases} c\dot{P}^{(M)}_{S-M} = -\left[\gamma^{+}_{S-M} + \gamma^{R+}_{S-M}\right] P^{(M)}_{S-M} \\ c\dot{P}^{(M)}_{m} = -\left[\gamma^{+}_{m} + \gamma^{R+}_{m}\right] P^{(M)}_{m} + \left[\gamma^{+}_{m-1} + \gamma^{R+}_{m-1}\right] P^{(M)}_{m-1}, \\ c\dot{P}^{(M)}_{S} = \left[\gamma^{+}_{S-1} + \gamma^{R+}_{S-1}\right] P^{(M)}_{S-1}, \end{cases} \tag{3.15}$$

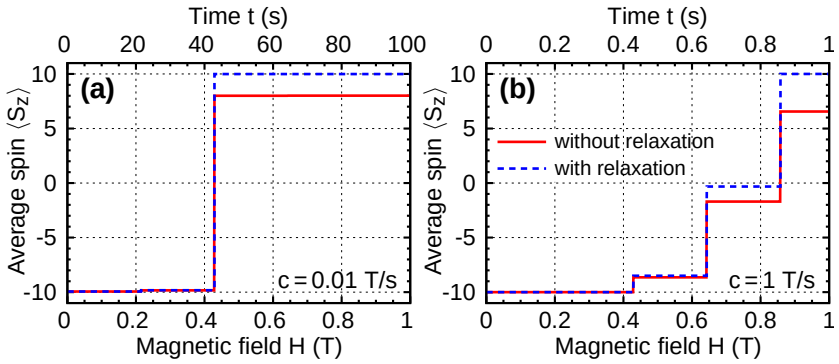

Figure 3.6: The average value of the SMM's spin, $\langle S_z \rangle$, as a function of an external magnetic field H in the case of the SMM coupled to electrodes (dashed lines), as well as for the SMM decoupled from the leads (solid lines). In both cases the intrinsic spin relaxation is neglected. The magnetic moments of the electrodes are in the *parallel* configuration and $P_L = P_R = 0.5$, whereas the other parameters are $K = 1$ meV, $\widetilde{D} = 0.5$ eV^{-1} per elementary unit, and $\tau_{\rm rel} = \infty$. The parameters assumed are typical for the Fe_8 molecule.

for $m \in \langle S - M + 1, S - 1 \rangle$.

The boundary conditions for the probabilities given in Eqs. (3.15) at the resonant magnetic field $H^{(M)}$ are

$$\begin{cases} P_{-S}^{(M)}\big(H^{(M)}\big) = 1 - \sum_{n=0}^{M} P_{-S,S-n}^{\rm LZ}, \\ P_{S-M}^{(M)}\big(H^{(M)}\big) = P_{-S,S-M}^{\rm LZ}, \\ P_{m}^{(M)}\big(H^{(M)}\big) = P_{m}^{(M-1)}\big(H^{(M)}\big), \end{cases} \tag{3.16}$$

for $m \in \langle S - M + 1, S \rangle$, and probabilities of finding the molecule in other states are equal to zero. By solving Eqs. (3.15) for the above boundary conditions, the mean value of the SMM's spin as a function of a magnetic field H is given by the formula

$$\Big\langle S_z^{(M)}(H) \Big\rangle = -S\left(1 - \sum_{n=0}^{M} P_{-S,S-n}^{\rm LZ}\right) + \sum_{n=0}^{M} (S-n) P_{S-n}^{(M)}(H), \tag{3.17}$$

where the first term does not depend on the field and its value is determined only by the Landau-Zener probability $P_{-S,S-n}^{\rm LZ}$, Eq. (3.4), at the resonant magnetic field $H^{(M)}$.

3.2.2 QTM in a Fe_8 molecule attached to ferromagnetic electrodes

Numerical results shown below have been obtained for the Fe_8 molecule, similarly as in the previous section. It has been assumed that the exchange interaction parameter is $K = 1$ meV, whereas the total DOS at the Fermi level in the leads is $\widetilde{D} = 0.5$ eV^{-1} (per elementary unit). The temperature of the system is assumed to be $T = 0.01$ K, which is below the blocking temperature $T_{\rm B} = 0.36$ K of the Fe_8 molecule.

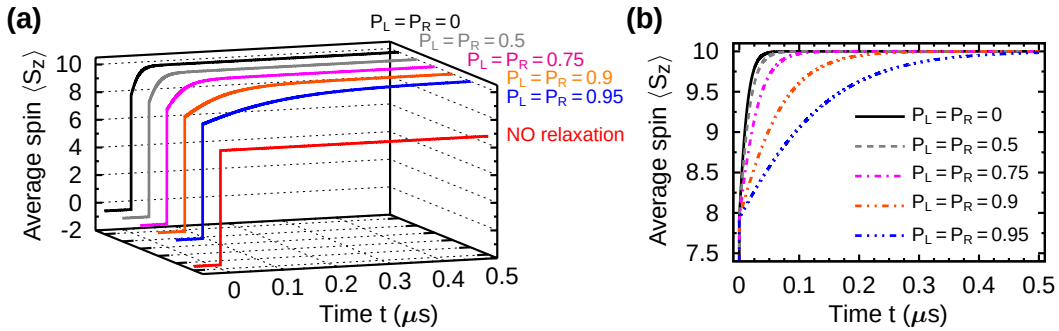

Figure 3.7: Dynamics of the relaxation process due to exchange coupling between the SMM and electrons in the leads, which the system undergoes after tunneling between the states $|-10\rangle$ and $|6\rangle$ at the resonant field $H^{(4)} = 0.858$ T, calculated in the *parallel* magnetic configuration for various values of the polarization parameters. The parameters assumed are typical for the Fe_8 molecule.

The average value of the z component of the SMM's spin in increasing external magnetic field with additional relaxation processes following from interaction of the SMM with ferromagnetic reservoirs is shown in Fig. 3.6 and compared with the case of QTM in the molecule detached from the leads (intrinsic spin relaxation is neglected in both cases, i.e. $\tau_{\rm rel} = \infty$). It is clear that the relaxation processes are indispensable to observe the full magnetic switching of a SMM. The dominating time scale, which also establishes the duration of the molecule's spin reversal, is set by the rate c at which the field H is augmented. Since for the parameters used in numerical calculations typical values of the transition times $1/\gamma_m^+$ are in the range of 10^{-9} to 10^{-6} s, the steps in Fig. 3.6 are very sharp.

To analyze details of the relaxation process, the time-evolution of the SMM's spin induced by the interaction of the molecule with electrodes after passing the resonant field $H^{(4)} = 0.858$ T [the third step in Fig. 3.6(b)] is presented in Fig. 3.7. It can be seen that in the parallel magnetic configuration of the electrodes, the larger polarization parameters of the leads, the longer is the time after which the state of the SMM's spin is stabilized. I call this characteristic time scale, the *stabilization time* $t_{\rm st}$.[2] According to Eq. (3.4), in the limiting case of $P_L = P_R = 1$, no relaxation should be visible because $\gamma_m^{\pm} = 0$ and consequently $t_{\rm st} = \infty$.

The stabilization time $t_{\rm st}$ is mainly determined by the magnetic configuration of the system. The dependence of $t_{\rm st}$ on the polarization parameters of the electrodes in the parallel and antiparallel configuration of the electrodes' magnetic moments is depicted in Fig. 3.8. The relaxation is most effective when both the electrodes are nonmagnetic, whereas in the case of magnetic leads the efficiency of the stabilization process relies on the relation between polarizations of the left and the right electrodes. In the parallel configuration the relaxation is fast only for small values of the parameters P_L and P_R,

[2]From a computational point of view, I define the stabilization time $t_{\rm st}$ as a time after which the average value of zth component of the molecule's spin reaches 99.999% of its stable value.

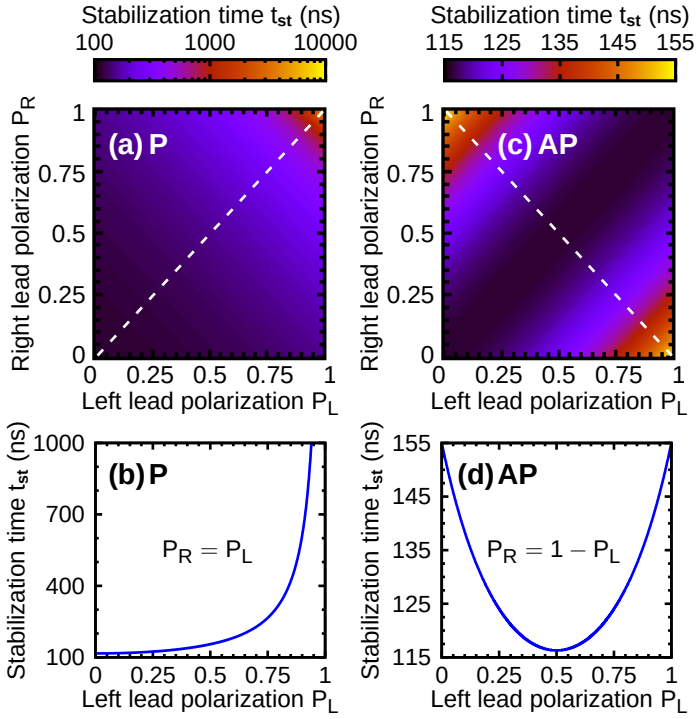

Figure 3.8: The dependence of the stabilization time $t_{\rm st}$ at the resonant field $H^{(4)} = 0.858$ T on the polarization parameters of the electrodes for the *parallel* (a) and *antiparallel* (c) magnetic configuration. The bottom panel shows cross sections of the plots above along the dashed lines. The other parameters as in Fig. 3.6.

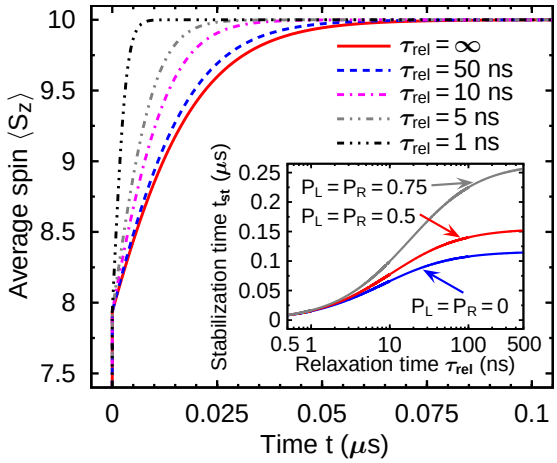

Figure 3.9: The effect of intrinsic-spin relaxation processes on the relaxation of the SMM's spin after the QTM at the resonant field $H^{(4)} = 0.858$ T. The electrodes are in the *parallel* magnetic configuration and $P_L = P_R = 0.5$. The inset presents how the stabilization time $t_{\rm st}$ depends on the intrinsic relaxation time $\tau_{\rm rel}$ for different values of the leads' polarization parameters. The other parameters as in Fig. 3.6.

while for the larger values the process becomes significantly decelerated, Fig. 3.8(a)-(b). On the other hand, in the antiparallel configuration the SMM's spin gets stabilized as fast as in the nonmagnetic case providing that $P_L \approx P_R$, and the process slows down only if $P_L \gg P_R$ (or $P_L \ll P_R$), Fig. 3.8(c)-(d).

Inclusion of additional intrinsic spin relaxation processes does not modify the results qualitatively, Fig. 3.9. Intrinsic spin relaxation can be neglected for $\tau_{\mathrm{rel}} \gg 1/\gamma_m^{\pm}$, as the relaxation due to the exchange interaction between the molecule's spin and spin-polarized reservoirs is then the dominating relaxation mechanism. In the opposite case, however, it must be taken into account.

CHAPTER 4

Dynamical aspects of transport through single-molecule magnets: current-induced magnetic switching

An external magnetic field is only one of possible means of manipulating the SMM's spin. However, if one intends to make use of a SMM as a part of a larger electronic circuit, the presence of the field may lead to undesired effects. To avoid any unnecessary complications that could occur in such a case, it would be an ideal solution if one could control the state of the SMM's spin using some generic properties of the system. It transpires that one of the most promising ways to fulfill such a requirement is to employ a spin-polarized current.

With establishing the physical origin of the GMR phenomenon it became clear that effects stemming from interaction between the electron spin and the magnetic moment of a medium through which an electron propagates bear a true potential for various applications in electronic (or spintronic, as I shall call them) circuits. Since the mechanism underlying the GMR is generally the current spin-filtering due to spin-dependent scattering of conduction electrons [155, 156], it is interesting to ask what the result of the reverse process could be, or in other words, how a spin-polarized current would affect the magnetic state of a medium. It has been predicted theoretically [157–161] that when a spin-polarized electric current passes through a nanometer-scale magnetic medium, the magnetic moment of the medium is effectively subjected to a torque resulting from the transfer of angular momentum from current to the magnetic medium. In consequence, for sufficiently large currents the *spin-transfer torque* can lead to the reversal and precession of the magnetization. In the case of the magnetization reversal due to flow of a spin-polarized current a term *'current-induced magnetic switching'* (CIMS) has been coined.

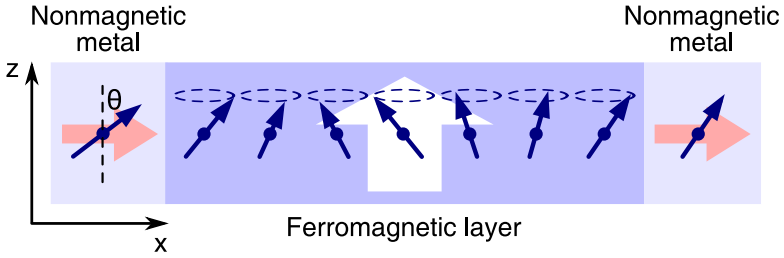

Figure 4.1: Schematic depiction of the behavior of a single electron travelling through a magnetic layer. It is assumed that the electron spin approaching the layer is polarized at the angle θ with respect to the magnetic moment of the layer, and θ lies in the xz plane. Moving in the layer the electrons spin precesses owing to the exchange field of the magnet. The idea adopted from Ref. [175].

The ingenious idea of applying a spin-polarized current to manipulate the magnetic state of a system has found experimental conformation in a number of different systems including point-contact junctions [162,163], nanowires [164], nanopillars [165–167], or individual superparamagnetic islands [168]. Furthermore, it turned out that a spin-transfer torque exerted on a domain wall results in displacement of the wall [169–172]. Recently, a group at IBM research division has developed a novel concept of nonvolatile memory device, so called the *magnetic domain-wall racetrack memory*, which utilizes as a key ingredient the possibility of controlling motion of a series of domain walls along a magnetic nanowire by pulses of a spin-polarized current [173,174].

The fundamental mechanism behind the spin-transfer phenomenon can be easily understood within a simplified semiclassical model of a single electron traversing a nonmagnetic metal towards a ferromagnetic layer[1] [175–178]. For this purpose let's assume that the spin of an electron moving along the x axis forms an angle θ with the z axis parallel to the magnetic moment of the layer, Fig. 4.1. When the electron encounters the interface between the nonmagnetic material and the magnet this will behave as a spin-filter, because due to a mismatch of density of states for spin-up and spin-down electrons on both sides of the interface the transmission probability is expected to be higher for majority (here spin-up) electrons. In consequence, after crossing the interface the electron spin should be tilted at smaller angle θ.

Next, travelling further through the magnet the electron experiences a strong exchange interaction with the magnet's moment, and it also starts precessing around the direction of the exchange field, which is parallel to the z axis. One should note there is no external magnetic field applied. Since angular momentum in the system need to be conserved, the moment of the magnet in principle should also precess around the electron spin. Nevertheless, taking into account the fact that the magnetic moment of the layer is much larger than that of an individual electron, the precessional motion of the former one can

[1] The following discussion is largely based on the picture presented in Ref. [175], where in a similarly intuitive way the case of spin-polarized transport through two magnetic layers, like in a spin-valve, is also considered.

be omitted for the sake of the present discussion. Such precession of the electron spin in general can be extremely rapid, so that the electron may undergo several precessions before it leaves the layer. Now, contrary to the zth component of the electron spin which should not be changed due to the precessional motion, final values of the xth and yth spin components will depend on the phase of the spin precession with which an electron leaves the magnetic layer.

Apparently, in a real system one deals not only with many electrons simultaneously moving through the layer, but also it has to be considered that they travel with various energies and arrive at the interface with slightly different angles θ. As a result, as long as the thickness of the magnetic layer significantly exceeds the precession length, for electrons exiting the layer one can anticipate a uniform directional distribution of spin components in the xy plane, i.e. there should be no perpendicular component of the total angular momentum originating from summing spins of all the electrons. It means that only the zth component (parallel to the magnetic moment of the layer) will not be equal to zero.

The question remains where the transverse component of electrons' angular momentum has disappeared. The key to the riddle lies in the conservation of angular momentum by the system. The missing transverse component of incoming spin angular momentum must have been transferred from the electrical current to the magnetic layer. Moreover, if the magnet responds as a single domain, then the entire magnetic moment of the layer can be expected to rotate towards the direction of the incident electrons' spin polarization. Thus the mechanism discussed above can be effectively viewed as if the spin-polarized current was exerting a torque on the moment of the magnetic layer. One should bear in mind, however, that the actual nature of the mechanism is far more complicated, as various additional scattering processes can occur as well.

With regard to possible applications of spin-transfer torques due to the flow of a spin-polarized current an important issue is the dynamics of the magnetization reversal process. The standard classical procedure allowing one to study time evolution of a magnetization $\mathbf{M}$ in the presence of real and fictitious fields is the macroscopic *Landau-Lifshitz-Gilbert equation* (LLG) [127, 128]. It has been shown by Slonczewski [157] that without considering the detailed microscopic mechanism governing the spin-transfer torque, the effect of the spin angular momentum transfer can be captured by introducing an additional term into the LLG equation [178, 179],

$$\frac{\mathrm{d}\mathbf{m}}{\mathrm{d}t} = -|\gamma|\mathbf{m}\times\mathbf{H}_{\mathrm{eff}} + \alpha\mathbf{m}\times\frac{\mathrm{d}\mathbf{m}}{\mathrm{d}t} + |\gamma|a_J\mathbf{m}\times(\mathbf{m}\times\hat{\mathbf{n}}_{\mathrm{s}}). \tag{4.1}$$

Here, $\mathbf{m}\equiv\mathbf{M}/M_{\mathrm{s}}$ is the magnetization vector normalized to its saturation value, whereas γ stands for the gyromagnetic ratio. The first term of Eq. (4.1) corresponds to the torque induced by the effective magnetic field $\mathbf{H}_{\mathrm{eff}}$, which generally can include the external field, the exchange field, the anisotropy field, the demagnetization field, and the random thermal field. The second term is the Gilbert damping term with α denoting the relevant damping coefficient. Finally, the last term proportional to an effective parameter a_J

represents the transverse component of the spin-transfer torque, where $\hat{\mathbf{n}}_s$ is an unit vector pointing the direction of spin polarization of the incoming current. Although originally only the *transverse* (or *in-plane*) component of the torque has been deduced, there can also be present the *out-of-plane* component [161]. It is worth noting that a_J depends mainly on the spin-polarization factor of a transport current and the current density J, but it also takes into account the angular dependence of the efficiency of the spin-angular momentum transfer between the current and the magnetization of the layer.

Returning to the main topic, since electronic transport through a single SMM is feasible, it seems just a matter of time before further advances in nanotechnology allow for changing magnetic state of the molecule by a spin-polarized current. In this context it seems legitimate to ask how the physical mechanism underlying CIMS would work in the case of a SMM, and, even more important, what theoretical tool could be used to study the dynamics of the SMM's spin reversal. As discussed in Chapter 2, SMMs with the approximately uniaxial type anisotropy are described in this thesis by a fully quantized model, i.e. the state of the molecule is completely described by there quantum numbers: the total spin S_t, the occupation number of the LUMO level n, and the zth component of the total spin S_t^z. It is thus quite obvious that one cannot apply here a semiclassical macrospin model employing the LLG equation, but a model considering the typical features of SMMs, such as a well defined spin value and a discrete magnetic spectrum, must be developed. Finally, although it seems a compelling idea to switch the magnetic state of a SMM with a spin-polarized current, experiments investigating the spin-transfer torque carried out so far indicate that rather high current density is required to exert a measurable effect on the magnetization [176]. It means that due to small cross-sectional dimensions of a device involving a SMM, performing a successful experiment with the SMM's spin reversal may turn out to be extremely challenging, if possible at all.

4.1 The mechanism of current-induced magnetic switching in single-molecule magnets

To address the issue of the CIMS of the SMM's spin, I consider the model of a molecule weakly coupled to metallic ferromagnetic leads, as discussed in Section 2.2. For simplicity the collinear configuration of the leads' spin moments is assumed, whereas the easy axis of the molecule can now be tilted away in the plane $x'z'$, forming an arbitrary angle φ, Fig. 2.3. Furthermore, contrary to the model considered in the preceding chapter, the assumption is made that a finite bias voltage and no external magnetic field are applied to the system.

Depending on the bias voltage V applied between electrodes one can distinguish two regimes of electronic transport through the molecule, Fig. 4.2(a). Let's analyze first the situation of sufficiently large voltages, when the transport takes place owing to tunneling between the electrodes and the LUMO level of the SMM. The CIMS can then appear as a consequence of exchange coupling between the spin of an electron occupying the LUMO level and the SMM's spin. The essential mechanism of the CIMS in SMMs rely on the

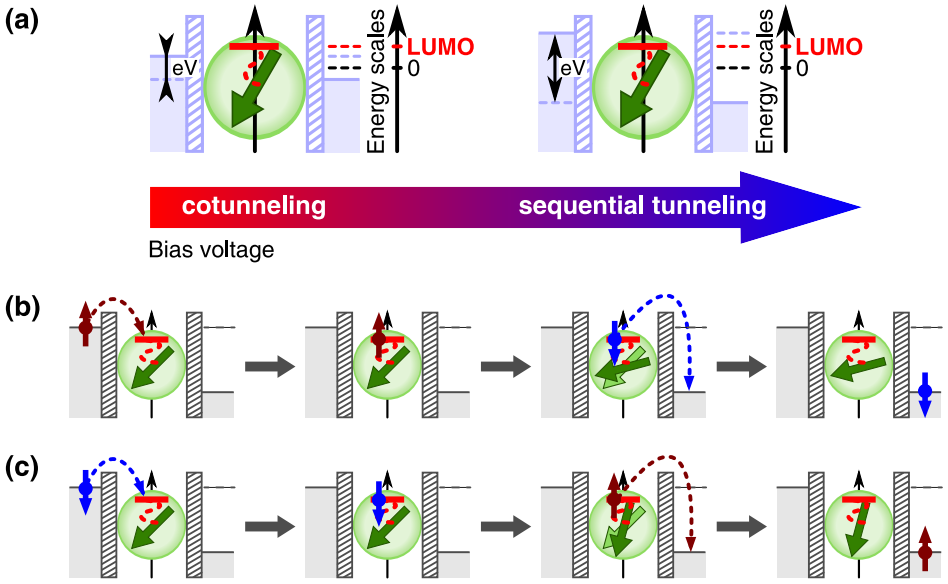

Figure 4.2: (a) The change of energy scales when moving from the *sequential tunneling* regime to the *cotunneling* regime. Schematics below represent the mechanism of the CIMS in the sequential tunneling regime leading to increasing (b) and decreasing (c) of the zth component of SMM's spin.

idea that electrons tunneling through the LUMO level can flip their spin orientations due to exchange interaction with the molecule's spin, which in turn corresponds to angular momentum transfer between conduction electrons and the molecule, Fig. 4.2(b)-(c). The change in the magnetic state of the molecule is thus stimulated by *inelastic* tunneling processes, as it will be discussed in further part of the present chapter as well as in the next chapter.

Such a voltage range within which electrons are energetically allowed to enter the LUMO level is referred to as a *sequential tunneling* (ST) regime. In the opposite limit of small voltages, on the other hand, electrons don't possess enough energy to overcome the tunneling barrier, and hence to occupy the LUMO level. In this case, known also as the *Coulomb blockade* (CB) region, the sequential tunneling processes are suppressed. Nevertheless, current still can flow due to higher order processes [so-called *cotunneling* (CT) regime] and the reversal of the SMM's spin can be observed, for the electrons virtually entering the LUMO can couple *via* exchange coupling to the molecule's spin. It should be noted that although higher order processes play a leading role only in the CB regime, they are active for all range of transport voltages. Furthermore, one should be careful when investigating the intermediate region where both sequential and cotunneling currents are comparable. Since the aim of the current chapter is to capture main dynamical features of the CIMS of SMMs, I use the simplest available theoretical tools, which are the standard perturbation approach and the master equation. Consequently, the approach allows me only to study separately either the cotunneling or sequential tunneling regime. More

universal theoretical approach employing the real-time diagrammatic technique, which permits considering both the regimes at the same time and therefore to study spin effects that can arise owing to the interplay of sequential tunneling and cotunneling of electrons, will be used in the next chapter.

In the following sections I will analyze the CIMS of the SMM's spin separately in the sequential tunneling (Section 4.2) and cotunneling (Section 4.3) regimes. In order to study quantitatively the switching process, the average value of the zth component of the total molecule's spin is considered,

$$\langle S_t^z \rangle = \sum_{n,m} \sum_{S_t} m P_{|S_t;n,m\rangle}, \tag{4.2}$$

and also current flowing through the system. For the sake of simplicity, from this moment I adhere to the convention that the positive bias corresponds to electrons flowing from left to right ($e > 0$). Furthermore, to calculate the quantities in question, one has to first determine the rates $\gamma_{q(qq')}^{|S_t;n,m\rangle|S_t';n',m'\rangle}$ describing transitions between the molecular spin states $|S_t;n,m\rangle$ and $|S_t';n',m'\rangle$ for sequential tunneling (cotunneling) processes. The probabilities $P_{|S_t;n,m\rangle}$ of finding the SMM in all accessible molecular states $|S_t;n,m\rangle$ are in turn obtained from the set of relevant master equations [103, 180, 181].

4.2 Current-induced magnetic switching in the sequential tunneling regime

In this section I consider the case when electrons possess enough energy to tunnel freely between electrodes and the LUMO level. The main idea is to develop an analytical scheme allowing to analyze the time evolution of the molecule's spin, and to be more precise the zth component of the spin, when a constant bias voltage is applied to the system.

4.2.1 The tunneling current and the average spin

The total current I flowing through the molecule in the sequential transport regime can be calculated as $I = (I_L - I_R)/2$, where I_q ($q = L, R$) is the *current* flowing from the qth lead to the molecule,

$$I_q = e \sum_{n,m} \sum_{n',m'} \sum_{S_t,S_t'} (n' - n) \gamma_q^{|S_t;n,m\rangle|S_t';n',m'\rangle} P_{|S_t;n,m\rangle}. \tag{4.3}$$

In order to keep the notation transparent, in the present section I assume $|S_t^\alpha; n_\alpha, m_\alpha\rangle \equiv |\alpha\rangle$, which also implies that $\sum_\alpha \equiv \sum_{m_\alpha} \sum_{n_\alpha} \sum_{S_t^\alpha}$.

In the second order (Fermi golden rule), the general formula for transition rates $\gamma_q^{|\alpha\rangle|\beta\rangle}$ between the states $|\alpha\rangle$ and $|\beta\rangle$ takes the form [103, 104]

$$\gamma_q^{|\alpha\rangle|\beta\rangle} = \sum_{\mathbf{k},\sigma\in q} \left\{ W_{|\beta\rangle}^{\mathbf{k}\sigma|\alpha\rangle} f_{\mathrm{FD}}(\varepsilon_{\mathbf{k}\sigma}^q) + W_{\mathbf{k}\sigma|\beta\rangle}^{|\alpha\rangle} \left[1 - f_{\mathrm{FD}}(\varepsilon_{\mathbf{k}\sigma}^q)\right] \right\}. \tag{4.4}$$

In the above equation, the first term represents the charge transfer from the qth lead to the molecule, whereas the second term stands for tunneling of electrons in the opposite direction. Furthermore, $W_f^i = (2\pi/\hbar)\big|\langle f|\mathcal{H}_{\rm tun}|i\rangle\big|^2\delta(E_f - E_i)$ is the rate of transitions from an initial state $|i\rangle$ to the final one $|f\rangle$, with $E_{i(f)}$ denoting the relevant energies. Replacing the summation with respect to a wave vector $\mathbf{k}$ by integration in Eq. (4.4), one obtains

$$\begin{aligned}\gamma_q^{|\alpha\rangle|\beta\rangle} = \sum_\sigma \frac{\Gamma_\sigma^q}{\hbar}\Bigg\{&\Big[\cos^2\frac{\varphi}{2}\left|C_{\alpha\beta}^{\sigma}\right|^2 + \sin^2\frac{\varphi}{2}\left|C_{\alpha\beta}^{\bar\sigma}\right|^2 - \sin\varphi\,\mathrm{Re}\big[C_{\alpha\beta}^{\sigma}C_{\alpha\beta}^{\bar\sigma *}\big]\Big] f_{\rm FD}\big(\epsilon_{\beta\alpha}-\mu_q\big)\\ &+\Big[\cos^2\frac{\varphi}{2}\left|C_{\beta\alpha}^{\sigma}\right|^2 + \sin^2\frac{\varphi}{2}\left|C_{\beta\alpha}^{\bar\sigma}\right|^2 - \sin\varphi\,\mathrm{Re}\big[C_{\beta\alpha}^{\sigma}C_{\beta\alpha}^{\bar\sigma *}\big]\Big]\\ &\times\Big[1 - f_{\rm FD}\big(\epsilon_{\alpha\beta}-\mu_q\big)\Big]\Bigg\},\end{aligned} \tag{4.5}$$

where $\epsilon_{\beta\alpha} = \epsilon_{|\beta\rangle} - \epsilon_{|\alpha\rangle}$ [see Eqs. (2.19)-(2.22)], and μ_q describes the electrochemical potential of the qth electrode. Using the results of Section 2.4, the nonzero coefficients $C_{\alpha\beta}^{\sigma} \equiv \langle\beta|c_\sigma|\alpha\rangle$ can be stated explicitly as follows

$$\begin{cases} C^{\sigma}_{|S-1/2;1,m\rangle|S;0,m'\rangle} = \mathbb{A}^{\mp}_{m}\delta_{\sigma\downarrow}\delta_{m',m+1/2} + \mathbb{B}^{\mp}_{m}\delta_{\sigma\uparrow}\delta_{m',m-1/2},\\ C^{\sigma}_{|S+1/2;1,m\rangle|S;0,m'\rangle} = \mathbb{A}^{\pm}_{m}\delta_{\sigma\downarrow}\delta_{m',m+1/2} + \mathbb{B}^{\pm}_{m}\delta_{\sigma\uparrow}\delta_{m',m-1/2},\\ C^{\sigma}_{|S;2,m\rangle|S-1/2;1,m'\rangle} = \mathbb{A}^{\mp}_{m'}\delta_{\sigma\uparrow}\delta_{m'+1/2,m} + \mathbb{B}^{\mp}_{m'}\delta_{\sigma\downarrow}\delta_{m'-1/2,m},\\ C^{\sigma}_{|S;2,m\rangle|S+1/2;1,m'\rangle} = \mathbb{A}^{\pm}_{m'}\delta_{\sigma\uparrow}\delta_{m'+1/2,m} + \mathbb{B}^{\pm}_{m'}\delta_{\sigma\downarrow}\delta_{m'-1/2,m}.\end{cases} \tag{4.6}$$

Now, taking into account the formulae above one can arrive at the conclusion that, owing to presence of the delta functions with respect to a spin σ and the spin number m, terms in Eq. (4.5) such as $\mathrm{Re}\big[C_{\alpha\beta}^{\sigma}C_{\alpha\beta}^{\bar\sigma *}\big]$ are equal to zero. Noting additionally that $1 - f_{\rm FD}(x) = f_{\rm FD}(-x)$, the ultimate expression for the transition rates is given as

$$\begin{aligned}\gamma_q^{|\alpha\rangle|\beta\rangle} = \sum_\sigma \frac{\Gamma_\sigma^q}{\hbar}\Bigg\{&\Big[\cos^2\frac{\varphi}{2}\left|C_{\alpha\beta}^{\sigma}\right|^2 + \sin^2\frac{\varphi}{2}\left|C_{\alpha\beta}^{\bar\sigma}\right|^2\Big] f_{\rm FD}\big(\epsilon_{\beta\alpha}-\mu_q\big)\\ &+\Big[\cos^2\frac{\varphi}{2}\left|C_{\beta\alpha}^{\sigma}\right|^2 + \sin^2\frac{\varphi}{2}\left|C_{\beta\alpha}^{\bar\sigma}\right|^2\Big] f_{\rm FD}\big(\epsilon_{\beta\alpha}+\mu_q\big)\Bigg\}.\end{aligned} \tag{4.7}$$

The coefficients $C_{\alpha\beta}^{\sigma} \equiv \langle\beta|c_\sigma|\alpha\rangle$ constitute therefore basic *selection rules* that govern transitions between molecular states, and hence they define the physical processes behind the CIMS of the SMM's spin. These selection rules state that tunneling of an individual electron between the molecule and leads is associated with the change of the SMM's oxidation state by one and $|\Delta S_t^z| = 1/2$. As a result, it means that the switching of the SMM's spin corresponds to a series of transitions between neighboring molecular states. An example of the formula for a transition rate between two states $|S;0,m\rangle$ and

$|S+1/2;1,m'\rangle$, satisfying the selection rules, is given below

$$\gamma_q^{|S;0,m\rangle|S+1/2;1,m'\rangle} = \left\{ \frac{\Gamma_\downarrow^q}{\hbar}\Big[\cos^2\frac{\varphi}{2}\left|\mathbb{A}^-_{m'}\right|^2\delta_{m,m'+\frac{1}{2}} + \sin^2\frac{\varphi}{2}\left|\mathbb{B}^-_{m'}\right|^2\delta_{m,m'-\frac{1}{2}}\Big] \right.$$
$$\left. + \frac{\Gamma_\uparrow^q}{\hbar}\Big[\cos^2\frac{\varphi}{2}\left|\mathbb{B}^-_{m'}\right|^2\delta_{m,m'-\frac{1}{2}} + \sin^2\frac{\varphi}{2}\left|\mathbb{A}^-_{m'}\right|^2\delta_{m,m'+\frac{1}{2}}\Big] \right\}$$
$$\times f_{\mathrm{FD}}\big(\epsilon_{|S+1/2;1,m'\rangle|S;0,m\rangle} - \mu_q\big). \quad (4.8)$$

As described in Sections 2.1 and 3.2, the magnetic state of a SMM can also be affected by intrinsic relaxation processes. Unlike relaxation stimulated by current flow through a molecule, the characteristic feature of intrinsic relaxation of the SMM's spin is that such processes do not change the oxidation state of the molecule. In addition, both the types of relaxation processes occur independently. Consequently, the transitions due to intrinsic relaxation take place between neighboring molecular states corresponding to the same occupation number of the LUMO level, which in the case of $n = 0$ [dots in Fig. 2.4(b,c)] and $n = 2$ [squares in Fig. 2.4(b,c)] means transitions within the same spin multiplet. For $n = 1$ [triangles and slanted squares in Fig. 2.4(b,c)], however, additional transitions between neighboring states of different spin multiplets become possible. In the situation under consideration, I assume that the spin relaxation within multiplets is fully described by phenomenological relaxation times $\tau_{\mathrm{rel},n}^{S_t\leftrightarrow S_t}$, which in general can be different for different spin multiplets. The corresponding relaxation rates take the form [180, 181],

$$\gamma_R^{|S_t;n,m\rangle|S_t;n,m\pm1\rangle} = \frac{1}{\tau_{\mathrm{rel},n}^{S_t\leftrightarrow S_t}} \times \frac{\exp\left[\frac{\Delta_{m,m\pm1}}{2k_BT}\right]}{2\cosh\left[\frac{\Delta_{m,m\pm1}}{2k_BT}\right]}, \quad (4.9)$$

with $\Delta_{m,m\pm1} = \epsilon_{|S_t;n,m\rangle} - \epsilon_{|S_t;n,m\pm1\rangle}$ [see Eqs. (2.19)-(2.22)]. The relaxation processes associated with transitions between two different spin multiplets for the case of a singly occupied LUMO level are characterized by $\tau_{\mathrm{rel},n=1}^{S+\frac{1}{2}\leftrightarrow S-\frac{1}{2}}$,

$$\gamma_R^{|S\pm\frac{1}{2};1,m\rangle|S\mp\frac{1}{2};1,m'\rangle} = \frac{\delta_{m',m-1}+\delta_{m',m+1}}{\tau_{\mathrm{rel},n=1}^{S+\frac{1}{2}\leftrightarrow S-\frac{1}{2}}} \times \frac{\exp\left[\frac{\Delta^\pm_{m,m'}}{2k_BT}\right]}{2\cosh\left[\frac{\Delta^\pm_{m,m'}}{2k_BT}\right]}, \quad (4.10)$$

where $\Delta^\pm_{m,m'} = \epsilon_{|S\pm1/2;1,m\rangle} - \epsilon_{|S\mp1/2;1,m'\rangle}$.

Taking into account the relaxation processes discussed above, the master equations for the probabilities $P_{|S_t;n,m\rangle}$ take the form,

$$\frac{\mathrm{d}P_{|S_t;n,m\rangle}}{\mathrm{d}t} = \sum_q \sum_{S_t',n',m'} \left\{ \left[\gamma_q^{|S_t';n',m'\rangle|S_t;n,m\rangle} + \gamma_R^{|S_t';n',m'\rangle|S_t;n,m\rangle}\right] P_{|S_t';n',m'\rangle} \right.$$
$$\left. - \left[\gamma_q^{|S_t;n,m\rangle|S_t';n',m'\rangle} + \gamma_R^{|S_t;n,m\rangle|S_t';n',m'\rangle}\right] P_{|S_t;n,m\rangle} \right\}. \quad (4.11)$$

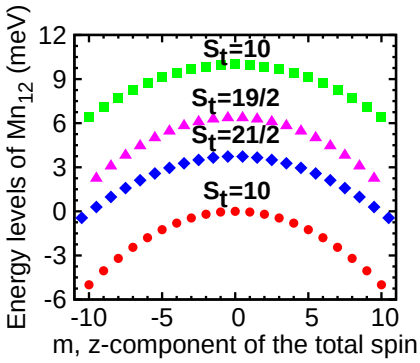

Figure 4.3: Energy spectra of the Mn_{12} molecule in the absence of an external magnetic field ($H_z = H_x = H_y = 0$) shown for the following parameters: $D = 0.05$ meV, $D_1 = -0.008$ meV, $D_2 = 0.0014$ meV [98], $J = 0.25$ meV, $\varepsilon = 5$ meV, and $U = 0$. Different parabolas correspond to indicated values of the SMM's total spin, S_t, and occupation states of the LUMO level: $|10;0,m\rangle$ (●), $|19/2;1,m\rangle$ (▲), $|21/2;1,m\rangle$ (♦), and $|10;2,m\rangle$ (■).

As a result, the analytical method allowing to study the dynamics of the SMM's CIMS has been devised. Assuming that initially the molecule is saturated for instance in the state $|S_t^0;n_0,m_0\rangle$, which corresponds to the boundary condition $P_{|S_t^0;n_0,m_0\rangle}(t_0 = 0) = 1$ and $P_{|S_t;n,m\rangle}(t_0 = 0) = 0$ for all $|S_t;n,m\rangle \neq |S_t^0;n_0,m_0\rangle$, at time $t \geqslant t_0$ one can apply a finite bias voltage V, and then study the dynamical response of the molecule's spin. It means that for a molecule of the spin S, one has to solve the set of $2S+1$ coupled differential equations for the situation of high LUMO level and $4(2S+1)$ equations in the general case — for the molecule Mn_{12} or Fe_8 with $S = 10$ one has to deal then with 84 equations.

4.2.2 Dynamical response of the Mn_{12} molecule's spin due to application of a constant voltage

Numerical results shown below have been obtained for the Mn_{12} molecule, whose energy spectrum is shown in Fig. 4.3. Since the results are going to be presented for an existing molecule, it seems suitable to comment on the choice of parameters used in calculations. When it comes to the parameters D, D_1 and D_2 describing the uniaxial anisotropy of the molecule, they can be deduced from the results of physicochemical experiments [67, 98, 100]. A more complicated situation is in the case of the coupling J between the LUMO level and the SMM's spin, which is the free parameter in the model under discussion. Because the exchange coupling can generally depend on the specific type of ligands used to stabilize the inner part of the molecule responsible form its magnetic properties, as well as on the structural geometry of the molecule, which can be additionally distorted due to the adsorption to a surface or electrodes (see Section 2.2), the parameter J can significantly vary even among different molecules belonging to the Mn_{12} family. One should therefore consider first whether J is positive or negative, for the sign of the coupling constant determines which of the spin multiplets $S + 1/2$ or $S - 1/2$ has lower

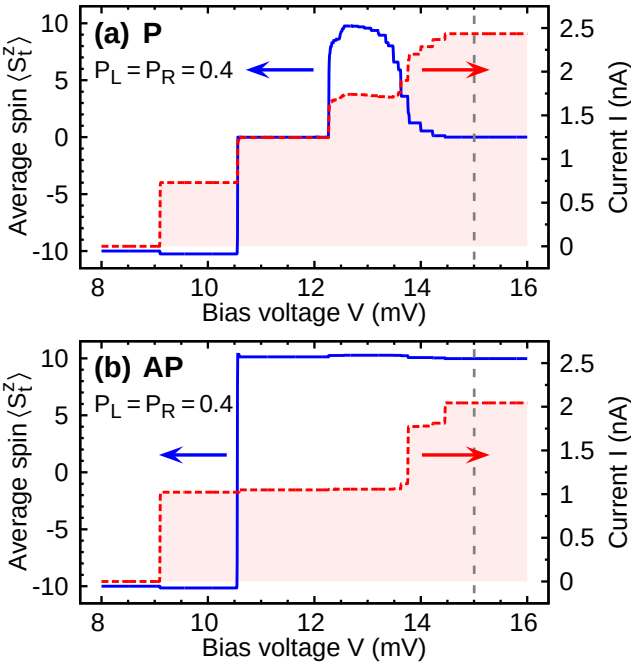

Figure 4.4: The average spin $\langle S_t^z \rangle$ and current I flowing through a Mn_{12} molecule in a stationary state as a function of bias voltage V for *parallel* (a) and *antiparallel* (b) magnetic configuration. Intrinsic relaxation processes are not taken into account. The other parameters are: $\varphi = 0$, $T = 0.01$ K and $\Gamma = 20$ μeV.

energy, and second, what is the value of J. Concerning the former point, there is a disagreement between the theory $(S + 1/2)$ [99] and experiments $(S - 1/2)$ [67, 98, 100]. More recent studies show that in fact both cases can take place [96]. Here, I have chosen $J > 0$ (the *ferromagnetic* coupling), however in Chapter 5 I will consider both the cases. Also the value of J can be hardly extracted from experimental results, so that the value assumed in Fig. 4.3 is chosen together with U, which in reality can be much larger, in order to get such a separation of spin multiplets that one can easily analyze their participation in transport processes. The larger Coulomb interaction U would mean that the states with a doubly occupied LUMO didn't take an active part in the CIMS process, whereas larger J would result in smaller energy gaps between states of the two lowest multiplets in Fig. 4.3.

In the following it is assumed that initially the molecule is saturated in the state $|10; 0, -10\rangle$, and then at time $t = 0$ a constant bias voltage V is applied. Figure 4.4 illustrates how the average spin $\langle S_t^z \rangle$ and current I flowing through the SMM in a stationary state depend on the bias voltage V. In the ST regime, the magnetic state of the molecule remains intact until the voltage reaches $V \approx 9.1$ mV, which corresponds to the energy gap between the states $|10; 0, -10\rangle$ and $|21/2; 1, -21/2\rangle$, Fig. 4.3. Since according to the selection rules the molecule can escape this state only *via* the state $|10; 2, -10\rangle$, whose energy is relatively large, the molecule becomes trapped in the state $|21/2; 1, -21/2\rangle$.

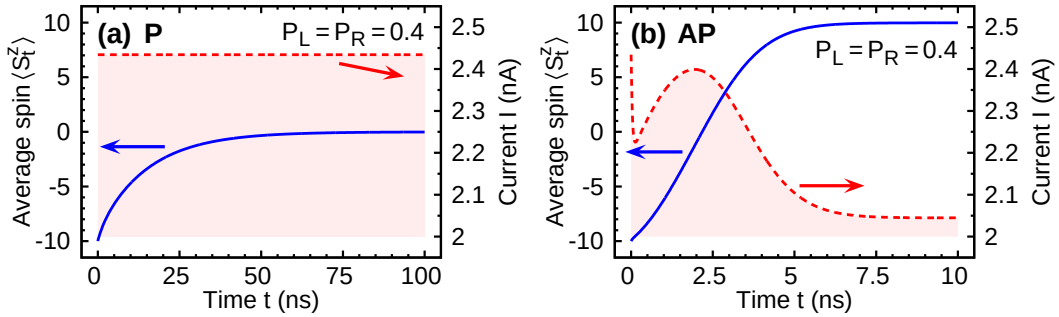

Figure 4.5: Dynamics of the SMM's switching in the *parallel* (a) and *antiparallel* (b) magnetic configuration for the bias voltage $V = 15$ mV. Other parameters as in Fig. 4.4.

The switching process begins when the next accessible level $|21/2; 1, -19/2\rangle$ enters the energy window set by the voltage V. For the case of both the electrodes characterized by the same polarization parameter, the switching of the SMM's spin is observed only in the antiparallel configuration of the leads' magnetic moments, whereas in the parallel configuration all molecular spin states gradually become equally probable. Such a behavior results from the left/right symmetry of the SMM's coupling to electrodes, resembling the absence of the spin accumulation in tunneling through a metallic nanoparticle [182]. On the other hand, the antiparallel configuration lacks such a symmetry, so that the molecular spin states become unequally occupied leading to the spin reversal.

Figure 4.5 presents the time evolution of the zth component of the molecule's total spin for a given value of a bias voltage. One of the most notable features of the CIMS is that the reversal of the SMM's spin is accompanied by an additional signal in the current flowing through the system, Fig. 4.5(b). The occurrence of this additional signal can be explained by considering transport channels through which electrons traverse the junction. As already mentioned in Section 4.1, during tunneling through the LUMO level the electron spin can flip its direction owing to exchange interaction with the molecule's spin, so that the transfer of spin angular momentum between the current and the molecule

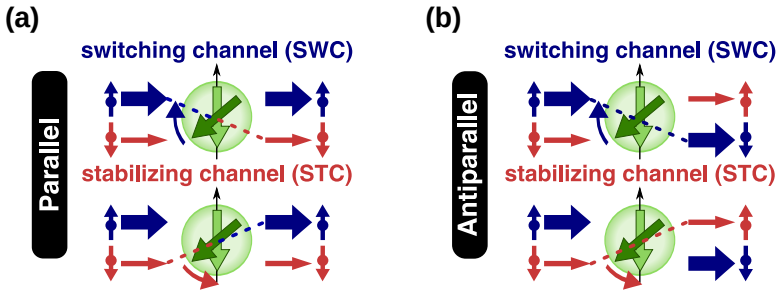

Figure 4.6: Schematic illustration of the concept of the switching (SWC) and stabilizing (STC) transport channels in the *parallel* (a) and *antiparallel* (b) configuration of the leads' spin moments.

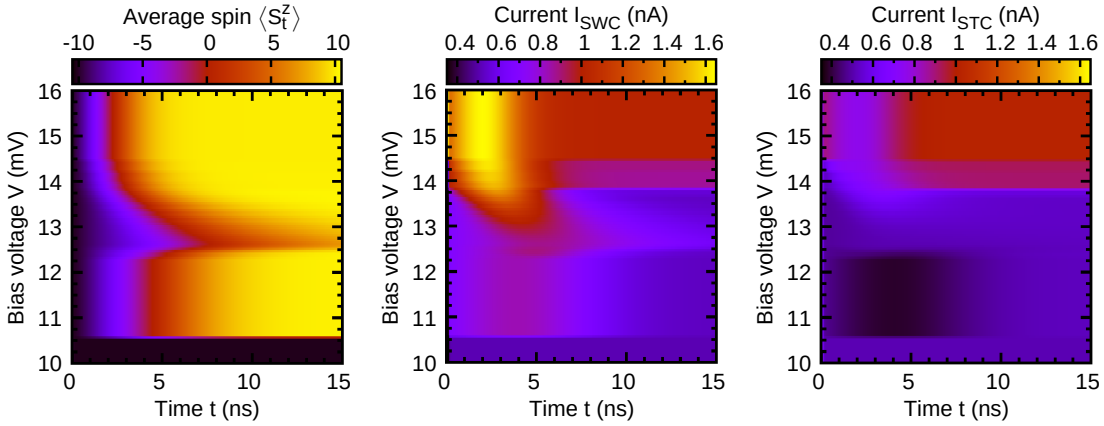

Figure 4.7: Dynamics of the SMM's switching in the *antiparallel* configuration of electrodes' magnetic moments for various bias voltages V: the average value of the zth component of the molecule's total spin, and the current flowing through the molecule *via* SWC channel I_{SWC} (b) and STC channel I_{STC} (c). Other parameters as in Fig. 4.4.

can take place, Fig. 4.2(b)-(c). When electrons change their spin orientation in such a way that the momentum transferred to the molecule tends to switch its magnetic moment, the corresponding transport channel is referred to as the '*switching channel*' (SWC). Accordingly, the transport channel in which electrons tunneling between the leads and the molecule tend to restore the initial state of the SMM's spin is called the '*stabilizing channel*' (STC), Fig. 4.6. Assuming that

$$I_q^{\mathrm{SWC(STC)}} = e \sum_{S_t, S_t'} \sum_{n,n',m} (n' - n) \gamma_q^{|S_t;n,m\rangle |S_t';n',m\pm 1\rangle} P_{|S_t;n,m\rangle} \tag{4.12}$$

describes the current flowing in the SWC (STC) from the qth lead to the molecule, the total resulting electronic current flowing through each of so defined channels is given by

$$I^{\mathrm{SWC(STC)}} = \frac{1}{2}\left[I_L^{\mathrm{SWC(STC)}} - I_R^{\mathrm{SWC(STC)}} \right]. \tag{4.13}$$

Analysis of Fig. 4.4 leads to a straightforward conclusion that for $P_L = P_R$ the reversal of the SMM's spin can be observed only for the antiparallel configuration of the electrodes' magnetic moments. Therefore it would be informative to take a look how the dynamics of the spin's switching in such a case depends on a bias voltage, Fig. 4.7(a). One can notice that for larger voltages the reversal occurs rather fast at the time of order of 12.5 ns, Fig. 4.8. However, before this range of voltages is reached one observes the transition through a bias region in which significant slowing down of the reversal process takes place. The stabilization time can then increase up to even 90 ns. On the other hand, in the parallel magnetic configuration typical time at which the molecule's become demagnetized is of order of 200 ns, but for the transitional region it can also be as long as 100 μs.

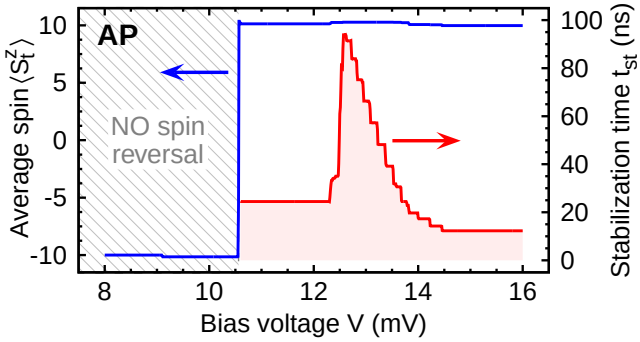

Figure 4.8: The dependence of the stabilization time t_{st}, which in this example can be understood as the *switching time*, plotted as a function of a bias voltage V for the antiparallel magnetic configuration of electrodes, see Fig. 4.4(b).

Let's now discuss in more detail the transport processes occurring during the SMM's spin reversal. Since in the antiparallel configuration spin directions of majority (and also minority) electrons in different leads are opposite, Fig. 4.6(b), tunneling probabilities through SWC and STC are not equal. There dominates transport through SWC, as this channel involves majority spins in both the electrodes. Consequently, the current adds more angular momentum to the molecule than it subtracts, Fig. 4.7(b)-(c), and the reversal of the SMM's spin takes place. The situation changes in the parallel configuration, where the channels become symmetric (at least for $P_L = P_R$), and both SWC and STC contribute equally to transport, so that no switching is observed. However, the symmetry of SWC/STC can be broken by allowing the polarization parameters of both the leads to differ ($P_L \neq P_R$), Fig. 4.9(a)-(d). Furthermore, it can be seen that in the antiparallel configuration the magnetic switching of a SMM can be observed for all the range of electrodes' polarization parameters, Fig. 4.9(e)-(h), whereas in the parallel configuration the spin of the molecule can be reversed only if $P_L > P_R$, Fig. 4.9(a)-(d). It should be thus emphasized that the pulse in current is a consequence of competition between SWC and STC transport channels which drive the molecule's spin to a stable state. Once the molecule reaches such a state the competition ceases, and both the channels start contributing equally to transport, Figs. 4.7(b)-(c).

Misalignment between the SMM's easy axis and the magnetic moments of the leads also affects the reversal process, Fig. 4.10. The effective spin orientation of electrons tunneling through the LUMO level perceived by the molecule varies with rotation of the molecule's anisotropy axis [183]. As a result, both the channels exchange their roles, i.e. the SWC (STC) gradually converts into STC (SWC).

Another important aspect of the SMM's spin reversal to be considered is intrinsic-spin relaxation. In the following it is assumed $\tau_{\mathrm{rel},0}^{10\leftrightarrow 10} = \tau_{\mathrm{rel},1}^{19/2\leftrightarrow 19/2} = \tau_{\mathrm{rel},1}^{21/2\leftrightarrow 21/2} = \tau_{\mathrm{rel},2}^{10\leftrightarrow 10} \equiv \tau_{\mathrm{rel}}$, and $\tau_{\mathrm{rel},1}^{21/2\leftrightarrow 19/2} = \tau'_{\mathrm{rel}}$. Figure 4.11 shows the case of relaxation processes occurring only within the individual spin multiplets. Apparently, intrinsic-spin relaxation processes lead to attenuation of the magnetic switching, increasing thus the time at which the spin

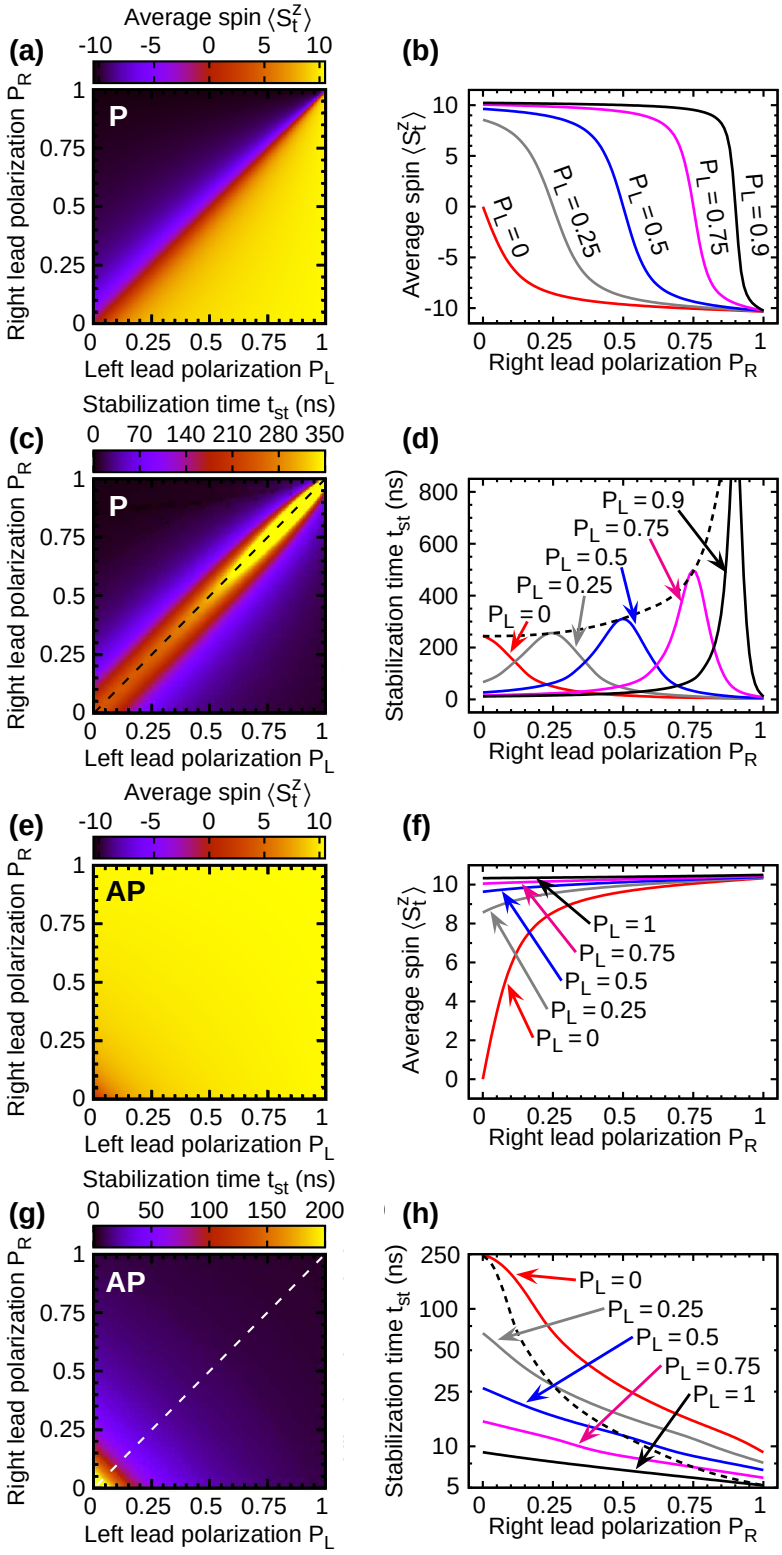

Figure 4.9: The influence of leads' polarization parameters on the final average spin state $\langle S_t^z \rangle$ of the molecule and the time $t_{\rm st}$ after which this state is reached in the *parallel* (a)-(d) and *antiparallel* (e)-(h) magnetic configuration of the system. Other parameters as in Fig. 4.4.

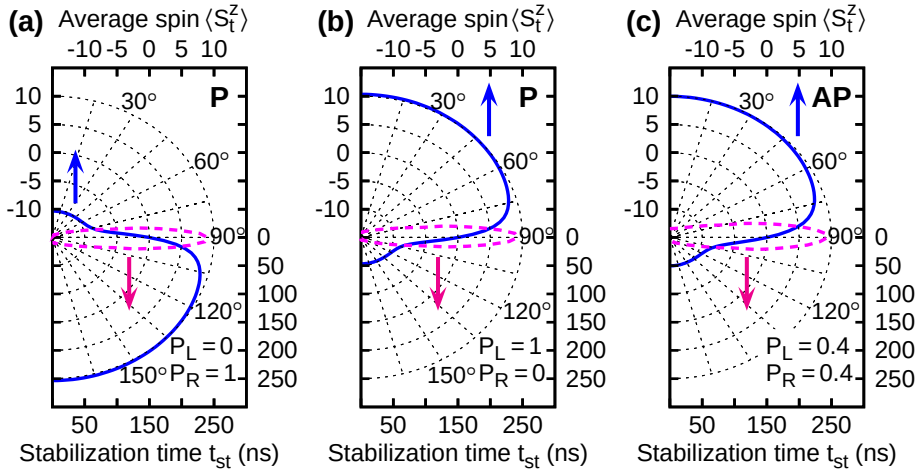

Figure 4.10: Variation of the average value $\langle S_t^z \rangle$ of the SMM's spin that can be reached for $V = 15$ mV and the stabilization time $t_{\rm st}$ due to rotation of the molecule's easy axis in the *parallel* (a)-(b) and *antiparallel* (c) magnetic configuration. The other parameters as in Fig. 4.4.

stabilizes. The appearance of such behavior results from significant contribution of the relaxation processes to competition between the SWC and the STC.

Further inclusion of the intrinsic relaxation between the two different spin multiplets corresponding to the singly occupied LUMO level shows that such processes only slightly modify the reversal of the molecule's spin, Fig. 4.12. The relaxation between different spin multiplets violates the selection rules in the sense that the processes under discussion allow the molecule for transitions satisfying $|\Delta S_t^z| = 1$, whose rate can be comparable or even higher than the rate of transitions induced by tunneling of electrons to/out of a LUMO level. Consequently, it turns out that the relaxation between different spin multiplets can facilitate spin switching and shorten the corresponding switching time.

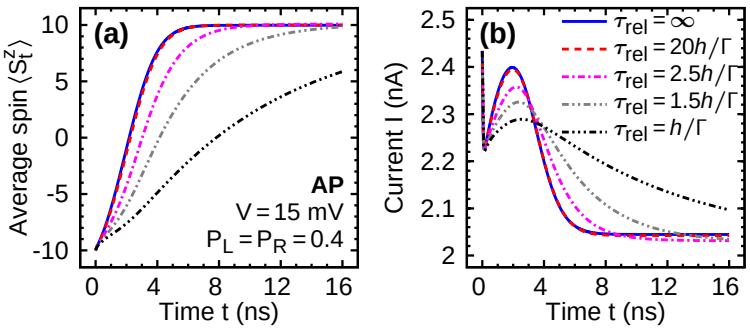

Figure 4.11: The effect of intrinsic relaxation processes on dynamics of the SMM's magnetic switching in the *antiparallel* magnetic configuration ($h/\Gamma = 0.2$ ns, $\varphi = 0$ and $\tau'_{\rm rel} = \infty$). The other parameters as in Fig. 4.4.

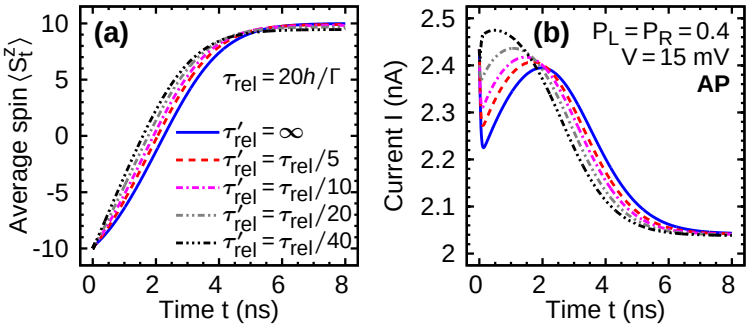

Figure 4.12: The reversal of the SMM's spin for different values of intrinsic-spin relaxation between the spin multiplets 21/2 and 19/2 that correspond to a singly occupied LUMO level. The other parameters as in Fig. 4.4.

4.3 Current-induced magnetic switching in the cotunneling regime

Cotunneling processes can in general be divided into two groups with respect to whether or not the molecule remains in its initial state after a cotunneling process, Fig. 4.13(a)-(b). Although the cotunneling events do not change the charge state of the molecule, they can, however, modify its spin state (inelastic cotunneling). Moreover, it turns out that inelastic cotunneling processes can lead to magnetic switching of the molecule's spin between two lowest energy states. This is because such processes involve angular momentum transfer between the molecule and tunneling electrons, as shown schematically in Fig. 4.13(b). It should be noted that in addition to *double-barrier* cotunneling processes which transfer charge between two different electrodes, there are also *single-barrier* cotunneling processes, where an electron involved in the cotunneling process returns back to the same electrode. Although the latter processes do not contribute directly to the current flowing through the system, they can affect all the transport properties in an indirect way, by altering spin state of the molecule.

Because in the Coulomb blockade regime electrons are not allowed to tunnel to the molecule, only the states with unoccupied LUMO level $|S;0,m\rangle$ can be realized. Consequently, the CIMS mechanism is active only if an electron being virtually in the LUMO level flips its spin orientation. Note, however, that by applying a gate voltage one can shift energy levels of a molecule, so that the molecule can instead be trapped in the states with a singly occupied LUMO level. This new situation permits that in the virtual state not only can the molecule accommodate an additional, second electron, but it is also allowed to release one electron, which effectively corresponds to tunneling a hole to the LUMO. Since my aim is to consider the dynamical aspects of the CIMS's basic mechanism in the CT regime, I focus in this section only on the conceptually easiest case of the unoccupied LUMO level in equilibrium. More detailed discussion on spin effects related to transport in the CT regime will be presented in the next chapter.

For the sake of notational clarity, similarly as in Chapter 3, I assume $|S;0,m\rangle \equiv |m\rangle$.

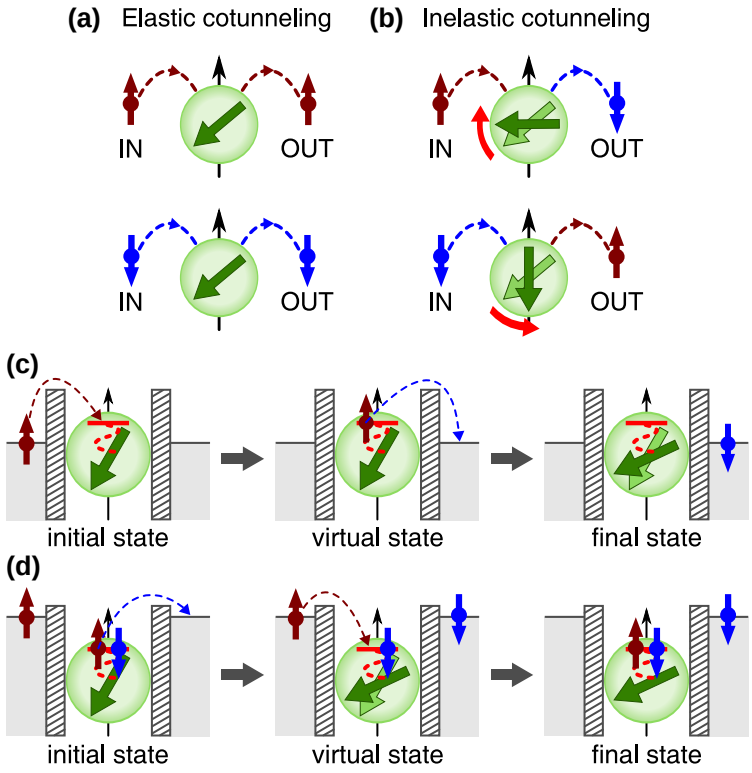

Figure 4.13: (a)-(b) Schematic representation of the *elastic* and *inelastic* electron cotunneling processes. The two bottom panels show examples of inelastic cotunneling processes leading to increase of the zth component of the SMM's spin in the situation when the LUMO level is: (c) empty and (d) doubly occupied. Note that in the present chapter I consider cotunneling processes only in the Coulomb blockade regime. For simplicity, in (c)-(d) I assume thus $V \to 0$, i.e. $\mu_L = \mu_R + 0^+$. If in the ground state the molecule was occupied by a single electron, inelastic processes could generally occur *via* two virtual states associated with empty and doubly occupied LUMO level.

In general, within the frame of the standard higher-order perturbation approach, the transition rate $\gamma_{qq'}^{|m\rangle|m'\rangle}$ for inelastic cotunneling processes can be written in the following manner [184, 185]

$$\gamma_{qq'}^{|m\rangle|m'\rangle} = \sum_{\mathbf{k}\sigma\in q} \sum_{\mathbf{k}'\sigma'\in q'} W_{q'\mathbf{k}'\sigma'|m'\rangle}^{q\mathbf{k}\sigma|m\rangle} \; f_{\mathrm{FD}}(\varepsilon_{\mathbf{k}\sigma}^{q}) \Big[1 - f_{\mathrm{FD}}(\varepsilon_{\mathbf{k}'\sigma'}^{q'})\Big]. \tag{4.14}$$

There are several theoretical methods which allow me to calculate the cotunneling rate [186–188]. Here, the $\mathcal{T}$-matrix approach that enables one to generalize Fermi's golden rule to higher-order processes is used. Accordingly, the probability amplitude that the system undergoes a transition from some initial eigenstate $|i\rangle$ of $\mathcal{H}_0 = \mathcal{H}_{\mathrm{SMM}} + \mathcal{H}_{\mathrm{el}}$ at t_0

to another eigenstate $|f\rangle$ at time $t > t_0$ reads[2]

$$\langle f|i(t)\rangle = \frac{\mathrm{e}^{\eta t}}{E_i - E_f + i\eta} \sum_{n=1}^{\infty} \langle f|\mathcal{T}|i\rangle, \tag{4.15}$$

where $\mathcal{T}$ is called the $\mathcal{T}$-matrix,

$$\begin{aligned}\mathcal{T} = \mathcal{H}_{\mathrm{tun}} &+ \mathcal{H}_{\mathrm{tun}} \frac{1}{E_i - \mathcal{H}_0 + i\eta} \mathcal{H}_{\mathrm{tun}} \\ &+ \mathcal{H}_{\mathrm{tun}} \frac{1}{E_i - \mathcal{H}_0 + i\eta} \mathcal{H}_{\mathrm{tun}} \frac{1}{E_i - \mathcal{H}_0 + i\eta} \mathcal{H}_{\mathrm{tun}} + \mathrm{h.o.}\end{aligned} \tag{4.16}$$

In consequence, the rate at which the system transfers from the initial state $|i\rangle$ to the final one $|f\rangle$ is given by

$$W_f^i = \frac{2\pi}{\hbar} \left| \sum_v \frac{\langle f|\mathcal{H}_{\mathrm{tun}}|v\rangle\langle v|\mathcal{H}_{\mathrm{tun}}|i\rangle}{E_i - E_v} \right|^2 \delta(E_f - E_i). \tag{4.17}$$

In Eq. (4.17), the initial and final states are defined as $|i\rangle \equiv |\mathbf{k}\sigma\rangle_q \otimes |m\rangle$ and $|f\rangle \equiv |\mathbf{k}'\sigma'\rangle_{q'} \otimes |m'\rangle$, where the first ket corresponds to the state of electrodes. From a physical point of view, the above equation represents the process during which one electron is moved from the lead q to the lead q' via a virtual state $|v\rangle \equiv |0\rangle|S \pm 1/2; 1, m''\rangle$. One should also note that summation in Eq. (4.17) runs over all molecular spin states belonging to multiplets $S + 1/2$ and $S - 1/2$, which correspond to a molecule with one extra electron. The electron virtually entering the LUMO level may then flip its spin orientation, altering *via* exchange interaction the state of the molecule's spin. Moreover, E_i, E_f and E_v in Eq. (4.17) denote the energies of the initial, final, and virtual states, respectively. To complete the present discussion, it is worth emphasizing that in the most general case for a finite Coulomb interaction U, one can also expect tunneling of electron pairs [189]. Nonetheless, it transpires that the contribution of such processes to the transport can be dominating only for some specific situations, e.g. for negative U, and one can neglect this contribution otherwise, as it has been done here.

As a result, the expression for the cotunneling transition rate takes the from

$$\begin{aligned}\gamma_{qq'}^{|m\rangle|m'\rangle} = \frac{\hbar}{2\pi} \sum_{\sigma\sigma'} \Gamma_\sigma^q \Gamma_{\sigma'}^{q'} \int d\epsilon \left| \sum_{S_t^\nu, m_\nu} \frac{\mathcal{A}_{mm'}^\nu}{\epsilon + \epsilon_{m\nu} + \mu_q} \right|^2 \\ \times f_{\mathrm{FD}}(\epsilon) \Big[1 - f_{\mathrm{FD}}(\epsilon + \epsilon_{mm'} + \mu_q - \mu_{q'}) \Big],\end{aligned} \tag{4.18}$$

with $\epsilon_{m\nu} \equiv \epsilon_{|m\rangle} - \epsilon_{|\nu\rangle}$, and $\epsilon_{|m(\nu)\rangle}$ being the energy of the SMM with an unoccupied (a

[2] To avoid further complications due to action of transient processes during switching on the perturbation (tunneling of electrons), it is assumed that the process occurs slowly. On the other hand, since the tunneling processes take place between the moments t_0 and t, the time of turning on the perturbation η^{-1} should be significantly shorter than the duration $t - t_0$ of the perturbation, i.e. $t - t_0 \gg \eta^{-1}$ [187].

singly occupied) LUMO level [see Eqs. (2.19)-(2.22)]. The coefficient $\mathcal{A}^{\nu}_{mm'}$ is defined as

$$\mathcal{A}^{\nu}_{mm'} = C^{\sigma'}_{m'\nu} C^{\sigma *}_{m\nu} \cos^2\frac{\varphi}{2} + \eta_q \eta_{q'} C^{\bar{\sigma}'}_{m'\nu} C^{\bar{\sigma} *}_{m\nu} \sin^2\frac{\varphi}{2} - \frac{1}{2}\sin\varphi\Big(\eta_q C^{\sigma'}_{m'\nu} C^{\bar{\sigma} *}_{m\nu} + \eta_{q'} C^{\bar{\sigma}'}_{m'\nu} C^{\sigma *}_{m\nu}\Big), \tag{4.19}$$

with $C^{\sigma'}_{m'\nu} \equiv \langle S_t; 0, m'|c_{\sigma'}|S^{\nu}_t; 1, m_\nu\rangle$, and the remaining coefficients formulated in a similar way — for exact expressions see two first lines of Eq. (4.6).

When tackling Eq. (4.18), one encounters divergence owing to the presence of the denominator. Several regularization procedures have been developed to deal with this problem [56, 190–193]. Here, I use the method described in Refs. [192, 193]. By noting that $f_{\rm FD}(\epsilon)\big[1 - f_{\rm FD}(\epsilon + a)\big] = f_{\rm BE}(-a)\big[f_{\rm FD}(\epsilon + a) - f_{\rm FD}(\epsilon)\big]$, where $f_{\rm BE}(\epsilon)$ is the Bose-Einstein distribution function, the integral in Eq. (4.18) can be split up into a sum of integrals of two types (with $n = 0$ and $n = 1$), which in the next step can be evaluated using contour integration, yielding

$$\int d\epsilon \frac{f_{\rm FD}(\epsilon + a)}{(\epsilon - b)^{n+1}} = \frac{1}{n!}\frac{{\rm d}^n}{{\rm d}b^n}\left[\Psi\Big(\frac{1}{2} + i\frac{a+b}{2\pi k_{\rm B}T}\Big) - \ln\frac{W}{2\pi k_{\rm B}T}\right]. \tag{4.20}$$

In the above equation, $\Psi(z)$ denotes the digamma function, and W is the cutoff parameter (the largest energy scale in the system). Ultimately, applying all aforementioned intermediate steps to Eq. (4.18), one derives the final expression for the tunneling rate between two neighboring spin states of a SMM,

$$\begin{aligned}
\gamma^{|m\rangle|m\pm1\rangle}_{qq'} = {} & \frac{\Gamma^{q}_{\uparrow(\downarrow)}\Gamma^{q'}_{\downarrow(\uparrow)}}{2\pi\hbar} f_{\rm BE}\Big(\Delta\epsilon^{|S;0,m\pm1\rangle}_{|S;0,m\rangle} + \mu_{q'} - \mu_q\Big) \\
& \times \Bigg\{ \big|\mathbb{A}^{-}_{m\pm1/2}\,\mathbb{B}^{-*}_{m\pm1/2}\big|^2 \Big[\widetilde{\Psi}'\Big(\Delta\epsilon^{|S+1/2;1,m\pm1/2\rangle}_{|S;0,m\pm1\rangle} - \mu_{q'}\Big) - \widetilde{\Psi}'\Big(\Delta\epsilon^{|S+1/2;1,m\pm1/2\rangle}_{|S;0,m\rangle} - \mu_q\Big)\Big] \\
& + \big|\mathbb{A}^{+}_{m\pm1/2}\,\mathbb{B}^{+*}_{m\pm1/2}\big|^2 \Big[\widetilde{\Psi}'\Big(\Delta\epsilon^{|S-1/2;1,m\pm1/2\rangle}_{|S;0,m\pm1\rangle} - \mu_{q'}\Big) - \widetilde{\Psi}'\Big(\Delta\epsilon^{|S-1/2;1,m\pm1/2\rangle}_{|S;0,m\rangle} - \mu_q\Big)\Big] \\
& + \frac{2{\rm Re}\big(\mathbb{A}^{-}_{m\pm1/2}\,\mathbb{A}^{+}_{m\pm1/2}\,\mathbb{B}^{-*}_{m\pm1/2}\,\mathbb{B}^{+*}_{m\pm1/2}\big)^{(*)}}{\Delta\epsilon^{|S+1/2;1,m\pm1/2\rangle}_{|S-1/2;1,m\pm1/2\rangle}} \\
& \quad \times \Big[\widetilde{\Psi}\Big(\Delta\epsilon^{|S+1/2;1,m\pm1/2\rangle}_{|S;0,m\pm1\rangle} - \mu_{q'}\Big) - \widetilde{\Psi}\Big(\Delta\epsilon^{|S+1/2;1,m\pm1/2\rangle}_{|S;0,m\rangle} - \mu_q\Big) \\
& \quad + \widetilde{\Psi}\Big(\Delta\epsilon^{|S-1/2;1,m\pm1/2\rangle}_{|S;0,m\rangle} - \mu_q\Big) - \widetilde{\Psi}\Big(\Delta\epsilon^{|S-1/2;1,m\pm1/2\rangle}_{|S;0,m\pm1\rangle} - \mu_{q'}\Big)\Big] \Bigg\},
\end{aligned} \tag{4.21}$$

where the following auxiliary notation has been introduced: $\widetilde{\Psi}(z) \equiv \Psi(1/2 + iz/(2\pi k_{\rm B}T))$, $\widetilde{\Psi}'(z) \equiv {\rm d}\widetilde{\Psi}(z)/{\rm d}z$ and $\Delta\epsilon^{|f\rangle}_{|i\rangle} = \epsilon_{|f\rangle} - \epsilon_{|i\rangle}$. Furthermore, Eq. (4.21) as stated is valid only for $2(D + D_1)J < 0$ [see Section 2.4], in the opposite case for $2(D + D_1)J > 0$ one should substitute $\mathbb{A}^{\pm}_{m\pm1/2}$ ($\mathbb{B}^{\pm}_{m\pm1/2}$) with $\mathbb{A}^{\mp}_{m\pm1/2}$ ($\mathbb{B}^{\mp}_{m\pm1/2}$).

Similarly as in the case of the ST regime, Eq. (4.11), one can put down the set of

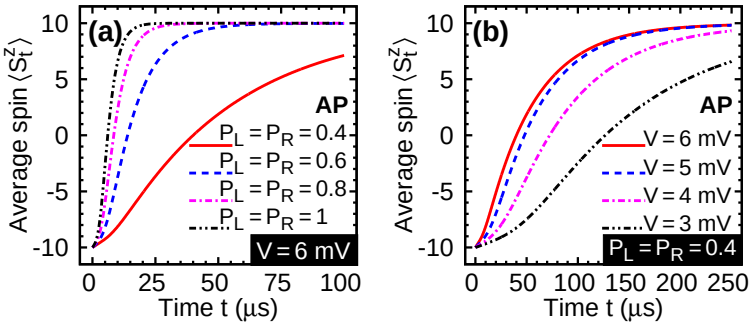

Figure 4.14: Dynamics of the average spin $\langle S_t^z \rangle$ in the antiparallel magnetic configuration for various polarization parameters $P_L = P_R$ (a) and different bias voltages V (b). The other parameters as in Fig. 4.4.

master equations describing the time evolution of the probability distribution,

$$\frac{\mathrm{d}P_{|m\rangle}}{\mathrm{d}t} = \sum_{q,q'} \Big\{ \Big[\gamma_{qq'}^{|m-1\rangle|m\rangle} + \gamma_R^{|m-1\rangle|m\rangle}\Big] P_{|m-1\rangle} + \Big[\gamma_{qq'}^{|m+1\rangle|m\rangle} + \gamma_R^{|m+1\rangle|m\rangle}\Big] P_{|m+1\rangle} - \Big[\gamma_{qq'}^{|m\rangle|m-1\rangle} + \gamma_{qq'}^{|m\rangle|m+1\rangle} + \gamma_R^{|m\rangle|m-1\rangle} + \gamma_R^{|m\rangle|m+1\rangle}\Big] P_{|m\rangle} \Big\}. \tag{4.22}$$

The main difference when compared to the analogous equation presented in Section 4.2 is that in the CT regime a SMM can occupy only the magnetic molecular states corresponding to an unoccupied LUMO level. For this reason, the probabilities of finding the molecule in other states can be assumed to be equal to zero, and hence there is no need to include them in the master equation. This significantly simplifies the considerations, as one have to deal now only with $2S + 1$ differential equations.

At the beginning it has to be emphasized that the basic ideas underling the CIMS in the CT regime do not differ qualitatively from those presented for the ST regime, compare Fig. 4.14 with Fig. 4.5(b). To start with, the reversal is also observed only when the voltage achieves a certain threshold value, which corresponds to the energy gap between the initial state $|-10\rangle$ and the nearest neighboring state $|-9\rangle$. Furthermore, since the transition rates, Eq. (4.21), are determined by the coupling parameters of the molecule to the electrodes q and q', described by Γ_σ^q and $\Gamma_{\sigma'}^{q'}$, switching of the SMM's spin strongly depends on magnetic configuration of the leads' magnetic moments, as shown in Figs. 4.14 and 4.15. In the antiparallel configuration the reversal occurs for the whole range of polarization parameters, whereas in the parallel case the switching is observed only for $P_L > P_R$. Such a behavior stems from the fact that for $\varphi = 0$ the probability of transfer through the SWC (STC) is proportional to $\Gamma_+^L \Gamma_-^R$ ($\Gamma_-^L \Gamma_+^R$) in the parallel case, and to $\Gamma_+^L \Gamma_+^R$ ($\Gamma_-^L \Gamma_-^R$) in the antiparallel one.

It has to be pointed out, however, that the numerical results shown in Fig. 4.14 and Fig. 4.15 have been obtained in the absence of intrinsic spin relaxation in the molecule.

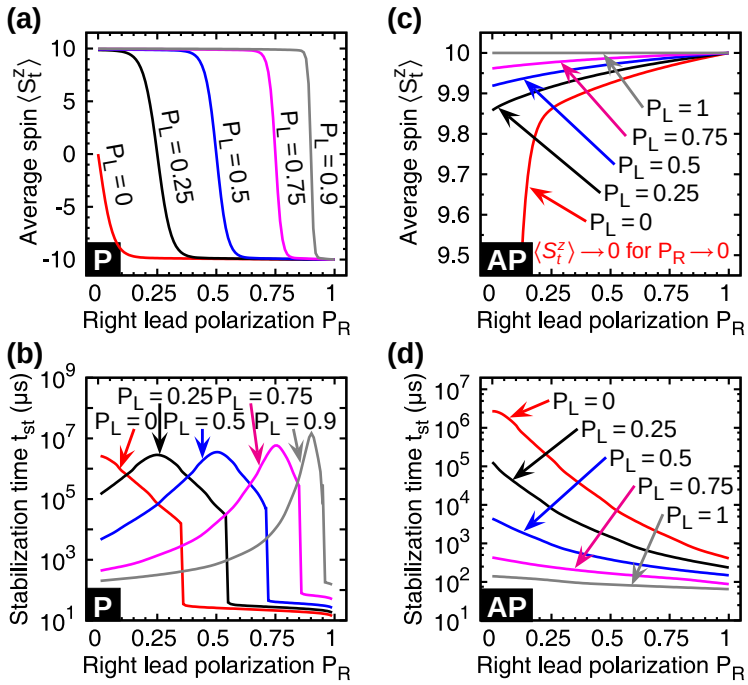

Figure 4.15: The average value of the SMM's spin $\langle S_t^z \rangle$ and the stabilization time t_{st} after which the state is reached as functions of polarization parameters of the leads for the parallel (a)-(b) and antiparallel (c)-(d) magnetic configuration of the system. ($V = 6$ mV) The other parameters as in Fig. 4.4.

In real system switching may be observed when the spin relaxation time is longer than the switching time found in the absence of spin relaxation. Comparison of numerical data with experimentally determined spin relaxation times indicates that current-induced switching in the cotunneling regime may be observed in some molecules and for favorable system parameters. The switching times obtained for the parameters assumed, however, seem to be too long for practical applications, contrary to transport in the sequential tunneling regime, where they are significantly shorter.

CHAPTER 5

Spin effects in stationary transport through single-molecule magnets in the sequential and cotunneling regimes

In the previous chapter I focused on analyzing the dynamics of the current-induced magnetic switching of SMMs separately in the sequential tunneling and cotunneling regimes. However, it should be noted that although higher-order processes play a substantial role mainly in the cotunneling regime, they remain active in the whole range of transport voltages, especially on resonance, leading to renormalization of the molecule levels and smearing of the Coulomb steps [194]. Therefore a suitable theoretical method should be used to properly investigate transport through molecules in the regime where both the sequential and cotunneling processes determine transport properties.

The existing analytical studies of electronic transport through SMMs in the *weak* coupling regime were based on the standard perturbation approach [103, 104, 110, 181, 185, 195–197], and they dealt separately either with the sequential or cotunneling regime, with one attempt of combining them [184]. Nevertheless, to properly take into account the nonequilibrium many-body effects such as on-resonance level renormalization or level splitting due to an effective exchange field, simple rate equation arguments are rather not sufficient.

Among different available methods, only a few enable one to analyze spin-dependent transport of the considered system in both the sequential and Coulomb blockade regimes within one fully consistent theoretical approach [198]. The aim of the present chapter is therefore to systematically study the electronic and spin stationary transport through a SMM, together with effects that can accompany such transport, in different orders with respect to tunneling processes between the molecule and external ferromagnetic

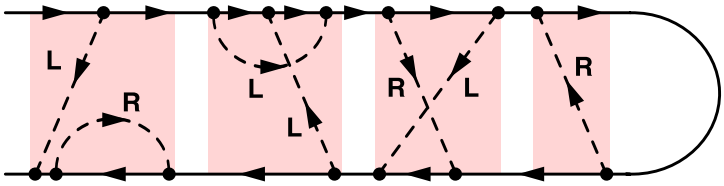

Figure 5.1: An example of a *Keldysh contour*, which is a graphical representation for the time evolution of the reduced density matrix. The top and bottom horizontal lines correspond to the forward and backward propagator, respectively. On the other hand, dashed lines connecting vertices in pairs depict tunneling of an electron between an electrode and the molecule, whereas arrows indicate whether the electron leaves or enters the molecule. Finally, the dark regions distinguish the irreducible diagrams.

leads. This is achieved by means of the *real-time diagrammatic technique* [194, 199–203], which has already proven its reliability and versatility in studying transport properties of various nanoscopic systems.

5.1 The real-time diagrammatic technique

The real-time diagrammatic technique relies on a systematic perturbation expansion of the reduced density matrix of the system under discussion and the operators of interest with respect to the coupling strength Γ between the LUMO level and the leads. All quantities, such as the current I, differential conductance G and the (zero-frequency) current noise S are essentially determined by the nonequilibrium time evolution of the reduced density matrix for the molecule's degrees of freedom. In the case considered in this thesis, the density matrix has only diagonal matrix elements, $p_\chi(t)$, which correspond to probability of finding the molecule in state $|\chi\rangle$ at time t. Following the matrix notation introduced by Thielmann *et al.* [201], the vector $\mathbf{p}(t)$ of the probabilities is given by the relation

$$\mathbf{p}(t) = \mathbf{\Pi}(t, t_0)\mathbf{p}(t_0)\,, \tag{5.1}$$

where $\mathbf{\Pi}(t, t_0)$ is the *propagator* matrix whose elements, $\Pi_{\chi'\chi}(t, t_0)$, describe the time evolution of the system that propagates from a state $|\chi\rangle$ at time t_0 to a state $|\chi'\rangle$ at time t, and $\mathbf{p}(t_0)$ is a vector representing the distribution of initial probabilities. In principle, the whole dynamics of the system is governed by the time evolution of the reduced density matrix. Furthermore, this time evolution can be schematically depicted as a sequence of irreducible diagrams on the Keldysh contour [194], Fig. 5.1, which after summing up correspond to *irreducible self-energy blocks* $W_{\chi'\chi}(t', t)$ [201]. Each vertex on the Keldysh contour represents the product of the Fermi operators of an electrode and the molecule's LUMO level. The vertex is then referred to as an *internal* or *external* vertex depending on whether it stems from the expansion of the tunneling Hamiltonian $\mathcal{H}_\mathrm{T}$ or any other operator of interest, respectively. Pairs of vertices are in turn connected by tunneling lines, which delineate contractions between pairs of electron operators. Within

such a picture, an *irreducible diagram* should be understand as a diagram for which it is impossible to draw a vertical line between two neighboring vertices without crossing at least one tunneling line.

The self-energy matrix $\mathbf{W}(t',t)$ is therefore the central quantity of the real-time diagrammatic technique, as its elements $W_{\chi'\chi}(t',t)$ can be interpreted as generalized transition rates between two arbitrary molecular states: $|\chi\rangle$ at time t and $|\chi'\rangle$ at time t'. Consequently, the Dyson equation for the propagator is obtained in the form [194, 201]

$$\mathbf{\Pi}(t,t_0) = \mathbf{1} + \int_{t_0}^{t} \mathrm{d}t_2 \int_{t_0}^{t_2} \mathrm{d}t_1 \mathbf{W}(t_2,t_1)\mathbf{\Pi}(t_1,t_0)\,. \tag{5.2}$$

By multiplying Eq. (5.2) from the right hand side with $\mathbf{p}(t_0)$, and differentiating it with respect to time t, one gets the general kinetic equation for the probability vector $\mathbf{p}(t)$,

$$\frac{\mathrm{d}}{\mathrm{d}t}\mathbf{p}(t) = \int_{t_0}^{t} \mathrm{d}t_1 \mathbf{W}(t,t_1)\mathbf{p}(t_1)\,. \tag{5.3}$$

In the limit of *stationary transport* the aforementioned formula reduces to the steady state master-like equation [199, 201]

$$\left[\widetilde{\mathbf{W}}\mathbf{p}^{\mathrm{st}}\right]_{\chi} = \Gamma\delta_{\chi\chi_0}\,, \tag{5.4}$$

where $\mathbf{p}^{\mathrm{st}} = \lim_{t\to\infty}\mathbf{p}(t) = \lim_{t_0\to-\infty}\mathbf{p}(0)$ is the stationary probability vector, independent of initial distribution. On the other hand, $\widetilde{\mathbf{W}}$ denotes the Laplace transform of the self-energy matrix $\mathbf{W}(t',t)$, whose one arbitrary row χ_0 has been replaced with $(\Gamma,\ldots,\Gamma)$ to include the normalization condition for the probabilities $\sum_\chi p_\chi^{\mathrm{st}} = 1$.

5.1.1 The tunneling current and crossover perturbation scheme

Knowing the probabilities, the electric current flowing through the system can be calculated from the formula [201]

$$I = \frac{e}{2\hbar}\mathrm{Tr}\left[\mathbf{W}^I\mathbf{p}^{\mathrm{st}}\right]\,, \tag{5.5}$$

where the matrix $\mathbf{W}^I$ denotes the self-energy matrix in which one internal vertex has been substituted with an external vertex for the current operator.

In order to calculate the transport quantities in both the deep Coulomb blockade and the sequential tunneling regime in each order in tunneling processes (the coupling strength $\Gamma \propto |T_{L(R)}|^2$), the perturbation expansion in Γ adopting the so-called *crossover perturbation scheme* is performed [203]. This scheme allows a smooth transition through the threshold voltage range where sequential tunneling processes start dominating over higher order tunneling processes, which are playing a leading role in the Coulomb blockade regime. The general idea of the crossover scheme relies on solving the master equation with first- and second-order self-energies, without expanding the probabilities, i.e. one

only expands the self-energy matrices,

$$\widetilde{\mathbf{W}} = \sum_{n=1}^{\infty} \widetilde{\mathbf{W}}^{(\mathrm{n})} \quad \text{and} \quad \mathbf{W}^{I} = \sum_{n=1}^{\infty} \mathbf{W}^{I(n)}. \tag{5.6}$$

Here, the first-order of expansion ($n = 1$) corresponds to sequential tunneling processes, while the second-order contribution ($n = 2$) is associated with cotunneling processes. In the present calculations both the first- and second-order diagrams are taken into account, which allows me to resolve the transport properties in the *full* weak coupling regime, i.e. in the cotunneling as well as in the sequential tunneling regimes. Furthermore, by considering the $n = 1$ and $n = 2$ terms of the expansion, the effects of LUMO level renormalization, cotunneling-assisted sequential tunneling, as well as effects associated with an exchange field exerted by ferromagnetic leads on the molecule are systematically included [203–205]. For $n \leq 2$, the stationary probabilities can be found from Eq. (5.4),

$$\left[\left(\widetilde{\mathbf{W}}^{(1)} + \widetilde{\mathbf{W}}^{(2)}\right)\mathbf{p}^{\mathrm{st}}\right]_{\chi} = \Gamma\delta_{\chi\chi_0}\,. \tag{5.7}$$

On the other hand, the current is explicitly given by the sum of two terms representing the current I_{sq} due to sequential tunneling processes and the current I_{cot} resulting from cotunneling of electrons,

$$I = I_{\mathrm{sq}} + I_{\mathrm{cot}} = \frac{e}{2\hbar}\mathrm{Tr}\left[\mathbf{W}^{I(1)}\mathbf{p}^{\mathrm{st}}\right] + \frac{e}{2\hbar}\mathrm{Tr}\left[\mathbf{W}^{I(2)}\mathbf{p}^{\mathrm{st}}\right]. \tag{5.8}$$

The key problem is now the somewhat lengthy but straightforward calculation of the respective self-energy matrices, which can be done using the corresponding diagrammatic rules [194,201,203]. An example of explicit formula for a second-order self-energy between arbitrary states $|\chi\rangle$ and $|\chi'\rangle$ can be found in Ref. [206].

5.1.2 The low frequency current noise

With recent progress in detection of ultra-small signals, it has become clear that the information about the system transport properties can also be extracted from the measurement of current noise [207]. In fact, the shot noise contains information about various correlations, coupling strengths, effective charges, etc., which is sometimes unaccessible just from measurements of electric current. Therefore, to make the analysis more self-contained, the zero-frequency shot noise is also calculated and discussed.

The *shot noise* is usually defined as the correlation function of the current operators, and its Fourier transform in the limit of low frequencies is given by [207]

$$S = 2\int_{-\infty}^{0} \mathrm{d}t\big[\langle I(t)I(0) + I(0)I(t)\rangle - 2\langle I\rangle^2\big]. \tag{5.9}$$

For $|eV| > k_{\mathrm{B}}T$, the current noise is dominated by fluctuations associated with the discrete nature of charge (shot noise), while for low bias voltages, the thermal noise

dominates [207].

Before putting down the general formula for the current noise within the language of real-time diagrammatic technique, it's instructive to note that the expression for the shot noise, Eq. (5.9), involves products of two current operators at different times. It means that such two current operators can appear either in one block $\mathbf{W}^{II}$, where two internal vertices have been replaced by external vertices for the current operator, or in two blocks $\mathbf{W}^{I}$. As a result, the current noise can be written as [201, 208]

$$S = \frac{e^2}{\hbar}\mathrm{Tr}\left[\mathbf{W}^{II}\mathbf{p}^{\mathrm{st}} + \mathbf{W}^{I}\mathbf{P}\mathbf{W}^{I}\mathbf{p}^{\mathrm{st}}\right], \tag{5.10}$$

with the matrix $\mathbf{P}$ given by

$$\mathbf{P} = \frac{1}{\hbar}\int_{-\infty}^{0} \mathrm{d}t\big[\mathbf{\Pi}(0,t) - \mathbf{\Pi}(0,-\infty)\big]. \tag{5.11}$$

Here, the constant propagator $\mathbf{\Pi}(0,-\infty)$ results from the term $\langle I\rangle^2$ in Eq. (5.9), and it ensures the convergence of the integral. Furthermore, applying the crossover perturbation scheme in an analogous manner as in the preceding section, one can decompose the total current noise, Eq. (5.10), into a sum of two terms representing different order of tunneling processes, $S = S_{\mathrm{sq}} + S_{\mathrm{cot}}$,

$$S_{\mathrm{sq}} = \frac{e^2}{\hbar}\mathrm{Tr}\left[\mathbf{W}^{II(1)}\mathbf{p}^{\mathrm{st}} + \mathbf{W}^{I(1)}\mathbf{P}\mathbf{W}^{I(1)}\mathbf{p}^{\mathrm{st}}\right], \tag{5.12}$$

$$\begin{aligned} S_{\mathrm{cot}} = \frac{e^2}{\hbar}\mathrm{Tr}\Big[&\mathbf{W}^{II(2)}\mathbf{p}^{\mathrm{st}} + \mathbf{W}^{I(2)}\mathbf{P}\mathbf{W}^{I(2)}\mathbf{p}^{\mathrm{st}} \\ &+\mathbf{W}^{I(1)}\mathbf{P}\mathbf{W}^{I(2)}\mathbf{p}^{\mathrm{st}} + \mathbf{W}^{I(2)}\mathbf{P}\mathbf{W}^{I(1)}\mathbf{p}^{\mathrm{st}}\Big]. \end{aligned} \tag{5.13}$$

The outline of the derivation, and also the most general expression for the noise S, can be found in Refs. [202, 208].

5.2 Basic transport characteristics: differential conductance and TMR

In order to discuss transport properties of a SMM, numerical results on charge current, differential conductance, shot noise and *tunnel magnetoresistance* (TMR) in the *linear* and *nonlinear response* regimes are presented in the remaining part of this chapter. Moreover, I should note that instead of current shot noise, I will rather consider the *Fano factor*,

$$F = \frac{S}{2e|I|}, \tag{5.14}$$

which describes deviation of the current noise from its Poissonian value, $S_P = 2e|I|$, characteristic of uncorrelated in time tunneling processes. On the other hand, the TMR

represents a change of transport properties when magnetic configuration of the device varies from antiparallel to parallel alignment – the conductance is usually larger in the parallel configuration and smaller in the antiparallel one, although opposite situation is also possible. The TMR is defined usually as [182, 203, 209]

$$\mathrm{TMR} = \frac{I_{\mathrm{P}} - I_{\mathrm{AP}}}{I_{\mathrm{AP}}}\,, \tag{5.15}$$

where I_{P} (I_{AP}) is the current flowing through the system in the parallel (antiparallel) magnetic configuration at a constant bias voltage V.

Contrary to the previous chapter, where I presented the results for the case of a Mn_{12} molecule ($S = 10$), here, numerical results have been obtained for a hypothetical SMM characterized by the spin number $S = 2$.[1] However, it should be emphasized that although in the following I assume $S = 2$, the considerations are still quite general and qualitatively valid for molecules with larger spin numbers. In fact, the choice of low molecule's spin allows performing a detailed analysis of various molecular states mediating the first and second-order tunneling processes that determine the transport properties. In the case of a greater spin number S, a much larger number of molecular states would make the discussion rather obscure. Apart from this, a symmetrical coupling of the molecule to the two external leads ($P_L = P_R = P$) and ferromagnetic exchange coupling between the molecule's magnetic core and electrons in the LUMO level is assumed. Later on, however, these restrictions will be relaxed and I will consider the situation where the exchange coupling is antiferromagnetic and also the case when one electrode is nonmagnetic while the other one is ferromagnetic. For clarity reasons, I neglect the role of the electron charge sign, i.e. assume that charge current and particle (electron) current flow in the same direction ($e > 0$).

To start the discussion, I first present some basic transport characteristics of the system under consideration. In Fig. 5.2 the differential conductance in the parallel and antiparallel configurations as a function of the bias voltage and position of the LUMO level is shown. The latter can be experimentally changed by sweeping the gate voltage. The density plot of the conductance displays the well-known Coulomb diamond pattern. The average charge accumulated in the LUMO level is

$$Q = \sum_{\chi} n(\chi) p_{\chi}^{\mathrm{st}} \quad \text{(in the units of } e\text{)}, \tag{5.16}$$

where $n(\chi) = 0, 1, 2$ denotes the number of additional electrons on the molecule in the state $|\chi\rangle$. With lowering energy of the LUMO level, the level becomes consecutively occupied with electrons. This leads in turn to forming two peaks in the linear conductance, separated approximately by U, which correspond to single and double occupancy, respectively, see Fig. 5.2 for $V = 0$.

Furthermore, in the nonlinear response regime, and outside the Coulomb blockade region, the differential conductance shows additional lines due to tunneling through excited

[1] Note that the assumption concerning the strong uniaxial magnetic anisotropy still holds.

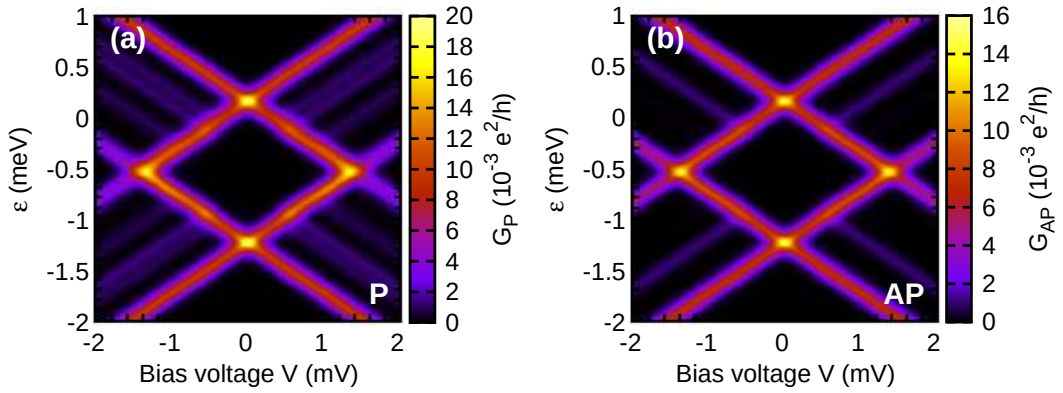

Figure 5.2: The total (first plus second order) differential conductance in the *parallel* (a) and *antiparallel* (b) configurations for the parameters: $S = 2$, $J = 0.2$ meV, $D = 0.05$ meV, $D_1 = -0.005$ meV, $D_2 = 0.002$ meV, $U = 1$ meV, $k_{\mathrm{B}}T = 0.04$ meV, $P_L = P_R = 0.5$, and $\Gamma = 0.002$ meV.

states of the molecule. These features are visible in both magnetic configurations. On the other hand, the hallmark of spin-depended tunneling is the difference in magnitude of the conductance in parallel and antiparallel configurations – the conductance in the parallel configuration is generally larger than in the antiparallel one, see Fig. 5.2. This difference is due to spin asymmetry of tunneling processes, which leads to suppression of the conductance when configuration changes from parallel to antiparallel one. Moreover, the difference between these two configurations strongly depends on spin polarization of the leads. For example, in the case of half-metallic ferromagnetic leads, the conductance in antiparallel alignment may be totally suppressed leading to a huge TMR.

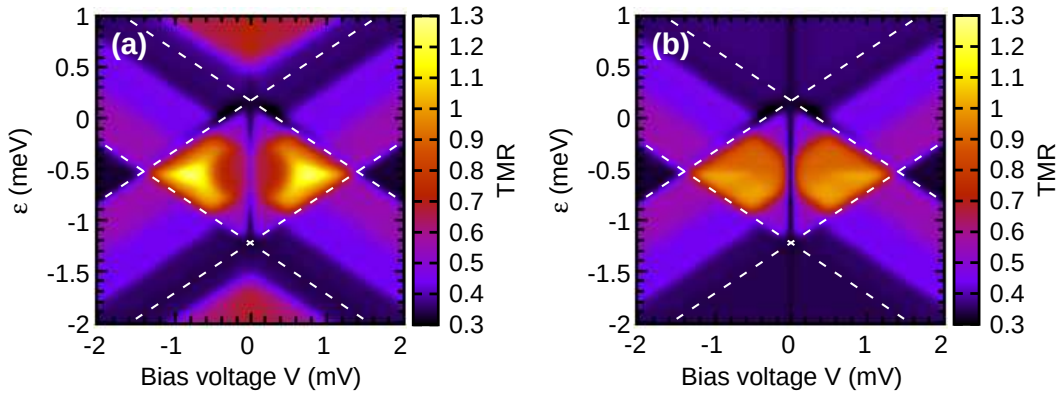

Figure 5.3: Density plot of the *total* (first plus second order) TMR (a) and TMR calculated in the *sequential tunneling approximation* (b) plotted in the same scale and for the same parameters as in Fig. 5.2. The sequential TMR is smaller than the total TMR. The dashed lines are only a guide for eyes, and they represent positions of the main conductance peaks, Fig. 5.2, separating thus regions corresponding to different occupation states of the LUMO level.

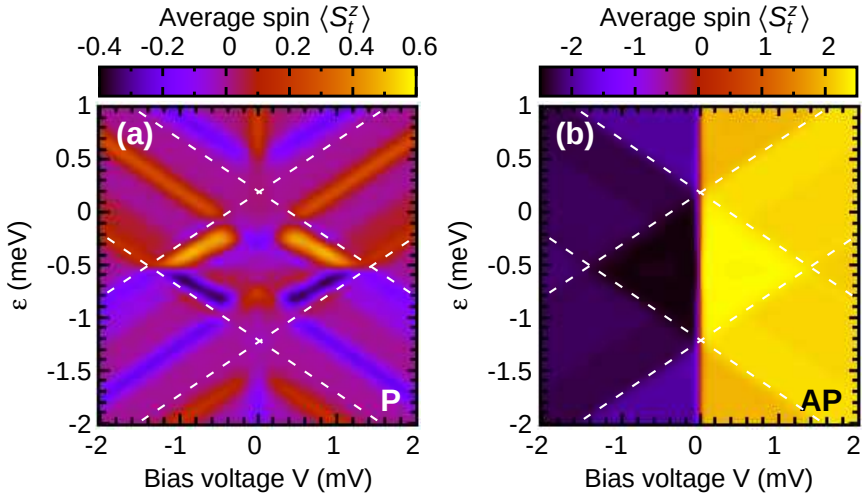

Figure 5.4: The average value of the zth component of the molecules's total spin $\langle S_t^z \rangle$ for the *parallel* (a) and *antiparallel* (b) magnetic configurations. All parameters as in Fig. 5.2.

Another aforementioned quantity characterizing transport through a SMM to be considered here is the TMR, whose density plot corresponding to Fig. 5.2 is shown in Fig. 5.3(a). The first notable feature of TMR is that its magnitude strongly depends on the transport regime. More precisely, TMR can range from approximately TMR $\approx P^2/(1-P^2) = 1/3$ (for $P = 0.5$), which is characteristic of sequential tunneling regime where all states of the LUMO level are active in transport [203], to roughly twice the value resulting from the *Julliere model* [209], TMR $\approx$ TMR$^{\text{Jull.}} = 4P^2/(1-P^2) = 4/3$, which can be observed in the nonlinear response regime of the Coulomb blockade diamond ($Q = 1$), see Fig. 5.3(a). For comparison, in Fig. 5.3(b) the TMR calculated using only the sequential tunneling processes is displayed. One can see that the first-order TMR is generally smaller than the total (first plus second order) TMR. Furthermore, it is also clear that the second-order tunneling processes modify TMR mainly in the Coulomb blockade regime ($Q = 1$) as well as in the cotunneling regimes where the LUMO level is either empty ($Q = 0$) or doubly ($Q = 2$) occupied. On the other hand, out of the cotunneling regime, the sequential processes dominate transport and the role of second-order tunneling is relatively small. As a consequence, the two results become then comparable, see Fig. 5.3(a) and Fig. 5.3(b).

As already shown in Chapter 4, spin-dependent transport through a SMM has a significant impact on its magnetic state. In Fig. 5.4 the average value of the molecule's spin zth component in the stationary state, $\langle S_t^z \rangle$, calculated as a function of the bias voltage V and energy of the LUMO level ε, is shown. In the *antiparallel* magnetic configuration, Fig. 5.4(b), the orientation of the molecule's spin is straightforwardly related to the bias voltage, and for $V > 0$ the spin is aligned along the easy axis $+z$, whereas for $V < 0$ it is aligned along the $-z$ axis. Note that in the regions corresponding to $Q = 0$ and $Q = 2$ the spin is equal to that of magnetic core, while for $Q = 1$ it also includes the

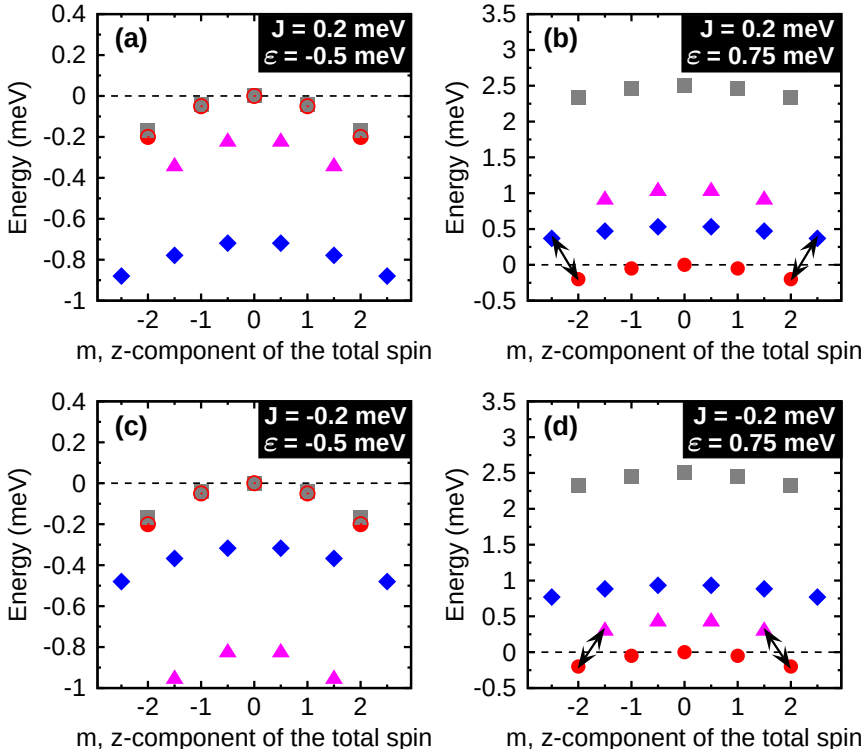

Figure 5.5: Energy spectrum of the molecule under consideration (relevant parameters given in the caption of Fig. 5.2) for $\varepsilon = -0.5$ meV (a,c) and $\varepsilon = 0.75$ meV (b,d) in the case of *ferromagnetic* (a)-(b) and *antiferromagnetic* (c)-(d) coupling between the SMM's core spin and the spin of electrons in the LUMO level. The dashed line symbolizes the Fermi level of the leads when no external voltage bias is applied ($V = 0$). Different sets of molecular states correspond to different values of the SMM's total spin S_t, and/or the occupation number of the LUMO level: $|2;0,m\rangle$ (●), $|5/2;1,m\rangle$ (♦), $|3/2;1,m\rangle$ (▲), and $|2;2,m\rangle$ (■). Note that in (a) and (c) the degeneracy between states $|2;0,m\rangle$ and $|2;2,m\rangle$ takes place only for $m = 0$.

contribution from an electron in the LUMO level. By contrast, in the *parallel* configuration, Fig. 5.4(a), the value of $\langle S_t^z \rangle$ in the stationary state can be both positive and negative for each sign of the bias voltage, and it varies in a rather limited range close to zero. Moreover, $\langle S_t^z \rangle$ in the parallel (antiparallel) magnetic configuration is an even (odd) function of the bias voltage V.

In order to account for the transport properties in different regimes, especially of TMR and shot noise, in the following two sections I will present and discuss the gate and bias voltage dependence corresponding to various cross-sections of the relevant density plots mentioned above. More specifically, I will first consider transport properties in the *linear response* regime (Section 5.3), and then transport in the *nonlinear* regime (Section 5.4). In addition, whenever advisable and possible, I will also compare and relate my findings to existing results on quantum dot systems. At this point, it is however worth emphasizing that the problem of electron transport through a SMM is much more complex and physically richer than in the case of single quantum dots [210]. This is because now

the transfer of electrons occurs through many different many-body states of the coupled LUMO level and molecule's magnetic core, see Eq. (2.5).

Because transport properties of a system are determined by its energy spectrum, it may be instructive to recall here some basic ideas from Chapter 2. For molecules with only uniaxial anisotropy considered in this thesis, the molecule's Hamiltonian $\mathcal{H}_{\mathrm{SMM}}$ can be diagonalized analytically, Section 2.4. Energy spectrum of the molecule under consideration is presented in Fig. 5.5 for two different values of the LUMO level energy ε and two values of the coupling parameter J. Each molecular state $|S_t; n, m\rangle$ is then labelled by the total spin number S_t, the occupation number n of the LUMO level, and the eigenvalue m of the zth component of the molecule's total spin, $S_t^z \equiv S_z + \frac{1}{2}(c_\uparrow^\dagger c_\uparrow - c_\downarrow^\dagger c_\downarrow)$, where the second term stands for the contribution coming form electrons in the LUMO level. The change of the LUMO level energy leads to the change in the energetic position of the spin-multiplets $|5/2; 1, m\rangle$, $|3/2; 1, m\rangle$ and $|2; 2, m\rangle$ with respect to $|2; 0, m\rangle$. The latter multiplet corresponds to uncharged molecule and therefore is independent of ε, see Fig. 5.5.

5.3 Transport in the linear response regime

As it has already been mentioned above, conductance in the *linear response* regime (see Fig. 5.2 for $V = 0$), displays two resonance peaks separated approximately by U. For $J > 0$ and $D(2S-1) \gg k_{\mathrm{B}}T$, one can assume that the molecule is in the spin states of lowest energy. The position of the conductance peaks (resonances) corresponds then to $\varepsilon = \varepsilon_{01}$,

$$\varepsilon_{01} = \frac{JS}{2} + D_1 S^2 + \frac{g\mu_{\mathrm{B}}|H_z|}{2}, \tag{5.17}$$

for the transition from zero to single occupancy of the LUMO level, and to $\varepsilon = \varepsilon_{12}$,

$$\varepsilon_{12} = -\frac{JS}{2} - U + (D_1 + D_2)S^2 - \frac{g\mu_{\mathrm{B}}|H_z|}{2}, \tag{5.18}$$

for the transition from single to double occupancy. It is worth noting that the above expressions may be useful for estimating the coupling constant J from transport measurements. Moreover, from the above formulas one can conclude that the middle of the Coulomb blockade ($Q = 1$ in Fig. 5.2) regime corresponds to $\varepsilon = \varepsilon_m$, with

$$\varepsilon_m = -\frac{U}{2} + \frac{2D_1 + D_2}{2} S^2\,, \tag{5.19}$$

which for the parameters assumed in calculations gives $\varepsilon_m = -0.516$ meV. Interestingly, ε_m is independent of the exchange coupling J, anisotropy constant D, and external magnetic field H_z, but it depends on the Coulomb interaction U, corrections D_1 and D_2 to the anisotropy due to finite occupation of the molecule, and the molecule's spin number S. In fact, owing to finite constants D_1 and D_2, the particle-hole symmetry is broken, which manifests itself in an asymmetric behavior of transport properties, as will be shown below.

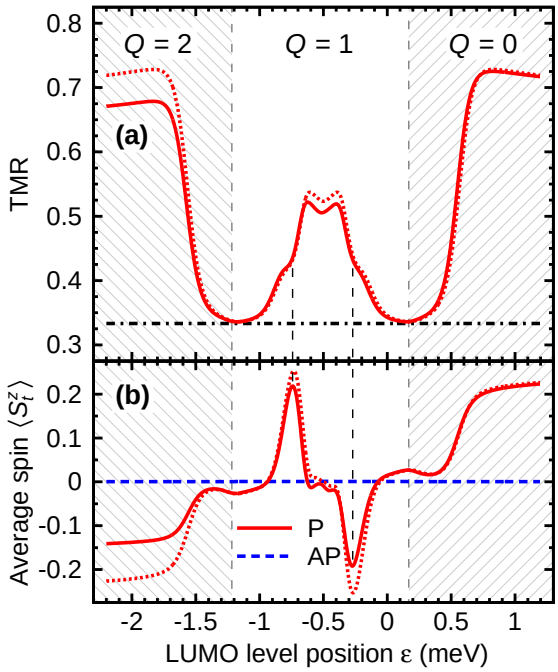

Figure 5.6: (a) TMR in the *linear response* regime for the parameters as in Fig. 5.2 (solid line). The dot-dashed line shows the TMR calculated in the first-order approximation. (b) Average value of the zth component of the molecule's total spin in the (P) *parallel* (solid line) and (AP) *antiparallel* (dashed line) magnetic configurations. The dotted lines in (a) and (b) correspond to the case of $D_1 = D_2 = 0$.

The total TMR in the linear response regime is shown in Fig. 5.6(a), where for comparison TMR in the sequential transport regime is also displayed (dash-dotted line). Clearly, the results obtained within the sequential tunneling approximation, which yields a constant TMR equal to $P^2/(1-P^2)$, are not sufficient as the total (first plus second order) linear TMR displays a nontrivial dependence on the gate voltage (LUMO level position). This behavior in fact stems from the dependence of the amount and type of second-order processes on the occupation number of the LUMO level.

5.3.1 Cotunneling regime with empty and doubly occupied LUMO level

Let's start from considering the situation when the LUMO level is either empty ($Q = 0$) or fully occupied ($Q = 2$). In such a case, the TMR in the corresponding cotunneling regions is slightly larger than the Julliere value, [209] $\mathrm{TMR}^{\mathrm{Jull.}} = 2P^2/(1-P^2)$ ($\mathrm{TMR}^{\mathrm{Jull.}} = 2/3$ for $P = 0.5$), see Fig. 5.6(a). Electron transport in these two regions is primarily due to elastic cotunneling processes which change neither the electron spin in the LUMO level nor the spin of molecule's core, and thus are fully coherent. An example of such process is sketched in Fig. 4.13(a). The enhancement of TMR above the Julliere value is then associated with the exchange coupling of the LUMO level to the molecule's core spin, which additionally admits inelastic cotunneling processes in these

regions. In addition, the enhanced TMR may also result from the fact that by using the *crossover* perturbation scheme [203], I also include some effects associated with third-order processes, which may further increase the TMR. Moreover, unlike the case of a single quantum dot [203,210], the maximal values of TMR reached for $Q = 0$ and $Q = 2$ do not necessarily have to be equal, see Fig. 5.6(a). To account for this asymmetry and the enhanced TMR, let's have a closer look at various elastic and inelastic cotunneling processes which affect the spin state of the molecule.

At low temperatures, a free-standing SMM (decoupled from electrodes, $Q = 0$) is with equal probabilities in one of the two states $|2;0,\pm 2\rangle$ of the lowest energy, Fig. 5.5(b). As the molecule becomes coupled to the electron reservoirs, the initial spin state of the molecule can be changed as a result of inelastic cotunneling, see Fig. 4.13(c). In the parallel magnetic configuration, inelastic transitions increasing (decreasing) the zth component of the SMM's spin are associated with transfer of electrons from spin majority (minority) to spin minority (majority) bands of the leads, and thus are of comparable probabilities for both spin orientations. However, due to exchange coupling between the LUMO level and molecules's core, there is a small difference in energy of virtual states with one spin-up or spin-down electron in the LUMO level. In consequence, the processes increasing zth component of the SMM's spin are initially slightly more probable, which in turn implies that the probability of finding the molecule in the state $|2;0,2\rangle$ is a little larger than in the state $|2;0,-2\rangle$. Thus, the average value of molecule's spin $\langle S_t^z\rangle$ is positive, see Fig. 5.6(b), although rather small. In the antiparallel configuration, on the other hand, the situation is significantly different. As follows from Fig. 5.4(b), the limit of $V = 0$ corresponds to the border between regions in which the molecule is fully magnetized in opposite directions. Thus, one can expect that the zth component of the molecule's spin vanishes in the linear response limit. Indeed this is the case, as shown in Fig. 5.6(b), and can be explained by taking into account spin asymmetries of cotunneling processes, similarly as for the parallel configuration.

The above discussion on the influence of inelastic cotunneling processes on the magnetic state of a SMM can now be useful to account for the enhanced TMR. From the energy spectrum displayed in Fig. 5.5(b) it follows that the dominant elastic transfer of electrons between the leads for $Q = 0$ takes place *via* the following virtual transitions: $|2;0,-2\rangle \leftrightarrow |5/2;1,-5/2\rangle$ and $|2;0,2\rangle \leftrightarrow |5/2;1,5/2\rangle$ [indicated with black arrows in Fig. 5.5(b)]. In the parallel configuration, the former transitions establish the transport channel for minority electrons, whereas the latter ones for majority electrons. The asymmetry between the occupation probabilities of the states $|2;0,-2\rangle$ and $|2;0,2\rangle$, where $|2;0,2\rangle$ is favored (as discussed above) gives rise to increased transport of majority electrons. On the other hand, there is no such asymmetry in the antiparallel configuration. This, in turn, leads to an enhancement of the TMR above the Julliere value, Fig. 5.6(a).

Similar analysis can be performed for the case of $Q = 2$, where the molecular states $|2;2,m\rangle$ correspond to double occupancy of the molecule's LUMO level. The fundamental difference compared to the situation discussed above ($Q = 0$) is that now an electron leaves the molecule in the virtual state, Fig. 4.13(d). Analysis similar to that

for $Q = 0$ shows that in the parallel configuration the inelastic cotunneling processes result in lowering of the zth component of the SMM's spin, see Fig. 5.6(b). Moreover, the asymmetry between the occupation probabilities of the states $|2; 2, -2\rangle$ and $|2; 2, 2\rangle$, where now $|2; 2, -2\rangle$ is favored, leads to increased elastic cotunneling of spin majority electrons and therefore gives rise to enhanced TMR for $Q = 2$.

Further analysis of Fig. 5.6(a) reveals another interesting feature of TMR in the linear response regime, i.e. the difference in its magnitude in the cotunneling regions corresponding to $Q = 0$ and $Q = 2$. This is contrary to the case of Anderson model, where the linear TMR was found to be symmetric with respect to the particle-hole symmetry point, $\varepsilon = -U/2$, seeRef. [203]. In the case considered here, the situation is different due to coupling of the LUMO level to the molecule's spin, and also due to occupation dependent corrections to the anisotropy constant, see Eq. (2.5). These corrections reduce the uniaxial anisotropy of the molecule with increasing number of electrons in the LUMO level. As a result, the height of the energy barrier between the two lowest molecular spin states is also diminished for $Q = 1$ and $Q = 2$, and so are the energy gaps between neighboring molecular states within the relevant spin multiplets. For this reason, the probability distribution of the molecular states for $Q = 2$ (and also for $Q = 1$) is more uniform than for $Q = 0$, see the solid line in Fig. 5.6(b). Consequently, the value of TMR for $Q = 2$ is smaller than for $Q = 0$. Thus, the observed asymmetry with respect to $\varepsilon = \varepsilon_m$ is due to the lack of particle-hole symmetry in the system when D_1 and D_2 are nonzero. However, if the influence of the LUMO level's occupation on the anisotropy were negligible, $D_1 \approx D_2 \approx 0$ (the states $|2; 0, m\rangle$ and $|2; 2, m\rangle$ in Fig. 5.5(a) were then degenerate for every m), the symmetry with respect to $\varepsilon = \varepsilon_m = -U/2$ would be restored. This situation is presented by the dotted curves in Fig. 5.6, which clearly show that the asymmetric behavior of TMR and $\langle S_t^z \rangle$ is related to the corrections to anisotropy constants and the lack of particle-hole symmetry.

5.3.2 Cotunneling regime with singly occupied LUMO level

Even more interesting behavior of the TMR is observed in the Coulomb blockade regime with one electron in the LUMO level, $Q = 1$, the TMR reaches local maxima close to the center of the Coulomb gap, and a local minimum just in the middle, i.e. for $\varepsilon = \varepsilon_m$. This behavior is opposite to that observed in single-level quantum dots, where linear TMR in the Coulomb blockade regime becomes suppressed and reaches a minimum when $\varepsilon = -U/2$, as shown in Ref. [203]. As in the case of $Q = 0$ and $Q = 2$ discussed above, the origin of increased TMR for $Q = 1$ can be generally assigned to the modification of the probability distribution of molecular states due to inelastic cotunneling processes, Fig. 4.13(b). In turn, the appearance of the local minimum in the center of the $Q = 1$ region is related to the fact that when $\varepsilon = \varepsilon_m$, the virtual states for leading inelastic cotunneling processes, which belong to spin multiplets $|2; 0, m\rangle$ and $|2; 2, m\rangle$, become pairwise degenerate (in the present situation, $|2; 0, \pm 2\rangle$ with $|2; 2, \pm 2\rangle$). This means that in the parallel configuration cotunneling processes involving empty and doubly occupied virtual states occur at equal rates. As a consequence, the average spin on the molecule

tends to zero, see Fig. 5.6(b), and TMR displays a local minimum for $\varepsilon = \varepsilon_m$.

It turns out that in the situation under consideration the sequential tunneling processes play a dominant role only for resonant energies, Eqs. (5.17)-(5.18), where the occupancy Q of the molecule changes. This results in the reduction of TMR to approximately half of the Julliere value [209], see the boundaries between the hatched and non-hatched areas in Fig. 5.6. The rate of first-order tunneling processes increases whenever the two neighboring charge states of the molecule become degenerate, provided that the conditions $|\Delta n| = 1$ and $|\Delta S_t^z| = 1/2$ are simultaneously satisfied, where $|\Delta n|$ and $|\Delta S_t^z|$ describe change in the occupation and spin of the molecule. This means that for $\varepsilon = \varepsilon_{01} \approx 0.18$ meV the degeneration between the empty and singly occupied states, $|2;0;\pm 2\rangle$ and $|5/2;1,\pm 5/2\rangle$, is observed, whereas for $\varepsilon = \varepsilon_{12} \approx -1.21$ meV the states with a single and two electrons on the LUMO level, $|5/2;1,\pm 5/2\rangle$ and $|2;2;\pm 2\rangle$, are degenerate. Moreover, note also that for $\Gamma \approx k_B T$, TMR can be reduced further due to increased role of second-order processes giving rise to the renormalization of the LUMO level [203].

5.4 Transport in the nonlinear response regime

As the bias voltage increases and one goes beyond the Coulomb blockade regime, the influence of sequential tunneling on transport characteristics, as well as on magnetic state of the SMM, becomes more evident. Figure 5.7 shows the bias dependence of current, differential conductance, TMR and Fano factor, calculated for $\varepsilon = -0.5$ meV and $\varepsilon = 0.75$ meV. The former case corresponds to the situation where the LUMO level in equilibrium is singly occupied, Fig. 5.5(a), while in the latter case it is empty, Fig. 5.5(b). The sequential tunneling is exponentially suppressed in the blockade regions, and the current flows then mainly due to the second-order cotunneling events. The inclusion of the latter processes is crucial for a proper description of transport behavior in the blockade regime, where the cotunneling processes significantly modify the first-order results, as one can see in Fig. 5.7, and this modification is most pronounced for TMR and shot noise.

5.4.1 Transport characteristics in the case of a singly occupied LUMO level in equilibrium

Let's consider first the case when in equilibrium the LUMO level is *singly* occupied, i.e. $\varepsilon_{01} > \varepsilon > \varepsilon_{12}$ (left panel of Fig. 5.7). At low temperatures and low voltages, the molecule with almost equal probabilities is in one of the two ground states $|5/2;1,\pm 5/2\rangle$, Fig. 5.5(a). When a small bias voltage is applied, some current flows due to cotunneling processes through virtual states of the system. If the bias voltage exceeds threshold for sequential tunneling, the current significantly increases and becomes dominated by first-order processes, when electrons tunnel one-by-one through the molecule. As discussed in Section 4.1, the spin state of the molecule can be changed by current due to a direct angular momentum transfer between the tunneling electrons and the molecule's spin

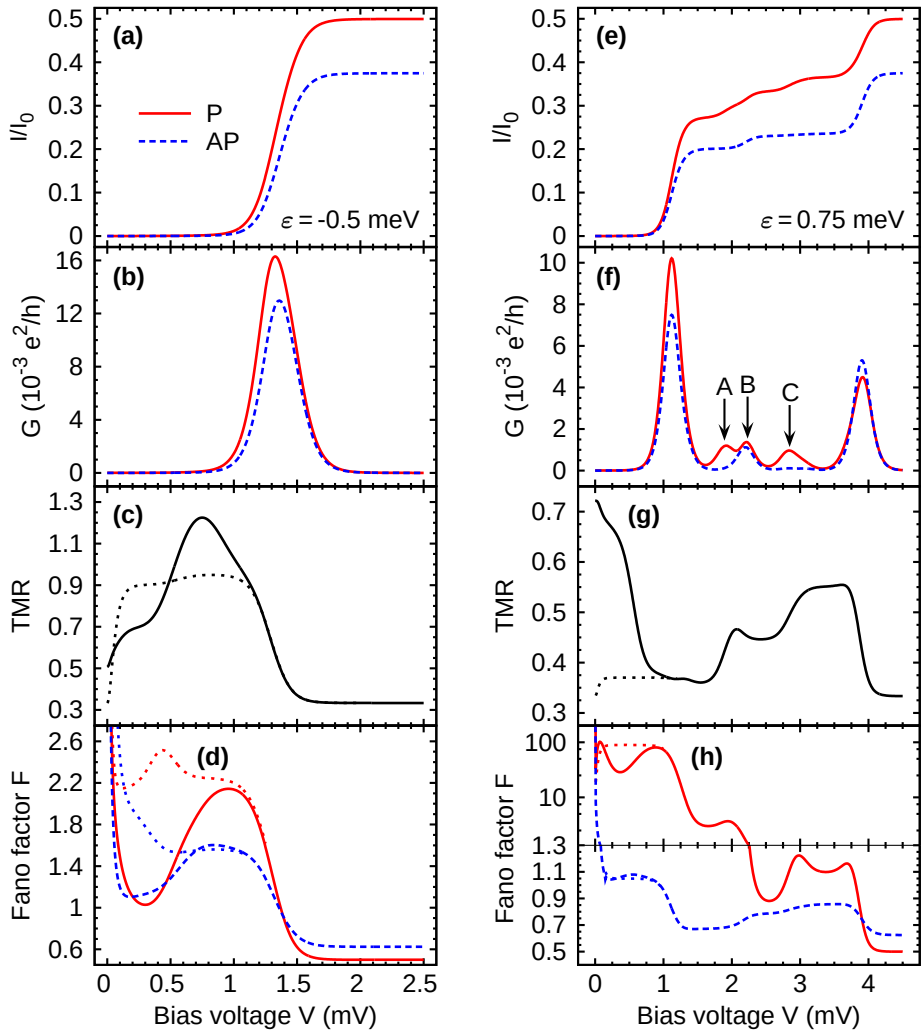

Figure 5.7: Bias dependence of the current (a,e), differential conductance (b,f), Fano factor (d,h) in the *parallel* (solid lines) and *antiparallel* (dashed lines) configurations and TMR (c,g) for $\varepsilon = -0.5$ meV (a)-(d) and $\varepsilon = 0.75$ meV (e)-(h). The parameters are the same as in Fig. 5.2, and $I_0 = e\Gamma/\hbar \approx 0.5$ nA. The dotted lines show the results obtained taking into account only first-order tunneling processes. The effect of cotunneling is most pronounced in the TMR and Fano factor.

(owing to the exchange interaction). In turn, transport of electrons through the system depends in a nontrivial way on its magnetic state. The general behavior of the molecule's spin is shown in Fig. 5.4. In the parallel magnetic configuration and for $\varepsilon = -0.5$ meV, the spin state of the molecule remains unchanged until $V \approx 0.34$ mV, where the Fermi level of the right electrode shifts below the states $|2; 2, \pm 2\rangle$, Fig. 5.4(a) (note that the voltage is applied symmetrically). Electrons can then tunnel sequentially *via* the LUMO level. Since spin-flip sequential tunneling processes with an electron from spin-majority band of the left electrode entering the LUMO level are slightly more probable than the other ones,

the molecule will be more often in the state $|5/2;1,5/2\rangle$. This results in a finite average spin of the molecule in the parallel configuration, although its value is relatively small, see Fig. 5.4(a). On the other hand, no such competition is observed in the antiparallel configuration, as transfer of electrons between the majority-spin bands of both electrodes implies that the molecule should be predominantly in the state $|5/2;1,5/2\rangle$. Therefore, for positive bias voltages the molecule's spin (including the contribution from electron in the LUMO level) becomes polarized along the $+z$ axis, see Fig. 5.4(b).

Since elastic cotunneling in the *antiparallel* configuration occurs essentially through the minority-majority and majority-minority channels, whereas for *paralle*l alignment through the majority-majority and minority-minority ones, one observes growth of TMR with increasing bias voltage, which reaches a local maximum just before the threshold for sequential tunneling. This is associated with nonequilibrium spin accumulation in the LUMO level for the antiparallel configuration, which leads to suppression of charge transport and thus to enhanced TMR. Further increase of transport voltage results in a decrease of TMR to approximately $1/3$ (for $P_L = P_R = 0.5$), which is typical of the sequential tunneling regime, when all molecular states actively participate in transport [203, 210]. In the parallel magnetic configuration each state is then equally populated, so that average magnetic moment of the molecule vanishes, $\langle S_t^z\rangle$=0. This differs from the antiparallel case, in which only the states with large positive zth component of the SMM's spin have finite probabilities. Finally, it is worth noting that the slight shift between the peaks in differential conductance corresponding to different magnetic configurations, see Fig. 5.7(b), is a consequence of nonequilibrium spin accumulation in the LUMO level in the antiparallel configuration. Similar behavior has been observed in the case of transport through ferromagnetic single-electron transistors [211].

In the end, to complete the current discussion, I consider also the Fano factor in the parallel ($F_{\rm P}$) and antiparallel ($F_{\rm AP}$) configurations, which is presented in Fig. 5.7(d). For low bias voltages, the shot noise is determined by thermal Johnson-Nyquist noise, which results in a divergency of the Fano factor for $V \to 0$ (current tends to zero). When a finite bias voltage is applied to the system, the Fano factor in both magnetic configurations drops to the value close to unity, which indicates that transport occurs mainly due to elastic cotunneling processes. Such processes are stochastic and uncorrelated in time, so the shot noise is Poissonian. When bias voltage increases further, the shot noise is enhanced due to bunching of inelastic cotunneling processes and reaches maximum just before threshold for sequential tunneling. At the threshold voltage, sequential tunneling processes start dominating transport and the noise becomes sub-Poissonian. This indicates that in the sequential tunneling regime, tunneling processes are correlated due to Coulomb correlation and Pauli principle, which generally gives rise to suppressed shot noise as compared to the Poissonian value. Furthermore, another feature clearly visible in the Coulomb blockade regime is the difference in Fano factors for parallel and antiparallel magnetic configurations. More specifically, shot noise in the parallel configuration is larger than in the antiparallel one. This is associated with the fact that in the parallel configuration transport occurs mainly through two competing channels

involving majority-majority and minority-minority spin bands, which in turn increases fluctuations, thus $F_{\mathrm{P}} > F_{\mathrm{AP}}$.

5.4.2 Transport characteristics for an empty LUMO level in equilibrium

Let's turn now to the situation corresponding to the *empty* LUMO level of the molecule in equilibrium ($\varepsilon > \varepsilon_{01}$),[2] which is shown in the right panel of Fig. 5.7. The initial large value of TMR, whose origin was discussed in the previous section, drops sharply as the bias voltage approaches the threshold value for sequential transport. The first pronounced peak in differential conductance appears when the following transitions become allowed: $|2;0,\pm2\rangle \leftrightarrow |5/2;1,\pm5/2\rangle$ [denoted by arrows is Fig. 5.5(b)]. It is important to note that, when a spin-multiplet enters the transport energy window, the first states that take part in transport are those with the largest $|\langle S_t^z\rangle|$ (lowest energy). Consequently, in the parallel magnetic configuration the system can be temporarily trapped in some molecular spin states of lower energy. This leads to $\langle S_z^t\rangle \neq 0$, see Fig. 5.4(a), and when $\langle S_t^z\rangle > 0$, it may result in an enhanced transport. Furthermore, as soon as all states within a certain spin-multiplet become energetically accessible, the probability of finding the molecule in each of these states becomes roughly equal. On the other hand, in the antiparallel configuration the system tends towards maximum value (for $V > 0$) of the zth component of SMM's spin. For these reasons, some regions of the increased TMR are present in Fig. 5.7(g).

One can also notice another interesting feature in differential conductance, Fig. 5.7(f), which in the sequential tunneling regime displays small peaks that can be observed in the parallel configuration, and some of them also in the antiparallel configuration. In general, these peaks are related to transitions involving states from the multiplet $|3/2;1,m\rangle$: $|2;0,\pm1\rangle \leftrightarrow |3/2;1,\pm3/2\rangle$ (A), $|2;0,\pm2\rangle \leftrightarrow |3/2;1,\pm3/2\rangle$ (B) and $|3/2;1,\pm3/2\rangle \leftrightarrow |2;2,\pm2\rangle$ (C), respectively, see Fig. 5.7(f). It should be noted that the energy gap corresponding to the transitions A/B is the smallest/largest gap between the spin-multiplets $|2;0,m\rangle$ and $|3/2;1,m\rangle$. In the parallel configuration all three peaks are visible, whereas for antiparallel alignment only the peak B can be clearly distinguished, which is a direct consequence of the probability distribution established in this configuration. Since in the antiparallel configuration tunneling processes tend to increase the zth component of the SMM's total spin, the probability of finding the molecule in any of the spin states $|2;0,m\rangle$ differs significantly from zero only for $m = 2$. As a consequence, in the antiparallel configuration most favorable transitions are those having the initial state $|2;0,2\rangle$, and thus the peaks A and C are suppressed, see Fig. 5.7(f).

Finally, the corresponding Fano factor is shown in Fig. 5.7(h). At low bias, the Fano factor drops with increasing voltage. However, its bias dependence is distinctively different in both magnetic configurations. In the antiparallel configuration, the Fano factor tends to unity, indicating that transport is due to uncorrelated tunneling events. In the parallel configuration, on the other hand, one observes large super-Poissonian shot noise. The increased current fluctuations result mainly from the interplay between different

[2] The relevant energy spectrum is presented in Fig. 5.5(b).

cotunneling processes and bunching of inelastic cotunneling. In addition, as mentioned previously, in the parallel configuration the molecule can be temporarily trapped in some molecular spin states of lower energy, which also gives rise to super-Poissonian shot noise. When the bias voltage is increased above the threshold for sequential tunneling, the Fano factor becomes suppressed and the shot noise is generally sub-Poissonian. Additionally, it is also worth noting that super-Poissonian shot noise in the cotunneling regime has already been observed in quantum dots and carbon nanotubes [210, 212–214], where the increased noise was associated with bunching of inelastic spin-flip cotunneling events.

5.5 Transport in the presence of a longitudinal external magnetic field

Up to this moment, all discussed effects have been considered under the assumption that no external magnetic field was present in the system. Now, I will analyze how the application of a finite magnetic field influences the already developed picture. When the field is along the easy axis of the molecule, its only effect is the modification of the energy of molecular spin states *via* the Zeeman term in Eq. (2.5). On the other hand, when the field possesses also a transversal component, the penultimate term on the right-hand side of Eq. (2.8), it leads to symmetry-breaking effects and the zth component of the SMM's total spin is no more a good quantum number [188]. If the magnetic field is additionally time-dependent, one can expect the phenomenon of quantum tunneling of magnetization to occur, as discussed in Chapter 3. Since the primary focus of the thesis is on transport through SMMs with only uniaxial anisotropy, in the following only a *longitudinal* magnetic field is considered.

The density plot of TMR for a magnetic field applied along the easy axis of a SMM is shown in Fig. 5.8(a). Despite rather modest value of the field (for comparison, in the experiment on the Mn_{12} molecule attached to nonmagnetic metallic electrodes by Jo *et al.*, the field of 8 T was used, Ref. [46]), a drastic change in transport properties of the system is observed [contrast Fig. 5.8(a) with Fig. 5.3(a)]. Not only does the field break the symmetry with respect to the bias reversal, but it allows for the situation when transport in the antiparallel magnetic configuration can be more effective than in the parallel one (black regions corresponding to negative TMR). Furthermore, the average spin $\langle S_t^z \rangle$ in the Coulomb blockade region can take large negative values, while in the absence of magnetic field the SMM's spin in the parallel configuration prefers orientation in the plane normal to the easy axis. This implies that the molecule's spin has tendency to orient almost antiparallel to the z-axis, Fig. 5.9(a). However, when the sequential tunneling processes are allowed, this tendency is generally reduced. In the antiparallel configuration, on the other hand, the behavior of the average molecule's spin is similar to that for $H_z = 0$, see Figs. 5.9(b) and 5.4(b).

In the *linear response* regime, a large change of TMR is observed when ε is comparable to ε_m, i.e. in the middle of the Coulomb blockade regime, see Fig. 5.8(b). This stems from the fact that at this point the dominating spin-dependent channel for transport

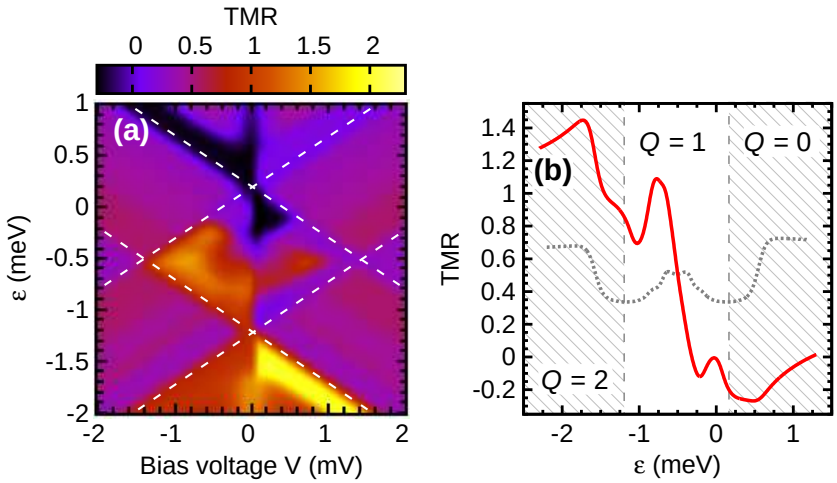

Figure 5.8: (a) Density plot of TMR in the case when an external magnetic field $H_z = 0.216$ T ($g\mu_B H_z = 0.025$ meV) is applied along the easy axis of the molecule. (b) TMR in the linear response regime (solid line). For comparison, TMR in the absence of external magnetic field (dotted line in (b)) is also shown. The other parameters are the same as in Fig. 5.2.

due to cotunneling processes in the parallel magnetic configuration switches from the minority-minority one (for $\varepsilon > \varepsilon_m$) to majority-majority channel (for $\varepsilon < \varepsilon_m$). In the antiparallel configuration, on the other hand, the dominant channel is rather associated with majority-minority spin bands, irrespective of the position of the LUMO level. As a consequence, for $\varepsilon > \varepsilon_m$ the current in the parallel configuration is smaller than that in the antiparallel one, leading to negative TMR, whereas for $\varepsilon < \varepsilon_m$ the situation is

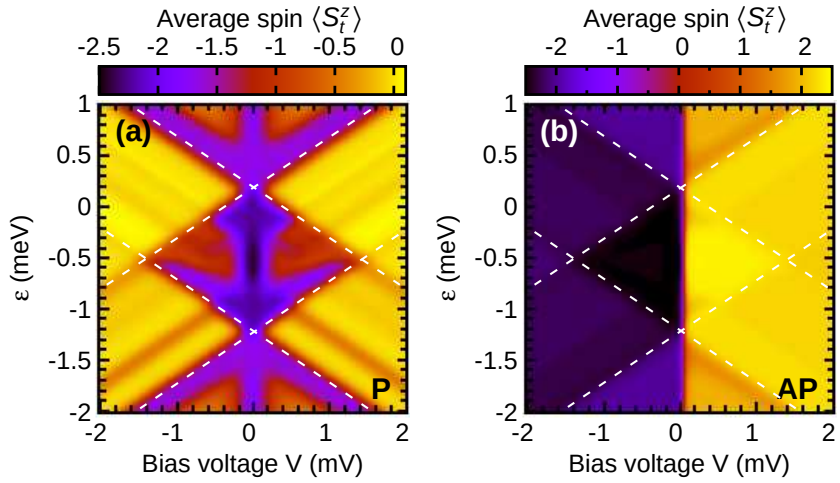

Figure 5.9: Average value of the zth component of the total molecule's spin in the parallel (a) and antiparallel (b) magnetic configurations, when an external field $H_z = 0.216$ T is applied along the z-axis. The other parameters are the same as in Fig. 5.2.

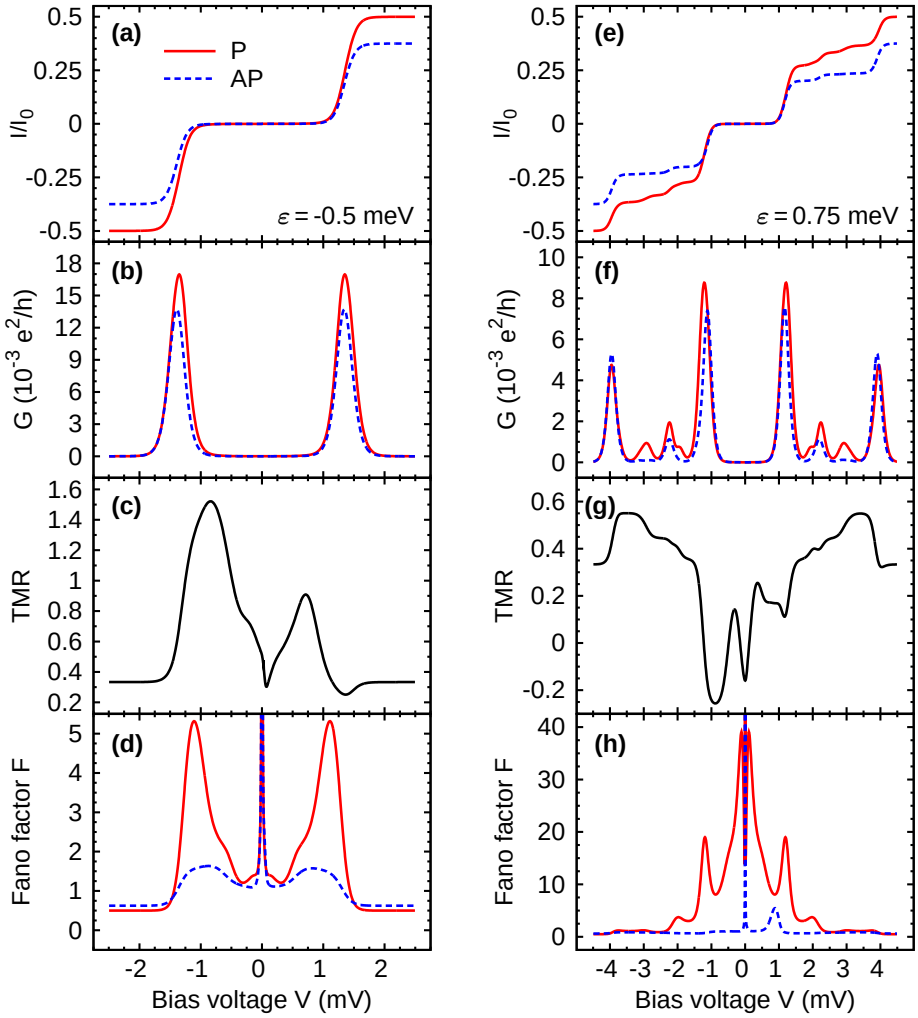

Figure 5.10: The current (a,e), differential conductance (b,f), Fano factor (d,h) in the *parallel* (solid lines) and *antiparallel* (dashed lines) configurations, and the TMR (c,g) for $\varepsilon = -0.5$ meV (a)-(d) and $\varepsilon = 0.75$ meV (e)-(h) as a function of the bias voltage. An external magnetic field $H_z = 0.216$ T is applied along the z-axis, while the other parameters are the same as in Fig. 5.2.

opposite and one finds a large positive TMR effect, see Fig. 5.8(b).

Figure 5.10 shows the transport characteristics in the *nonlinear response* regime, and in the presence of external magnetic field. The left (right) panel corresponds there to the situation where in the ground state the molecule is singly occupied (empty). The asymmetry with respect to the bias reversal is clearly visible, especially in the tunnel magnetoresistance, see Fig. 5.10(c) and (g). Interestingly, this asymmetric behavior is mainly observed in the cotunneling regime, as can be also seen in Fig. 5.8(a). This results from the fact that for $H_z \neq 0$ the degeneracy of the molecule's ground state is removed and SMM becomes polarized. In the cotunneling regime, transport depends mainly on the system's ground state, which is the initial state for the cotunneling processes. In ad-

dition, due to the Zeeman splitting, at low voltages only the elastic processes contribute, which gives rise to Poissonian shot noise, see Fig. 5.10(d). As a consequence, in the parallel configuration the current is always mediated by electrons belonging to the same spin bands of the leads, whereas in the antiparallel configuration, the dominant transport channel is associated either with majority or minority electrons, depending on the direction of the current flow. Thus, the current in the antiparallel configuration becomes in general asymmetric with respect to the bias reversal, which gives rise to associated asymmetric behavior of the TMR.

As voltages start exceeding the splitting due to the Zeeman term ($g\mu_{\mathrm{B}}H_z = 0.025$ meV), the inelastic cotunneling processes start taking part in transport. The competition between the elastic and inelastic cotunneling leads in turn to large super-Poissonian shot noise, which in the parallel configuration is enhanced due to additional fluctuations associated with cotunneling through majority-majority and minority-minority spin channels, see Fig. 5.10(d) and (h). On the other hand, when the voltage exceeds threshold for sequential tunneling, more states take part in transport and the asymmetry with respect to the bias reversal is suppressed. The same tendency is observed in the shot noise, which in the sequential tunneling regime becomes generally sub-Poissonian.

5.6 Antiferromagnetic coupling between the LUMO level and SMM's core spin

Until now, I have focused on discussing numerical results only for the case of *ferromagnetic* coupling ($J > 0$) between the LUMO level and the SMM's core spin. However, since the type of such an interaction generally depends on the SMM's internal structure, the coupling can also be of *antiferromagnetic* type ($J < 0$). In this section I thus consider how the main transport properties of the system change when the exchange coupling parameter becomes antiferromagnetic.

Analyzing Fig. 5.11(a), it becomes clear that the most apparent new feature of TMR for $J < 0$ is its negative value in the Coulomb blockade regime ($Q = 1$). The negative TMR occurs in transport regimes where the maximum of TMR was observed for $J > 0$, i.e. close to the threshold for sequential tunneling, see Fig. 5.3(a). Such behavior of TMR originates from the fact that now spin-multiplets $|5/2; 1, m\rangle$ and $|3/2; 1, m\rangle$ exchange their positions, Fig. 5.5(c)-(d), so that the multiplet corresponding to smaller total spin of the molecule for antiferromagnetic coupling is characterized by lower energy. Consequently, in the Coulomb blockade the current flowing in the antiparallel configuration is larger than that in the parallel configuration, which gives rise to negative TMR effect.

Furthermore, the *linear response* TMR is shown in Fig. 5.12(a). Unlike the case of ferromagnetic coupling, the values of TMR for $Q = 0$ and $Q = 2$ are smaller as compared to those in the case of transport through single-level quantum dots [203, 210]. On the other hand, for $Q = 1$ the TMR can take values exceeding those found in the case of ferromagnetic exchange coupling. For $\varepsilon > \varepsilon_{01}$, the equilibrium probability distribution of different molecular spin states $|2; 0, m\rangle$ becomes changed owing to inelastic cotunneling

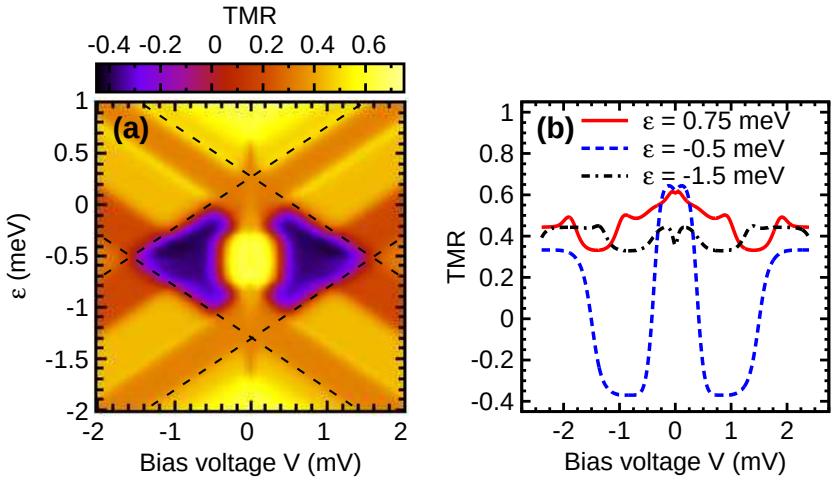

Figure 5.11: (a) The total tunnel magnetoresistance in the case of *antiferromagnetic* coupling between the SMM's core spin and the spin in the LUMO level, calculated for $J = -0.2$ meV and other parameters as in Fig. 5.2. (b) Representative cross-sections of the density plot in (a) for several values of the LUMO level energy ε.

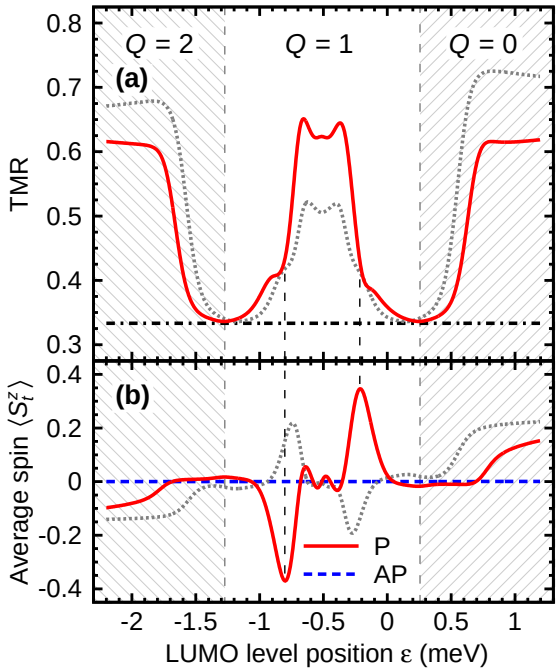

Figure 5.12: Tunnel magnetoresistance (a) and the zth component of the molecule's total spin (b) calculated in the linear response regime for the antiferromagnetic coupling of the SMM's core spin with the spin of the LUMO level ($J = -0.2$ meV and other parameters as in Fig. 5.2). Dotted lines show the results obtained for the case of *ferromagnetic* exchange coupling, see Fig. 5.6 – in (b) the dotted line corresponds to the *parallel* configuration.

processes, similarly as described in Section 5.3. The key difference with respect to $J > 0$ is that now dominating elastic cotunneling transitions for $Q = 0$ are those with initial states $|2; 0, \pm 2\rangle$ and virtual states $|3/2; 1, \pm 3/2\rangle$ [indicated by black arrows in Fig. 5.5(d)].

Finally, it should be noted that in the case of antiferromagnetic coupling between the LUMO level and molecule's core spin the formulas estimating the position of conductance resonances need some modification. Equations (5.17)-(5.18) were derived assuming the degeneracy between the states $|2; 0, \pm 2\rangle$ ($|5/2; 1, \pm 5/2\rangle$) and $|5/2; 1, \pm 5/2\rangle$ ($|2; 2, \pm 2\rangle$). For $J < 0$, however, the condition has to be modified by changing $|5/2; 1, \pm 5/2\rangle$ into $|3/2; 1, \pm 3/2\rangle$, where the upper signs apply for $H_z < 0$, and the lower ones for $H_z > 0$. The relevant equations take now the following form:

$$\varepsilon_{01} = \frac{|J|}{4} + D_1 S^2 - \Delta\varepsilon \tag{5.20}$$

for the transition from empty to singly occupied states, and

$$\varepsilon_{12} = -\frac{|J|}{4} - U + (D_1 + D_2)S^2 + \Delta\varepsilon \tag{5.21}$$

for the transition between singly and doubly occupied states, where

$$\Delta\varepsilon = D^{(1)}\frac{2S-1}{2} + \frac{g\mu_{\rm B}|H_z|}{2} - \sqrt{D^{(1)}(D^{(1)} + |J|)\frac{(2S-1)^2}{4} + \frac{J^2}{16}(2S+1)^2}, \tag{5.22}$$

with $D^{(1)} = D + D_1$.

5.7 Spin diode behavior in transport through single-molecule magnets

An interesting situation arises when a SMM is coupled to ferromagnetic leads with unequal spin polarizations. As already predicted in the case of quantum dots [215–217], transport properties of such systems exhibit a significant asymmetry with respect to the bias reversal – for one bias polarization the current is suppressed, which is a key feature of diodes. In addition, due to coupling to ferromagnetic leads and the spin dependence of tunneling processes, the current flowing through a diode device becomes spin polarized and, interestingly, the spin polarization may change with reversing the bias voltage. In other words, the system behaves like a *spin diode*, as well. In fact, very recently spin diode behavior was predicted and observed experimentally in another class of molecular structures, namely in single-wall carbon nanotubes [218, 219].

Consequently, in this section I consider transport properties of a SMM coupled to a nonmagnetic lead on the left and a ferromagnetic lead of high spin polarization on the right. Due to large spin asymmetry in coupling of the SMM to the ferromagnetic lead, the tunneling probability for spin-majority (spin-up) electrons is much larger than that for spin-minority (spin-down) electrons. On the other hand, the rate of tunneling processes between the molecule and the nonmagnetic lead is the same for both spin orientations.

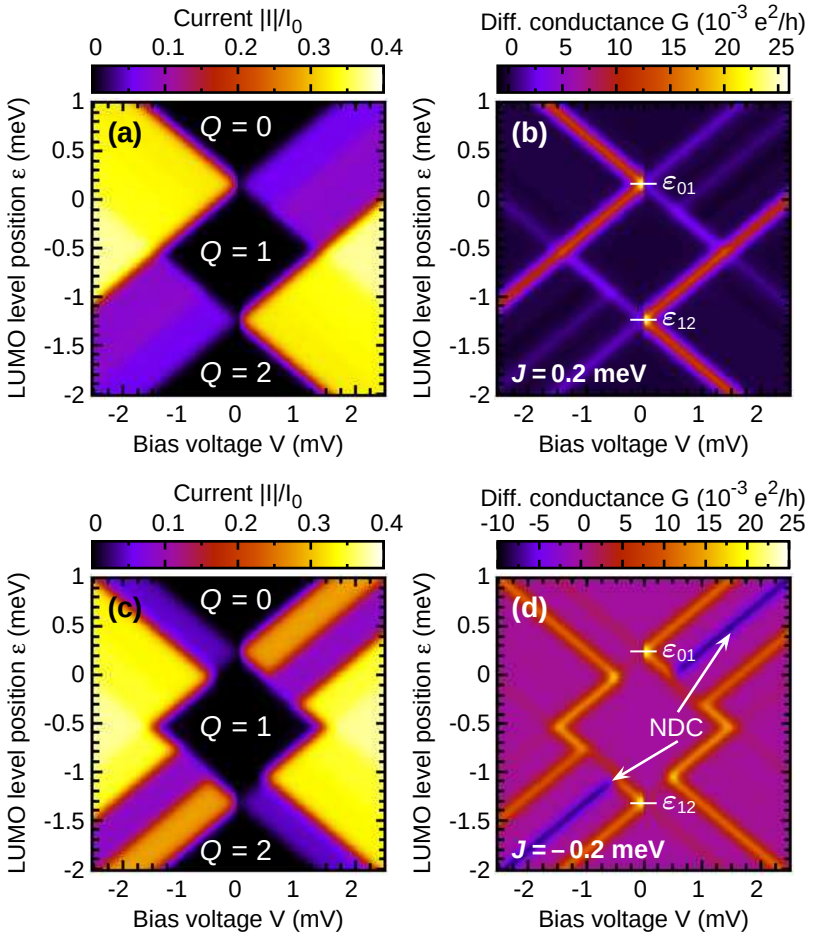

Figure 5.13: (a,c) The absolute value of the current I in units of $I_0 = 2e\Gamma/\hbar \approx 0.5$ nA, and (b,d) differential conductance G as a function of the bias voltage V and the LUMO level position ε for (a)-(b) *ferromagnetic* ($J > 0$) and (c)-(d) *antiferromagnetic* ($J < 0$) exchange coupling, $|J| = 0.2$ meV. Q in (a,c) represents the average charge accumulated in the LUMO level. Except $P_L = 0$ and $P_R = 0.9$, the other parameters are as in Fig. 5.2.

This generally leads to some asymmetry of tunneling current with respect to the bias reversal.

Let's first discuss the current and differential conductance as a function of the LUMO level position and bias voltage for *ferromagnetic* ($J > 0$) interaction between the LUMO level and the SMM's spin, Fig. 5.13(a)-(b). Close to the first resonance, $\varepsilon \approx \varepsilon_{01}$, see Fig. 5.13(b), current can flow easily from the ferromagnetic lead to the nonmagnetic one ($V < 0$), while it is suppressed for the opposite direction ($V > 0$); see solid line in Fig. 5.14(a). To understand this behavior one should take into account the following facts. First, the molecule's states with one extra electron in the LUMO level correspond to the total spin number $S = 5/2$ and $S = 3/2$, with the former being of lower energy. Second, orientation of the molecule's spin depends significantly on the current direction, and for $V > 0$ the SMM's spin tends towards antiparallel orientation with respect to the

electrode's magnetic moment, whereas for $V < 0$ the spin prefers the parallel alignment. Thus, for low bias transport can occur mainly *via* the state corresponding to $S = 5/2$, and this requires spin-down electrons for $V > 0$ and spin-up electrons for $V < 0$. Unfortunately, tunneling rate for spin-down electrons is significantly reduced due to fewer available states in the minority spin band of the ferromagnetic lead, which effectively leads to the suppression of current for $V > 0$. When bias voltage increases, then the state corresponding to $S = 3/2$ becomes active in transport as well, leading only to a small increase of the current due to the spin blockade. However, the blockade for positive bias is removed when double occupancy of the LUMO level is admitted, which takes place for bias voltages exceeding some threshold value. Furthermore, the electron flow from ferromagnetic lead to the nonmagnetic one is spin polarized and degree of this polarization depends mainly on the spin polarization of the lead. In fact, in the case of a perfect halfmetallic ferromagnet ($P_R \to 1$), the current flowing towards halfmetallic lead would be totally blocked. Moreover, different time scales associated with spin-majority and spin-minority electrons lead in turn to considerable current fluctuations and super-Poissonian shot noise, see Fig. 5.14(c) for $\varepsilon = 0.2$ meV.

The situation becomes significantly different when the LUMO level is doubly occupied in equilibrium; $\varepsilon = -1.5$ meV in Fig. 5.14(a). Now, the behavior of the current is reversed as compared to the case of $Q = 0$, since the current is suppressed for $V < 0$, i.e. for electrons tunneling from the magnetic lead. This is associated with the fact that an electron first has to tunnel out of the LUMO level and then another electron can enter the molecule. Thus, for positive bias a spin-up electron can easily tunnel out to the ferromagnetic lead. On the other hand, when the bias is reversed and the spin-down electron tunnels out of the molecule leaving it in the state corresponding to $S = 5/2$, the current becomes suppressed, as the rate for tunneling of spin-down electrons from the ferromagnetic lead to the molecule is relatively small. This also leads to super-Poissonian shot noise, as shown in Fig. 5.14(c).

More complex transport characteristics are observed when the exchange interaction is *antiferromagnetic* ($J < 0$); Fig. 5.13(c)-(d). The most striking difference is the appearance of additional peaks in the current when the LUMO level is initially either empty or doubly occupied, Figs. 5.13(c) and 5.14(d), which are accompanied by negative differential conductance (NDC); Figs. 5.13(d) and 5.14(e). Consider first the case of empty LUMO level in equilibrium, $\varepsilon = 0.2$ meV in Fig. 5.14(d). The key difference is that now the molecule's state corresponding to the total spin number $S = 3/2$ has lower energy and determines transport properties at low voltages. Thus spin-up electrons are involved in charge transport for $V > 0$ and spin-down electrons for $V < 0$. Consequently, the current is suppressed for negative bias and can easily flow for positive one. When the bias voltage reaches values admitting transport through the $S = 5/2$ state, the current for positive bias becomes suppressed by a spin down electron tunneling to the LUMO level, while suppression for negative voltage becomes then lifted. In turn, when bias increases further admitting doubly occupation of the LUMO level, the blockade for positive bias becomes removed as well. Transport characteristics for doubly occupied LUMO level in

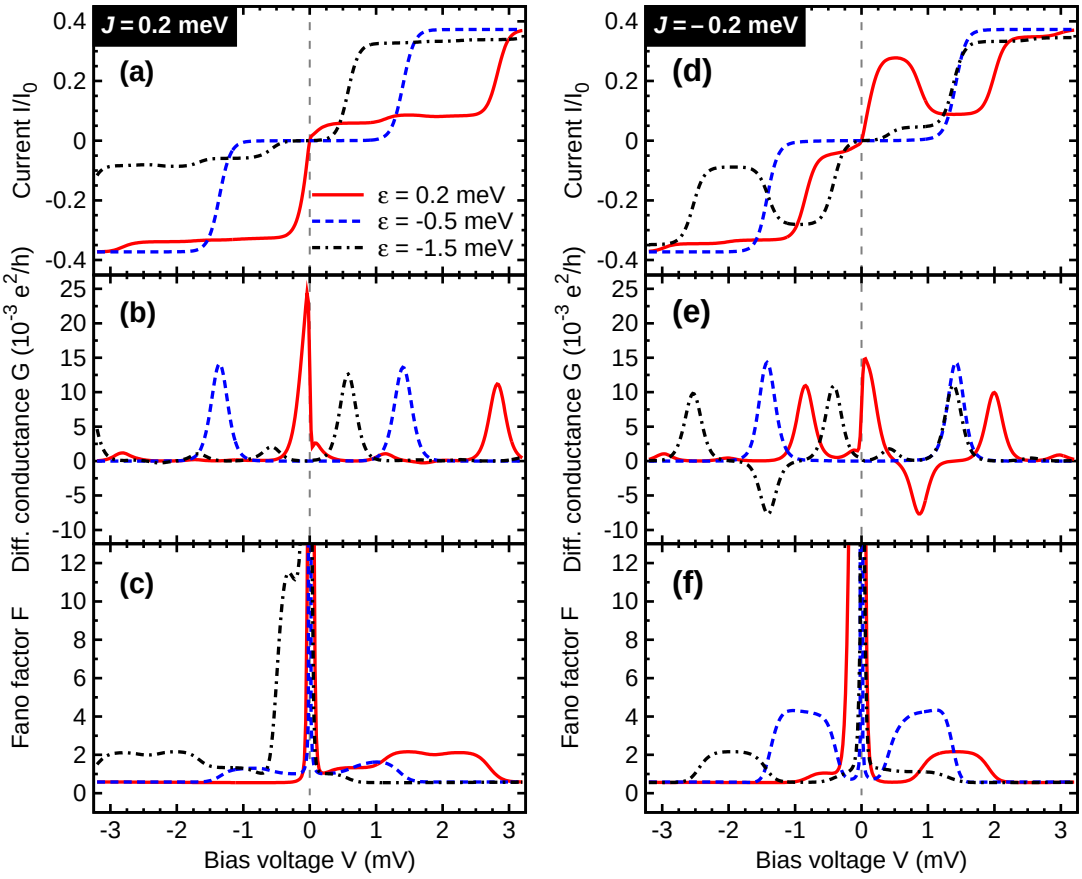

Figure 5.14: Selected cross-sections of density plots in Fig. 5.13 for specific values of the LUMO level position ε, which depict the current I flowing through the system (a,d), differential conductance G (b,e), and Fano factor F (c,f) as a function of the bias voltage V for the *ferromagnetic* (left panel) and *antiferromagnetic* (right panel) exchange couplings. The other parameters are the same as in Fig. 5.2.

equilibrium can be explained in a similar way.

On the other hand, when the LUMO level is singly occupied and its position corresponds approximately to the middle of the Coulomb blockade region [dashed line in Figs. 5.14(a,d)], the diode behavior disappears and the current recovers symmetry with respect to the bias reversal regardless of the type of the exchange interaction J. This is due to the fact that now with increasing the bias voltage all charge states of the molecule start taking part in transport at the same time, i.e. once the bias voltage reaches the threshold. The transport characteristics become then symmetric with respect to the bias reversal and the noise is rather sub-Poissonian, indicating the role of single-electron charging effects in transport. Note, however, that in the Coulomb blockade regime bunching of inelastic cotunneling processes may still result in enhancement of the shot noise; see dashed lines in Figs. 5.14(c,f). Furthermore, it is visible that the enhancement is much more pronounced in the case of the antiferromagnetic coupling, Fig. 5.14(f). Such

a behavior stems from the fact that for $J < 0$ both energetically lowest lying molecular magnetic states $S_t^z = \pm 3/2$ allow the possibility of occupying the LUMO level by an electron either with the spin up or down, whereas for $J > 0$ the state $S_t^z = +5/2$ ($S_t^z = -5/2$) can only accommodate an electron with spin up (down). For this reason, in the former case both majority and minority electrons of the ferromagnetic lead can participate in the transport, thus increasing the fluctuations.

Finally, it is worth emphasizing that operation of the SMM spin diode strongly depends on the number of electrons occupying the LUMO level. Thus, when assuming a specific bias polarization, one can tune the functionality of such device by changing the occupation number of the LUMO level, e.g. by shifting the position of the LUMO level with a gate voltage. It should also be emphasized that the key requirement for observing the spin diode behavior of a SMM is the presence of considerable spin asymmetry in the couplings to the left and right electrodes, and well-defined spin states in the molecule, i.e. $J, D \gg T$, where T is the experimental temperature.

CHAPTER 6

Equilibrium transport in the Kondo regime – the numerical renormalization group approach

Up to this moment I have been considering transport properties of a SMM assuming that the molecule is only *weakly* coupled to reservoirs of spin-polarized electrons. However, in real experiments such assumption not necessarily has to be satisfied, so that it seems reasonable to address also the limit of *strong* coupling, which will be the subject of the present and the next chapter.

To begin with, one shall ask what consequences of the coupling strength to electrodes for transport through nanoscopic objects, such as molecules or quantum dots, are. It is important to notice that the energy spectrum of these objects is characterized by a set of discrete energy levels, and the spectrum becomes modified upon introducing the coupling to electrodes [28]. Due to the interaction between localized electron states of the molecule and extended electron states in the electrodes, the possibility of electron tunneling arises. When the mixing of the states is rather weak (the *weak coupling regime*), the original molecular states undergo broadening, but a structure of well-defined energy levels can still be distinguished. As a result, in such a case one can consider tunneling of electrons *via* molecular levels, as it was done in Chapters 4 and 5.

However, if the overlapping is significant (the *strong coupling regime*), the molecular states can no longer serve as an appropriate approximation for describing transport of electrons. Therefore one has to replace them by new hybrid states, which take into account the fact that now electrons are to some extent delocalized between electrodes and the molecule. Since electrons can easily tunnel back and forth between electrodes and the molecule, when the latter is occupied by an odd number of electrons, such processes

may lead to reversing the spin of the unpaired electron. This in turn can result in an additional resonance in the density of states near the Fermi level of electrodes, known as the *Kondo* (sometimes also *Abrikosov-Suhl*) *resonance*. For this reason, the strong coupling regime is often referred to as the *Kondo regime*.

The *Kondo effect* is a well-studied phenomenon in condensed-matter physics [220–226], and it occurs for metallic systems containing magnetic impurities, manifesting as the increase of resistance below some characteristic temperature T_K, called the *Kondo temperature*. The effect originates from the interaction of a magnetic impurity with surrounding conduction electrons of a non-magnetic host metal, and it can be qualitatively understood on the ground of the simplest *Anderson magnetic impurity model* [227]. If the impurity accommodates one electron, for instance with the spin 'up', as in Fig. 6.1(a), the electron can tunnel out providing it possesses enough energy, otherwise it remains trapped. Nevertheless, within the time scale allowed by the Heisenberg uncertainty principle a virtual state can be formed, in which the electron can either temporarily escape the impurity or another electron of the opposite spin can additionally arrive.[1] When the system reaches the final state, it may turn out that due to virtual exchange processes the direction of the impurity spin becomes effectively flipped to the opposite one. In the present case this means the change from the 'up' to 'down' direction. In consequence, such spin exchange processes between a localized electron and free-electron states qualitatively modify the energy spectrum of the system, leading to generation of a new state at the Fermi level, the *Kondo resonance*, Fig. 6.1(b). Now, since transport properties of a system are determined by the behavior of electrons with energies in the vicinity of the Fermi level, the additional resonance can drastically change these properties.

At the end of the 1990s, it was shown that the Kondo effect can occur not only in bulk systems, but also it is observed in transport through nanoscopic objects like quantum dots [228–230], nanotubes [231], and different types of molecules: coordination complexes in which a Co(II) ion is bonded within an approximately octahedral environment to two terpyridinyl linker molecules with thiol end groups [232]; divanadium molecules [(N, N′, N″-trimethyl-1,4,7-triazacyclononane)$_2$-V$_2$(CN)$_4$(m-C$_4$N$_4$)] [233]; and C_{60} molecules attached to gold [234] or ferromagnetic nickel electrodes [235]. Furthermore, it should be noted that although the physical processes governing the formation of the Kondo effect are always the same, regardless of whether one considers bulk metal systems or nanoscopic magnetic objects, there is the fundamental difference in the behavior of measured transport quantities between such two cases. Whereas for metals, scattering of electrons on the impurities causes the increase of resistance below T_K, in the case of quantum dots and molecules, one observes the increase of conductance instead. Because electrons, in order to get from one electrode to the opposite one, have to travel through the central region of the device, the Kondo resonance becomes a kind of a 'bridge', allowing for easier mixing of electron states belonging to two different electrodes, and hence it enhances tunneling of electrons across the device [226].

[1] Note that I assume here symmetrical position of singly and doubly occupied states of the impurity with respect to the Fermi level of electrodes.

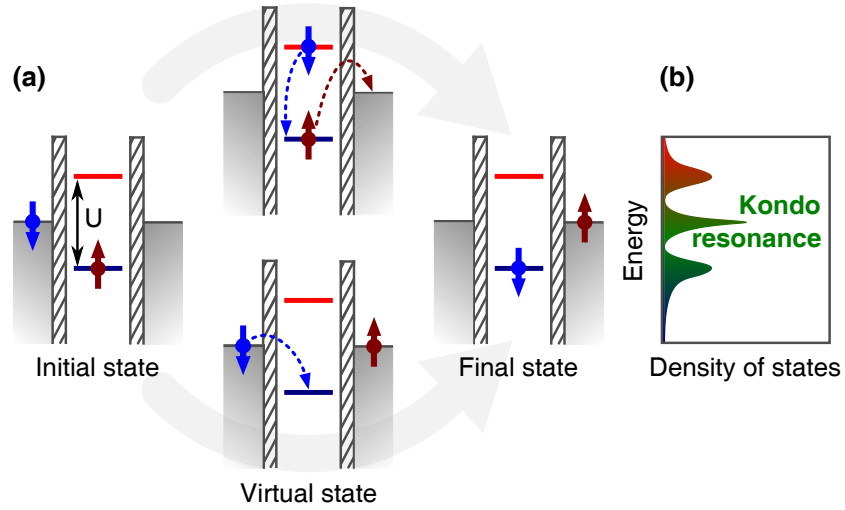

Figure 6.1: Illustration of spin exchange processes (a) that can lead to formation of the *Kondo resonance* at the Fermi level of electrodes (b), shown schematically in the case of the *Anderson magnetic impurity model*. The general idea adopted from Ref. [226].

More recently, it has been demonstrated that for systems characterized by larger spins ($S > 1/2$), e.g. a Co atom of $S = 3/2$, the role of the magnetic anisotropy in the physics of the Kondo effect cannot be neglected [236, 237]. Moreover, the key conclusion is that the Kondo effect can be tuned by changing the magnitude and orientation of the magnetic anisotropy, which sets the ground for a novel class of Kondo systems in which the effect could be handled directly by controlling the local environment [236]. In this context, SMMs seem to be a very promising material for research. Although few theoretical works focused on studying transport related issues in SMMs in the Kondo regime have hitherto been published [50–54, 238], no experimental evidence of the Kondo effect in transport through SMMs have been found yet. Let's therefore briefly discuss the current state of knowledge concerning transport through SMMs in the Kondo regime.

In the Coulomb blockade regime, where the charge of a molecule doesn't alter, for linear transport through a half-integer spin SMM, whose spin is *weakly* exchange-coupled to conduction electrons, it has been shown that due to presence of the transverse anisotropy the interaction can result in spin fluctuations [50]. Thus the pseudo-spin 1/2 Kondo effect is there a consequence of a joint action between the quantum tunneling of the molecule's spin and spin exchange processes between the SMM and tunneling electrons. Moreover, the effect should arise only for particular values of the SMM's spin, determined by the symmetry of the transverse anisotropy. The situation becomes even more intriguing for the *strong* interaction, because then the Kondo temperature can be substantially larger than the tunnel splittings Δ, see Chapter 3. It means that excited SMM's magnetic states which belong to topologically different sectors, with respect to rotations around the easy axis, can also contribute to the Kondo effect [51], so that the effect can occur for full-integer spin molecules as well.

It was soon realized that qualitative differences between mechanisms of the Kondo effect in the case of molecules with half- and full-integer spins disappear with application of even a moderate transverse magnetic field [52]. Furthermore, it has been demonstrated how, with the use of the Schrieffer-Wolff transformation, the Anderson-type Hamiltonian describing the SMM can be mapped onto a spin-1/2 anisotropic Kondo Hamiltonian [53]. It turned out that, depending on whether due to tunneling of an electron the total molecule's spin is either reduced or augmented in the charged state, the Kondo Hamiltonian is characterized by an antiferromagnetic and ferromagnetic coupling, respectively. In the former case the Kondo effect manifests itself, whereas in the latter one, owing to renormalization of the transverse coupling to zero, no resonance at the Fermi level is present. Finally, the oscillatory behavior of the Kondo effect as a function of the transverse field amplitude has been demonstrated to stem from the Berry-phase periodical modulation of the tunnel splitting.

To complete the present review, it should be mentioned that also the nonequilibrium spin dynamics of a SMM, triggered by a sudden change in the magnetic field amplitude, with the main emphasis on the time evolution of the Kondo screening, has been studied [54]. Interestingly enough, the manner in which the molecule's spin relaxes in the presence of the transverse anisotropy is related to its parity. For a half-integer spin, because of the combined effect of the QTM and spin screening by conduction electrons, the pseudospin-1/2 Kondo effect arises and on a long-time scale the reduction of the SMM's average spin is seen. On the other hand, for a full-integer spin, the QTM occurs directly between two ground states, so that no screening takes place, and consequently one observes only damped *Rabi oscillations*.[2]

In view of the above discussion, it is clear that in the case of the *strong* coupling one cannot any longer anticipate that only the states in the vicinity of the Fermi level of electrodes will significantly contribute to transport. In fact, any state belonging to the conduction band cannot arbitrarily be excluded from participating in tunneling processes, and therefore one should in principle consider a wide range of energies corresponding to the whole width of the conduction band. Consequently, at this point I need to abandon perturbation schemes used so far, and apply a method that allows me to describe an interacting many-body quantum-mechanical system characterized by a broad continuous spectrum of excitation energies. The problem of electron transport through a SMM strongly coupled to two ferromagnetic metallic electrodes can be efficiently treated with the renormalization group approach. In particular, I employ here *Wilson's numerical renormalization group* method [225, 240, 241], referred to as NRG in the following, whose great advantage is being non-perturbative in all system parameters.

The general NRG strategy applied by Wilson to analyze the behavior of a *magnetic impurity* coupled to non-interacting electrons of a conduction band can be briefly summarized as a sequence of three substantial steps. First, he discretized the conduction band logarithmically, using a discretization parameter $\Lambda > 1$, and dividing the band into

[2]The term *'Rabi oscillations'* is generally used to call oscillations that arise in an effective two-level system due to the occurrence of a momentary or periodic change in an external field [239].

intervals $[\Lambda^{-(n+1)}\omega_c, \Lambda^{-n}\omega_c]$ and $[-\Lambda^{-n}\omega_c, -\Lambda^{-(n+1)}\omega_c,]$ with $n = 0, 1, 2, 3, \ldots$ Then he mapped the discretized model onto a semi-infinite chain with the impurity representing the first node of the chain. Finally, the model in the form of the semi-infinite chain was diagonalized iteratively, starting from the impurity site and adding degrees of freedom to the chain in each successive step. Since moving along the chain effectively means accessing smaller and smaller energy scales in the calculations, the method developed by Wilson provides a non-perturbative description of the crossover from a free magnetic impurity at high temperatures to a screened spin at low temperatures [241].

Since the mathematical formulation of NRG method has been broadly discussed in the literature [225, 240, 242–251], I omit in the following all redundant derivations, and I recall only formulae indispensable for keeping the current discussion logically consistent.

6.1 The numerical renormalization group (NRG) method – basic ideas

The NRG method is in general applicable to all systems which can be reduce to the model of a quantum-mechanical impurity coupled to a bath of fermions or bosons. Whereas there are in principle no constraints concerning the form of the impurity term of the Hamiltonian, it is required that the bath consists of non-interacting fermions of bosons. For this reason, in order to use the NRG method efficiently, I have to first transform the previously studied model of a SMM coupled to two metallic ferromagnetic electrodes into a model where the molecule interacts effectively only with a single spin-polarized electron reservoir.

It has been shown that this can be achieved by means of a *canonical transformation* [187, 252, 253] of the tunneling Hamiltonian,[3] Eq. (2.3),

$$\begin{pmatrix} a^e_{\mathbf{k}\sigma} \\ a^o_{\mathbf{k}\sigma} \end{pmatrix} = \frac{1}{\sqrt{|T^L_{\mathbf{k}\sigma}|^2 + |T^R_{\mathbf{k}\sigma}|^2}} \begin{pmatrix} T^{L*}_{\mathbf{k}\sigma} & T^{R*}_{\mathbf{k}\sigma} \\ -T^R_{\mathbf{k}\sigma} & T^L_{\mathbf{k}\sigma} \end{pmatrix} \begin{pmatrix} a^L_{\mathbf{k}\sigma} \\ a^R_{\mathbf{k}\sigma} \end{pmatrix}, \tag{6.1}$$

with the label $e(o)$ denoting the odd (even) combination of leads operators. Such a rotation in the space of left-right electron operators results in separation of the total Hamiltonian, Eq. (2.1), into two independent parts, among which one involves the LUMO level coupled to a single electron reservoir described by the even combination of the leads' electron operators, while the other one describes merely a non-interacting electron gas described by the odd combination of the leads' electron operators. The tunnling Hamiltonian in the collinear configuration of the leads' magnetic moments and the molecule's easy axis ($\varphi = 0$) reads as

$$\mathcal{H}_{\mathrm{tun}} = \sum_{\mathbf{k}\sigma} \mathcal{V}_{\mathbf{k}\sigma} \left[a^{e\dagger}_{\mathbf{k}\sigma} c_\sigma + c^\dagger_\sigma a^e_{\mathbf{k}\sigma} \right], \tag{6.2}$$

[3] Note that although the tunneling matrix element $T^q_{\mathbf{k}\sigma}$ can formally depend on a wave vector $\mathbf{k}$ and a spin σ, which is assumed for the purpose of the present discussion, in the further part of this section I will relax the assumption, requiring only the spin-dependence.

where $\mathcal{V}_{\mathbf{k}\sigma} = \sqrt{|T^L_{\mathbf{k}\sigma}|^2 + |T^R_{\mathbf{k}\sigma}|^2}$ is a renormalized, effective LUMO level-lead coupling. For convenience of further discussion, I leave out the superscript 'e'.

Consequently, the model under discussion can be reformulated so that it resembles now a quantum impurity model, described by the total Hamiltonian

$$\mathcal{H} = \mathcal{H}_{\text{SMM}} + \mathcal{H}_{\text{res}} + \mathcal{H}_{\text{SMM-res}}. \tag{6.3}$$

Here, $\mathcal{H}_{\text{SMM}}$ plays a role of the impurity, and is given by Eq. (2.5), $\mathcal{H}_{\text{res}} = \sum_{\mathbf{k}\sigma} \varepsilon_{\mathbf{k}\sigma} a^\dagger_{\mathbf{k}\sigma} a_{\mathbf{k}\sigma}$ describes the reservoir (bath), and $\mathcal{H}_{\text{SMM-res}} \equiv \mathcal{H}_{\text{tun}}$ represents the interaction between the molecule and the reservoir, Eq. (6.2). As it can be seen in the equations above, at this stage I explicitly keep spin-dependance for the reservoir's energy dispersion relation $\varepsilon_{\mathbf{k}\sigma}$, as well as for the tunneling matrix element $\mathcal{V}_{\mathbf{k}\sigma}$. However, I would like to point out that ferromagnetism of the bath can formally be included either by a spin-dependent DOS $\rho_\sigma(\omega)$ or $\mathcal{V}_{\mathbf{k}\sigma}$, without no need of assuming simultaneously spin-dependency of both of these parameters. Since, as long as transport properties of the system are concerned, both these pictures are equivalent [251,254], I lump all spin and energy dependence into $\mathcal{V}_{\mathbf{k}\sigma}$. Furthermore, for simplicity I assume a flat conduction band stretching within the interval $[-\mathfrak{D}, \mathfrak{D}]$, with $\mathfrak{D} > 0$ and $\mathfrak{D} = 1$ being the the largest (cutoff) energy scale of the system, so that $\rho(\omega) = \sum_\sigma \rho_\sigma(\omega) \equiv \rho = \frac{1}{2\mathfrak{D}}$. Finally, I also neglect the energy dependence of the tunneling matrix $\mathcal{V}_{\mathbf{k}\sigma} = \mathcal{V}_\sigma$ [242]. As a result, the overall effect of the reservoir on the SMM is then completely determined by the coupling (hybridization) function[4]

$$\Gamma_\sigma = \pi\rho|\mathcal{V}_\sigma|^2. \tag{6.4}$$

The model established in the previous two paragraphs constitutes conceptually the easiest system to be treated with the NRG method. The *general strategy* of the approach under discussion can be divided into following steps [241]:

- Division of a continuous spectrum of a reservoir into a discrete set of states, and subsequent discretization of the model, Fig. 6.2(a)-(b).
- Mapping of the discretized model onto a semi-infinite chain, Fig. 6.2(c).
- Iterative diagonalization of this chain.
- Analysis of data obtained due to the iterative diagonalization procedure.

Starting with the first point, Wilson has shown that the most suitable choice for discretization of the conduction band is the logarithmic discretization, which introduces a set of energy points at $x_n = \pm\Lambda^{-n}$ ($\Lambda > 1$, $n = 1, 2, 3, \ldots$) in place of a continuous spectrum. The advantage of the logarithmic distribution of points is that the low-energy resolution depends exponentially on the number of sites into which the model is divided. Then, within each logarithmic interval, characterized by the width $d_n = \Lambda^{-n}(1 - \Lambda^{-n})$,

[4] It should be noted that the definition of the coupling function used in this chapter differs slightly form that introduced in Section 2.2, i.e. here the factor 2 is missing. The present form of Γ_σ is according to the Flexible DM-NRG code to be applied in this chapter [255,256].

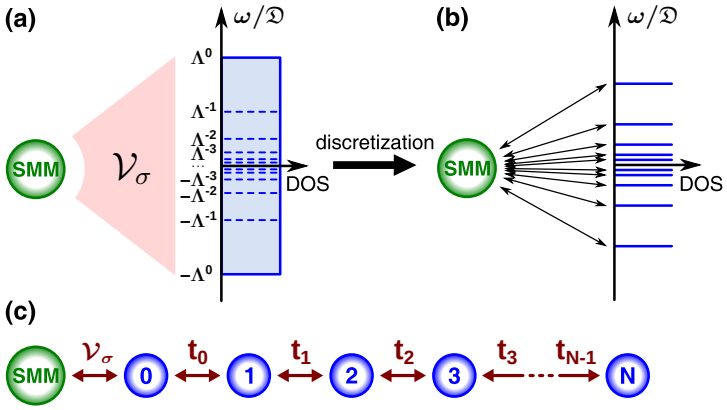

Figure 6.2: A schematic representation of the major steps in the NRG method. (a) The continuous density of states (DOS) of a reservoir is separated into a set of logarithmic intervals, whose lengths are determined by the discretization parameter Λ. (b) Within each of such defined intervals, the continuous spectrum is replaced by a single state. (c) The discretized model is then mapped onto a semi-infinite chain, whose first node corresponds to the molecule. The idea adopted from Ref. [241].

one expands the *continuous* conduction band operators $a_{\varepsilon\sigma}$ in a Fourier series in an orthonormal basis spanned by functions [225, 240, 241]

$$\psi^{\pm}_{np}(\varepsilon) = \begin{cases} d_n^{-1/2} \mathrm{e}^{\pm i\omega_n p\varepsilon} & \text{for } x_{n+1} < \pm\varepsilon < x_n, \\ 0 & \text{if } \varepsilon \text{ lies outside the above interval,} \end{cases} \tag{6.5}$$

with $\omega_n = 2\pi/d_n$ denoting the fundamental frequency in the nth interval. The discretization procedure applied to the Hamiltonian (6.3) yields [225, 240, 241]

$$\mathcal{H} = \mathcal{H}_{\mathrm{SMM}} + \underbrace{\sum_{\sigma,n=0}^{\infty} \frac{1+\Lambda^{-1}}{2\Lambda^n} \left[a^{(+)\dagger}_{n\sigma} a^{(+)}_{n\sigma} - a^{(-)\dagger}_{n\sigma} a^{(-)}_{n\sigma}\right]}_{\text{reservoir}} + \underbrace{\sum_{\sigma} \mathcal{V}_\sigma \left[c^\dagger_\sigma f_{0\sigma} + f^\dagger_{0\sigma} c_\sigma\right]}_{\text{SMM-reservoir interaction}}, \tag{6.6}$$

where an auxiliary fermionic operator $f_{0\sigma}$, defined as

$$f_{0\sigma} = \sum_{n=0}^{\infty} \sqrt{\frac{d_n}{2}} \left[a^{(+)}_{n\sigma} + a^{(-)}_{n\sigma}\right] \quad \text{and} \quad a^{(\pm)}_{n\sigma} = \int_{-1}^{1} \mathrm{d}\varepsilon \left[\psi^{\pm}_{n0}(\varepsilon)\right]^* a_{\varepsilon\sigma}, \tag{6.7}$$

has been introduced.

In the next step, the discretized Hamiltonian is mapped onto a semi-infinite chain. Analyzing the structure of the Hamiltonian (6.6), one can notice that the LUMO level couples directly only to one conduction electron degree of freedom *via* operators $f_{0\sigma}$ ($f^\dagger_{0\sigma}$) [see the third term of Eq. (6.6)]. Thus these operators correspond to the first node of the conduction electron part of the chain. Because the operators $f_{0\sigma}$ ($f^\dagger_{0\sigma}$) are not orthogonal to the operators $a^{(\pm)}_{n\sigma}$ ($a^{(\pm)\dagger}_{n\sigma}$), therefore it is convenient to construct a new set of mutually

orthogonal operators $f_{n\sigma}$ ($f^\dagger_{n\sigma}$) from $f_{0\sigma}$ ($f^\dagger_{0\sigma}$) and $a^{(\pm)}_{n\sigma}$ ($a^{(\pm)\dagger}_{n\sigma}$), which corresponds to mapping of the second (reservoir) term of Eq. (6.6) onto a semi-infinite chain, Fig. 6.2(c). Consequently, one obtains the sought expression for the chain Hamiltonian in the form

$$\mathcal{H} = \mathcal{H}_{\mathrm{SMM}} + \sum_{\sigma,n=0}^{\infty} t_n \big[f^\dagger_{n\sigma} f_{n+1\sigma} + f^\dagger_{n+1\sigma} f_{n\sigma} \big] + \sum_\sigma \mathcal{V}_\sigma \big[c^\dagger_\sigma f_{0\sigma} + f^\dagger_{0\sigma} c_\sigma \big]. \tag{6.8}$$

The operators $f_{n\sigma}$ ($f^\dagger_{n\sigma}$) represent the nth node of the conduction electron part of the chain, Fig. 6.2(c), which is also described by the hopping matrix element t_n [241],

$$t_n = \frac{(1+\Lambda^{-1})(1-\Lambda^{-n-1})\Lambda^{-n/2}}{2\sqrt{1-\Lambda^{-2n-1}}\sqrt{1-\Lambda^{-2n-3}}} \quad \xrightarrow{\text{for large } n} \quad t_n \approx \frac{1}{2}(1+\Lambda^{-1})\Lambda^{-n/2}. \tag{6.9}$$

The fact that the value of the hopping matrix element falls off exponentially with distance from the impurity is the key feature of the NRG method, as it essentially means that adding each consecutive node to the chain corresponds to diminishing the relevant energy scale by a factor of $\sqrt{\Lambda}$.

It should be noted that up to this moment none of performed transformations have revealed the *'renormalization group'* character of the discussed approach. The chain Hamiltonian, Eq. (6.8), can actually be seen as a series of Hamiltonians $\mathcal{H}_N$ ($N = 1, 2, 3, \ldots$), from which the initial Hamiltonian, Eq. (6.3), is recovered in the limit of the infinitely long chain [225, 240, 241],

$$\mathcal{H} = \lim_{N\to\infty} \Lambda^{-(N-1)/2} \mathcal{H}_N \tag{6.10}$$

where the Hamiltonian $\mathcal{H}_N$ contains the first N nodes of the Wilson chain,

$$\mathcal{H}_N = \Lambda^{(N-1)/2} \Bigg\{ \mathcal{H}_{\mathrm{SMM}} + \sum_{\sigma,n=0}^{N-1} t_n \big[f^\dagger_{n\sigma} f_{n+1\sigma} + f^\dagger_{n+1\sigma} f_{n\sigma} \big] + \sum_\sigma \mathcal{V}_\sigma \big[c^\dagger_\sigma f_{0\sigma} + f^\dagger_{0\sigma} c_\sigma \big] \Bigg\}. \tag{6.11}$$

Here, the factors $\Lambda^{\pm(N-1)/2}$ have been inserted into the last two equations to cancel the N-dependence of the hopping matrix element t_{N-1} between the two final nodes of $\mathcal{H}_N$. The starting Hamiltonian $\mathcal{H}_0$, which corresponds to a two-site cluster formed by the SMM coupled to the first conduction electron node, is therefore given by

$$\mathcal{H}_0 = \Lambda^{-1/2} \Bigg\{ \mathcal{H}_{\mathrm{SMM}} + \sum_\sigma \mathcal{V}_\sigma \big[c^\dagger_\sigma f_{0\sigma} + f^\dagger_{0\sigma} c_\sigma \big] \Bigg\}, \tag{6.12}$$

whereas two successive Hamiltonians $\mathcal{H}_{N+1}$ and $\mathcal{H}_N$ are recursively related as follows

$$\mathcal{H}_{N+1} = \sqrt{\Lambda}\mathcal{H}_N + \Lambda^{N/2} \sum_\sigma t_N \big[f^\dagger_{N\sigma} f_{N+1\sigma} + f^\dagger_{N+1\sigma} f_{N\sigma} \big]. \tag{6.13}$$

The last expression is then the point where the renormalization scheme comes into play, as Eq. (6.13) defines a mapping $\mathcal{H}_{N+1} = R\big[\mathcal{H}_N\big]$ which transforms the Hamiltonian in question into another Hamiltonian of the same form, but characterized by lower energy scales. As a result, to solve the chain Hamiltonian, Eq. (6.8), one has to diagonalize iteratively $\mathcal{H}_N$, i.e. diaginalize the chain Hamiltonian afer adding each consecutive node to the chain.

Let's assume that, for a given N, the Hamiltonian $\mathcal{H}_N$ has been diagonalized and it can be described by the many-body energies $E_N(i)$, so that $\mathcal{H}_N|\psi_i\rangle_N = E_N(i)|\psi_i\rangle_N$ $(i = 1, 2, \ldots, N_s)$, where $|\psi_i\rangle_N$ are the eigenstates and N_s is the dimension of $\mathcal{H}_N$. To proceed with diagonalization of $\mathcal{H}_{N+1}$, one first constructs a new basis $|\psi_i; \phi_s\rangle_{N+1} = |\psi_i\rangle_N \oplus |\phi_s\rangle_{N+1}$, whose states are product states of the eigenbasis of $\mathcal{H}_N$ and a proper basis for the added degrees of freedom. The matrix of $\mathcal{H}_{N+1}$ has then the form

$$\mathcal{H}_{N+1}(is, i's') = {}_{N+1}\langle\psi_i; \phi_s|\mathcal{H}_{N+1}|\psi_{i'}; \phi_{s'}\rangle_{N+1}. \tag{6.14}$$

Diagonalization of the matrix above yields the new set of eigenenergies $E_{N+1}(j)$ and corresponding eigenstates $|\psi_j\rangle_{N+1}$. Since the number of states taking part in calculation increases with adding each next node to the chain, a truncation procedure need to be devised so that for large N numerical diagonalization can be still performed. The standard solution of this problem is, first, to employ the symmetries of the system, and, second, to keep after each diagonalization step only $N_{\max}$ eigenstates with the lowest energies [241, 256]. In consequence, one fixes the dimension of the Hilbert space to $N_{\max}$ along the chain. The iterative diagonalization procedure should be continued until the system reaches its low-temperature fixed point.

To complete the present section, I would like to briefly comment on the effect of a finite temperature of the system on the NRG procedure. Since in the Nth iteration step one gains access to energy scales $\omega_N \sim \Lambda^{-(N-1)/2}\mathfrak{D}$, at $T = 0$ one can then increase N to get insight into lower and lower energy properties of the system. On the other hand, in the case of a finite temperature $(T \neq 0)$, the energy resolution granted by the method is limited by the thermal energy. It means that the NRG calculations have to be ceased once ω_N approaches the scale $k_{\mathrm{B}}T = \frac{1}{2}(1 + \Lambda^{-1})\Lambda^{-(N_T-1)/2}\mathfrak{D}$, Eq. (6.9), where N_T corresponds to the number of iterations necessary to reach the energy scale $k_{\mathrm{B}}T$.

6.2 Calculation of equilibrium transport with NRG

Diagonalizing the Hamiltonian (6.11) for a given chain site N, one obtains the set of eigenenergies $E_N(i)$, with $i = 1, 2, \ldots, N_{\max}$, and corresponding eigenstates $|\psi_i\rangle_N$, the knowledge of which allows for calculating the physical properties of the system at the energy (or temperature) scale $\omega_N \sim \Lambda^{-(N-1)/2}\mathfrak{D}$ $(k_{\mathrm{B}}T_N \sim \Lambda^{-(N-1)/2}\mathfrak{D})$.

A central quantity of interest when describing the transport properties of the system under consideration is the spin-dependent LUMO level *spectral function* $A_\sigma(\omega, T)$ [241,

257], which is defined as

$$A_\sigma(\omega,T) = -\frac{1}{\pi}\mathrm{Im}\,\mathcal{G}^{\mathrm{r}}_\sigma(\omega,T). \tag{6.15}$$

In the above equation, $\mathcal{G}^{\mathrm{r}}_\sigma(\omega,T)$ denotes the Fourier transform of the *retarded Green function* $\mathcal{G}^{\mathrm{r}}_\sigma = -i\theta(t)\big\langle\{c_\sigma(t),c^\dagger_\sigma(0)\}\big\rangle_\rho$ [258], and $\rho(T)$ is the density matrix of the full system at temperature T ($k_{\mathrm{B}}T = \beta^{-1}$). In the Nth iteration the expression for the spectral function $A^N_\sigma(\omega,T)$ takes the following form [241]

$$A^N_\sigma(\omega,T) = \frac{1}{\mathcal{Z}_N(T)}\sum_{ij}\Big[\mathrm{e}^{-\beta E_N(i)} + \mathrm{e}^{-\beta E_N(j)}\Big] \times \big|{}_N\langle\psi_j|c^\dagger_\sigma|\psi_i\rangle_N\big|^2\delta\big(\omega - [E_N(j) - E_N(i)]\big), \tag{6.16}$$

where $\mathcal{Z}_N(T) = \sum_i \mathrm{Exp}[-\beta E_N(i)]$ is the partition function. At this point, it should be emphasized that because the method under discussion is a fully numerical approach, Eq. (6.16) requires replacing the delta function by some smooth distribution. As the NRG method is not the main subject of this thesis, but rather one of theoretical tools used for analysis of the problem, I omit here further technical details concerning application of the method. They have been broadly described for instance in Refs. [248, 250, 255].

Knowing the spectral function, I can make use of the *Landauer-Wingreen-Meir formula* for the *linear-response regime* conductance [187, 259–263],

$$G = \frac{e^2}{h}\sum_\sigma\int_{-\infty}^{\infty}\mathrm{d}\omega\,\frac{\partial f_{\mathrm{FD}}(\omega)}{\partial\omega}\cdot\frac{2\Gamma^L_\sigma(\omega)\Gamma^R_\sigma(\omega)}{\Gamma^L_\sigma(\omega)+\Gamma^R_\sigma(\omega)}\cdot\frac{1}{\pi}\mathrm{Im}\,\mathcal{G}^{\mathrm{r}}_\sigma(\omega,T), \tag{6.17}$$

with $f_{\mathrm{FD}}(\omega)$ denoting the Fermi-Dirac distribution function. Noting that I focus only on the case for $T = 0$, where $-\frac{\partial f_{\mathrm{FD}}(\omega)}{\partial\omega} = \delta(\omega)$, and that I have assumed only the spin-dependance of the coupling functions, $\Gamma^{L(R)}_\sigma = \pi\big|T^{L(R)}_\sigma\big|^2/(2\mathfrak{D})$, the equation above, after employing Eq. (6.15), takes much simpler form

$$G = \frac{e^2}{h}\sum_\sigma\frac{2\Gamma^L_\sigma\Gamma^R_\sigma}{\Gamma^L_\sigma+\Gamma^R_\sigma}\cdot A_\sigma(0,T=0). \tag{6.18}$$

In the next step, I can express the coupling functions in terms of the electrodes' polarization parameters in a similar way as in Section 2.2, obtaining:

- for the *parallel* magnetic configuration

$$\Gamma^L_{\uparrow(\downarrow)} = \frac{\Gamma}{2}(1\pm P_L) \quad\text{and}\quad \Gamma^R_{\uparrow(\downarrow)} = \frac{\Gamma}{2}(1\pm P_R), \tag{6.19}$$

- for the *antiparallel* magnetic configuration

$$\Gamma^L_{\uparrow(\downarrow)} = \frac{\Gamma}{2}(1\pm P_L) \quad\text{and}\quad \Gamma^R_{\uparrow(\downarrow)} = \frac{\Gamma}{2}(1\mp P_R). \tag{6.20}$$

In consequence, for the system with electrodes characterized by the same polarization

parameters, $P_L = P_R = P$, the linear conductance $\widetilde{G}$ (in units of e^2/h) in the parallel and antiparallel magnetic configurations of the leads reads as

$$\begin{cases} \widetilde{G}_{\mathrm{P}} = \dfrac{\Gamma}{2}\big[(1+P)A^{\mathrm{P}}_{\uparrow}(0) + (1-P)A^{\mathrm{P}}_{\downarrow}(0)\big], \\ \widetilde{G}_{\mathrm{AP}} = \dfrac{\Gamma}{2}(1-P^2)A^{\mathrm{AP}}(0). \end{cases} \tag{6.21}$$

Here, for the sake of brevity, I skipped the temperature argument of the spectral function. Finally, in calculating $A^{\mathrm{A(AP)}}_{\sigma}(\omega)$, the magnetic configuration of the electrodes' spin moments is taken into account through the effective coupling between the molecule and the reservoir: $\mathcal{V}^{\mathrm{AP}}_{\uparrow} = \mathcal{V}^{\mathrm{AP}}_{\downarrow} = \sqrt{\frac{\Gamma}{\pi\rho}} \equiv \mathcal{V}$ for the *antiparallel* configuration, and $\mathcal{V}^{\mathrm{P}}_{\uparrow(\downarrow)} = \mathcal{V}\sqrt{1 \pm P}$ for the *parallel* one.

6.3 Transport through a single-molecule magnet in the linear response regime

Numerical results presented below have been obtained with the use of the Flexible DM-NRG code [255,256]. Similarly as in the previous chapter I have considered a hypothetical SMM characterized by $S = 2$ and strong uniaxial anisotropy. The parameters of the NRG procedure are assumed to be: $\lambda = 2$, $N = 60$ (the number of iterative steps) and $N_{\mathrm{max}} = 2000$ (the number of states kept after each diagonalization step). Furthermore, in order to facilitate numerical calculations, the $U_{\mathrm{charge}}(1) \times U_{\mathrm{spin}}(1)$ symmetry of the model was used, so that the zth component of the total spin S^z_t and the charge Q were employed as quantum numbers according to which the multiplets of the Hamiltonian were classified during computation. Finally, it should be emphasized that all energies cited in this section are given in units of $\mathfrak{D}$, and the height of spectral functions is normalized to $A_0 \equiv A(0)$[5] for $J = 0$ in the antiparallel configuration of the leads' magnetic moments.[6]

Since the Kondo regime is defined by the presence of the Kondo resonance in the spectral function, I should first derive the Kondo temperature T_{K} of the system. At $T = 0$, the Kondo temperature can be estimated from the half-width at half-maximum of the Kondo resonance [225,237]. As a result, considering the total spectral function for $J = 0$, I obtain $T_{\mathrm{K}} \approx 0.00066$ – I note here that for simplicity, throughout the remaining part of this chapter I assume $k_{\mathrm{B}} \equiv 1$, i.e. temperatures are also given in units of $\mathfrak{D}$. Now, turning on slowly the interaction between the electron spin in the LUMO level and the SMM's core spin, I can analyze how this interaction affects the shape of the spectral function in the Kondo regime, Figs. 6.3 and 6.4.

As it should be expected, for small values of J, where the behavior of the system should resemble that of a quantum dot, one observes a well pronounced Kondo peak in the antiparallel configuration of the electrodes' magnetic moments, Fig. 6.3, whereas in

[5] Numerically, the value of the spectral function $A(\omega)$ at $\omega = 0$ has been obtained by averaging values of $A(\omega)$ within the range $\langle 10^{-8}, 10^{-6}\rangle$, in which the spectral function is already constant.

[6] It's worth noting that in the situation under discussion there is neither quantitative nor qualitative difference between the antiparallel case and the case of nonmagnetic electrodes.

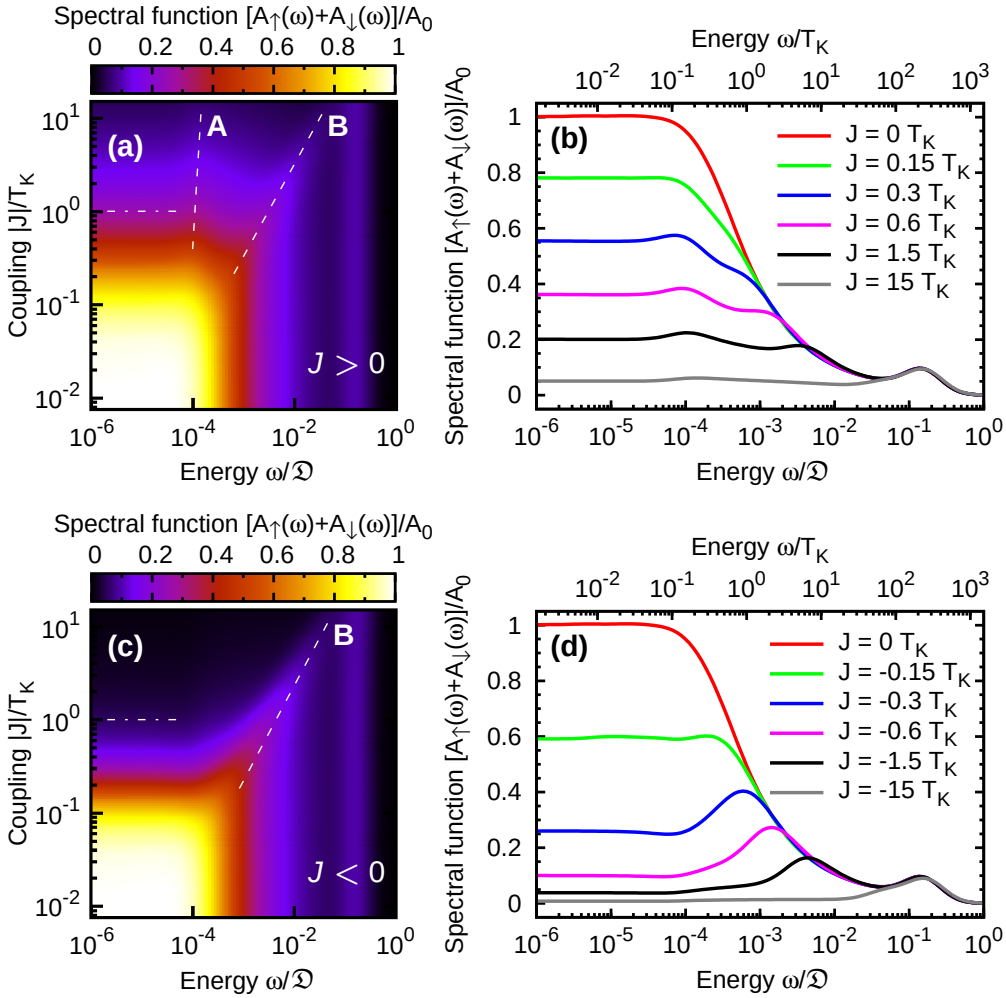

Figure 6.3: The total LUMO level spectral function $A(\omega) = \sum_\sigma A_\sigma(\omega)$ as a function of the coupling J between the electron spin occupying the LUMO level and the SMM's core spin for the *antiparallel* magnetic configuration of electrodes. Results for both types of the coupling are presented: (a)-(b) *ferromagnetic* ($J > 0$), and (c)-(d) *antiferromagnetic* ($J < 0$). Panels (b) and (d) represent cross-sections of the density plots (a) and (c), respectively, for selected values of J. Note that all spectral functions are normalized to $A_0 \equiv A(0)$ for $J = 0$. The parameters describing the molecule are as follows: $D = 5 \cdot 10^{-5}$, $D_1 = -5 \cdot 10^{-6}$, $D_2 = 2 \cdot 10^{-6}$, $\varepsilon = -0.1$ and $U = 0.3$ (all given in units of $\mathfrak{D}$). Other parameters are: $P = 0.5$, $\Gamma = 0.0225$ ($\mathcal{V}_\uparrow^{\mathrm{AP}} = \mathcal{V}_\downarrow^{\mathrm{AP}} = 0.12$).

the parallel case a strong suppression of the peak is visible, Fig. 6.4. Such a behavior is related to the fact that for identical electrodes in the *parallel* magnetic configuration, the density of states for majority (minority) electrons are the same in both electrodes. Since spin exchange processes leading to creation of the Kondo resonance require transfer of electrons between majority (minority) and minority (majority) conduction bands, the overall effect is much weaker than in the antiparallel case. In particular, the asymmetry between the densities of states in the opposite electrodes in the *antiparallel* magnetic

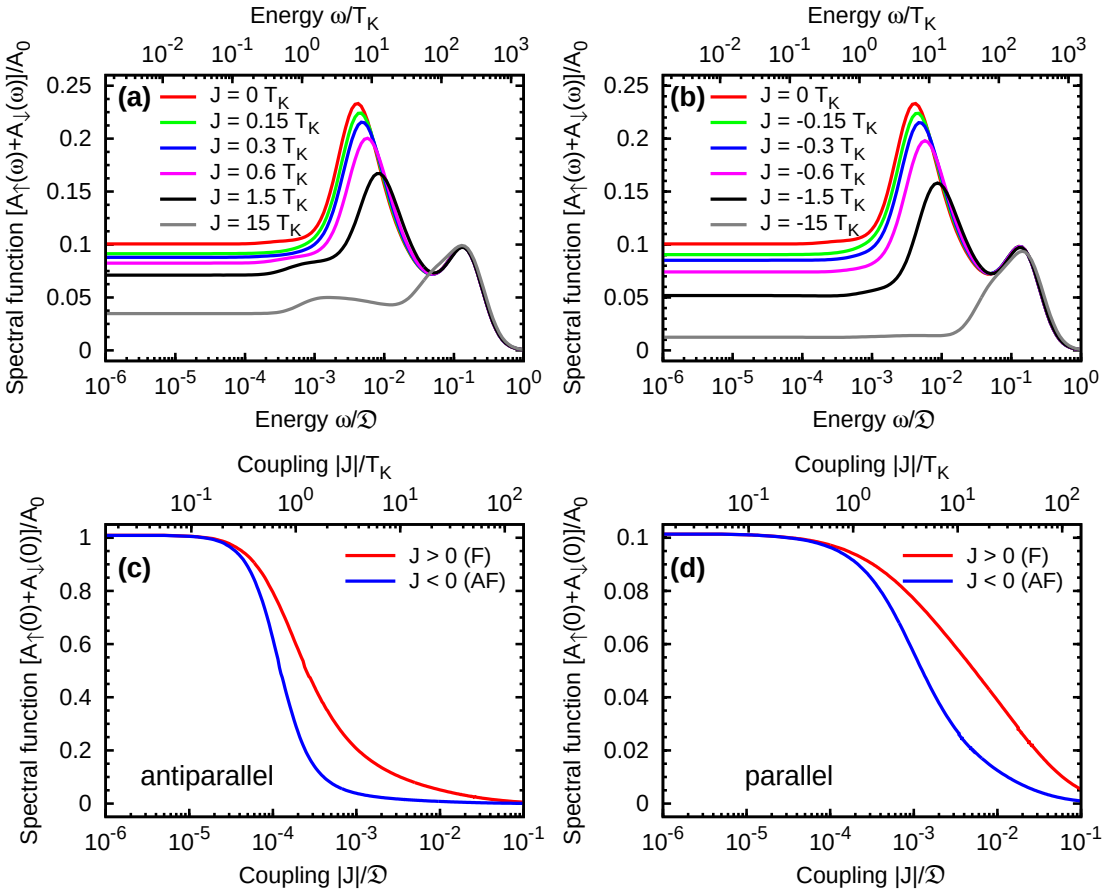

Figure 6.4: The total LUMO level spectral function $A(\omega) = \sum_\sigma A_\sigma(\omega)$ shown for selected values of the coupling J in the case of the *parallel* magnetic configuration of electrodes for both types of the coupling between the LUMO level and the SMM's core spin: (a) *ferromagnetic* ($J > 0$), and (b) *antiferromagnetic* ($J < 0$). Bottom panels present the dependance of the height of the total spectral function at $\omega \approx 0$ on the coupling parameter J for *antiparalel* (c) and *antiparallel* (d) magnetic configurations of the leads. Except $\mathcal{V}_\uparrow^{\mathrm{P}} = 0.147$ and $\mathcal{V}_\downarrow^{\mathrm{P}} = 0.085$, all parameters are the same as in Fig. 6.3.

configuration means that the processes in question occur through the majority-majority (and also through the minority-minority) channel, and thus they are more effective, resulting in the sharp resonance.

With the increase of J, the height of the peak becomes reduced, and for $|J| \gg T_{\mathrm{K}}$ it almost completely vanishes. It can also be seen that the disappearance of the resonance is faster in the case of the antiferromagnetic coupling, Figs. 6.4(c)-(d). Furthermore, as the coupling J grows stronger, some additional features of spectral functions emerge. Apart from the Hubbard peak, stemming form the Coulomb repulsion of two electrons in the LUMO level, there are two additional resonances for the coupling between the LUMO level spin and the SMM's core spin of the ferromagnetic type ($J > 0$), Figs. 6.3(a)-(b) and 6.4(a), and one resonance in the antiferromagnetic case ($J < 0$), Figs. 6.3(c)-(d)

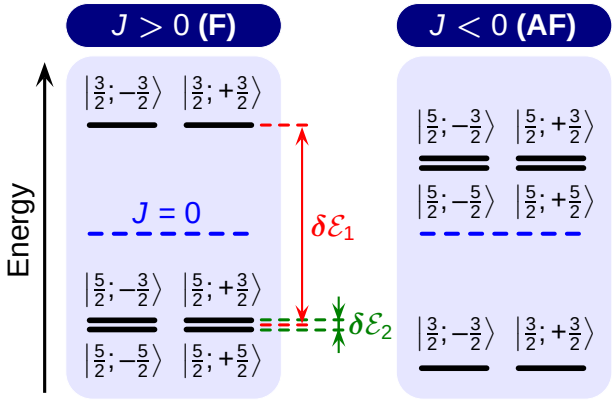

Figure 6.5: Illustration shows schematically the position of selected lowest lying states within spin multiplets corresponding to single occupation of the LUMO level, which participate in formation of resonances in the Kondo effect. The dashed line represents the position of the LUMO level in the absence of the exchange coupling ($J = 0$).

and 6.4(b). Among the two resonances for $J > 0$, the position of one depends on energy very weakly (line A), whereas the other one moves towards larger energies with increasing J (line B), see the dashed lines in Fig. 6.3(a). The behavior of the latter peak suggests that it has the same origin as the peak appearing for $J < 0$, Fig. 6.3(c).

In order to explain the mechanism responsible for creation of the resonances under consideration, it can be useful to consider the role of the lowest lying molecular states corresponding to single occupation of the LUMO level, Fig. 6.5. It should be noted, however, that although such a simplified picture can be helpful here, in fact it is not entirely correct. Due to the application of the NRG procedure, the energy spectrum of the molecule can no longer be described by means of formulae given in Section 2.4, because now one deals with new hybridize states resulting from the strong coupling between electron states in electrodes and the LUMO level of a SMM. Nevertheless, I will use the spectrum of a free-standing molecule to draw at least some quantitative conclusions about the origin of the additional resonances.

First of all, I shall recall that the many-body states belonging to spin-multiplets corresponding to a singly occupied SMM have the general form

$$|S_t = S \pm 1/2; 1, m\rangle = \mathbb{A}_m|{\downarrow}\rangle_{\rm orb} \otimes |m{+}1/2\rangle_{\rm mol} + \mathbb{B}_m|{\uparrow}\rangle_{\rm orb} \otimes |m{-}1/2\rangle_{\rm mol}, \qquad (6.22)$$

where the significance of coefficients $\mathbb{A}_m$ and $\mathbb{B}_m$ was discussed in Section 2.4. It has been shown that the coupling between the electron spin occupying the LUMO level and the SMM's core spin leads to decomposition of molecular magnetic states into two spin-multiplets for $Q = 1$, and the sign of the coupling parameter J decides whether the multiplet $S + 1/2$ or $S - 1/2$ has lower energy, see Fig. 2.4(b)-(c). Since in the present chapter I consider only the case of $T = 0$, thus it seems justified to assume that only the states of lowest energy in both spin-multiplets contribute significantly to the effect.

In some sense, this situation is similar to the case of a quantum dot subjected to an external magnetic field, which leads to splitting the Kondo resonance [228, 264]. The main difference is that for a quantum dot, one level splits into two, whereas in the case of a SMM one gets much more complex energy structure. Moreover, except the states $|5/2;1,\pm 5/2\rangle$, all molecular states for $Q=1$ are the admixture of states corresponding to the LUMO level containing an electron with the spin 'up' and 'down'.

Let's analyze the situation for $J>0$, the left panel of Fig. 6.5, and assume that initially the molecule occupies the state $|5/2;-5/2\rangle$.[7] As it was introduced at the beginning of this chapter, in the virtual state the molecule can either accommodate another electron or release one, and then upon returning to the initial state the spin direction of the electron in the LUMO level can be reversed. However, in the situation under consideration it means that the SMM can end up in one of three states: $|5/2;-5/2\rangle$ (i.e. it goes back to the same state – no contribution to the Kondo effect), $|5/2;-3/2\rangle$ and $|3/2;-3/2\rangle$. Using Eqs. (2.19)-(2.22), it can be estimated that for $J \gg D^{(1)}$, with $D^{(1)}=D+D_1$, the energy gaps shown in Fig. 6.5 are

$$\begin{cases} \delta\mathcal{E}_1 \approx \dfrac{2S+1}{2}J, \\ \delta\mathcal{E}_2 \approx 2SD^{(1)}\left[1-\dfrac{2J-2D^{(1)}}{(2S+1)(J-2D^{(1)})}\right]. \end{cases} \tag{6.23}$$

Consequently, it transpires that the origin of the resonance marked by the line A is related to transitions characterized by the energy gap $\delta\mathcal{E}_2$, while the resonance indicated by the line B by $\delta\mathcal{E}_1$.

The situation changes slightly for the exchange coupling of the antiferromagnetic type ($J<0$), Fig. 6.3(c), because then the position of the spin-multiplets $S+1/2$ and $S-1/2$ is interchanged with respect to the case of $J>0$. Assuming that the SMM is at the beginning in the state $|3/2;-3/2\rangle$, due to processes resulting in reversing the spin of an electron occupying the LUMO level, the molecule can in principle be transferred into five different states: $|5/2;-5/2\rangle$, $|5/2;-3/2\rangle$, $|5/2;-1/2\rangle$, $|3/2;-3/2\rangle$, and $|3/2;-1/2\rangle$. However, taking into account all possible transitions, it turns out that the dominating contribution should just come from transitions to the state $|5/2;-3/2\rangle$ (characterized by the energy gap $\delta\mathcal{E}_1$), and, as a result, only the resonance denoted by the line B is visible. It is also worth highlighting that for $J<0$ the resonance is even more distinct than the analogous peak for $J>0$. Finally, the origin of resonances in the case of the parallel magnetic configuration, Fig. 6.4(a)-(b), can be qualitatively analyzed in a similar way.

Figure 6.6 presents how the total LUMO level spectral function $A(\omega)=\sum_\sigma A_\sigma(\omega)$ depends on the position of the LUMO level ε. It can be seen that most significant modifications of the spectral function, with respect to the case of $J=0$, appear in the region corresponding to single occupation of the LUMO level ($Q=1$). Let's focus on analyzing the behavior of the spectral functions for low energies. First of all, for $J=0$ in

[7] For notational clarity, I omit here the number of electrons occupying the LUMO level, as in the current case it is always $Q=1$.

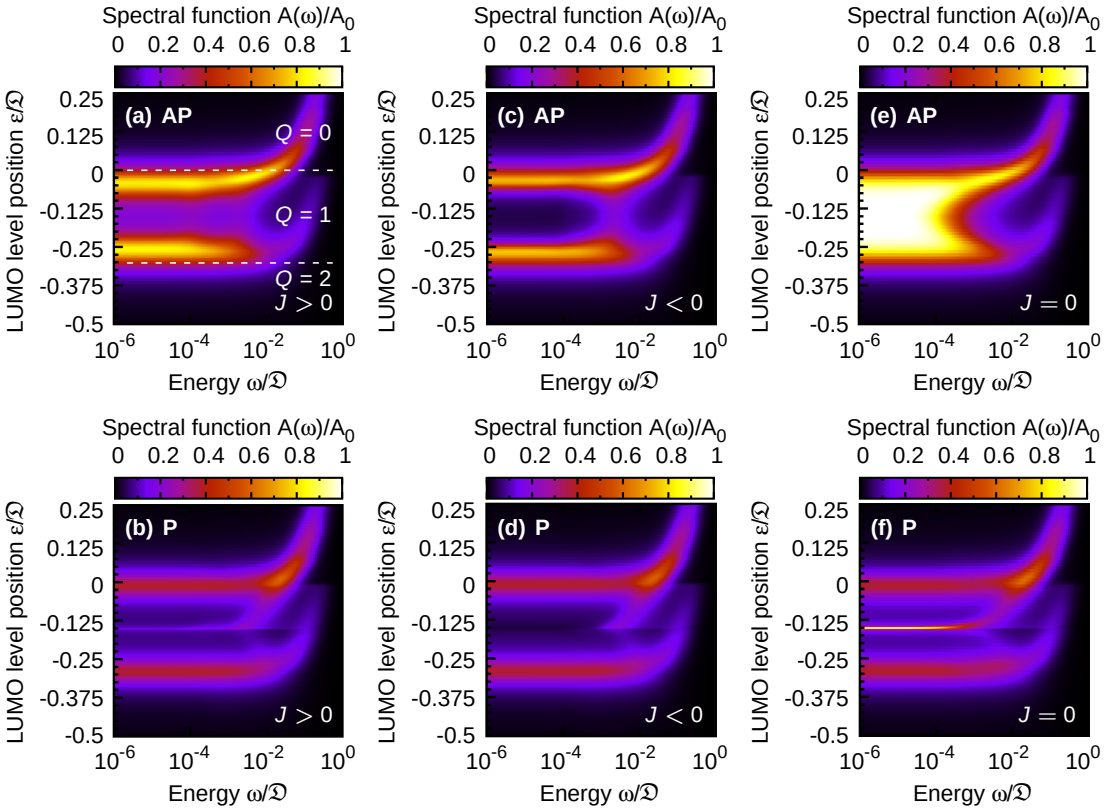

Figure 6.6: The dependance of the total LUMO level spectral function $A(\omega) = \sum_\sigma A_\sigma(\omega)$ on the position of the LUMO level ε for the *antiparallel* (a,c,e) and *parallel* (b,d,f) magnetic configuration of electrodes, in the case of the *ferromagnetic* (a,b) and *antiferromagnetic* (c,d) coupling between the LUMO level spin and the SMM's core spin. For comparison the rightmost panels show the spectral function when $J = 0$. Here, $|J| = 0.0005$, and the remaining parameters are as in Fig. 6.3 and 6.4.

the antiparallel magnetic configuration, Fig. 6.6(e), it can be seen that when the LUMO level is occupied by one electron, the clearly pronounced Kondo resonance arises, and it survives until the population of the level by another electron is energetically allowed. The vanishment of the Kondo effect in the situation when the LUMO level accommodates two electrons of opposite spins is related to the fact that the effective spin of the level is then equal to zero, so that spin exchange processes due to tunneling of electrons cease to operate. For the antiparallel orientation of electrodes' magnetic moments, one observes the maximal value of $A(\omega)$ in the whole region of the LUMO level position ε corresponding to $Q = 1$, because, as discussed above, one of the transport channels, responsible for reversing the spin of an electron in the LUMO level, involves only the majority spin bands of the electrodes.

The situation alters completely in the parallel magnetic configuration, Fig. 6.6(f), where for $Q = 1$ the Kondo effect becomes suppressed for almost all values of ε except those that are very close to the position of the LUMO level at which the character of

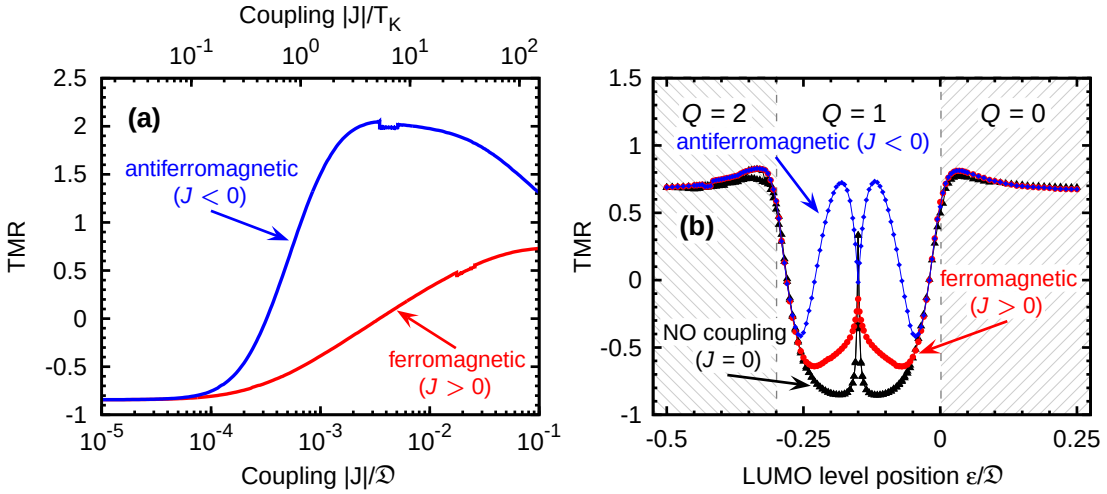

Figure 6.7: (a) Tunnel magnetoresistance (TMR) as a function of the exchange coupling parameter J for the position of the LUMO level $\varepsilon = -0.1$. (b) Comparison of TMR as a function of ε when $|J| = 0.0005$ for the two types of the exchange coupling between the LUMO level and the SMM's core spin with the case of $J = 0$.

transport changes from particle- to hole-type (i.e. the *particle-hole symmetry point*, mentioned in Section 5.3.1). In such a point, the Fermi level of electrodes lies exactly in the middle of the energy gap between the states corresponding to single and double electron occupancy of the level, Fig. 6.1(a). Consequently, in the vicinity of this point both hole-like [the bottom path in Fig. 6.1(a)] and particle-like [the top path in Fig. 6.1(a)] mechanisms of transport leading to creation of the Kondo peak are active. The superposition of these two processes, in turn, allows for circumvention of the problems with spin exchanging transport processes stemming from the parallel magnetic configuration of electrodes. If I now turn on the interaction between the LUMO level and the SMM's core spin ($J \neq 0$), Figs. 6.6(a)-(d), this generally results in quenching of the spectral function in the region where the LUMO level is singly occupied. Furthermore, the suppression of the Kondo resonance is more noticeable for the antiferromagnetic type of the coupling. The nature of such a behavior can be understood on the basis of analogous arguments that I used earlier to explain the dependance of the Kondo resonance on the coupling parameter J.

Employing the data presented in Figs. 6.4(c)-(d) and 6.6, as well as the formulae for conductance of the system, Eqs. (6.21), I can calculate tunnel magnetoresistance as

$$\mathrm{TMR} = \frac{\widetilde{G}_{\mathrm{P}} - \widetilde{G}_{\mathrm{AP}}}{\widetilde{G}_{\mathrm{AP}}}. \tag{6.24}$$

The result is shown in Fig. 6.7. First of all, it can be noticed that for small values of the coupling J between the LUMO level spin and the SMM's core spin, transport in the antiparallel magnetic configuration can dominate over transport in the parallel

configuration, which is represented by the negative TMR. However, as $|J|$ gets increased, the trend becomes reversed. I recall here that the growth of the coupling strength J is associated with broadening the energy gap $\delta\mathcal{E}_1$ between the key states participating in formation of the Kondo resonance, Eq. (6.23) – the energy gap $\delta\mathcal{E}_1$ remains approximately constant.

Even more interesting seems to be the dependance of TMR on the LUMO level position, Fig. 6.7(b), as this figure allows me to make a qualitative comparison between the results obtained for the *weak* and *strong* regime of coupling between the molecule and electrodes; for TMR in the *weak* coupling regime see Figs. 5.6(a) and 5.12(a). To begin with, it should be emphasized that the curve for $J = 0$ agrees with the result obtained by means of the same method for a quantum dot coupled to ferromagnetic leads [254]. One can see that in the case of a SMM, TMR differs greatly from that for a simple quantum dot. Furthermore, similarly as in the case when the molecule was only *weakly* coupled to electrodes, Figs. 5.6 and 5.12, TMR is sensitive to the type of the exchange coupling between the electron spin at the LUMO level and the SMM's core spin. Interestingly enough, it seems that there exist some correspondence between main features of the curves in the *strong* and the *weak* coupling regime. For instance, the increase of TMR in the vicinity of the middle point ε_m[8] is observed, and generally TMR for $J < 0$ is larger than for $J > 0$ in this region. The most striking difference, on the other hand, concerns the fact that in the present situation TMR can be negative for the position of the LUMO level ε corresponding to the level occupied by a single electron ($Q = 1$).

[8]Note that in the situation under consideration this point doesn't correspond to the particle-hole symmetry point. It is worth recalling that owing to the presence of corrections D_1 and D_2, representing the influence of the LUMO level's occupation on to the anisotropy, the Hamiltonian describing a SMM (2.5) doesn't exhibit the the particle-hole symmetry.

CHAPTER 7

Optically stimulated current-induced magnetic switching of a single-molecule magnet

From the point of view of potential applications of all mechanisms that can lead to the reversal of a magnetic moment, and hance serve to write a bit of information, an important issue is the time at which the process can take place. In the case of the switching due to a precessional motion in the presence of a perpendicular magnetic field pulse, it has been shown that deterministic magnetization reversal ceases for pulses shorter than a few picoseconds [265]. The main problem with fast magnetic switching concerns the fact that an ultrafast stimulus usually enforces the system into a strongly nonequilibrium thermodynamic state [266], as in such a case the time scale at which thermalization of a magnetic excitation occurs is much longer than that associated with the excitation mechanism. It would be therefore desired to utilize some non-thermal mechanizm, which would allow avoiding the major obstacle stemming from limitation of the repetition rate by the cooling time, i.e. one wouldn't have to wait until the system returns to the initial (ground) state before application of the next pulse.

Generally, experiments employing optical methods for controlling the magnetic state of a system can be divided into two groups depending on whether an optical pulse is absorbed or not. Since in the former case the absorption of photons is followed by an increase of temperature, such methods are referred to as *thermal* ones, and consequently the latter group encompasses so called *non-thermal* methods. As already mentioned above, the major problem for obtaining fast magneto-optical demagnetization or switching with thermal methods is relatively long time which the system needs to recover an equilibrium state [267–269]. Moreover, the complete reversal of the magnetization occurs

only in the presence of an external magnetic field [270]. As a result, during previous years much effort has been devoted to exploring properties of non-thermal processes, and it has been experimentally demonstrated that ultrafast magnetic processes can be effectively induced and studied with the use of laser pulses [266, 271–274].

One of the most compelling ideas suggested so far is the possibility of using circularly polarized light to manipulate a magnetic system with the resultant effect analogous to a magnetic field oriented parallel to the wave vector. Although this mechanism, called the *inverse Faraday effect*, was proposed [275, 276] and shown to work [277] almost half a century ago, only the recent development of modern high-power and ultrafast lasers raises hope for exploiting the latent technological potential of this effect. An important property of the inverse Faraday effect is that it employs Raman-type coherent optical scattering processes *via* virtual states with strong spin-orbit coupling, and thus no absorption of photons is involved [278]. It means that the effect of light on the magnetization is non-thermal [279]. It should also be stressed that no external magnetic field is necessary for the process to take place and the final magnetic state of the system depends only on the helicity of the laser pulse.

Up to now, circularly polarized femtosecond pulses have been proven to control spin oscillations in a weak ferromagnet $DyFeO_3$ [279]. Additionally, reproducible reversal of the magnetization in an amorphous ferrimagnet alloy GdFeCo by a single 40 fs circularly polarized laser pulse [278, 280] as well as optical control of the magnetization in ferrimagnetic garnet films [281] have been demonstrated. Although the general theory of the mechanism [276, 282–285] has been generally accepted, the universal microscopic mechanism is still the subject of debate as it is not clear which reservoir, i.e. the crystal lattice or photons, is the source of angular momentum required for the magnetic switching [286–288]. Moreover, it has been shown that it is rather unlikely that the effect arises owing to the direct magnetic-dipole interaction between the angular momentum of a medium and the magnetic field of the light wave, because such a mechanism would require much larger beam intensities than those actually used in experiments [289]. The general conclusion is that the switching of magnetization caused by the inverse Faraday effect occurs as a complex multistage process in which orbital, spin, photon and phonon systems participate.

From a fundamental perspective, both the Faraday and inverse Faraday effect derive from the same free energy [276, 277, 290], and thus from a thermodynamical point of view they constitute a pair of reciprocal processes [291, 292]. One should therefore expect that if a magnetic system is capable of inducing the rotation of the polarization plane of electromagnetic (EM) wave passing through it (the Faraday effect), the reverse process should in principle also operate, i.e. circularly polarized light can influence the magnetization of the system (the inverse Faraday effect). This point motivates my interest in application of optical methods for manipulating the magnetic state of SMMs, as at least one SMM species (the Mn_{12} family) has been shown to exhibit the Faraday effect[1] [293].

[1]Note that the experiment was performed on a sample consisting of iso-oriented single crystals, and not on a single molecule.

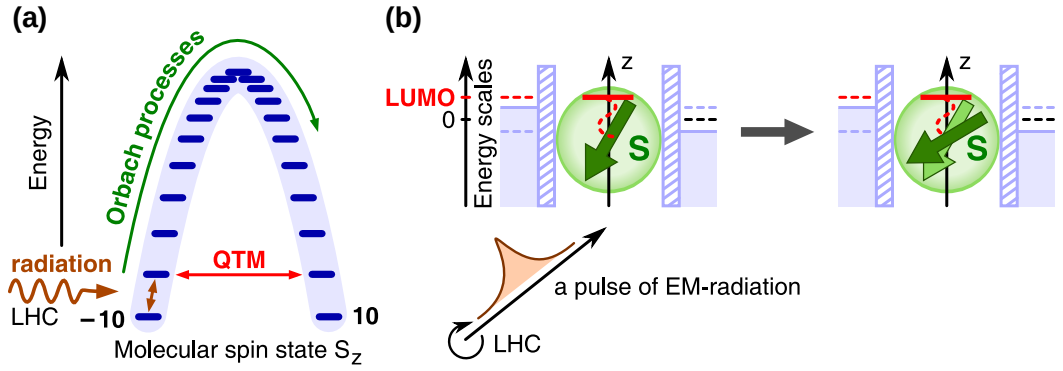

Figure 7.1: (a) Schematic depiction of various processes relevant for the spin dynamics that can arise after resonant absorption of the *left-handed circularly polarized* (LHC) EM-radiation. (b) Symbolic illustration of the application of a short LHC EM-radiation pulse to stimulate the CIMS of the SMM's spin in the *Coulomb blockade* regime.

However, despite growing interest in investigating optical properties of SMMs, not much is known about their non-thermal response to EM-radiation, even in a crystal form. On the other hand, attempts to control the magnetization dynamics of SMMs (bulk samples) by absorption of continuous or pulsed radiation turned out to be more successful.

It has been demonstrated that the partial reversal of the magnetization of a system of Fe_8 molecules induced by applying radiation at resonant frequency is feasible [294, 295]. In such a case, the absorption of radiation triggers transition between two lowest energy levels, and this in turn is subsequently followed by thermal (Orbach) or tunneling relaxation processes [296], Fig. 7.1(a). Moreover, time-resolved magnetization experiments in the presence of EM-radiation provide valuable information about the spin relaxation time or spin decoherence time [297]. On the experimental ground, the situation becomes even more interesting if the radiation of frequency resonant with transition between two excited states is used. Because of the much larger phonon DOS, when the spin system returns to the a state of lower energy after the excitation, it will most likely release a phonon instead of a photon. Thermalization of these phonons leads to augmenting the temperature of the sample, and in consequence also to the increased population of excited states. This means that more photons can be absorbed, and thus the system is driven towards higher temperatures as an effect of such a feedback mechanism [298, 299]. Furthermore, the problem of heating can be circumvented by performing experiments at much shorter time scale. Subjecting the crystal of Fe_8 molecules to an intense and short microwave pulses, it turns out that the *phonon bottleneck effect*[2] starts playing a dominant role in the magnetization dynamics, for it puts a constraint on the spin-phonon relaxation [73, 297, 306].

[2] In general, the *phonon bottleneck effect* arises as a consequence of some hindrance in energy transfer from the spin system to the phonon bath [300–302]. It is worth mentioning that in the case of molecular magnets which don't exhibit an energy barrier against the spin reversal, the effect is responsible for the occurrence of characteristic butterfly-like hysteresis loops [303–305].

The main objective of this thesis is to analyze transport properties of SMMs with dominating *uniaxial* anisotropy in terms of possible mechanism allowing the manipulation of the molecule's spin. Therefore in the following section I will focus primarily on the absorption of circularly polarized light in the context of its application to stimulate CIMS in the *Coulomb blockade* regime, Fig. 7.1(b). Since there is no external magnetic field applied, and very low temperatures are assumed, all thermal and quantum tunneling-based reversal processes are disregarded. The main emphasis is put on analyzing the effect of transitions between molecular magnetic states induced by tunneling of electrons and interaction of the molecule with EM-radiation. Nonetheless, the temperature dependent spin relaxation processes are taken into account on a phenomenological level, as discussed in Section 4.2.

7.1 The effective Hamiltonian of interaction between a single-molecule magnet and EM-radiation

In order to model the interaction between a SMM and EM-radiation, the Hamiltonian of the form characteristic to the *linear magnetoelectric effect* is adopted [284, 307, 308]

$$\mathcal{H}_{\text{eff}}^{\text{mol-EM}} = -\sum_{i,j=x,y,z} \alpha_{ij} E_i H_j. \tag{7.1}$$

Here, α_{ij} is a second-rank tensor, in general unsymmetrical, called the *magnetoelectric* (ME) *susceptibility tensor*. Making the substitution $H_j \to M_j = -g\mu_{\text{B}} S_j$, where $\mathbf{S} = [S_x, S_y, S_z]$ denotes the spin of a molecule, one therefore obtains

$$\mathcal{H}_{\text{eff}}^{\text{mol-EM}} = g\mu_{\text{B}} \sum_{i,j=x,y,z} \alpha_{ij} E_i S_j. \tag{7.2}$$

Although the above expression fails to provide an actual physical mechanism governing the interaction, and hence Eq. (7.2) should be considered merely as the representation of a phenomenological model, it allows to capture symmetry features of the system. As discussed in Section 2.2, in the case of a molecule deposited onto a surface or attached to electrodes, symmetry-related issues may play a dominat role in describing transport through the molecule.

To keep calculations maximally clear, it is assumed that EM-wave propagates along the z-axis $\boldsymbol{E} = (E_x, E_y, 0)$, so that the Hamiltonian can be put down explicitly as follows,

$$\begin{aligned}\mathcal{H}_{\text{eff}}^{\text{mol-EM}} = g\mu_{\text{B}} \Big\{ &\alpha_{xx} E_x S_x + \alpha_{xy} E_x S_y + \alpha_{xz} E_x S_z \\ &+ \alpha_{yx} E_y S_x + \alpha_{yy} E_y S_y + \alpha_{yz} E_y S_z \Big\}.\end{aligned} \tag{7.3}$$

Furthermore, introducing the ladder operators for the SMM's spin operator $S_\pm = S_x \pm$

iS_y, and then using the auxiliary operators

$$\begin{cases} \widetilde{S}_x = \alpha_{xx}(S_+ + S_-) + i\alpha_{xy}(S_- - S_+) + 2\alpha_{xz}S_z, \\ \widetilde{S}_y = \alpha_{yx}(S_+ + S_-) + i\alpha_{yy}(S_- - S_+) + 2\alpha_{yz}S_z, \end{cases} \tag{7.4}$$

the Hamiltonian is cast in a more compact form

$$\mathcal{H}_{\text{eff}}^{\text{mol-EM}} = \frac{g\mu_{\text{B}}}{2}\Big(E_x\widetilde{S}_x + E_y\widetilde{S}_y\Big). \tag{7.5}$$

Within the quantum-mechanical model of the EM-field, the electric-field operator can be expressed as [239, 309, 310]

$$\mathbf{E}(\mathbf{r},t) = i\sum_{\mathbf{k},s}\sqrt{\frac{\hbar\omega_k}{2\varepsilon_0 V}}\mathbf{e}_{\mathbf{k}s}\Big[a_{\mathbf{k}s}\mathrm{e}^{i(\mathbf{k}\cdot\mathbf{r}-\omega_k t)} - a_{\mathbf{k}s}^{\dagger}\mathrm{e}^{-i(\mathbf{k}\cdot\mathbf{r}-\omega_k t)}\Big], \tag{7.6}$$

where $\mathbf{k}$ is a wavevector describing the propagation of a EM-wave, ω_k is an angular frequency for the $\mathbf{k}$-mode, and $\mathbf{e}_{\mathbf{k}s}$ $(s = 1, 2)$ are two orthogonal unit polarization vectors (i.e. $\mathbf{e}_{\mathbf{k}s}\cdot\mathbf{e}_{\mathbf{k}s'} = \delta_{ss'}$), which satisfy the condition $\mathbf{e}_{\mathbf{k}s}\cdot\mathbf{k} = 0$.

Since in the case under consideration, I am interested only in a one-mode field, all redundant $\mathbf{k}$-indices are omitted. Furthermore, making use of the fact that the EM-field oscillations take place in the xy plane, I align polarization versors along x and y axes. Finally, because the wave length λ of radiation to be employed is much larger that the size of the molecule characterized by $\mathbf{r}_{\text{mol}}$, the *dipole approximation* [239] is applied,

$$\frac{\lambda}{2\pi} = \frac{1}{|\mathbf{k}|} \gg |\mathbf{r}_{\text{mol}}| \quad \Rightarrow \quad \mathrm{e}^{\pm i\mathbf{k}\cdot\mathbf{r}} \approx 1 \pm i\mathbf{k}\cdot\mathbf{r} + \text{h.o.}, \tag{7.7}$$

so that the exponential term can be replaced by unity. As a result, one derives

$$\mathbf{E}(t) = i\sqrt{\frac{\hbar\omega}{2\varepsilon_0 V}}\Big\{\big[\mathbf{e}_x a_x + \mathbf{e}_y a_y\big]\mathrm{e}^{-i\omega t} - \big[\mathbf{e}_x a_x^{\dagger} + \mathbf{e}_y a_y^{\dagger}\big]\mathrm{e}^{i\omega t}\Big\}. \tag{7.8}$$

Because the primary objective of this chapter is to consider transfer of angular momentum between photons and a molecule, the choice of a proper basis for the polarization of photons is of major importance. Up to this point, the polarization of the beam has been described by versors along x and y axes, i.e. photons in the beam are polarized either along x or y axis. Since the key feature of the system under investigation is to be the presence of circularly polarized light, thus such a basis will not be very convenient to handle in further analysis. Consequently, one would prefer a basis which inherently expressed the polarization of the beam in terms of left-handed and right-handed circularly polarized photons. For this purpose, I use a *canonical transformation* for photon-field operators and polarization versors [311]:

$$\begin{pmatrix} a_L \\ a_R \end{pmatrix} = \frac{1}{\sqrt{2}}\begin{pmatrix} 1 & -i \\ 1 & i \end{pmatrix}\begin{pmatrix} a_x \\ a_y \end{pmatrix} \quad \text{and} \quad \begin{pmatrix} \mathbf{e}_+ \\ \mathbf{e}_- \end{pmatrix} = \frac{1}{\sqrt{2}}\begin{pmatrix} 1 & i \\ 1 & -i \end{pmatrix}\begin{pmatrix} \mathbf{e}_x \\ \mathbf{e}_y \end{pmatrix}, \tag{7.9}$$

which yields

$$\mathbf{E}(t) = iE_0(\omega)\Big\{\big[\mathbf{e}_+ a_L + \mathbf{e}_-\ a_R\big]\mathrm{e}^{-i\omega t} - \big[\mathbf{e}_- a_L^\dagger + \mathbf{e}_+ a_R^\dagger\big]\mathrm{e}^{i\omega t}\Big\}, \tag{7.10}$$

with $E_0(\omega) = \sqrt{\hbar\omega/(2\varepsilon_0 V)}$. It is worth noting that the transformation in Eq. (7.9) doesn't change the number of photons,

$$\mathbf{a}^\dagger\mathbf{a} = a_x^\dagger a_x + a_y^\dagger a_y = a_L^\dagger a_L + a_R^\dagger a_R. \tag{7.11}$$

The x and y components of the electric-field operator in the new basis is given by

$$\begin{cases} E_x(t) = \mathbf{E}(t)\cdot\mathbf{e}_x = iE_0(\omega)\Big\{\big[a_L + a_R\big]\mathrm{e}^{-i\omega t} - \big[a_L^\dagger + a_R^\dagger\big]\mathrm{e}^{i\omega t}\Big\}, \\ E_y(t) = \mathbf{E}(t)\cdot\mathbf{e}_y = -E_0(\omega)\Big\{\big[a_L - a_R\big]\mathrm{e}^{-i\omega t} + \big[a_L^\dagger - a_R^\dagger\big]\mathrm{e}^{i\omega t}\Big\}, \end{cases} \tag{7.12}$$

so that the final expression for the interaction Hamiltonian takes the form

$$\begin{aligned} \mathcal{H}_{\text{eff}}^{\text{mol-EM}}(t) = \frac{1}{2}g\mu_{\text{B}}E_0(\omega)\Big\{ & i\big[a_L + a_R\big]\widetilde{S}_x\mathrm{e}^{-i\omega t} - i\big[a_L^\dagger + a_R^\dagger\big]\widetilde{S}_x\mathrm{e}^{i\omega t} \\ & -\big[a_L - a_R\big]\widetilde{S}_y\mathrm{e}^{-i\omega t} - \big[a_L^\dagger - a_R^\dagger\big]\widetilde{S}_y\mathrm{e}^{i\omega t}\Big\}. \end{aligned} \tag{7.13}$$

Some additional auxiliary operators,

$$\begin{array}{ll} \mathcal{A}_{x(1)} = \big[a_L + a_R\big]\widetilde{S}_x, & \\ \mathcal{A}_{x(2)} = \big[a_L^\dagger + a_R^\dagger\big]\widetilde{S}_x, & \end{array} \quad \text{and} \quad \begin{array}{ll} \mathcal{A}_{y(1)} = \big[a_L - a_R\big]\widetilde{S}_y, & \\ \mathcal{A}_{y(2)} = \big[a_L^\dagger - a_R^\dagger\big]\widetilde{S}_y, & \end{array} \tag{7.14}$$

allow me to retype the equation in an abbreviated form

$$\mathcal{H}_{\text{eff}}^{\text{mol-EM}}(t) = \frac{1}{2}g\mu_{\text{B}}E_0(\omega)\Big\{\big[i\mathcal{A}_{x(1)} - \mathcal{A}_{y(1)}\big]\mathrm{e}^{-i\omega t} - \big[i\mathcal{A}_{x(2)} + \mathcal{A}_{y(2)}\big]\mathrm{e}^{i\omega t}\Big\}. \tag{7.15}$$

7.2 Transition rates

Transition rates between neighboring magnetic molecular states due to the interaction of a SMM with circularly polarized EM-radiation are found by employing Fermi golden rule, similarly as in Chapters 3 and 4. The general expression for the first order transition probability amplitude, for the transition of the state $|l\rangle$ to another orthogonal state $|k\rangle$ [312], is given by

$$c_{l\to k} = \frac{1}{i\hbar}\lim_{T\to\infty}\int_{-T/2}^{T/2}\langle k|H_{\text{eff}}^{\text{mol-EM}}(\tau)|l\rangle\mathrm{e}^{i(\omega_k-\omega_l)\tau}\mathrm{d}\tau. \tag{7.16}$$

Using the Hamiltonian (7.15), it is derived

$$c_{l\to k} = \frac{\pi g\mu_{\text{B}}E_0(\omega)}{\hbar}\Big\{\big[\mathcal{A}_{kl}^{x(1)} + i\mathcal{A}_{kl}^{y(1)}\big]\delta(\omega_{kl}-\omega) - \big[\mathcal{A}_{kl}^{x(2)} - i\mathcal{A}_{kl}^{y(2)}\big]\delta(\omega_{kl}+\omega)\Big\}. \tag{7.17}$$

Here, $\mathcal{A}_{kl}^{x(1)} \equiv \langle k|\mathcal{A}_{x(1)}|l\rangle$, and the remaining terms are defined in analogous way. Moreover, $\omega_{kl} = \omega_k - \omega_l$ and two Dirac's deltas have appeared due to $\lim_{y\to\infty}\int_{-y}^{y}\exp[iax]\mathrm{d}x = 2\pi\delta(a)$. The transition rate $P_{l\to k} = |c_{l\to k}|^2$ reads then as

$$P_{l\to k} = \left(\frac{\pi g\mu_{\mathrm{B}}E_0(\omega)}{\hbar}\right)^2 \Big\{\big|\mathcal{A}_{kl}^{x(1)} + i\mathcal{A}_{kl}^{y(1)}\big|^2\delta^2(\omega_{kl}-\omega) + \big|\mathcal{A}_{kl}^{x(2)} - i\mathcal{A}_{kl}^{y(2)}\big|^2\delta^2(\omega_{kl}+\omega)\Big\}. \tag{7.18}$$

Before I proceed to deriving the sought expression for the transition rates, first I have to deal with the product of Dirac's deltas present in the equation above. I can get rid of one of the deltas in the following way [312]:

$$\delta(a-b)\delta(a-b) = \lim_{T\to\infty}\delta(a-b)\frac{1}{2\pi}\int_{-T/2}^{T/2}\mathrm{e}^{i(a-b)x}\mathrm{d}x = \delta(a-b)\lim_{y\to\infty}\frac{T}{2\pi}, \tag{7.19}$$

where the rightmost formula was obtained by noting that the Dirac's delta in front of the integral differs from zero only if $a = b$, so that the trick is to substitute the integrand with $a = b$. As a result,

$$R_{l\to k} = \frac{P_{l\to k}}{T} = \frac{\pi}{2}\left(\frac{g\mu_{\mathrm{B}}E_0(\omega)}{\hbar}\right)^2 \Big\{\overbrace{\big|\mathcal{A}_{kl}^{x(1)} + i\mathcal{A}_{kl}^{y(1)}\big|^2\delta(\omega_{kl}-\omega)}^{\text{photon's absorption}} + \underbrace{\big|\mathcal{A}_{kl}^{x(2)} - i\mathcal{A}_{kl}^{y(2)}\big|^2\delta(\omega_{kl}+\omega)}_{\text{photon's emission}}\Big\} \tag{7.20}$$

The classical formula for the irradiance of a EM-wave reads as $\mathcal{I} = c\varepsilon_0|\boldsymbol{E}|^2/2$. According to the *correspondence principle* [309, 313] in the limit of large number n of photons in a box of volume V, one can directly relate the quantum energy density to the one following from the classical treatment,

$$\frac{n\hbar\omega}{V} = \frac{1}{2}\varepsilon_0|\boldsymbol{E}|^2 \quad\Rightarrow\quad |\boldsymbol{E}| = 2\sqrt{n}E_0(\omega). \tag{7.21}$$

It allows me to substitute the electric field $E_0(\omega)$ for the intensity $\mathcal{I}(\omega)$ of a laser beam, which is a more preferable parameter to be used in laser spectroscopy experiments. Consequently,

$$\mathcal{I}(\omega) = 2nc\varepsilon_0E_0^2(\omega). \tag{7.22}$$

Last but not least, I take into account the fact that in real systems due to various types of interactions, mainly with the environment, the system can stay excited only for a limited period of time, after which it returns to a state of lower energy. As a result, energy levels acquire finite widths, and transitions between two states can also occur for energies slightly detuned from the resonant value [302]. Equation (7.20) should be thus multiplied by the line shape function $\mathcal{F}_{kl}(\omega)$ that describes broadening of the energy

of two states $|l\rangle$ and $|k\rangle$ involved in the transition process,[3] and then integrated over transition energies,

$$R_{l\to k} = \Big(\frac{g\mu_{\rm B}}{\hbar}\Big)^2 \frac{\pi\mathcal{I}(\omega)}{4nc\varepsilon_0}\Big\{\underbrace{\big|\mathcal{A}^{x(1)}_{kl} + i\mathcal{A}^{y(1)}_{kl}\big|^2\mathcal{F}_{kl}(\omega)}_{\text{photon's absorption}} + \underbrace{\big|\mathcal{A}^{x(2)}_{kl} - i\mathcal{A}^{y(2)}_{kl}\big|^2\mathcal{F}_{kl}(-\omega)}_{\text{photon's emission}}\Big\}. \quad (7.23)$$

Now, I can apply the above equation to the case under consideration. In general, the energy of the radiation can be tuned in order to stimulate specific transitions between two neighboring molecular magnetic states within a certain spin multiplet. It should be noted, however, that for SMMs, due to the presence of uniaxial anisotropy, absorption (as well as emission) of a photon may lead either to increase or decrease of the molecule's zth component of spin ,$S^z_t = m$, depending on whether m is larger or smaller than zero. Therefore for $H_z = 0$, i.e. no external longitudinal magnetic field, the expressions for transitions induced by EM-radiation are classified in the following way:

- for $m \leqslant 1$ ($m \geqslant 1$) *absorption* of a photon results in increasing (decreasing) m

$$\gamma^{|S_t;n,m\rangle|S_t;n,m\pm1\rangle}_{\text{EM-radiation}} = \Big(\frac{g\mu_{\rm B}}{\hbar}\Big)^2 \frac{\pi\mathcal{I}(\omega)}{4c\varepsilon_0}\Big|\big(\sqrt{\eta_L}+\sqrt{\eta_R}\big)\widetilde{S}^x_{m\pm1,m} + i\big(\sqrt{\eta_L}-\sqrt{\eta_R}\big)\widetilde{S}^y_{m\pm1,m}\Big|^2\mathcal{F}_{m\pm1,m}(\omega), \quad (7.24)$$

- for $m \leqslant 0$ ($m \geqslant 0$) *emission* of a photon results in decreasing (increasing) m

$$\gamma^{|S_t;n,m\rangle|S_t;n,m\mp1\rangle}_{\text{EM-radiation}} = \Big(\frac{g\mu_{\rm B}}{\hbar}\Big)^2 \frac{\pi\mathcal{I}(\omega)}{4c\varepsilon_0}\Big|\big(\sqrt{\eta_L}+\sqrt{\eta_R}\big)\widetilde{S}^x_{m\mp1,m} - i\big(\sqrt{\eta_L}-\sqrt{\eta_R}\big)\widetilde{S}^y_{m\mp1,m}\Big|^2\mathcal{F}_{m\mp1,m}(-\omega). \quad (7.25)$$

Here, the abbreviated notation has been used $\widetilde{S}^{x(y)}_{m',m} \equiv \langle S_t;n,m'|\widetilde{S}_{x(y)}|S_t;n,m\rangle$. I have also assumed that the molecule is exposed to large number of photons. Moreover, since from Eq. (7.11) it follows that $n = n_L + n_R$, the total intensity is $\mathcal{I}(\omega) = \mathcal{I}_L(\omega) + \mathcal{I}_R(\omega)$, and $\mathcal{I}_{L(R)} = \eta_{L(R)}\mathcal{I}(\omega)$, where $\eta_{L(R)} = n_{L(R)}/n$ describes the fraction of left-handed (right-handed) circularly polarized photons in a beam. Finally, the line shape function in the above equations is assumed to be the Lorentz function,

$$\mathcal{F}_{kl}(\pm\omega) = \frac{2t^*}{1+(\pm\omega-\omega_{kl})^2 t^{*2}}, \quad (7.26)$$

with t^* denoting a characteristic relaxation time, for simplicity assumed here $t^* = \tau_{\rm rel}$.

The processes of EM-radiation-stimulated transitions between molecular magnetic states, described by Eqs. (7.24) and (7.25), can be then formally incorporated into the master equation (4.11), introduced in Section 4.2. Such approach allows me to study dynamics of the system only in the first approximation, i.e. only sequential tunneling

[3] From the physical point of view, $\mathcal{F}(\omega)$ can be interpreted as the probability density (per frequency unit) of photon's emission or absorption.

processes are taken into account. Since in Chapter 5 it has been shown that second-order (cotunneling) processes can play a fundamental role in the mechanism of the current-induced magnetic switching of the molecule's spin, especially in the Coulomb blockade regime, I should justify why one can with impunity omit higher-order processes in the following discussion. The key are different time scales of the spin's dynamics set by tunneling processes of various orders. Because the spin's reversal due to cotunneling processes occurs at time t_{st} of the order of $10^1 - 10^3$ μs (or even slower, Section 4.3),[4] which is much longer than in the case of the magnetic switching resulting from sequential tunneling of electrons ($t_{\mathrm{st}} \sim 10^1 - 10^3$ ns, Section 4.2), I neglect the former processes as insignificant for the case under consideration.

7.3 The effect of EM-radiation on the magnetic state of a single-molecule magnet

Similarly as in previous three chapters, numerical results are presented for a hypothetical single-molecule magnet of spin $S = 2$ with strong uniaxial magnetic anisotropy. To begin with, it is worth recalling that the magnetic state of a molecule in the absence of bias voltage depends on temperature, Fig. 7.2, which in the model under discussion is straightforwardly related to relaxation processes. Throughout this work I assume that the system is always kept at temperature lower than the blocking temperature T_{B}, which excludes the possibility of occurring thermally activated magnetic relaxation. On the other hand, I take into consideration the fact that the molecule can suffer intrinsic relaxation processes, which on a phenomenological level are included in the model through Eqs. (4.9) and (4.10). For temperatures lower than some characteristic temperature $\widetilde{T}$, when the relaxation processes are frozen, the molecule's spin is trapped in one of two metastable states corresponding to the maximal value of its zth component, the region denoted as ① in Fig. 7.2. It means that once the molecule is saturated in the state $S_z = \pm S$, it should remain in this state for an infinitely long time. Increasing temperature above $\widetilde{T}$, one enters the region ②, where intrinsic spin relaxation starts playing a prominent role, eventually leading to complete dephasing of the molecule's spin. Moreover, it can be seen that the higher the temperature is, the faster the molecule demagnetizes.

The idea of using a pulse of circularly polarized light is to induce instantaneous nonequilibrium in the probability distribution for the states either with the positive or negative zth component of the molecule's spin in order to initiate the magnetic switching. Therefore it matters whether the process takes place in the region ① or ②, as for low bias voltages, i.e. voltages lower than the threshold voltage for CIMS, the effective strength of spin relaxation determines the final magnetic state of the molecule.

To study dynamics of the SMM's spin I solve Eq. (4.11) with additional terms corresponding to transitions induced by EM-radiation, Eqs. (7.24) and (7.25). As previously, it is assumed that at $t = 0$ the molecule occupies only the state $|2; 0, -2\rangle$. Consequently,

[4] It should be noted that this time is comparable or even longer than typical relaxation times experimentally observed in the real molecules, see Section 2.1.

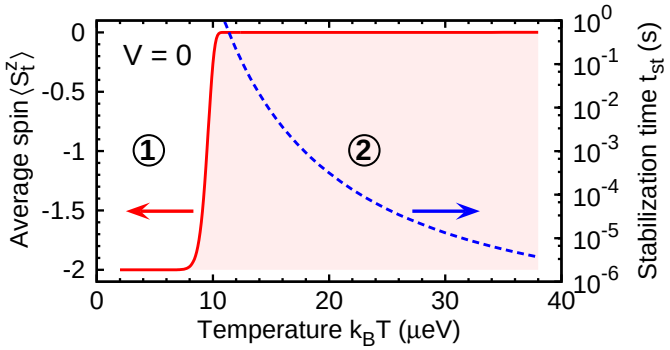

Figure 7.2: Dependance of the average value of the molecule's spin $\langle S_t^z \rangle$ in a *steady state* (solid line) and the time $t_{\rm st}$ the system needs to reach such a state (dashed line) on temperature $k_{\rm B}T$ of the system (expressed in units of energy) in the case of *no* external bias voltage applied ($V = 0$). The molecule of spin $S = 2$ is characterized by the same parameters as in Section 5.2 (i.e. $J = 0.2$ meV, $D = 0.05$ meV, $D_1 = -0.005$ meV, $D_2 = 0.002$ meV, $U = 1$ meV, $\varepsilon = 0.75$ meV), so that the SMM's spectrum is represented by Fig. 5.5(b). The other parameters of the system are: $\tau_{\rm rel} = 1$ ns, $P_L = P_R = 0.5$ and $\Gamma = 0.002$ meV.

in the Coulomb regime only the spin multiplet $|2;0,m\rangle$ participates in the switching mechanism. Furthermore, if the wavelength of the radiation is chosen to be resonant with the transition energy between the states $|2;0,-2\rangle$ and $|2;0,-1\rangle$, the transitions stimulated by light also appear only within this multiplet. Below the explicit form of terms $\widetilde{S}^{x(y)}_{m\pm1,m}$ for transitions within the spin multiplet $|2;0,m\rangle$ is given

$$\begin{cases} \widetilde{S}^{x}_{m\pm1,m} = \mathcal{C}^{\pm}_{m}(\alpha_{xx} \mp i\alpha_{xy}), \\ \widetilde{S}^{y}_{m\pm1,m} = \mathcal{C}^{\pm}_{m}(\alpha_{yx} \mp i\alpha_{yy}), \end{cases} \tag{7.27}$$

where $\mathcal{C}^{\pm}_{m} = \sqrt{S(S+1) - m(m \pm 1)}$. One can note that this is exactly the point where the symmetry of a SMM enters the model *via* elements of the magnetoelectric susceptibility tensor. Since the amount of available information concerning distortion of a SMM's spatial structure during deposition on a surface is still rather modest, see Section 2.2, I limit the following analysis to the simplest case of $\alpha_{xx} = \alpha_{yy} = 10^{-10}$ s/m (typical values [308]) and $\alpha_{xy} = \alpha_{yx} = 0$. Finally, the time evolution of a pulse is described by the Lorentz function

$$f(t) = \frac{t_{\rm WHM}/2}{(t_{\rm WHM}/2)^2 + (t - t_{\rm pos})^2}, \tag{7.28}$$

with $t_{\rm WHM}$ denoting the width of a pulse at half maximum, whereas $t_{\rm pos}$ is the position of a pulse on a time-scale. It should be emphasized that here position of the pulse means position of the maximum value of the pulse.

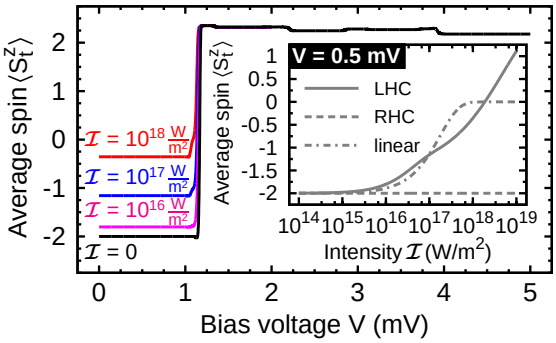

Figure 7.3: Dependance of a *stable state* of the molecule's spin $\langle S_t^z \rangle$ on a bias voltage V for various beam intensities $\mathcal{I}$ in the *antiparallel* magnetic configuration. The parameters describing the light pulse are $\eta_L = 1$ (i.e. left-handed circular polarization), $t_{\mathrm{WHM}} = 75$ ps and $t_{\mathrm{pos}} = 100$ ns (other parameters as for Fig. 7.2). The inset shows how the steady average value of the spin $\langle S_t^z \rangle$ is related to the intensity $\mathcal{I}$ for the voltage $V = 0.5$ mV and $k_{\mathrm{B}}T = 5$ μeV in the case of *left-handed circularly polarized* (LHC, solid line), *right-handed circularly polarized* (RHC, dashed line), and linearly polarized light (dash-dotted line).

7.3.1 The region of a fully blocked spin

I start with considering how the EM-radiation pulse affects the stable state of the SMM's spin, Fig. 7.3. It can be seen that the pulse leaves a permanent mark on the molecule's magnetic state only for voltages not exceeding the threshold voltage for the current-induced magnetic switching. For larger bias voltages, the final state of the molecule is independent of whether it was illuminated or not. This can be easily explained by noticing that transitions stimulated by flow of electrons *via* the LUMO level are characterized by much larger rates than those stemming from interaction of the molecule with EM-radiation. Furthermore, since the former transitions dominate in the system, the light may exert a temporary effect on the spin, but ultimately it is tunneling of electrons that determines the stable state of the SMM's spin. It should also be noted that in the example discussed, the light can affect the state of the molecule's spin only if it is *left-handed circularly polarized*, the inset in Fig. 7.3. For the *right-handed circular polarization* the initial state $|2; 0, -2\rangle$ of the SMM remains unaltered, whereas for the *linearly polarized* light and large intensities the molecule becomes demagnetized.

In the range of voltages corresponding to the Coulomb blockade, where the effect of the EM-radiation on the SMM's spin state is most pronounced, the final state of the system results from the interplay of three independent relaxation processes. First of all, there are processes originating from interaction of the molecule with spin-polarized currents, which are the main topic of this thesis. However, in the case under consideration, when the SMM's spin is saturated in the state of minimal energy and bias voltage is below the threshold value for initiating the CIMS, such processes alone cannot change the molecule's magnetic state. Second, one should also expect some intrinsic spin relaxation dependent on temperature to occur, as discussed above. Finally, the third type of relaxation that can take place in the system are processes stimulated by the light pulse,

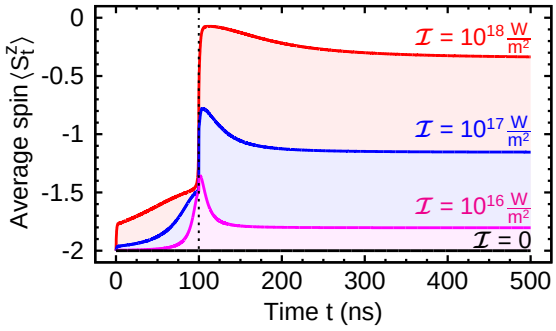

Figure 7.4: Time evolution of the molecule's zth component of the spin when a light pulse is applied to the system at $V = 0.5$ mV. The dotted line depicts the position of the pulse, $t_{\mathrm{pos}} = 100$ ns and $t_{\mathrm{WHM}} = 75$ ps. Remaining parameters the same as for Fig. 7.2.

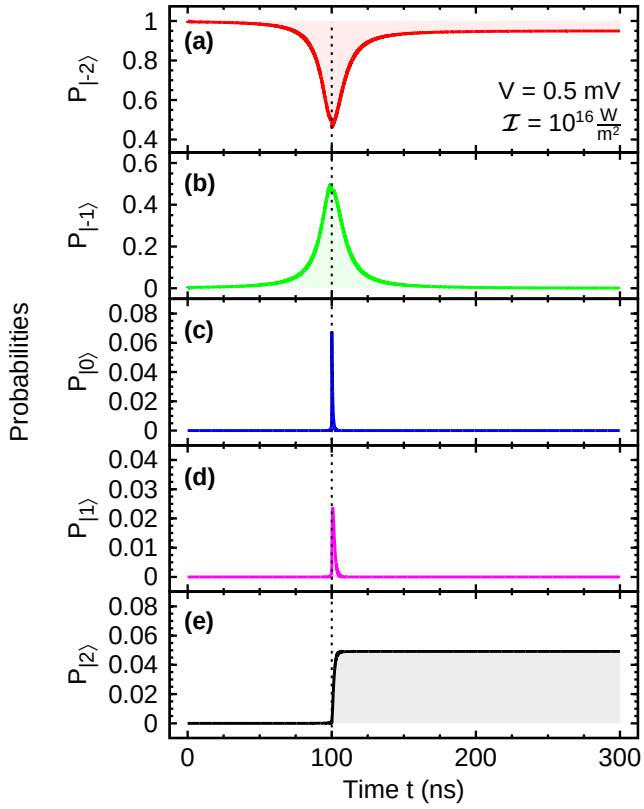

Figure 7.5: Time-dependance of the probabilities for finding a SMM in the state $|2;0,m\rangle \equiv |m\rangle$. The above plots fully correspond to the case of $\mathcal{I} = 10^{16}$ W/m^2 shown in Fig. 7.4.

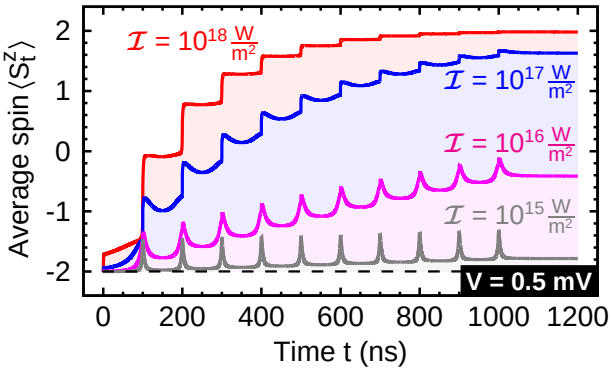

Figure 7.6: Dynamics of the average value of the SMM's spin $\langle S_t^z \rangle$ for the molecule exposed to a series of 10 EM-radiation pulses shown for different maximal pulse intensities $\mathcal{I}$. The time separation of pulses is 100 ns, and the other parameters are as in Figs. 7.3 and 7.4. The dashed line represents the initial state of the molecule's spin.

which are the subject of the present chapter. It transpires then that the last mechanism plays a role of a trigger for a more complex mechanism. Absorbing the pulse, the molecule becomes temporarily excited, so that for a brief moment the energy barrier for the CIMS stemming from too low bias voltage can be circumvented. Therefore it can be seen that the EM-radiation pulse serves here to activate the relaxation processes due to interaction with tunneling electrons, and consequently the intensity beam determines the final magnetic state of a SMM in the Coulomb blockade.

For reasons mentioned above, I focus on analyzing the process of interest only in the Coulomb blockade regime. In Fig. 7.4, the dynamical response of the molecule's spin to a EM-radiation pulse is presented. At $t_{\mathrm{pos}} = 100$ ns, where the pulse reaches its maximal intensity, a significant change in the magnetic state of the molecule is observed, and then during next one to a few hundred nanoseconds the SMM's spin relaxes to the stable state. This behavior of the molecule's spin in the presence of EM-radiation can be qualitatively understood on the basis of the time-evolution of the probability distribution between states of the spin multiplet $|2; 0, m\rangle$, for convenience referred to as $|m\rangle$, Fig. 7.5. At the beginning ($t = 0$), the molecule is saturated in the state $|-2\rangle$, which formally corresponds to $P_{|-2\rangle} = 1$ in Fig. 7.5(a). Since the radiation is tuned to the transition energy between the states $|-2\rangle$ and $|-1\rangle$, when the pulse approaches its maximum intensity at t_{pos}, the building up of the finite probability for finding the molecule in the state $|-1\rangle$ becomes visible, Fig. 7.5(b). Once the maximum value of the intensity $\mathcal{I}$ is reached, the part of the probability is transferred *via* intermediate states to the final state $|2\rangle$. This is possible due to the presence of the line shape function $\mathcal{F}(\omega)$ in Eqs. (7.24) and (7.25), as in a limited range it also admits non-resonant light-induced transition between molecular magnetic states.

The main drawback of the mechanism is the value of the beam intensity $\mathcal{I}$ needed to observe the change in the molecule's spin. Furthermore, the values of $\mathcal{I} \sim 10^{17} - 10^{18}$ W/m^2, which give the most pronounced effect, are definitively beyond the reach of

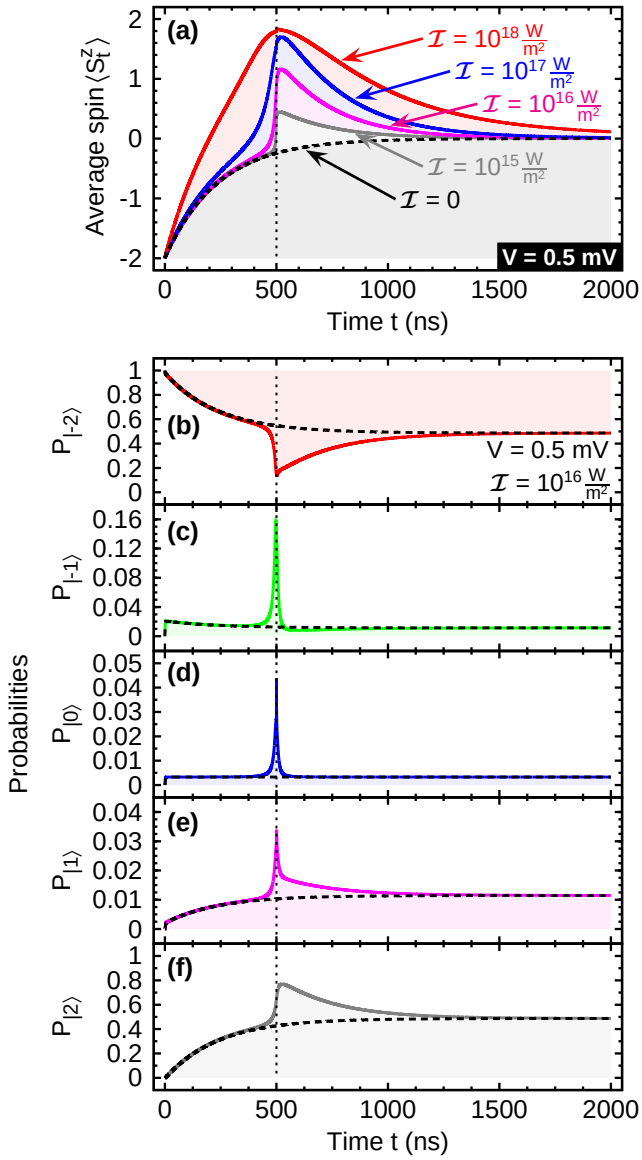

Figure 7.7: (a) Time evolution of the average value of the molecule's spin $\langle S_z^t \rangle$ for different maximal laser pulse intensities $\mathcal{I}$ in the case of $k_{\mathrm{B}}T = 40$ μeV, when intrinsic spin-relaxation processes leads to complete demagnetization of the molecule in a steady state. Remaining parameters except $t_{\mathrm{pos}} = 500$ ns (marked by the dotted line) are the same as in Figs. 7.3 and 7.4. (b)-(f) Probabilities $P_{|m\rangle}$ as a function of time t for the situation corresponding to $\mathcal{I} = 10^{16}$ W/m^2 in (a). The dashed lines represent the relevant probabilities in the case when the molecule is not exposed to EM-radiation.

experiment, and most probably they would lead to destruction of a sample. However, for smaller $\mathcal{I}$ it still should be possible to obtain a significant increase of the molecule's spin by application of a series of light pulses, Fig. 7.6.

7.3.2 The region of significant intrinsic spin relaxation

The situation changes drastically, when one moves to region ②, in which intrinsic relaxation processes start playing an important role. It can be seen that in the absence of the EM-radiation pulse ($\mathcal{I} = 0$) the relaxation processes drive the molecule towards the nonmagnetic state by trying to equalize the probabilities of finding the SMM's spin in one of two states $|\pm 2\rangle$ of the lowest energy. However, because a finite bias voltage is applied, no equal distribution of probabilities between these two states is actually reached, see dashed lines in Fig. 7.7(b)-(f). The final average value of the SMM's spin is slightly larger than zero. Illumination of the molecule with an ultrashort laser pulse induces then only a temporary disequilibrium in the probability distribution seen as an increase of the average value $\langle S_t^z \rangle$, and as soon as the pulse ceases the relaxation processes again tend to restore the even occupation of states $|\pm 2\rangle$.

Concluding remarks and outlook

With the recent development of experimental techniques allowing one to measure transport properties of nanoscopic systems, such as individual molecules, nanotubes or nanowires, a growing interest in describing and understanding transport phenomena through such systems has been observed. Taking into account possible applications in novel spintronic devices, especially promising seem to be single-molecule magnets (SMMs). Not only for this reason, but also for understanding the most fundamental physics underlying transport processes in SMMs, theoretical studies of these systems attract more and more attention. Under this respect, the present dissertation, whose main objective is to investigate transport of charge and spin through a SMM, aims at making a contribution towards advancing the current comprehension of mechanisms governing transport processes through SMMs.

After reviewing some basic properties of SMMs at the beginning of Chapter 2, I focused on introducing formally the model to be discussed throughout the thesis. Since the interface-related issues, following from the actual manner through which a SMM and electrodes are connected, can affect transport through such a system in various ways, I considered here only the minimal model, which allowed for capturing the basic features of the type of molecule under discussion. The model system consisted of a SMM inserted between two metallic, ferromagnetic electrodes of collinear magnetizations. Furthermore, the assumption was made that electronic transport through the molecule occurs only *via* the lowest unoccupied molecular orbital (LUMO) of the SMM, which is in turn exchange coupled with the molecule's core spin. Finally, except Chapter 3, I limited the analysis to the case of molecules which, with a sufficient approximation, can be assumed to be characterized only by the uniaxial anisotropy. Thanks to this assumption I could analytically digonalize the molecular Hamiltonian in the basis of states labeled by the zth component of the molecules total spin, which was crucial from the point of view of theoretical methods to be used in the further part of the thesis.

Next, in Chapter 3 I studied how the presence of reservoirs of spin-polarized electrons

can influence the *quantum tunneling of magnetization* (QTM) in SMMs, which is one of the most recognizable features of many SMMs. Using the *Landau-Zener model* for describing the QTM mechanism, and the perturbation approach (Fermi golden rule) for including the effect of spin-polarized tunneling electrons on the molecule's spin, I showed that relaxation processes stemming from scattering of electrons on the molecule's spin can facilitate the spin reversal due to the QTM.

In the subsequent chapter I investigated the phenomenon of *current-induced magnetic switching* (CIMS) in the case of an individual SMM. The essential mechanism of CIMS relies on angular momentum transfer between tunneling current and a molecule, which is possible due to the presence of the interaction between the spin of an electron occupying the LUMO level and the SMM's core spin. The problem was analyzed in terms of the dynamical response of the molecule's magnetic state to a constant bias voltage. I discussed two distinctive ranges of voltages: the first one, corresponding to the *Coulomb blockade*, where only higher order tunneling processes can occur, and the second one, so-called the *sequential tunneling* regime, in which electrons possess sufficient energy to tunnel freely between the molecule and electrodes. The obtained results suggest that, under certain conditions, the spin reversal induced by a spin-polarized current can take place over a timescale as short as of a few tens of nanoseconds. In addition, the magnetic switching of a SMM is accompanied by an additional signal in the current flowing through the system.

A more general description of various spin effects that can arise in the molecule owing to flow of spin-polarized electrons was provided in Chapter 5. Employing the *real-time diagrammatic technique*, which enabled me to systematically analyze electronic transport through the system in different orders with respect to tunneling processes between electrodes and the molecule, I considered how inclusion of electron cotunneling, i.e. higher-order tunneling processes, modifies transport characteristics of the system in the *linear* and *nonlinear* voltage regime. It transpires that cotunneling processes play a vital role especially in the blockade regime. Moreover, one observes there a complex interplay between inelastic cotunneling, which affects the molecule's spin state, and elastic tunneling of electrons. With the purpose to complete the discussion, I also studied the transport in the situation when electrodes exhibit a significant asymmetry in their spin-polarization parameters, drawing a conclusion that a SMM acts then as a *spin diode*.

The analysis on transport properties of SMMs conducted in Chapters 3-5 concerned only the case of a SMM *weakly* coupled to electrodes. In order order to complement the results of preceding chapters, the opposite limit of *strong* coupling regime was addressed in Chapter 6. By means of the *Wilson's numerical renormalization group*, I investigated the influence of the LUMO level-SMM's core spin coupling strength on the formation of the *Kondo effect*. It turns out that not only does the increase of the coupling parameter J lead to suppression of the Kondo resonance, but also one can notice the occurrence of some extra resonances. Additionally, I computed tunnel magnetoresistance (TMR) as a function of the LUMO level position in the *linear response* regime, so that I could perform qualitative comparison between the result for the weak and strong coupling

regime. It seems there is some general correspondence between the main features of TMR curves in these two cases. However, one should note that in the strong coupling limit, negative TMR is seen, which means that the transfer of electrons is easier for the antiparallel magnetic configuration of leads.

The final chapter was devoted to studying the possibility of applying electromagnetic radiation for stimulation of the CIMS in SMMs. Since the mechanism of CIMS has its origin in angular momentum transfer between the molecule and its environment, therefore it occurs that also a pulse of *circularly polarized electromagnetic radiation* can in principle serve as the source of angular momentum. Following this idea, I showed that in the Coulomb blockade, when a bias voltage is below the threshold value for initiation of CIMS, a short pulse of electromagnetic radiation can be engaged to trigger a series of processes leading to the reversal of the SMM's spin. The precise switching mechanism results in this case from the interplay of relaxation processes stemming from the interaction of a molecule with spin-polarized currents, intrinsic spin relaxation processes and processes induced by absorption of a light pulse. Furthermore, the brief excitation of a SMM due to the radiation absorption allows for temporary circumvention of the energy barrier for the CIMS, which is a consequence of too low bias voltage. The main drawback of the mechanism under discussion is related to extremely large beam intensities at which one could observe the effect. Nevertheless, one possible solution enabling elimination of this problem would be to use a succession of pulses characterized by lower intensities, instead of one high-power pulse.

Although the results presented in this thesis seem to be encouraging for further studies of SMMs in terms of utilizing them as elements of spintronic devices, it should be clearly stated that, from the experimental point of view, the ideas under consideration are still pretty far from realization. One of the major obstacles are low temperatures at which such devices would operate. Thus enormous efforts are concentrated on synthesizing new SMMs of even higher blocking temperatures, which at the same time would be characterized by a decent energy barrier for the spin reversal. In regard to theoretical aspects of SMM's transport properties, it seems that at the moment it is important to gain understanding how the deposition of a molecule onto a surface changes properties of the molecule that can be crucial for the electronic transport. Furthermore, as it transpires that spin polarized transport will most probably be observed first in the system comprising a SMM on a metallic but nonmagnetic substrate and the scanning tunneling microscope with a magnetic tip, it could also be interesting to analyze how ballistic transport of electrons through a molecule affects its structure and magnetic state.

Streszczenie – Summary of the thesis in Polish

W tradycyjnych układach elektronicznych przetwarzanie informacji odbywa się z wykorzystaniem ładunku elektronu. Jednakże oprócz ładunku, elektrony posiadają również drugi stopień swobody, którym jest spin. Wraz z odkryciem w układach składających się z wielu warstw magnetycznych zjawiska *gigantycznego magnetooporu* (nazywanego potocznie efektem GMR – od angielskiego *'gigant magnetoresistance'*) [4,5], stało się jasne, że także spin elektronu może zostać użyty jako kluczowy składnik mechanizmu działania nowej klasy urządzeń. Obecnie układy, w których spinowy stopień swobody elektronów odgrywa pierwszorzędną rolę nazywamy układami *elektroniki spinowej*.[5] Duże praktyczne znaczenie takich układów wynika z faktu, że w porównaniu z klasycznymi układami elektronicznymi, powinny się one charakteryzować nieulotnością, wyższą prędkością działania oraz znacznie mniejszymi rozmiarami [10–12]. Szerokie wprowadzenie układów spintronicznych na rynek komercyjny oznaczałoby prawdziwy przełomem technologiczny, czym należy tłumaczyć obecne ożywienie w badaniach na tymi układami.

Ostatecznym celem przyświecającym działaniom zmierzającym do coraz większej miniaturyzacji układów elektronicznych jest osiągnięcie poziomu molekularnego, gdzie molekuła byłaby wykorzystywana jako w pełni funkcjonujący składnik większego układu. Molekuły budzą duże zainteresowanie głównie dzięki swoim własnością optycznym, magnetycznym oraz mechanicznym, gdyż mogą one zostać użyte do skonstruowania układów hybrydowych, które cechowałyby własności praktycznie nieosiągalne w przypadku dostępnych obecnie klasycznych układów elektronicznych bazujących na krzemie [9,24–28]. Jednym z przykładów takich unikalnych własności jest wzajemne oddziaływanie pomiędzy skwantowanymi elektronowymi i mechanicznymi stopniami swobody [18]. Warto również zauważyć, że ponieważ molekuły są otrzymywane na drodze syntezy chemicznej,

[5] W literaturze wspomniane układy występują również pod nazwą *układów spintronicznych* lub *magnetotronicznych*.

stąd w procesie ich przygotowania, molekuły można wyposażyć w określone własności.

Spośród wielu różnych klas molekuł, przez które można badać transport elektronu i spinu, szczególnie interesujące wydają się być molekuły posiadające wewnętrzny moment magnetyczny [29]. Wykazują one bowiem potencjał do wykorzystania w obszarze technologii związanych z przechowywaniem i przetwarzaniem informacji [9, 31]. Aby molekuła mogła w ogóle być brana pod uwagę jako baza dla molekularnej komórki pamięci, musi ona spełniać dwa podstawowe warunki. Po pierwsze, molekuła taka powinna być magnetycznie bistabilna, oraz po drugie, jej stan nie powinien podlegać dekoherencji dla odpowiednio długiego czasu [32]. Okazuję się, że układami wypełniającymi powyższe wymagane kryteria są *pojedyncze magnetyczne molekuły* (w skrócie SMM – od angielskiego *'single-molecule magnet'*).

Celem niniejszej pracy jest zbadanie transportu ładunku i spinu przez pojedyncze magnetyczne molekuły oraz jego wpływu na magnetyczny stan tychże molekuł. W szczególności analizie poddany jest mechanizm oddziaływania pomiędzy prądem tunelowym a momentem magnetycznym molekuły, który odpowiedzialny jest za wystąpienie tzw. *indukowanego prądem magnetycznego przełączania* molekuły. Następnie skupiam się na rozważeniu ewolucji czasowej magnetycznego stanu molekuły wynikającej z przyłożenia do układu stałego napięcia transportowego. W kolejnym rozdziale badam efekty spinowe towarzyszące stacjonarnemu przepływowi spinowo-spolaryzowanego prądu. Dalsza część pracy poświęcona jest analizie wpływu wielkości oddziaływania pomiędzy molekułą a elektrodami na charakter transportu przez molekułę oraz jej stan. W ostatnim rozdziale rozważam możliwość zastosowania kołowo spolaryzowanego światła do stymulowania indukowanego prądem magnetycznego przełączania molekuły.

Po wprowadzeniu do tematyki związanej z rozważanymi przeze mnie zagadnieniami oraz przedstawieniu uzasadnienia podjęcia badań (rozdział 1), przechodzę w rozdziale 2 do omówienia podstawowych własności pojedynczych magnetycznych molekuł. W ramach poruszanych w pracy problemów, przez pojedynczą magnetyczną molekułę rozumiem układ wykazujący trwały moment magnetyczny, a w konsekwencji również histerezę magnetyczną, który ma czysto molekularne pochodzenie, tzn. wynika z silnych oddziaływań pomiędzy jonami magnetycznymi tworzącymi molekułę [37, 38, 57, 58]. Cechą charakterystyczną rozważanej klasy molekuł jest powolna relaksacja magnetyczna pojawiająca się w niskich temperaturach. Bariera energetyczna ΔE, którą molekuła musi pokonać w celu odwrócenia swojego momentu magnetycznego, jest wynikiem połączenia dużego spinu S stanu podstawowego oraz znacznej anizotropii jednoosiowej (typu Isinga), opisanej przez parametr D.

Badania doświadczalne pokazały, że w niskich temperaturach pojedyncze magnetyczne molekuły swoim zachowaniem przypominają molekuły superparamagnetyczne [34, 59]. Powyżej pewnej temperatury granicznej T_{B}, zwanej *temperaturą blokowania*, wskutek wzbudzania termicznego spin molekuły może swobodnie się obracać. Kiedy jednak temperatura ulega obniżeniu poniżej T_{B}, energia termiczna staje się niewystarczająca dla pokonania bariery energetycznej ΔE i spin molekuły zostaje uwięziony w jednej z dwóch dozwolonych orientacji. Zachowanie to stanowi podstawę dla zastosowań omawianych

molekuł jako komórek pamięci. Ponieważ w tym kontekście istotna jest również relaksacja spinowa oraz utrata koherencji w wyniku oddziaływania molekuły z otoczeniem, oba te aspekty są także przedyskutowane.

W kolejnej części rozdziału 2 rozważam model sprzężenia molekuły z elektrodami. Dotychczas zaproponowano kilka różnych geometrii (rys. 2.2), w jakich molekułę można przyłączyć do metalicznych, a w szczególności magnetycznych, elektrod [28]. Należy przy tym zauważyć, że dostępne w literaturze wyniki pomiarów transportu przez pojedyncze magnetyczne molekuły zostały uzyskane w geometrii złamanego złącza [44, 46, 47] oraz z wykorzystaniem skaningowego mikroskopu tunelowego [48, 49], wyłącznie dla przypadku elektrod niemagnetycznych. Okazuje się ponadto, że przymocowanie molekuły do elektrod nastręcza wiele trudności technicznych. W pracy rozważam koncepcyjnie najprostszy model (rys. 2.3), składający się z molekuły umieszczonej pomiędzy dwiema magnetycznymi elektrodami, których momenty magnetyczne mogą być ustawione równolegle lub antyrównolegle. Elektrody scharakteryzowane są przez nieoddziałujące elektrony wędrowne, rów.(2.2), natomiast procesy tunelowania elektronów pomiędzy elektrodami a molekułą opisuje hamiltonian (2.3). Napięcie transportowe jest przykładane do elektrod symetrycznie.

Do opisu procesów transportu elektronów przez molekułę wykorzystuję model, w ramach którego zakładam, iż redukcji molekuły odpowiada obsadzenie *najniższego nieobsadzonego poziomu molekularnego* (w skrócie nazywanego LUMO – od angielskiego *'lowest unoccupied molecular orbital'*) przez maksymalnie dwa elektrony, rów. (2.5). Spin poziomu LUMO ulega następnie efektywnemu sprzężeniu wymiennemu z wewnętrznym spinem molekuły, rów. (2.6), które opisane jest przez stałą J. Warto podkreślić dwa fakty dotyczące hamiltonianu (2.5). Po pierwsze, hamiltonian ten można wykorzystać tylko do opisu molekuły wykazującej wyłącznie anizotropię jednoosiową. Po drugie, zawiera on dwa człony proporcjonalne do D_1 oraz D_2, które uwzględniają eksperymentalnie pokazany efekt [98–100], polegający na tym, że zmiana obsadzenia poziomu LUMO może wpływać na wielkość anizotropii molekuły.

Należy jednak zauważyć, że w ogólnym przypadku, molekuła może również wykazywać anizotropię poprzeczną, rów. (2.8). Za wyjątkiem rozdziału 3, w którym obecność członu (2.8) jest kluczowa dla wystąpienia omawianych tam efektów, w pozostałej części pracy skupiam się jedynie na molekułach, dla których anizotropia poprzeczna jest zaniedbywalnie mała i molekuły takie można z dobrym przybliżeniem uznawać za układy o anizotropii jednoosiowej. W takim przypadku okazuje się, że hamiltonian molekuły może zostać zdiagonalizowany analitycznie [103, 104], a poszczególne stany molekularne opisane są przez następujące trzy liczby kwantowe: całkowity spin molekuły S_t (przez który rozumiem sumę spinu poziomu LUMO oraz wewnętrznego spinu molekuły), składową z całkowitego spinu molekuły S_t^z odpowiadającą liczbie elektronów n obsadzających poziom LUMO, gdzie $n = 0, 1, 2$. Pozostała część rozdziału 2 poświęcona jest przedstawieniu wzorów analitycznych opisujących stany, rów. (2.9)-(2.16), oraz energie, rów. (2.19)-(2.22), dla przypadku molekuły wykazującej anizotropię jednoosiową.

W rozdziale 3 rozważam najbardziej charakterystyczny efekt występujący w przy-

padku pojedynczych magnetycznych molekuł, umieszczonych w zewnętrznym, zależnym od czasu polu magnetycznym, jakim jest *kwantowe tunelowanie wektora namagnesowania* (w skrócie QTM – od angielskiego *'quantum tunneling of magnetization'*). Zjawisko QTM jest przykładem efektu makroskopowego tunelowania i objawia się tym, że dla określonych wartości zewnętrznego pola magnetycznego wartość składowej z spinu molekuły może ulegać skokowym zmianom. Takie zachowanie spinu molekuły jest typowe dla obiektu kwantowego i różni się od tradycyjnego opisu zjawiska tunelowania cząstki przez barierę potencjału jedynie tym, że w przypadku QTM, akt tunelowania odbywa się w przestrzeni momentu pędu. Występowanie efektu QTM prowadzi do powstania pętli histerezy o charakterystycznym kształcie, rys. 3.1, składającym się serii następujących po sobie płaskich obszarów oraz stromych schodków. Celem tego rozdziału jest zbadanie jak sprzężenie pojedynczej magnetycznej molekuły z rezerwuarami spinowo-spolaryzowanych elektronów wpływa na zjawisko QTM.

W części 3.1 przechodzę do omówienia teoretycznego modelu służącego do opisu efektu QTM. Przede wszystkim na początku rozważam fizyczne źródło mechanizmu QTM. Okazuje się, że badane zjawisko tunelowania jest wynikiem obecności w układzie anizotropii poprzecznej lub słabego, poprzecznego, przyłożonego z zewnątrz pola magnetycznego, które prowadzą do mieszania stanów opisanych przez różne liczby spinowe S_t^z[6] oraz zniesienia degeneracji energii pomiędzy odpowiednimi stanami znajdującymi się po przeciwnych stronach bariery energetycznej. W rezultacie, dla pól rezonansowych zamiast krzyżowania się poziomów energetycznych obserwuje się pojawienie przerw energetycznych Δ, rys. 2.5 oraz 3.2.

Następnie rozważam, powszechnie stosowany do modelowania zjawiska QTM, *mechanizm tunelowania Landaua-Zenera* [70,101,136–144]. W ramach tego modelu zakłada się, że w zakresie wartości pola magnetycznego bliskich danej wartości pola rezonansowego, zachowanie układu można opisać przez efektywny hamiltonian dla układu dwupoziomowego, rów. (3.1). Rozwiązując zależne od czasu równanie Schrödingera dla funkcji w przybliżeniu adiabatycznym, rów. (3.2), można pokazać [83,146], że prawdopodobieństwo przetunelowania spinu molekuły między odpowiednimi stanami znajdującymi sie po przeciwnych stronach bariery energetycznej, jak pokazano schematycznie na rys. 3.3(a)-(c), opisane jest wówczas równaniem (3.4).

W celu zilustrowania wyników analitycznych, rozważam zjawisko QTM dla przypadku molekuły Fe_8, rys. 3.4. Najistotniejszą cechą przedstawionej średniej wartości składowej z spinu molekuły w funkcji amplitudy podłużnego pola magnetycznego, jest jej silna zależność od szybkości narastania wartości pola. Do tego momentu rozważałem sytuację, w której proces tunelowania był jedynym mechanizmem odpowiedzialnym za zmianę stanu magnetycznego molekuły. Jednakże w rzeczywistych układach może występować również relaksacja spinu molekuły związana ze sprzężeniem molekuły z otoczeniem, rys. 3.3(d). Szczególnym przypadkiem takiego oddziaływania są procesy rozpraszania elektronów, tunelujących pomiędzy dwiema elektrodami, na spinie pojedynczej magnetycznej mole-

[6] W dalszej części odwołując się do stanów molekuły opisanych przez liczbę spinową S_t^z, stany te będę nazywał *stanami magnetycznymi molekuły*.

kuły. Wspomniane procesy matematycznie uwzględniam w rozważaniach przy pomocy hamiltonianu Appelbauma [83,146,153,154], rów. (3.6), który opisuje efektywne oddziaływanie wymienne pomiędzy elektronami przewodnictwa z elektrod a spinem molekuły. Zakładam ponadto, że między elektrodami nie jest przyłożone napięcie transportowe, a położenie poziomu LUMO dobrane jest w taki sposób, iż pozostaje on nieobsadzony.

Wykorzystując złotą regułę Fermiego (tj. rachunek zaburzeń drugiego stopnia względem stałej K opisującej sprzężenie wymienne spinu molekuły z elektronami przewodnictwa) wyznaczam częstości przejść między sąsiednimi stanami magnetycznymi molekuły, rów. (3.11), które są wynikiem rozpraszania elektronów przewodnictwa z elektrod na spinie molekuły. Wszystkie inne procesy prowadzące do relaksacji spinu molekuły uwzględniam w postaci pojedynczego fenomenologicznego parametru, czasu relaksacji τ_{rel}, a odpowiadająca im częstość przejść opisana jest rów. (3.12). Dysponując wyrażeniami na częstości przejść pomiędzy stanami magnetycznymi molekuły, mogę zapisać układ równań bilansu prawdopodobieństw (tzw. *równanie master*) dla poszczególnych zakresów pola magnetycznego pomiędzy kolejnymi wartościami rezonansowymi pola, rów. (3.14). Znalezione wcześniej, w oparciu o model Landau-Zenera, prawdopodobieństwa tunelowania spinu molekuły pomiędzy odpowiednimi stanami pełnią tutaj rolę warunków początkowych dla każdego z rozważanych przedziałów wartości pola magnetycznego. Tym samym, aby wyznaczyć zależność średniej wartości składowej z spinu molekuły od pola magnetycznego, rów. (3.17), muszę obliczyć z równania bilansu prawdopodobieństwa znalezienia molekuły w każdym z jej stanów magnetycznych.

Wyniki numeryczne ponownie przedstawiam dla molekuły Fe_8. Rysunek 3.6 pokazuje, iż obecność procesów relaksacyjnych (przerywana linia) jest niezbędna dla całkowitego przełączenia spinu molekuły między dwiema orientacjami przy pomocy efektu QTM. Dynamika procesów relaksacyjnych wynikających z rozpraszania spinów elektronów na spinie molekuły zależy od własności magnetycznych elektrod, a dokładnie od stopnia ich spinowej polaryzacji, opisanego przez parametry P_L oraz P_R, oraz konfiguracji magnetycznej momentów spinowych elektrod. W celu jakościowej analizy omawianych zjawisk, posługuję się pojęciem tzw. *czasu stabilizacji* t_{st} magnetycznego stanu molekuł, przez który rozumiem czas po jakim średnia wartość składowej z spinu molekuły osiąga 99.999% wartości odpowiadającej stanowi stabilnemu molekuły (tj. dla $t \to \infty$).

Na rys. 3.7 oraz 3.8 rozważam zachowanie spinu molekuły po akcie tunelowania równoważnemu trzeciemu schodkowi na rys. 3.6(b), w przypadku równoległej konfiguracji magnetycznej elektrod. Procesy relaksacji związane są z odwróceniem kierunku spinów elektronów przewodnictwa wskutek ich rozpraszania na spinie molekuły. Dla *równoległego* ustawienia momentów spinowych elektrod, zwiększenie stopnia polaryzacji elektrod prowadzi do osłabienia efektu relaksacji, rys. 3.8(a), ponieważ jest on związany z transferem elektronów pomiędzy kanałami mniejszościowymi a większościowymi elektrod. Inaczej sytuacja prezentuje się w przypadku *antyrównoległego* ustawienia momentów spinowych elektrod, rys. 3.8(c), kiedy spowolnienie procesów relaksacyjnych następuje, gdy parametry polaryzacji spinowej elektrod znacząco różnią się od siebie. Natomiast dla $P_L = P_R$, relaksacja przebiega najszybciej. Ponadto uwzględnienie do-

datkowych procesów relaksacyjnych może prowadzić do dalszego skrócenia czasu stabilizacji, o ile $1/\tau_{\mathrm{rel}}$ jest większe niż częstości przejść wywołane rozpraszaniem elektronów przewodnictwa na spinie molekuły, rys. 3.9.

W rozdziale 4 skupiam się na przeanalizowaniu dynamicznych aspektów związanych z transportem elektronów przez pojedyncze magnetyczne molekuły. Szczególną uwagę poświęcam rozważeniu mechanizmu prowadzącego do wystąpienia w molekule *indukowanego prądem magnetycznego przełączania* (w skrócie CIMS – od angielskiego *'current-induced magnetic switching'*). W odniesieniu do wcześniejszego rozdziału, w którym przedyskutowałem zjawisko QTM, obecnie zakładam, że molekuła jest charakteryzowana wyłącznie przez anizotropię jednoosiową oraz między elektrodami jest przyłożone skończone napięcie transportowe.

Zanim przechodzę do sformułowania problemu zjawiska CIMS w przypadku pojedynczych magnetycznych molekuł, na początku omawiam ogólną ideę wspomnianego zjawiska. Termin CIMS używany jest w szerszym kontekście do opisu zjawisk związanych z przepływem spinowo-spolaryzowanego prądu przez magnetyczne układy o rozmiarach nanoskopowych. Okazuje się bowiem, że w takim przypadku moment magnetyczny układu poddany jest działaniu momentu obrotowego, będącego wynikiem przepływu momentu pędu pomiędzy prądem a układem. Zjawisko CIMS zostało teoretycznie przewidziane niezależnie przez Slonczewskiego oraz Bergera [157–161], a następnie idea manipulowania momentem magnetycznym przy pomocy prądu została eksperymentalnie potwierdzona w wielu różnych układach, takich jak: złącza typu punktowego [162, 163], nanodruty [164], nanokolumny [165–167] oraz indywidualne wyspy superparamagnetyczne [168]. W dalszej części wstępu do rozdziału 4 omawiam mechanizm CIMS dla spinowo-spolaryzowanego prądu płynącego przez pojedynczą magnetyczną warstwę, rys. 4.1.

Z punktu widzenia możliwych zastosowań mechanizmu CIMS, istotną kwestią jest dynamika procesu odwrócenia momentu magnetycznego. Standardową metodą badania ewolucji czasowej zachowania momentu magnetycznego w obecności rzeczywistych oraz efektywnych pól magnetycznych jest *makroskopowe równanie Landaua-Lifszyca-Gilberta* (LLG) [127, 128]. Slonczewski pokazał [157], że bez konieczności rozważania mikroskopowego mechanizmu, zjawisko wymiany momentu pędu między układem a prądem może zostać uwzględnione w równaniu LLG jako dodatkowy człon [178, 179], patrz ostatni człon w rów. (4.1).[7] Oczywistym jest, że układ zawierający warstwę magnetyczną różni się zasadniczo od układu z pojedynczą magnetyczną molekułą, w przypadku której mam do czynienia z dyskretnym widmem stanów magnetycznych. Nie mogę w związku z tym zastosować do opisu dynamiki spinu molekuły półklasycznego modelu makrospinu wykorzystującego równanie LLG, co oznacza, że istnieje konieczność zaproponowania innego modelu, który uwzględniałby specyficzne własności rozważanych molekuł.

W zależności on wartości napięcia V przyłożonego do elektrod można rozróżnić dwa

[7] W powyższym równaniu uwzględniona jest jedynie, pierwotnie zaproponowana, składowa poprzeczna (tzn. leżąca w płaszczyźnie warstwy) momentu obrotowego wynikającego z przepływu momentu pędu. Oprócz niej może również występować składowa działająca w płaszczyźnie prostopadłej do płaszczyzny warstwy [161].

podstawowe obszary transportu elektronów przez molekułę. Zakres napięć, dla których elektrony posiadają energię wystarczającą dla obsadzenia poziomu LUMO nazywany jest zakresem *tunelowania sekwencyjnego*. Jeżeli natomiast napięcie jest zbyt małe i elektrony mają zbyt małą energię, aby pokonać barierę tunelową, a tym samym transport sekwencyjny jest niemożliwy, to mówi się o zakresie *blokady kulombowskiej*. Warto jednak zauważyć, że nadal można obserwować przepływ prądu przez układ, który jest wynikiem występowania procesów tunelowania wyższego rzędu, stąd też alternatywna nazwa tzw. zakres *współtunelowania*. W obu wspomnianych przypadkach, rozważany przeze mnie efekt CIMS w odniesieniu do pojedynczych magnetycznych molekuł pojawia się jako wynik oddziaływania wymiennego pomiędzy spinem elektronu znajdującego się na poziomie LUMO a wewnętrznym spinem molekuły. Mechanizm CIMS polega zasadniczo na założeniu, że wskutek oddziaływania ze spinem molekuły elektrony tunelujące przez LUMO mogą zmieniać swoją orientację spinu na przeciwną, co z kolei odpowiada przekazywaniu momentu pędu pomiędzy elektronami przewodnictwa a molekułą. Tym samym, zmiana stanu magnetycznego molekuły wywoływana jest nieelastycznymi procesami tunelowymi, rys. 4.2(b)-(c). Ponieważ w omawianym rozdziale skupiam się przede wszystkim na analizie głównych cech dynamiki odwracania spinu molekuły, stąd korzystam z najprostszej dostępnej metody, jaką jest rachunek zaburzeń w postaci złotej reguły Fermiego oraz równanie bilansu prawdopodobieństw. Należy w tym miejscu zauważyć, że zastosowanie wspomnianej metody jest fizycznie uprawnione tylko dla konkretnego zakresu, tzn. albo zakresu tunelowania sekwencyjnego albo zakresu współtunelowania. Obszar przejściowy, gdzie istotną rolę mogą odgrywać procesy tunelowe różnych rzędów, wymaga zastosowania nieco innego podejścia, jak zostanie pokazane w rozdziale 5.

Dyskusję rozpoczynam od analizy problemu dla zakresu tunelowania sekwencyjnego, podrozdział 4.2. Na początku przedstawiam ogólną postać formuły na prąd tunelowy płynący pomiędzy elektrodą a molekułą, rów. (4.3), która zwiera wyrażenia opisujące częstość przejść pomiędzy różnymi stanami magnetycznymi molekuły wskutek transportu elektronów przez poziom LUMO molekuły, rów. (4.4). Korzystając z wyników rozdziału 2, wyprowadzam ogólne wyrażenie na częstość przejść, rów. (4.7), w którym współczynnik $C^{\sigma}_{\alpha\beta}$ ustanawia *reguły wyboru* rządzące przejściami pomiędzy stanami magnetycznymi molekuły, a stąd także definiuje fizyczne procesy stanowiące podstawę mechanizmu CIMS w przypadku molekuł. Podobnie jak w rozdziale 3, wszystkie inne procesy relaksacji, niezwiązane z transportem elektronów, uwzględnione są na poziomie fenomenologiczny przy pomocy rów. (4.9)-(4.10).[8] Następnie zapisuję stosowny układ równań bilansu, które rozwiązuję dla określonych warunków początkowych. Warto podkreślić, że liczba równań wynosi $2S+1$ (S – wartość spinu swobodnej molekuły), a tym samym w przypadku molekuł takich jak Mn_{12} czy Fe_8, dla których $S = 10$, mam do czynienia z układem 84 równań.

Dyskusję wyników numerycznych, którą prowadzę dla przypadku molekuły Mn_{12},

[8]Równanie (4.9) opisuje procesy relaksacji w obrębie jednego multipletu spinowego dla określonej liczby obsadzenia poziomu LUMO oraz całkowitego spinu molekuły, podczas gdy rów. (4.10) reprezentuje procesy relaksacyjne, które mogą zachodzić pomiędzy dwoma różnymi multipletami dla poziomu LUMO obsadzonego prze jeden elektron.

rozpoczynam od zaprezentowania zależności średniej wartości składowej z całkowitego spinu molekuły oraz prądu płynącego przez układ od napięcia transportowego po osiągnięciu stanu stacjonarnego, rys. 4.4. W rozważanym przypadku zakładam, że początkowo molekuła znajduje się w stanie spinowym $S_t^z = -10$, a następnie w chwili $t = 0$ do elektrod symetrycznie przykładane jest stałe napięcie. Widać, że gdy uwzględnione są tylko procesy tunelowania sekwencyjnego, zmiana stanu magnetycznego molekuły wskutek przepływu prądu pojawia się po przekroczeniu pewnej wartości progowej napięcia, która odpowiada przerwie energetycznej pomiędzy początkowym a najbliższym stanem magnetycznym spełniającym reguły wyboru. Należy ponadto zauważyć, że dla dużych napięć, dla których w transporcie uczestniczą wszystkie stany molekuły, efekt CIMS spinu molekuły obserwowany jest tylko dla antyrównoległej konfiguracji momentów magnetycznych elektrod. Na kolejnym wykresie, rys. 4.5, przedstawiam ewolucję czasową magnetycznego stanu molekuły. Szczególnie interesujący jest kształt krzywej prądowej w przypadku antyrównoległej magnetycznej konfiguracji elektrod, rys. 4.5(b), bowiem można zauważyć, że procesowi obracania spinu molekuły towarzyszy pojawienie się dodatkowego sygnału w prądzie.

Obecność impulsu prądowego można wytłumaczyć rozważając kanały prądowe, przez jakie elektrony przemierzają złącze. Jak już wcześniej wspomniałem, podczas tunelowania elektronu przez poziom LUMO molekuły, w wyniku oddziaływania wymiennego z wewnętrznym spinem molekuły, orientacja spinu elektronu może ulec zmianie na przeciwną, z czym związany jest przepływ momentu pędu pomiędzy prądem a molekułą. Jeżeli elektrony zmieniają orientację swoich spinów w taki sposób, że przepływ momentu pędu prowadzi do obrócenia spinu molekuły, to wówczas odpowiadający takiemu zachowaniu kanał prądowy nazywam *kanałem przełączającym* (w skrócie SWC – od angielskiego *'switching channel'*). Jeżeli natomiast omawiane procesy dążą do zachowania początkowego stanu molekuły, to taki kanał nazywam *kanałem stabilizującym* (w skrócie STC – od angielskiego *'stabilizing channel'*). Idea nieelastycznych kanałów transportowych zilustrowana jest schematycznie na rys. 4.6. Można tam zauważyć, że dla równoległego ustawienia momentów magnetycznych elektrod, rys. 4.6(a), oba kanały są symetryczne, podczas gdy w przypadku antyrównoległym dominuje kanał SWC, rys. 4.6(b), co prowadzi do powstania dodatkowego impulsu w prądzie.

Dalsza część analizy wyników dotyczy wpływu parametrów polaryzacji elektrod na czas stabilizacji stanu magnetycznego molekuły, rys. 4.9, efektów wynikających z niewspółliniowego ustawienia osi łatwej molekuły względem momentów magnetycznych elektrod, rys. 4.10, oraz dodatkowych procesów relaksacyjnych, rys. 4.11 oraz 4.12.

Ostatni fragment rozdziału 4, podrozdział 4.3, zawiera dyskusję mechanizmu CIMS w zakresie blokady kulombowskiej (współtunelowania). Zakładając, że napięcie bramkujące dobrane jest w ten sposób, że poziom LUMO pozostaje nieobsadzony, okazuje się, że mechanizm CIMS w omawianym zakresie napięć różni się od mechanizmu w obszarze tunelowania sekwencyjnego wyłącznie tym, iż w obecnej sytuacji odwrócenie kierunków spinów elektronów przewodnictwa na przeciwny może nastąpić tylko w stanie wirtualnym, rys. 4.13(c)-(d). Ostateczny wzór na częstość przejść między sąsiednimi sta-

nami magnetycznymi molekuły wskutek procesów tunelowych wyższego rzędu dany jest rów. (4.21). Wyniki numeryczne nie odbiegają jakościowo od tych uzyskanych wcześniej dla transportu sekwencyjnego. Jedyna różnica dotyczy skali czasowej, w jakiej zachodzi proces odwrócenia spinu molekuły, który jest znacznie dłuższy niż w uprzednio rozważanym przypadku. Biorąc pod uwagę, że uzyskane przeze mnie czasy przełączania w zakresie współtunelowania mogą być dłuższe niż czasy relaksacji wewnętrznej spinu molekuły, wydaje się, iż w rzeczywistych układach zaobserwowanie efektu CIMS dla rozważanego zakresu napięć może okazać się bardzo trudne, a być może niemożliwe.

Dotychczas skupiłem się na analizie problemu dynamiki przełączania spinu molekuły przy pomocy prądu spinowo-spolaryzowanego osobno dla zakresu napięć odpowiadających blokadzie kulombowskiej oraz transportowi sekwencyjnemu elektronów. Należy jednak zauważyć, że chociaż procesy tunelowe wyższego rzędu odgrywają znaczącą rolę głównie w obszarze blokady kulombowskiej, to pozostają one aktywne dla całego zakresu napięć, również w obszarze rezonansu, prowadząc na przykład do rozmycia schodków kulombowskich [194]. W związku z tym, korzystając z *techniki diagramowej* [194, 199–203], w rozdziale 5 badam transport elektronów przez pojedynczą magnetyczną molekułę, uwzględniając możliwość jednoczesnego występowania procesów tunelowania sekwencyjnego oraz współtunelowania.

Stosowana przeze mnie technika diagramowa polega na systematycznym rozwinięciu zredukowanej macierzy gęstości układu oraz interesujących mnie operatorów względem sprzężenia Γ pomiędzy poziomem LUMO molekuły a elektrodami. Prawdopodobieństwa znalezienia molekuły w różnych stanach magnetycznych w dowolnej chwili można wyznaczyć z rów. (5.1), gdzie $\mathbf{\Pi}(t, t_0)$ jest macierzą propagacji, a jej elementy opisują w jaki sposób układ ewoluuje pomiędzy danym stanem początkowym w chwili t_0, a stanem docelowym w chwili t. W ramach omawianej metody, ewolucję tę można schematycznie przedstawić jako serię nieredukowalnych diagramów na konturze Keldysh'a [194], rys. 5.1, które po zsumowaniu odpowiadają nieredukowalnym blokom energii własnych $W_{\chi'\chi}(t', t)$ (ang. *'irreducible self-energy blocks'*) [201]. Macierz energii własnych $\mathbf{W}(t', t)$ jest zatem jedną z najważniejszych wielkości w omawianej metodzie, ponieważ jej elementy $W_{\chi'\chi}(t', t)$ można zinterpretować jako uogólnione częstości przejść pomiędzy dwoma dowolnymi stanami magnetycznymi molekuły. Operatory opisujące własności transportowe rozważanego układu, takie jak prąd I oraz szum prądowy S, można następnie wyrazić w języku techniki diagramowej, rów. (5.5) oraz (5.10). W *stanie stacjonarnym* prawdopodobieństwa znalezienia układu w poszczególnych stanach otrzymywane są w oparciu o rów. (5.4), które rozwiązuję używając tzw. *podejścia perturbacyjnego w obszarze przejściowym* (ang. *'crossover perturbation scheme'*). Idea tego podejścia polega na rozwinięciu jedynie macierzy $\mathbf{W}(t', t)$, bez rozwijania prawdopodobieństw, aż do drugiego rzędu względem Γ.

Inaczej niż we wcześniejszych rozdziałach, w rozdziale 5 wyniki numeryczne przedstawiam dla hipotetycznej molekuły o spinie $S = 2$, charakteryzującej się dominującą anizotropią jednoosiową. Należy jednak w tym miejscu zaznaczyć, że poczynione obserwacje, na poziomie jakościowym, obowiązują także dla molekuł o większej wartości spinu.

Wybór stosunkowo małego spinu dla zilustrowania wyników podyktowany jest tym, że pozwala on na dość wnikliwą analizę udziału różnych stanów magnetycznych molekuły w procesach transportowych, co byłoby znacznie utrudnione w przypadku większych wartości spinu. Efekty dyskutowane w podrozdziałach 5.3-5.5 prezentowane są dla *ferromagnetycznego* ($J > 0$) sprzężenia pomiędzy elektronem na poziomie LUMO a spinem wewnętrznym molekuły, a uogólnienie na przypadek *antyferromagnetyczny* ($J < 0$) zamieszczone jest w podrozdziale 5.6.

Dyskusję wyników rozpoczynam od konduktancji różniczkowej, rys. 5.2, oraz odpowiadającego jej współczynnika TMR (od angielskiego *'tunnel magnetoresistance'*), rys. 5.3, który opisuje jak własności transportowe układu zmieniają się przy przejściu od konfiguracji antyrównoległej do równoległej ustawienia momentów magnetycznych elektrod [182,203,209]. Porównując rys. 5.3(a), przedstawiający TMR obliczony przy uwzględnieniu pierwszego oraz drugiego rzędu rachunku zaburzeń, z rys. 5.3(b), na którym TMR policzony został w przybliżeniu transportu sekwencyjnego (tylko pierwszy rząd), widać, że uwzględnienie procesów współtunelownia jest niezbędne dla uzyskania poprawnego opisu transportu. Rysunek 5.4 potwierdza wcześniejsze obserwacje z rozdziału 4, iż przepływ prądu spinowo-spolaryzowanego przez pojedynczą magnetyczną molekułę wpływa na jej stan magnetyczny. Dla *antyrównoległej* konfiguracji magnetycznej elektrod, rys. 5.4(b), orientacja spinu molekuły jest nie tylko ściśle powiązana z kierunkiem przepływu prądu, ale przede wszystkim widoczna jest preferencja spinu do ustawiania się wzdłuż osi łatwej molekuły. Natomiast w przypadku *równoległym*, rys. 5.4(a), średnia wartość składowej z spinu tylko nieznacznie różni się od zera (spin preferuje płaszczyznę prostopadłą do osi łatwej molekuły) i jest parzystą funkcją napięcia transportowego.

Podrozdział 5.3 poświęcony jest analizie transportu przez molekułę w zakresie *liniowej odpowiedzi* układu. Na rys. 5.6 zamieszczona jest zależność współczynnika TMR oraz średniej wartości składowej z spinu molekuły od położenia poziomu LUMO. Uzyskana krzywa TMR, w obszarze odpowiadającym poziomowi LUMO obsadzonemu przez jeden elektron ($Q = 1$), znacznie różni się jakościowo od tej uzyskanej dla układu zawierającego kropkę kwantową [203,210]. Wynika to stąd, że widmo stanów wielociałowych molekuły, przez które mogą tunelować elektrony, jest znacznie bogatsze niż w przypadku kropki. Inną interesującą własnością krzywej TMR jest jej asymetria, tzn. różnica pomiędzy maksymalnymi wartościami obserwowanymi dla $Q = 0$ oraz $Q = 2$. Zachowanie to odbiega od zachowania typowego dla modelu Andersona, gdzie TMR jest symetryczny względem punktu $\varepsilon = -U/2$ [203]. W obecnej sytuacji brak symetrii spowodowany jest uwzględnieniem poprawek do anizotropii podłużnej, wynikających z obsadzenia poziomu LUMO molekuły, rów. (5.19).

Uzupełnieniem wyników dla zakresu linowej odpowiedzi jest podrozdział 5.4, w którym dyskutuję zachowanie się układu dla skończonych wartości napięcia transportowego. W kolejnym podrozdziale 5.5, uwzględniam ponadto wpływ podłużnego, stałego pola magnetycznego. Okazuje się, że nawet pole o małej wartości może znacząco modyfikować własności transportowe układu. Nie tylko ulega złamaniu symetria współczynnika TMR względem zmiany znaku napięcia transportowego, rys. 5.8(a), ale także pojawia się możli-

wość, że transport w przypadku antyrównoległego ustawienia momentów magnetycznych elektrod może być bardziej efektywny niż dla ustawienia równoległego, co odpowiada ujemnemu współczynnikowi TMR na rys. 5.8 oraz 5.10(c,g). Podobną sytuację obserwuję dla *antyferromagnetycznego* ($J < 0$) sprzężenia elektronu na poziomie LUMO ze spinem molekuły, rys. 5.11.

Ciekawa sytuacja pojawia się, gdy pojedyncza magnetyczna molekuła jest przyłączona do elektrod charakteryzujących się różnymi parametrami polaryzacji, co jest przedmiotem analizy ostatniej części rozdziału 5. W szczególności rozważam układ, w którym lewa elektroda jest niemagnetyczna, natomiast prawą cechuje wysoki stopień polaryzacji spinowej. Własności transportowe tak zdefiniowanego układu wykazują wyraźną asymetrię wobec zmiany polaryzacji napięcia transportowego, tzn. dla jednej z polaryzacji napięcia układ słabo przewodzi prąd, rys. 5.14(a,d). Własność ta jest typową dla układów zachowujących się jak dioda. Ponadto wskutek sprzężenia do elektrody ferromagnetycznej oraz zależności procesów tunelowych od kierunku spinu, prąd płynący przez rozważany układ ulega spinowej polaryzacji, a dodatkowo polaryzacja ta może ulec zmianie przy odwróceniu kierunku przepływu prądu. Tym samym mam do czynienia z układem pełniącym funkcję *diody spinowej* [215–217]. Jak pokazano na rys. 5.13 oraz 5.14, szczegółowe własności prostujące układu zależą od tego, jaki typ sprzężenia występuje między elektronem na poziomie LUMO a wewnętrznym spinem molekuły.

Wszystkie rozważane do tego momentu zjawiska, wynikające z transportu ładunku przez pojedynczą magnetyczną molekułę, dotyczą przypadku, kiedy molekuła jest *słabo* sprzężona do elektrod. Jednakże w rzeczywistym eksperymencie, założenie takie niekoniecznie musi być spełnione. Należałoby zatem zapytać, jakim modyfikacją ulegają własności transportowe układu, gdy molekuła jest *silnie* sprzężona z elektrodami, co stanowi przedmiot dyskusji rozdziału 6. Na wstępie warto zauważyć, iż tunelowanie elektronów pomiędzy elektrodami a molekułą jest wynikiem oddziaływania pomiędzy stanami zlokalizowanymi molekuły oraz stanami rozciągłymi elektronów z elektrod. Kiedy molekuła jest jedynie słabo sprzężona z elektrodami, a tym samym mieszanie wspomnianych stanów jest niewielkie, jej poziomy molekularne ulegają tylko nieznacznemu poszerzeniu, a tym samym nadal mam do czynienia z widmem dyskretnym molekuły. Gdy natomiast przekrywanie się stanów jest znaczne, to wówczas stany molekularne nie mogą być wykorzystane do opisu transportu elektronów i należy jest zastąpić nowymi stanami hybrydowymi, które będą uwzględniały to, że elektrony w takiej sytuacji są do pewnego stopnia zdelokalizowane pomiędzy elektrodami a molekułą. Co więcej, w przypadku gdy molekuła jest obsadzona przez nieparzystą liczbę elektronów, omawiane procesy mogą prowadzić do odwrócenia spinu niesparowanego elektronu, a co za tym idzie do pojawienia się dodatkowego rezonansu w gęstości stanów dla energii bliskich poziomowi Fermiego elektrod, znanego jako *rezonans Kondo* (czasami również jako *rezonans Abrikosova-Shula*).

Efekt Kondo jest zjawiskiem dobrze znanym w obrębie fizyki ciała stałego [220–226], gdzie w układach metalicznych zawierających magnetyczne domieszki objawia się jako wzrost oporności poniżej pewnej temperatury T_{K}, zwanej *temperaturą Kondo*. Pod koniec

lat 90-tych okazało się, że występowanie tego efektu nie ogranicza się wyłącznie do układów masywnych, ale można go również zaobserwować w transporcie przez układy nansokopowe takie, jak kropki kwantowe [228–230], nanorurki węglowe [231] oraz różnego typu molekuł [232–235]. Warto zaznaczyć, że mimo, iż mechanizm fizyczny prowadzący do utworzenia rezonansu Kondo jest taki sam zarówno dla układów masywnych jak i nanoskopowych, to występuje jedna zasadnicza różnica. Mianowicie w przypadku tych drugich układów, zamiast wzrostu oporności poniżej T_{K}, następuje wzrost przewodności, ponieważ dodatkowy rezonans odgrywa rolę mostu, który ułatwia mieszanie się stanów elektronowych należących do różnych elektrod, a tym samym wspomaga tunelowanie elektronów przez układ. Schemat procesów prowadzących do powstania rezonansu Kondo w przypadku modelu domieszki magnetycznej zaproponowanej przez Andersona przedstawiony jest na rys. 6.1(a). W dalszej części wstępu do rozdziału 6 dokonuję szczegółowego przeglądu obecnego stanu wiedzy na temat zjawisk mogących pojawić się w pojedynczych magnetycznych molekułach w sytuacji silnego sprzężenia molekuły z elektrodami.

W świetle powyższej dyskusji, staje się jasne, że, gdy molekuła jest silnie sprzężona z elektrodami, nie mogę oczekiwać, że jedynie stany o energiach bliskich energii Fermiego elektrod będą wnosiły istotny wkład do procesów transportowych. W rzeczywistości, żaden stan z pasma przewodnictwa elektron nie może zostać w sposób dowolny wykluczony z rozważań, a tym samym, badając transport elektronów przez molekułę, powinienem w obecnym przypadku wziąć pod uwagę w zasadzie wszystkie stany z pasma przewodnictwa elektrod. W związku z tym, muszę dotychczas stosowane metody perturbacyjne zastąpić innym podejściem, które uwzględni szerokie, ciągłe spektrum stanów elektronowych elektrod. W niniejszej pracy wykorzystuję *numeryczną grupę renormalizacji* (w skrócie NRG – od angielskiego *'numerical renormalization group'*), w postaci zaproponowanej przez Wilsona [225,240,241], której główną cechą jest to, że jest metodą nieperturbacyjną ze względu na wszystkie parametry układu.

Ogólne podejście NRG wykorzystane przez Wilsona do zbadania zachowania domieszki magnetycznej sprzężonej z morzem nieoddziałujący elektronów w elektrodzie można krótko przedstawić jako sekwencję trzech kroków, rys. 6.2. Po pierwsze, dokonuje się logarytmicznej dyskretyzacji pasma przewodnictwa. Następnie tak zdyskretyzowany model zostaje odwzorowany na półnieskończony łańcuch, którego pierwszy węzeł reprezentuje domieszkę. W ostatnim kroku, układ w postaci półnieskończonego łańcucha podlega iteracyjnej diagonalizacji, zaczynając od węzła odpowiadającego domieszce, a w każdym następnym kroku iteracyjnym dodawany jest kolejny energetyczny stopień swobody. Ponieważ wędrówka wzdłuż łańcucha równoznaczna jest z uwzględnianiem w obliczeniach coraz mniejszych skal energetycznych, rozwinięta przez Wilsona metoda dostarcza nieperturbacyjnego opisu przejścia od układu swobodnej domieszki magnetycznej, w wysokich temperaturach, do układu silnie ekranowanego spinu, w niskich temperaturach [241]. Szczegóły teoretyczne zastosowanej metody w odniesieniu do pojedynczych magnetycznych molekuł są szeroko dyskutowane w podrozdziale 6.1.

Wynikiem zastosowania procedury numerycznej NRG[9] jest zbiór stanów oraz energii własnych układu, w oparciu o które mogę następnie wyznaczyć funkcję spektralną układu $A_\sigma(\omega, T)$. Znajomość tej wielkości wystarcza do znalezienia, w oparciu o równanie Landauera-Wingreena-Meira [187, 259–263], charakterystyk transportowych molekuły w zakresie *odpowiedzi liniowej*, jak pokazano w podrozdziale 6.2. Przewodność układu G opisana jest rów. (6.18). Pozostała część rozdziału poświęcona jest analizie uzyskanych wyników dla hipotetycznej molekuły o spinie $S = 2$.

Dyskusję rozpoczynam od znalezienia temperatury Kondo układu dla zadanych parametrów, którą w rozważanym przypadku dla $T = 0$ można oszacować z szerokości połówkowej odpowiadającej połowie maksymalnej wartości rezonansu Kondo [225, 237]. Za punkt odniesienia przyjąłem krzywą dla $J = 0$, uzyskując wartość $T_\mathrm{K} = 0.00066$ – dla uproszczenia w ramach tego podrozdziału zakładam, że $k_\mathrm{B} \equiv 1$, a energie są wyrażone w jednostce połowy szerokości pasma przewodnictwa $\mathfrak{D}$, która reprezentuje największą skalę energetyczną w układzie. Na rys. 6.3 oraz 6.4 przedstawiona jest zależność całkowitej funkcji spektralnej $A(\omega)$ od wielkości sprzężenia pomiędzy spinem poziomu LUMO a wewnętrznym spinem molekuły dla obu typów sprzężenia (tj. *ferromagnetycznego*, $J > 0$, oraz *antyferromagnetycznego*, $J < 0$), zarówno dla *antyrównoległej* (rys. 6.3), jak i *równoległej* (rys. 6.4) konfiguracji magnetycznej elektrod. Widać, że ze wzrostem wartości J następuje stopniowy zanik rezonansu Kondo. Co ciekawe, dla dużych wartości sprzężenia, w widmie ujawniają się dodatkowe rezonanse, których powstanie można jakościowo wytłumaczyć w oparciu o widmo niesprzężonej molekuły. Należy jednak podkreślić, iż taka analiza ma dość ogólny charakter, ponieważ zastosowanie procedury NRG prowadzi do renormalizacji poziomów energetycznych molekuły. Następnie przechodzę do przeanalizowania jak funkcja spektralna, rys. 6.6, oraz własności transportowe molekuły, a dokładnie współczynnik TMR, rys. 6.7, zależą od położenia poziomu LUMO dla wybranej wartości sprzężenia J. Rysunek 6.7 umożliwia dokonanie jakościowego porównania pomiędzy wynikami uzyskanymi dla przypadku *słabego* oraz *silnego* sprzężenia pomiędzy molekułą a elektrodami. Okazuje się, że ogólny charakter krzywych TMR jest podobny w obu przypadkach, z jednym wszakże wyjątkiem. W rozważanej obecnie sytuacji TMR może przyjmować wartości ujemne, co oznacza, że układ łatwiej przewodzi prąd dla antyrównoległej konfiguracji momentów magnetycznych elektrod.

Ostatni rozdział niniejszej pracy (rozdział 7), poświęcam przedyskutowaniu możliwości wykorzystania światła spolaryzowanego kołowo w procesie magnetycznego przełączania pojedynczych magnetycznych molekuł. W minionych latach pokazano bowiem, że światło spolaryzowane kołowo można wykorzystać do zmiany stanu namagnesowania układu [266, 271–274], a uzyskany efekt równoważny jest temu, jaki można by zaobserwować, gdyby przyłożyć pole magnetyczne w kierunku wektora falowego. Omawiany efekt nosi nazwę *odwrotnego efektu Faradaya* i chociaż został on zaproponowany [275, 276] oraz pierwszy raz eksperymentalnie potwierdzony [277] ponad pół wieku temu, to dopiero obecny rozwój technologii związanych z wytwarzaniem wiązek laserowych daje nadzieję na pełne wykorzystanie tkwiącego w tym efekcie potencjału technologicznego. Dotych-

[9] W pracy wykorzystuję kod Flexible DM-NRG [255, 256].

czas pokazano, że odwrotny efekt Faradaya można wykorzystać do manipulowania namagnesowania w amorficznym stopie magnetycznym GdFeCo [278, 280] oraz ferrimagnetycznych warstwach granatu [281]. Ważną własnością odwrotnego efektu Faradaya jest to, że wykorzystuje on procesy ramanowskiego spójnego rozpraszania optycznego, a co za tym idzie, nie występuje absorpcja fotonów [278]. Jednakże, mimo, iż ogólna teoria omawianego zjawiska jest dobrze znana [276, 282–285], nadal szeroko dyskutowany jest mikroskopowy mechanizm, gdyż nie jest oczywiste skąd dokładnie (tzn. czy z sieci krystalicznej, czy z fotonów) pochodzi moment pędu niezbędny do wystąpienia magnetycznego przełączenia [286–288].

Ponieważ zarówno zwykły jak i odwrotny efekt Faradaya wynikają z tego samego wyrażenia na energię swobodną [276, 277, 290], z termodynamicznego punktu widzenia stanowią one parę procesów odwrotnych [291, 292]. Należałoby zatem spodziewać się, że jeżeli układ magnetyczny jest w stanie wymusić obrót płaszczyzny polaryzacji przechodzącej przez niego fali elektromagnetycznej (efekt Faradaya), to również powinno być możliwe wystąpienie procesu odwrotnego, tzn. fala elektromagnetyczna spolaryzowana kołowo powinna zmieniać stan magnetyczny układu (odwrotny efekt Faradaya). Powyższe stwierdzenie uzasadnia moje zainteresowanie zastosowaniem optycznych metod do kontrolowania magnetycznego stanu pojedynczych magnetycznych molekuł, ponieważ co najmniej jeden typ molekuł (grupa molekuł Mn_{12}) wykazuje efekt Faradaya [293]. Należy jednakże zauważyć, iż nadal niewiele wiadomo na temat własności optycznych pojedynczych magnetycznych molekuł w zakresie procesów związanych z prostym i odwrotnym elektem Faradaya. Z drugiej jednak strony, bardziej owocne okazały się próby kontroli dynamiki momentu magnetycznego molekuły poprzez absorpcję promieniowania [294–299]. W związku z tym, w rozdziale 7 skupiam się na rozważeniu absorpcji spolaryzowanego kołowo promieniowania elektromagnetycznego w kontekście możliwości jego wykorzystania do stymulowania zjawiska CIMS w molekułach w zakresie blokady kulombowskiej.

W celu opisania oddziaływania między molekułą a promieniowaniem elektromagnetycznym, wykorzystuję hamiltonian o postaci typowej dla linowego zjawiska magnetoelektrycznego [284, 307, 308], rów. (7.2), gdzie α_{ij} jest tensorem drugiego rzędu (w ogólności niesymetrycznym), nazywanym *tensorem podatności magnetoelektrycznej*. Chociaż używany przeze mnie hamiltonian (7.2) nie opisuje rzeczywistego mikroskopowego mechanizmu rządzącego oddziaływaniem między molekułą a promieniowaniem, a stąd reprezentuje on czysto fenomenologiczny model, to jednak pozwala on uwzględnić pewne cechy symetrii układu. Jak przedyskutowano w podrozdziale 2.2, w przypadku molekuły umieszczonej na podłożu lub dołączonej do elektrod, efekty związane z symetrią molekuły mogą odgrywać znaczącą rolę przy opisie transportu przez taką molekułę. Aby uprościć nieco rozważania, zakładam, że promieniowanie ulega propagacji w kierunku składowej z, rys. 2.2. Następnie dokonuję kwantyzacji operatora pola elektrycznego [239, 309, 310], rów. (7.6), oraz wykorzystuję *przybliżenie dipolowe* [239], rów. (7.7). W ostatnim kroku zmieniam bazę dla wektorów polaryzacji fotonów tak, aby wiązka promieniowania składała się z fotonów spolaryzowanych kołowo lewo- lub prawoskrętnie [311], rów. (7.9).

Ostateczna postać hamiltonianu oddziaływania dana jest rów. (7.15).

Częstości przejść między dwoma sąsiednimi stanami magnetycznymi molekuły, wywołanych oddziaływaniem z promieniowaniem elektromagnetycznym, znajduję, podobnie jak w rozdziałach 3 oraz 4, w oparciu o złotą regułę Fermiego, podrozdział 7.2. Szukane wyrażenia dane są rów. (7.24) oraz (7.25), gdzie $\mathcal{F}_{kl}(\omega)$ jest funkcją kształtu opisującą poszerzenie poziomów energetycznych, pomiędzy którymi zachodzi przejście. Znalezione częstości przejść wstawiam następnie do równania bilansu prawdopodobieństw (4.11). Wyniki numeryczne ponownie uzyskuję dla hipotetycznej molekuły o spinie $S = 2$, która początkowo znajduje się w stanie $S_t^z = -2$, a jej poziom LUMO pozostaje nieobsadzony.

W ciągu całej pracy przyjmuję założenie, że układ utrzymywany jest w temperaturze niższej niż temperatura blokowania T_B, co wyklucza możliwość wystąpienia termicznie aktywowanych procesów relaksacyjnych. Z drugiej jednak strony, w swoich rozważaniach biorę pod uwagę relaksację wewnętrzną spinu, która na poziomie fenomenologicznym uwzględniona jest przez rów. (4.9) oraz (4.10). Rysunek 7.2 przedstawia zależność średniej wartości składowej z spinu molekuły od temperatury. Widać na nim, że poniżej pewnej charakterystycznej temperatury, kiedy procesy relaksacyjne są "zamrożone", spin molekuły jest unieruchomiony w jednym z dwóch stanów metastabilnych, odpowiadających maksymalnej wartości składowej z spinu (obszar ①). Zwiększając temperaturę wkraczam w obszar ②, w którym procesy relaksacji wewnętrznej spinu odgrywają istotną rolę, prowadząc do całkowitego rozfazowania spinu molekuły. Celem wykorzystania impulsu promieniowania spolaryzowanego kołowo jest wytworzenie chwilowej nierównowagi w rozkładzie prawdopodobieństw tak, aby zapoczątkować magnetyczne przełączanie. W tym kontekście, duże znaczenie ma czy rozważam proces w obszarze ①, czy ②, ponieważ dla małych napięć (blokada kulombowska) efektywna wielkość relaksacji spinowej określa końcowy stan magnetyczny molekuły.

Na rys. 7.3 pokazana jest zależność średniej wartości składowej z spinu molekuły od napięcia transportowego w przypadku, gdy molekuła wystawiona jest na działanie impulsu promieniowania elektromagnetycznego. Widać, że promieniowanie wywiera trwały efekt na stanie magnetycznym molekuły jedynie w zakresie blokady kulombowskiej. Ponadto można zauważyć, ramka na rys. 7.3, że promieniowanie wpływa na stan magnetyczny molekuły jedynie, kiedy jest spolaryzowane kołowo lewoskrętnie (linia ciągła). Natomiast dla polaryzacji kołowej prawoskrętnej stan molekuł nie ulega zmianie, a promieniowanie spolaryzowane liniowo prowadzi, dla dużych natężeń, do rozmagnesowania molekuły.

Okazuje się, że w omawianym zakresie napięć, wpływ promieniowania elektromagnetycznego na stan magnetyczny molekuły jest wynikiem współgrania trzech niezależnych procesów. Po pierwsze, występują procesy wynikające ze sprzężenia molekuły z prądem spinowo-spolaryzowanym, które są głównym przedmiotem badań tejże rozprawy. Jednakże, w obszarze blokady kulombowskiej, kiedy napięcie transportowe jest mniejsze niż jego wartość progowa, przy której następuje zapoczątkowanie mechanizmu CIMS, wspomniane procesy nie są w stanie zmienić stanu molekuły. Po drugie, w układzie obecne są procesy wewnętrznej relaksacji spinu. Ostatnią grupę procesów stanowią pro-

cesy stymulowane przez impuls promieniowania, które dyskutuję w obecnym rozdziale. Wydaje się, że ostatni z wymienionych mechanizmów, pełni funkcję inicjującą dla bardziej złożonego mechanizmu. Absorbując impuls promieniowania, molekuła ulega czasowemu wzbudzeniu, a w konsekwencji przez krótki moment zmniejszeniu ulega bariera energetyczna dla zjawiska CIMS, wynikająca ze zbyt małego napięcia transportowego. W rozważanym przypadku, promieniowanie elektromagnetyczne służy zatem do stymulowania procesów relaksacji wynikających z oddziaływania molekuły z elektronami przewodnictwa, a natężenie promieniowania decyduje o końcowym stanie magnetycznym molekuły, rys. 7.4.

Głównym problemem związanym z zastosowaniem analizowanego przeze mnie mechanizmu jest wartość natężeń promieniowania, dla których można by obserwować zmianę stanu magnetycznego molekuły. Uzyskane wartości są zdecydowanie niemożliwe obecnie do uzyskania w ramach zaproponowanego eksperymentu i prawdopodobnie doprowadziłyby do zniszczenia próbki. Jednocześnie powyższy problem można by spróbować ominąć, używając, zamiast jednego impulsu o dużym natężeniu, serię impulsów o mniejszym natężeniu, rys. 7.6. Na koniec, warto zauważyć, że główna różnica pomiędzy wpływem promieniowania na stan magnetyczny molekuły w obszarze ① oraz ② polega na tym, że w tym drugim promieniowanie tylko chwilowo może zmienić stan molekuły, rys. 7.7(a), po czym molekuła ulega rozmagnesowaniu, które jest wynikiem silnej relaksacji spinowej.

Chociaż wyniki powyższej pracy wydają się być zachęcające dla dalszych badań nad pojedynczymi magnetycznymi molekułami, pod kątem ich wykorzystania jako elementów urządzeń spintronicznych, to jednak należy jasno powiedzieć, że z doświadczalnego punktu widzenia, realizacja przedstawionych w tej pracy pomysłów jest dość odległą perspektywą. Głównym problemem w obecnej chwili są zbyt niskie temperatury, w jakich omawiane urządzenia wykazywałyby oczekiwane własności. W związku z tym, podejmowane są ogromne starania w celu zsyntetyzowania nowych molekuł, które cechowałaby znacznie wyższa temperatura blokowania, a jednocześnie rozsądna wartość bariery energetycznej dla odwrócenia spinu molekuły. W odniesieniu do teoretycznych aspektów badań nad własnościami transportowymi pojedynczych magnetycznych molekuł, jednym z ważniejszych zadań to poznanie szczegółowego mechanizmu, jak osadzenie molekuły na powierzchni wpływa na własności molekuły odpowiedzialne za transport elektronów. Ponieważ wiele na to wskazuje, że spinowo-spolaryzowany transport przez rozważane molekuły zostanie po raz pierwszy zaobserwowany w układzie składającym się z molekuły umieszczonej na metalicznym, niemagnetycznym podłożu oraz skaningowego mikroskopu tunelowego o magnetycznym ostrzu, interesujące może okazać się rozważenie jak transport balistyczny elektronów przez molekułę wpływa na jej strukturę przestrzenną oraz stan magnetyczny.

List of publications

1. M. Misiorny and J. Barnaś,
   Magnetic switching of a single molecular magnet due to spin-polarized current,
   Physical Review B **75** (2007), no. 13, 134425.

2. M. Misiorny and J. Barnaś,
   Spin polarized transport through a single-molecule magnet: Current-induced magnetic switching,
   Physical Review B **76** (2007), no. 5, 54448; also in Vir. J. Nan. Sci. & Tech. **16** (2007), iss. 11, sec. Nanomagnetism and Spintronics.

3. M. Misiorny and J. Barnaś,
   Effects of intrinsic spin-relaxation in molecular magnets on current-induced magnetic switching,
   Physical Review B **77** (2008), no. 17, 172414; also in Vir. J. Nan. Sci. & Tech. **17** (2007), iss. 23, sec. Nanomagnetism and Spintronics.

4. M. Misiorny, I. Weymann and J . Barnaś,
   Spin effects in transport through single-molecule magnets in the sequential and cotunneling regimes,
   Physical Review B **79** (2009), no. 22, 224420; also in Vir. J. Nan. Sci. & Tech. **19** (2007), iss. 26, sec. Nanomagnetism and Spintronics.

5. M. Misiorny and J. Barnaś,
   Quantum tunneling of magnetization in single molecular magnets coupled to ferromagnetic reservoirs,
   Europhysics Lett. 78 (2007), no. 2, 27003.

6. M. Misiorny, I. Weymann and J. Barnaś,
   Spin diode behavior in transport through single-molecule magnets,
   Europhysics Lett. – accepted for publication.

7. J. Barnaś, M. Gmitra, M. Misiorny, V. K. Dugaev, and H. W. Kunert,
Current-induced magnetic switching and dynamics in spin valves,
Journal of Non-Crystalline Solids **354** (2008), no. 35-39, 4181.

8. M. Misiorny and J. Barnaś,
Switching of molecular magnets (feature article),
Physica Status Solidi B **246** (2009), no. 4, 695.

9. J. Barnaś, M. Gmitra, M. Misiorny oraz V. Dugaev,
Current-induced switching in spin-valve structures,
Physica Status Solidi B **244** (2007), no. 7, 2304.

10. M. Misiorny and J. Barnaś,
Dynamics of current-induced magnetic switching of a single-molecule magnet,
IEEE Transactions on Magnetics **44** (2008), no. 11, 2523.

11. M. Misiorny and J. Barnaś,
Current-induced magnet switching of an arbitrary oriented single-molecule magnet in the cotunneling regime,
Journal of Magnetism and Magnetic Materials – in press (available online).

12. M. Misiorny and J. Barnaś,
Current-induced switching of a single magnetic molecule with an arbitrary orientation of the magnetic easy axis,
Solid State Sciences **11** (2009), no. 4, 772.

13. M. Misiorny oraz J. Barnaś,
Spin reversal processes in a single molecular magnet between two ferromagnetic leads,
Materials Science – Poland **25** (2007), no. 2, 505.

14. M. Misiorny oraz J. Barnaś,
Current–induced switching of a single–molecule magnet with arbitrary oriented easy axis,
Materials Science – Poland **25** (2007), no. 4, 1236.

Bibliography

[1] S. Gray, *An account of some new electrical experiments. By Mr. Stephen Gray*, Phil. Trans. (1683-1775) **31** (1720-1721), no. 366, 104.

[2] S. Gray, *A letter to Cromwell Mortimer, M. D. Secr. R. S. containing several experiments concerning electricity; By Mr. Stephen Gray*, Phil. Trans. (1683-1775) **37** (1731-1732), no. 417, 18.

[3] M. Ben-Chaim, *Social mobility and scientific change: Stephen Gray's contribution to electrical research*, The British Journal for the History of Science **23** (1990), no. 1, 3.

[4] M. N. Baibich, JM Broto, A. Fert, F. N. Van Dau, F. Petroff, P. Eitenne, G. Creuzet, A. Friederich, and J. Chazelas, *Giant magnetoresistance of (001) Fe/(001) Cr magnetic superlattices*, Phys. Rev. Lett. **61** (1988), no. 21, 2472.

[5] G. Binasch, P. Grünberg, F. Saurenbach, and W. Zinn, *Enhanced magnetoresistance in layered magnetic structures with antiferromagnetic interlayer exchange*, Phys. Rev. B **39** (1989), no. 7, 4828.

[6] J.F. Gregg, I. Petej, E. Jouguelet, and C. Dennis, *Spin electronics – a review*, J. Phys. D: Appl. Phys. **35** (2002), no. 18, R121.

[7] R. E. Camley and J. Barnaś, *Theory of giant magnetoresistance effects in magnetic layered structures with antiferromagnetic coupling*, Phys. Rev. Lett. **63** (1989), no. 6, 664.

[8] J. Barnaś, A. Fuss, R. E. Camley, P. Grünberg, and W. Zinn, *Novel magnetoresistance effect in layered magnetic structures: Theory and experiment*, Phys. Rev. B **42** (1990), no. 13, 8110.

[9] C. Joachim, J. K. Gimzewski, and A. Aviram, *Electronics using hybrid-molecular and mono-molecular devices*, Nature (London) **408** (2000), no. 6812, 541.

[10] S. A. Wolf, D. D. Awschalom, R. A. Buhrman, J. M. Daughton, S. von Molnar, M. L. Roukes, A. Y. Chtchelkanova, and D. M. Treger, *Spintronics: a spin-based electronics vision for the future*, Science **294** (2001), no. 5546, 1488.

[11] D. D. Awschalom and M. E. Flatté, *Challenges for semiconductor spintronics*, Nature Phys. **3** (2007), no. 3, 153.

[12] H. Dery, P. Dalal, L. Cywinski, and L. J. Sham, *Spin-based logic in semiconductors for reconfigurable large-scale circuits*, Nature (London) **447** (2007), no. 7144, 573.

[13] W. G. van der Wiel, S. De Franceschi, J. M. Elzerman, T. Fujisawa, S. Tarucha, and L. P. Kouwenhoven, *Electron transport through double quantum dots*, Rev. Mod. Phys. **75** (2002), no. 1, 1.

[14] S. J. Tans, M. H. Devoret, H. Dai, A. Thess, R. E. Smalley, L. J. Geerligs, and C. Dekker, *Individual single-wall carbon nanotubes as quantum wires*, Nature (London) **386** (1997), no. 6624, 474.

[15] S.J. Tans, A.R.M. Verschueren, and C. Dekker, *Room-temperature transistor basedon a single carbonnanotube*, Nature (London) **393** (1998), 49.

[16] K. Tsukagoshi, B. W. Alphenaar, and H. Ago, *Coherent transport of electron spin in a ferromagnetically contacted carbon nanotube*, Nature (London) **401** (1999), no. 6753, 572.

[17] J. P. Cleuziou, W. Wernsdorfer, V. Bouchiat, T. Ondarçuhu, and M. Monthioux, *Carbon nanotube superconducting quantum interference device*, Nature Nanotech. **1** (2006), 53.

[18] H. Park, J. Park, A.K.L. Lim, E.H. Andeson, A.P. Alivisatos, and P.L. McEuen, *Nanomechanical oscillations in a single-C_{60} transistors*, Nature (London) **407** (2000), 57.

[19] M. A. Reed, C. Zhou, C. J. Muller, Burgin T. P., and J. M. Tour, *Conductance of a molecular junctions*, Science **278** (1997), 252.

[20] D. Porath, Y. Levi, M. Tarabiah, and O. Millo, *Tunneling spectroscopy of isolated C_{60} molecules in the presence of charging effects*, Phys. Rev. B **56** (1997), no. 15, 9829.

[21] D. Porath, A. Bezryadin, S. de Vries, and C. Dekker, *Direct measurements of electrical transport through DNA molecules*, Nature (London) **403** (2000), 635.

[22] J. Reichert, R. Ochs, D. Beckmann, H. B. Weber, M. Mayor, and H. Löhneysen, *Driving current through single organic molecules*, Phys. Rev. Lett. **88** (2002), no. 17, 176804.

[23] J. E. Grose, E. S. Tam, C. Timm, M. Scheloske, B. Ulgut, J. J. Parks, H. D. Abruña, W. Harneit, and D. C. Ralph, *Tunneling spectra of individual magnetic endofullerene molecules*, Nature Mater. **7** (2008), 884.

[24] A. Nitzan and M. A. Ratner, *Electron transport in molecular wire junctions*, Science **300** (2003), no. 5624, 1384.

[25] A. R. Rocha, V. M. Garcia-Suarez, S. W. Bailey, C. J. Lambert, J. Ferrer, and S. Sanvito, *Towards molecular spintronics*, Nature Mater. **4** (2005), no. 4, 335.

[26] N. J. Tao, *Electron transport in molecular junctions*, Nature Nanotech. **1** (2006), no. 3, 173.

[27] W. J. M. Naber, S. Faez, and W. G. van der Wiel, *Organic spintronics*, J. Phys. D: Appl. Phys. **40** (2007), no. 12, R205.

[28] L. Bogani and W. Wernsdorfer, *Molecular spintronics using single-molecule magnets*, Nature Mater. **7** (2008), no. 3, 179.

[29] S. J. Blundell and F. L. Pratt, *Organic and molecular magnets*, J. Phys.: Condens. Matter **16** (2004), no. 24, R771.

[30] M. Mannini, F. Pineider, P. Sainctavit, C. Danieli, E. Otero, C. Sciancalepore, A.M. Talarico, M.A. Arrio, A. Cornia, D. Gatteschi, and R. Sessoli, *Magnetic memory of a single-molecule quantum magnet wired to a gold surface*, Nature Mater. **8** (2009), no. 3, 194.

[31] O. Kahn and C. J. Martinez, *Spin-transition polymers: from molecular materials toward memory devices*, Science **279** (1998), no. 5347, 44.

[32] W. Wernsdorfer, *A long-lasting phase*, Nature Mater. **6** (2007), 174.

[33] R. Sessoli, D. Gatteschi, A. Caneschi, and M. A. Novak, *Magnetic bistability in a metal-ion cluster*, Nature (London) **365** (1993), no. 6442, 141.

[34] D. Gatteschi, A. Caneschi, L. Pardi, and R. Sessoli, *Large clusters of metal ions: the transition from molecular to bulk magnets*, Science **265** (1994), no. 5175, 1054.

[35] G. Christou, D. Gatteschi, D. N. Hendrickson, and R. Sessoli, *Single-molecule magnets*, Mater. Res. Soc. Bull. **25** (2000), no. 11, 66.

[36] G. Christou, *Single-molecule magnets: a molecular approach to nanoscale magnetic materials*, Polyhedron **24** (2005), no. 16–17, 2065.

[37] D. Gatteschi, R. Sessoli, and J. Villain, *Molecular nanomagnets*, Oxford University Press, New York, 2006.

[38] A. Caneschi, D. Gatteschi, C. Sangregorio, R. Sessoli, L. Sorace, A. Cornia, and M. Novak, *Molecular approach to nanoscale magnetism*, J. Mag. Mag. Mater. **200** (1999), no. 1, 182s.

[39] M.N. Leuenberger and D. Loss, *Quantum computing in molecular magnets*, Nature (London) **410** (2001), no. 6830, 789.

[40] B. Zhou, R. Tao, S.-Q. Shen, and J.-Q. Liang, *Quantum computing of molecular magnet Mn_{12}*, Phys. Rev. A **66** (2002), no. 1, 010301.

[41] F. Troiani, A. Ghirri, M. Affronte, S. Carretta, P. Santini, G. Amoretti, S. Piligkos, G. Timco, and R.E.P. Winpenny, *Molecular engineering of antiferromagnetic rings for quantum computation*, Physical review letters **94** (2005), no. 20, 207208.

[42] A. Ardavan, O. Rival, J. J. L. Morton, S. J. Blundell, A. M. Tyryshkin, G. A. Timco, and R. E. P. Winpenny, *Will spin-relaxation times in molecular magnets permit quantum information processing?*, Phys. Rev. Lett. **98** (2007), no. 5, 57201.

[43] M. Affronte, F. Troiani, A. Ghirri, A. Candini, M. Evangelisti, V. Corradini, S. Carretta, P. Santini, G. Amoretti, F. Tuna, G. Timco, and R.E.P. Winpenny, *Single molecule magnets for quantum computation*, J. Phys. D: Appl. Phys. **40** (2007), no. 10, 2999.

[44] H. B. Heersche, Z. de Groot, J. A. Folk, H. S. J. van der Zant, C. Romeike, M. R. Wegewijs, L. Zobbi, D. Barreca, E. Tondello, and A. Cornia, *Electron transport through Single Mn_{12} molecular magnets*, Phys. Rev. Lett. **96** (2006), no. 20, 206801.

[45] C. Ni, S. Shah, D. Hendrickson, and P. R. Bandaru, *Enhanced differential conductance through light induced current switching in Mn_{12} acetate molecular junctions*, Appl. Phys. Lett. **89** (2006), no. 21, 212104.

[46] M.-H. Jo, J. E. Grose, K. Baheti, M. M. Deshmukh, J. J. Sokol, E. M. Rumberger, D. N. Hendrickson, J. R. Long, H. Park, and D. C. Ralph, *Signatures of molecular magnetism in single-molecule transport spectroscopy*, Nano Lett. **6** (2006), no. 9, 2014.

[47] J. J. Henderson, C. M. Ramsey, E. del Barco, A. Mishra, and G. Christou, *Fabrication of nanogapped single-electron transistors for transport studies of individual single-molecule magnets*, J. Appl. Phys. **101** (2007), 09E102.

[48] S. Voss, M. Fonin, U. Rüdiger, M. Burgert, and U. Groth, *Experimental observation of a band gap in individual Mn_{12} molecules on Au(111)*, Appl. Phys. Lett. **90** (2007), no. 13, 133104.

[49] S. Voss, O. Zander, M. Fonin, U. Rüdiger, M. Burgert, and U. Groth, *Electronic transport properties and orientation of individual Mn_{12} single-molecule magnets*, Phys. Rev. B **78** (2008), no. 15, 155403.

[50] C. Romeike, M. R. Wegewijs, W. Hofstetter, and H. Schoeller, *Quantum-tunneling-induced Kondo effect in single molecular magnets*, Phys. Rev. Lett. **96** (2006), no. 19, 196601.

[51] C. Romeike, M. R. Wegewijs, W. Hofstetter, and H. Schoeller, *Kondo-transport spectroscopy of single molecule magnets*, Phys. Rev. Lett. **97** (2006), no. 20, 206601.

[52] M. N. Leuenberger and E. R. Mucciolo, *Berry-phase oscillations of the Kondo effect in single-molecule magnets*, Phys. Rev. Lett. **97** (2006), no. 12, 126601.

[53] G. Gonzalez, M. N. Leuenberger, and E. R. Mucciolo, *Kondo effect in single-molecule magnet transistors*, Phys. Rev. B **78** (2008), 054445.

[54] D. Roosen, M. R. Wegewijs, and W. Hofstetter, *Nonequilibrium dynamics of anisotropic large spins in the Kondo regime: Time-dependent numerical renormalization group analysis*, Phys. Rev. Lett. **100** (2008), no. 8, 087201.

[55] D. V. Averin and A. A. Odintsov, *Macroscopic quantum tunneling of the electric charge in small tunnel junctions*, Phys. Lett. A **140** (1989), no. 5, 251.

[56] D. V. Averin and Y. V. Nazarov, *Virtual electron diffusion during quantum tunneling of the electric charge*, Phys. Rev. Lett. **65** (1990), no. 19, 2446.

[57] W. Wernsdorfer and R. Sessoli, *Quantum phase interference and parity effects in magnetic molecular clusters*, Science **284** (1999), no. 5411, 133.

[58] G. Aromí and E. K. Brechin, *Synthesis of 3d metallic single-molecule magnets*, Struct. Bond. **122** (2006), 1.

[59] A. L. Barra, P. Debrunner, D. Gatteschi, C. E. Schulz, and R. Sessoli, *Superparamagnetic-like behavior in an octanuclear iron cluster*, Europhys. Lett. **35** (1996), no. 2, 133.

[60] C. P. Bean and J. D. Livingston, *Superparamagnetism*, J. Appl. Phys. **30** (1959), no. 4, S120.

[61] S. Bedanta and W. Kleemann, *Superparamagnetism*, J. Phys. D: Appl. Phys. **42** (2009), no. 1, 013001.

[62] D. Gatteschi and R. Sessoli, *Quantum tunneling of magnetization and related phenomena in molecular materials*, Angew. Chem. Int. Ed. **42** (2003), no. 3, 268.

[63] L. Thomas, F. Lionti, R. Ballou, D. Gatteschi, R. Sessoli, and B. Barbara, *Macroscopic quantum tunnelling of magnetization in a single crystal of nanomagnets*, Nature (London) **383** (1996), no. 6596, 145.

[64] S. Accorsi, A. L. Barra, A. Caneschi, G. Chastanet, A. Cornia, A. C. Fabretti, D. Gatteschi, C. Mortalo, E. Olivieri, F. Parenti, P. Rosa, R. Sessoli, L. Sorace, W. Wernsdorfer, and L. Zobbi, *Tuning anisotropy barriers in a family of tetrairon(III) single-molecule magnets with an $S = 5$ ground state*, J. Am. Chem. Soc. **128** (2006), no. 14, 4742.

[65] C. J. Milios, A. Vinslava, W. Wernsdorfer, S. Moggach, S. Parsons, S. P. Perlepes, G. Christou, and E. K. Brechin, *A record anisotropy barrier for a single-molecule magnet*, J. Am. Chem. Soc. **129** (2007), no. 10, 2754.

[66] A. L. Barra, D. Gatteschi, and R. Sessoli, *High-frequency EPR spectra of $[Fe_8O_2(OH)_{12}(rmtacn)_6]Br_8$: A critical appraisal of the barrier for the reorientation of the magnetization in single-molecule magnets*, Chem. Euro. J. **6** (2000), no. 9, 1608.

[67] N. E. Chakov, S. C. Lee, A. G. Harter, P. L. Kuhns, A. P. Reyes, S. O. Hill, N. S. Dalal, W. Wernsdorfer, K. A. Abboud, and G. Christou, *The properties of the $[Mn_{12}O_{12}(O_2CR)_{16}(H_2O)_4]$ single-molecule magnets in truly axial symmetry: $[Mn_{12}O_{12}(O_2CCH_2Br)_{16}(H_2O)_4] \cdot 4CH_2Cl_2$*, J. Am. Chem. Soc. **128** (2006), no. 21, 6975.

[68] O. Waldmann, *A criterion for the anisotropy barrier in single-molecule magnets*, Inorg. Chem. **46** (2007), no. 24, 10035.

[69] A. Morello, O. N. Bakharev, H. B. Brom, R. Sessoli, and L. J. de Jongh, *Nuclear spin dynamics in the quantum regime of a single-molecule magnet*, Phys. Rev. Lett. **93** (2004), no. 19, 197202.

[70] W. Wernsdorfer, R. Sessoli, A. Caneschi, D. Gatteschi, and A. Cornia, *Nonadiabatic Landau-Zener tunneling in Fe_8 molecular nanomagnets*, Europhys. Lett. **50** (2000), no. 4, 552.

[71] S. Bahr, K. Petukhov, V. Mosser, and W. Wernsdorfer, *Pump-probe experiments on the single-molecule magnet Fe_8: Measurement of excited level lifetimes*, Phys. Rev. Lett. **99** (2007), no. 14, 147205.

[72] S. Bahr, K. Petukhov, V. Mosser, and W. Wernsdorfer, *Energy level lifetimes in the single-molecule magnet Fe_8: Experiments and simulations*, Phys. Rev. B **77** (2008), no. 6, 64404.

[73] M. Bal, J. R. Friedman, W. Chen, M. T. Tuominen, C. C. Beedle, E. M. Rumberger, and D. N. Hendrickson, *Radiation- and phonon-bottleneck-induced tunneling in the Fe_8 single-molecule magnet*, Europhys. Lett. **82** (2007), no. 1, 17005.

[74] W. Wernsdorfer, A. Caneschi, R. Sessoli, D. Gatteschi, A. Cornia, V. Villar, and C. Paulsen, *Effects of nuclear spins on the quantum relaxation of the magnetization for the molecular manomagnet Fe_8*, Phys. Rev. Lett. **84** (2000), no. 13, 2965.

[75] A. Morello, P. C. E. Stamp, and I. S. Tupitsyn, *Pairwise decoherence in coupled spin qubit networks*, Phys. Rev. Lett. **97** (2006), no. 20, 207206.

[76] N. V. Prokof'ev and P. C. E. Stamp, *Quantum relaxation of magnetisation in magnetic particles*, Journal of Low Temperature Physics **104** (1996), no. 3, 143.

[77] N. V. Prokof'ev and P. C. E. Stamp, *Low-temperature quantum relaxation in a system of magnetic nanomolecules*, Phys. Rev. Lett. **80** (1998), no. 26, 5794.

[78] T. Ohm, C. Sangregorio, and C. Paulsen, *Non-exponential relaxation in a resonant quantum tunneling system of magnetic molecules*, J. Low Temp. Phys. **113** (1998), no. 5, 1141.

[79] L. Thomas, A. Caneschi, and B. Barbara, *Nonexponential dynamic scaling of the magnetization relaxation in Mn_{12} acetate*, Phys. Rev. Lett. **83** (1999), no. 12, 2398.

[80] W. Wernsdorfer, N. Aliaga-Alcalde, D. N. Hendrickson, and G. Christou, *Exchange-biased quantum tunnelling in a supramolecular dimer of single-molecule magnets*, Nature (London) **416** (2002), no. 6879, 406.

[81] W. Wernsdorfer, S. Bhaduri, R. Tiron, D. N. Hendrickson, and G. Christou, *Spin-spin cross relaxation in single-molecule magnets*, Phys. Rev. Lett. **89** (2002), no. 19, 197201.

[82] S. Hill, R. S. Edwards, N. Aliaga-Alcalde, and G. Christou, *Quantum coherence in an exchange-coupled dimer of single-molecule magnets*, Science **302** (2003), no. 5647, 1015.

[83] G. H. Kim and T. S. Kim, *Electronic transport in single-molecule magnets on metallic surfaces*, Phys. Rev. Lett. **92** (2004), no. 13, 137203.

[84] H. Park, A. K. L. Lim, A. P. Alivisatos, J. Park, and P. L. McEuen, *Fabrication of metallic electrodes with nanometer separation by electromigration*, Appl. Phys. Lett. **75** (1999), no. 2, 301.

[85] A. Cottet, T. Kontos, S. Sahoo, H. T. Man, M. S Choi, W. Belzig, C. Bruder, A. F. Morpurgo, and C. Schönenberger, *Nanospintronics with carbon nanotubes*, Semicond. Sci. Technol. **21** (2006), no. 11, S78.

[86] L. E. Hueso, J. M. Pruneda, V. Ferrari, G. Burnell, J. P. Valdes-Herrera, B. D. Simons, P. B. Littlewood, E. Artacho, A. Fert, and N. D. Mathur, *Transformation of spin information into large electrical signals using carbon nanotubes.*, Nature (London) **445** (2007), no. 7126, 410.

[87] M. Fonin, S. Voss, S. Herr, G. de Loubens, A.D. Kent, M. Burgert, U. Groth, and U. Rüdiger, *Influence of the ligand shell on the surface orientation of Mn_{12} single molecule magnets*, Polyhedron **28** (2009), no. 9-10, 1977.

[88] A.N. Abdi, J.P. Bucher, P. Rabu, O. Toulemonde, M. Drillon, and P. Gerbier, *Magnetic properties of bulk $Mn_{12}Pivalates_{16}$ single molecule magnets and their self assembly on functionnalized gold surface*, J. Appl. Phys. **95** (2004), no. 11, 7345.

[89] A. Cornia, A.F. Costantino, L. Zobbi, A. Caneschi, D. Gatteschi, M. Mannini, and R. Sessoli, *Preparation of novel materials using SMMs*, Struct. Bond. **122** (2005), 133.

[90] L. Zobbi, M. Mannini, M. Pacchioni, G. Chastanet, D. Bonacchi, C. Zanardi, R. Biagi, U.D. Pennino, D. Gatteschi, A. Cornia, and R. Sessoli, *Isolated single-molecule magnets on native gold*, Chem. Commun. **12** (2005), 1640.

[91] A. Naitabdi, J.P. Bucher, P. Gerbier, P. Rabu, and M. Drillon, *Self-assembly and magnetism of Mn_{12} nanomagnets on native and functionalized gold surfaces*, Adv. Mater. **17** (2005), no. 13, 1612.

[92] M. Burgert, S. Voss, S. Herr, M. Fonin, U. Groth, and U. Rüdiger, *Single-molecule magnets: A new approach to investigate the electronic structure of Mn_{12} molecules by scanning tunneling spectroscopy*, J. Am. Chem. Soc. **129** (2007), no. 46, 14362.

[93] S. Barraza-Lopez, M.C. Avery, and K. Park, *First-principles study of a single-molecule magnet Mn_{12} monolayer on the Au(111) surface*, Phys. Rev. B **76** (2007), no. 22, 224413.

[94] S. Barraza-Lopez, M.C. Avery, and K. Park, *The interaction between a monolayer of single-molecule magnets and a metal surface*, J. Appl. Phys. **103** (2008), no. 7, 07B907.

[95] S. Barraza-Lopez, K. Park, V. García-Suárez, and J. Ferrer, *Spin-filtering effect in the transport through a single-molecule magnet Mn_{12} bridged between metallic electrodes*, J. Appl. Phys. **105** (2009), no. 7, 07E309.

[96] S. Barraza-Lopez, K. Park, V. García-Suárez, and J. Ferrer, *First-principles study of electron transport through the single-molecule magnet Mn_{12}*, Phys. Rev. Lett. **102** (2009), no. 24, 246801.

[97] C.D. Pemmaraju, I. Rungger, and S. Sanvito, *Ab initio calculation of the bias-dependent transport properties of Mn_{12} molecules*, Phys. Rev. B **80** (2009), no. 10, 104422.

[98] M. Soler, W. Wernsdorfer, K. A. Abboud, J. C. Huffman, E. R. Davidson, D. N. Hendrickson, and G. Christou, *Single-molecule magnets: two-electron reduced version of a Mn_{12} complex and environmental influences on the magnetization relaxation of $(PPh_4)_2[Mn_{12}O_{12}(O_2CCHCl_2)_{16}(H_2O)_4]$*, J. Am. Chem. Soc **125** (2003), no. 12, 3576.

[99] K. Park and M.R. Pederson, *Effect of extra electrons on the exchange and magnetic anisotropy in the anionic single-molecule magnet Mn_{12}*, Phys. Rev. B **70** (2004), no. 5, 054414.

[100] R. Basler, A. Sieber, G. Chaboussant, H. U. Gudel, N. E. Chakov, M. Soler, G. Christou, A. Desmedt, and R. Lechner, *Inelastic neutron scattering study of electron reduction in Mn_{12} derivatives*, Inorg. Chem. **44** (2005), no. 3, 649.

[101] V. V. Dobrovitski and A. K. Zvezdin, *Macroscopic quantum tunnelling and hysteresis loops of mesoscopic magnets*, Europhys. Lett. **38** (1997), no. 5, 377.

[102] L. Michalak, C.M. Canali, M.R. Pederson, V.G. Benza, and M. Paulsson, *Theory of tunneling spectroscopy in a Mn_{12} single-electron transistor by DFT methods*, Arxiv preprint arXiv:0812.1058 (2008).

[103] M. Misiorny and J. Barnaś, *Spin polarized transport through a single-molecule magnet: Current-induced magnetic switching*, Phys. Rev. B **76** (2007), no. 5, 054448.

[104] C. Timm and F. Elste, *Spin amplification, reading, and writing in transport through anisotropic magnetic molecules*, Phys. Rev. B **73** (2006), no. 23, 235304.

[105] R. Caciuffo, G. Amoretti, A. Murani, R. Sessoli, A. Caneschi, and D. Gatteschi, *Neutron spectroscopy for the magnetic anisotropy of molecular clusters*, Phys. Rev. Lett. **81** (1998), no. 21, 4744.

[106] J. Perenboom, J. S. Brooks, S. Hill, T. Hathaway, and N. S. Dalal, *Relaxation of the magnetization of Mn_{12} acetate*, Phys. Rev. B **58** (1998), no. 1, 330.

[107] J. Schnack, *Quantum theory of molecular magnetism* (*Lecture notes of the 36th spring school of the Institute of Solid State Research: Magnetism goes nano – electron correlations, spin transport and molecular magnetism*, S. Blügel, T. Brückel, and M. Schneider, eds.), Schriften des Forschungzentrums Jülich – Matter and Materials, vol. 26, Institut für Festkörperforschung, Forschunszentrum Jülich GmbH, 2005.

[108] G. Kamieniarz and R. Matysiak, *Simulations of the low-dimensional magnetic systems by the quantum transfer-matrix technique*, Comput. Mater. Sci. **28** (2003), no. 2, 353.

[109] G. Kamieniarz, M. Haglauer, A. Caramico D'Auria, F. Esposito, and D. Gatteschi, *Simulations of the low-dimensional molecular-based spin systems: dodecanuclear nickel ring*, J. Mag. Mag. Mater. **290** (2005), no. 2, 970.

[110] C. Romeike, M. R Wegewijs, and H. Schoeller, *Spin quantum tunneling in single molecular magnets: Fingerprints in transport tpectroscopy of current and noise*, Phys. Rev. Lett. **96** (2006), no. 19, 196805.

[111] B. Barbara, L.C. Sampaio, J.E. Wegrowe, B.A. Ratnam, A. Marchand, C. Paulsen, M.A. Novak, J.L. Tholence, M. Uehara, and D. Fruchart, *Quantum tunneling in magnetic systems of various sizes*, J. Appl. Phys. **73** (1993), no. 10, 6703.

[112] B. Barbara, W. Wernsdorfer, L.C. Sampaio, J.G. Park, C. Paulsen, M.A. Novak, R. Ferré, D. Mailly, R. Sessoli, A. Caneschi, K. Hasselbach, A. Benoit, and L. Thomas, *Mesoscopic quantum tunneling of the magnetization*, J. Mag. Mag. Mater. **140–144** (1995), no. 3, 1825.

[113] J. Tejada, R.F. Ziolo, and X.X. Zhang, *Quantum tunneling of magnetization in nanostructured materials*, Chem. Mater. **8** (1996), no. 8, 1784.

[114] E. M. Chudnovsky and J. Tejada, *Macroscopic quantum tunneling of the magnetic moment*, Cambridge Studies in Magnetism, Cambridge University Press, New York, 1998.

[115] B. Barbara, L. Thomas, F. Lionti, I. Chiorescu, and A. Sulpice, *Macroscopic quantum tunneling in molecular magnets*, J. Magn. Magn. Mater. **200** (1999), no. 1, 167.

[116] W. Wernsdorfer, *Classical and quantum magnetization reversal studied in nanometer-sizeed particles and clusters*, Adv. Chem. Phys. **118** (2001), 99.

[117] J.R. Friedman, *Resonant magnetization tunneling in molecular magnets* (*Exploring the quantum/classical frontier: recent advances in macroscopic and mesoscopic quantum phenomena*, J.R. Friedman, and S. Han, eds.), Nova Science, Huntington, NY, 2003.

[118] M. Enz and R. Schilling, *Magnetic field dependence of the tunnelling splitting of quantum spins*, J. Phys. C: Solid State Phys. **19** (1986), no. 30, L711.

[119] J.L. van Hemmen and A. Sütő, *Tunnelling of quantum spins*, Europhys. Lett. **1** (1986), no. 10, 481.

[120] E. M. Chudnovsky and L. Gunther, *Quantum tunneling of magnetization in small ferromagnetic particles*, Phys. Rev. Lett. **60** (1988), no. 8, 661.

[121] E. M. Chudnovsky and L. Gunther, *Quantum theory of nucleation in ferromagnets*, Phys. Rev. B **37** (1988), no. 16, 9455.

[122] P.C.E. Stamp, *Quantum dynamics and tunneling of domain walls in ferromagnetic insulators*, Phys. Rev. Lett. **66** (1991), no. 21, 2802.

[123] D.A. Garanin, *Spin tunnelling: a perturbative approach*, J. Phys. A: Math. Gen. **24** (1991), no. 2, L61.

[124] J. Tejada, X.X. Zhang, and L. Balcells, *Nonthermal viscosity in magnets: Quantum tunneling of the magnetization*, J. Appl. Phys. **73** (1993), no. 10, 6709.

[125] J. Tejada and X.X. Zhang, *On magnetic relaxation in antiferromagnetic horse-spleen ferritin proteins*, J. Phys.: Condens. Matter **6** (1994), no. 1, 263.

[126] J. R. Friedman, M. P. Sarachik, J. Tejada, and R. Ziolo, *Macroscopic measurement of resonant magnetization tunneling in high-spin molecules*, Phys. Rev. Lett. **76** (1996), no. 20, 3830.

[127] A.H. Morrish, *The physical principles of magnetism*, John Wiley & Sons, 1965. (Polish trans. *Fizyczne podstawy magnetyzmu*, PWN, 1970).

[128] R. Skomski, *Simple models of magnetism*, Oxford University Press, 2008.

[129] A. L. Barra, A. Caneschi, A. Cornia, D. Gatteschi, L. Gorini, L. P. Heiniger, R. Sessoli, and L. Sorace, *The origin of transverse anisotropy in axially symmetric single molecule magnets*, J. Am. Chem. Soc. **129** (2007), no. 35, 10754.

[130] W. Wernsdorfer, M. Murugesu, and G. Christou, *Resonant tunneling in truly axial aymmetry Mn_{12} single-molecule magnets: Sharp crossover between thermally assisted and pure quantum tunneling*, Phys. Rev. Lett. **96** (2006), no. 5, 057208.

[131] W. Wernsdorfer, N.E. Chakov, and G. Christou, *Quantum phase interference and spin-parity in Mn_{12} single-molecule magnets*, Phys. Rev. Lett. **95** (2005), no. 3, 037203.

[132] W. Wernsdorfer, T.C. Stamatatos, and G. Christou, *Influence of the Dzyaloshinskii-Moriya exchange interaction on quantum phase interference of spins*, Phys. Rev. Lett. **101** (2008), no. 23, 237204.

[133] A. Garg, *Topologically quenched tunnel splitting in spin systems without kramers' degeneracy*, Europhys. Lett. **22** (1993), no. 3, 205.

[134] M.N. Leuenberger and D. Loss, *Spin tunneling and topological selection rules for integer spins*, Physical Review B **63** (2001), no. 5, 054414.

[135] S. Datta, *Electronic transport in mesoscopic systems*, Cambridge Studies in Semiconductor Physics and Microelectronic Engineering, vol. 3, Cambridge University Press, 2002.

[136] C. Zener, *Non-adiabatic crossing of energy levels*, Proc. R. Soc. London **137** (1932), 696.

[137] L.D. Landau and E.M. Lifshitz, *Quantum mechanics, Non-relativistic theory*, 3rd ed., Course of Theoretical Physics, vol. III, Pergamon Press, 1977. (Polish trans. *Mechanika kwantowa. Teoria nierelatywistyczna*, PWN, 1979).

[138] S. Miyashita, *Dynamics of the magnetization with an inversion of the magnetic field*, J. Phys. Soc. Jpn. **64** (1995), no. 9, 3207.

[139] S. Miyashita, *Observation of the energy gap due to the quantum tunneling making use of the Landau-Zener mechanism*, J. Phys. Soc. Jpn. **65** (1996), no. 8, 2734.

[140] H. De Raedt, S. Miyashita, K. Saito, D. García-Pablos, and N. García, *Theory of quantum tunneling of the magnetization in magnetic particles*, Phys. Rev. B **56** (1997), no. 18, 11761.

[141] L. Gunther, *Spin tunneling in a swept magnetic field*, Europhys. Lett. **39** (1997), no. 1, 1.

[142] W. Wernsdorfer, R. Sessoli, A. Caneschi, D. Gatteschi, A. Cornia, and D. Mailly, *Landau–Zener method to study quantum phase interference of Fe_8 molecular nanomagnets*, J. Appl. Phys. **87** (2000), no. 9, 5481.

[143] M. N. Leuenberger and D. Loss, *Incoherent Zener tunneling and its application to molecular magnets*, Phys. Rev. B **61** (2000), no. 18, 12200.

[144] E. Rastelli and A. Tassi, *Dynamics of large-spin molecules in a time-dependent magnetic field*, Phys. Rev. B **64** (2001), no. 6, 064410.

[145] L.I. Schiff, *Quantum mechanics*, 3rd Ed., McGraw-Hill Book Company, 1968. (Polish trans. *Mechanika kwantowa*, PWN 1977).

[146] M. Misiorny and J. Barnaś, *Quantum tunneling of magnetization in single molecular magnets coupled to ferromagnetic reservoirs*, Europhys. Lett. **78** (2007), no. 2, 27003.

[147] W. Wernsdorfer, T. Ohm, C. Sangregorio, R. Sessoli, D. Mailly, and C. Paulsen, *Observation of the distribution of molecular spin states by resonant quantum tunneling of the magnetization*, Phys. Rev. Lett. **82** (1999), no. 19, 3903.

[148] W. Wernsdorfer, T. Ohm, C. Sangregorio, R. Sessoli, D. Gatteschi, and C. Paulsen, *Quantum hole digging in magnetic molecular clusters*, Physica B **284-288** (2000), 1229.

[149] N. V. Prokof'ev and P. C. E. Stamp, *Theory of the spin bath*, Rep. Prog. Phys **63** (2000), 669.

[150] D. A. Garanin and E. M. Chudnovsky, *Thermally activated resonant magnetization tunneling in molecular magnets: $Mn_{12}Ac$ and others*, Phys. Rev. B **56** (1997), no. 17, 11102–11118.

[151] C. Sangregorio, T. Ohm, C. Paulsen, R. Sessoli, and D. Gatteschi, *Quantum tunneling of the magnetization in an iron cluster nanomagnet*, Phys. Rev. Lett. **78** (1997), no. 24, 4645.

[152] A. Fort, A. Rettori, J. Villain, D. Gatteschi, and R. Sessoli, *Mixed quantum-thermal relaxation in Mn_{12} acetate molecules*, Phys. Rev. Lett. **80** (1998), no. 3, 612.

[153] J. Appelbaum, *"s-d" Exchange model of zero-bias tunneling anomalies*, Phys. Rev. Lett. **17** (1966), no. 2, 91.

[154] J.A. Appelbaum, *Exchange model of zero-bias tunneling anomalies*, Phys. Rev. **154** (1967), no. 3, 633.

[155] A. Barthélémy, A. Fert, J.P. Contour, M. Bowen, V. Cros, J.M. De Teresa, A. Hamzic, J.C. Faini, J.M. George, J. Grollier, F. Montaigne, F. Pailloux, F. Petroff, and C. Vouille, *Magnetoresistance and spin electronics*, J. Mag. Mag. Mater. **242** (2002), no. 1, 68.

[156] S.M. Thompson, *The discovery, development and future of GMR: The Nobel prize 2007*, J. Phys. D: Appl. Phys. **41** (2008), no. 9, 1.

[157] J. Slonczewski, *Current-driven excitation of magnetic multilayers*, J. Mag. Mag. Mater. **159** (1996), L1.

[158] L. Berger, *Emission of spin waves by a magnetic multilayer traversed by a current*, Phys. Rev. B **54** (1996), no. 13, 9353.

[159] J. Slonczewski, *Excitation of spin waves by an electric current*, J. Mag. Mag. Mater. **195** (1999), L261.

[160] M. D. Stiles and A. Zangwill, *Anatomy of spin-transfer torque*, Phys. Rev. B **66** (2002), no. 1, 14407.

[161] J. Barnaś, A. Fert, M. Gmitra, I. Weymann, and V. K. Dugaev, *From giant magnetoresistance to current-induced switching by spin transfer*, Phys. Rev. B **72** (2005), no. 2, 24426.

[162] M. Tsoi, A. G. M. Jansen, J. Bass, W. C. Chiang, M. Seck, V. Tsoi, and P. Wyder, *Excitation of a magnetic multilayer by an electric current*, Phys. Rev. Lett. **80** (1998), no. 19, 4281. (see also Erratum, Phys. Rev. Lett. **81** (1998), no. 2, 493).

[163] E. B. Myers, D. C. Ralph, J. A. Katine, R. N. Louie, and R. A. Buhrman, *Current-induced switching of domains in magnetic multilayer devices*, Science **285** (1999), no. 5429, 867.

[164] J.E. Wegrowe, D. Kelly, Y. Jaccard, P. Guittienne, and J.P. Ansermet, *Current-induced magnetization reversal in magnetic nanowires*, Europhys. Lett. **45** (1999), no. 5, 626.

[165] J. A. Katine, F. J. Albert, R. A. Buhrman, E. B. Myers, and D. C. Ralph, *Current-driven magnetization reversal and spin-wave excitations in Co/Cu/Co pillars*, Phys. Rev. Lett. **84** (2000), no. 14, 3149.

[166] J. Grollier, V. Cros, A. Hamzic, J.M. George, H. Jaffres, A. Fert, G. Faini, J.B. Youssef, and H. Legall, *Spin-polarized current induced switching in Co/Cu/Co pillars*, Appl. Phys. Lett. **78** (2001), no. 23, 3663.

[167] I.N. Krivorotov, N.C. Emley, J.C. Sankey, S.I. Kiselev, D.C. Ralph, and R.A. Buhrman, *Time-domain measurements of nanomagnet dynamics driven by spin-transfer torques*, Science **307** (2005), no. 5707, 228.

[168] S. Krause, L. Berbil-Bautista, G. Herzog, M. Bode, and R. Wiesendanger, *Current-induced magnetization switching with a spin-polarized scanning tunneling microscope*, Science **317** (2007), no. 5844, 1537.

[169] G. Tatara and H. Kohno, *Theory of current-driven domain wall motion: Spin transfer versus momentum transfer*, Phys. Rev. Lett. **92** (2004), no. 8, 086601.

[170] S.E. Barnes and S. Maekawa, *Current-spin coupling for ferromagnetic domain walls in fine wires*, Phys. Rev. Lett. **95** (2005), no. 10, 107204.

[171] M. Yamanouchi, D. Chiba, F. Matsukura, and H. Ohno, *Current-induced domain-wall switching in a ferromagnetic semiconductor structure*, Nature (London) **428** (2004), no. 6982, 539.

[172] D. Ravelosona, D. Lacour, J.A. Katine, B.D. Terris, and C. Chappert, *Nanometer scale observation of high efficiency thermally assisted current-driven domain wall depinning*, Phys. Rev. Lett. **95** (2005), no. 11, 117203.

[173] S.S.P. Parkin, M. Hayashi, and L. Thomas, *Magnetic domain-wall racetrack memory*, Science **320** (2008), no. 5873, 190.

[174] M. Hayashi, L. Thomas, R. Moriya, C. Rettner, and S.S.P. Parkin, *Current-controlled magnetic domain-wall nanowire shift register*, Science **320** (2008), no. 5873, 209.

[175] D. C. Ralph and R. A. Buhrman, *Spin-transfer torques and nanomagnets* (*Concepts in spin electronics* S. Maekawa, ed.), Oxford University Press, 2006.

[176] M.D. Stiles, *Handbook of magnetism and advanced magnetic materials* (H. Kronmüller and S. Parkin, eds.), Vol. 2: *Micromagnetism*, John Wiley & Sons, 2007. (Chap. *Theory of spin-transfer torques*, p. 1147).

[177] J. Slonczewski, *Handbook of magnetism and advanced magnetic materials* (H. Kronmüller and S. Parkin, eds.), Vol. 5: *Spintronics and magnetoelectronics*, John Wiley & Sons, 2007. (Chap. *Theory of spin-polarized current and spin-transfer torque in magnetic multilayers*, p. 2648).

[178] J.Z. Sun, *Handbook of magnetism and advanced magnetic materials* (H. Kronmüller and S. Parkin, eds.), Vol. 5: *Spintronics and magnetoelectronics*, John Wiley & Sons, 2007. (Chap. *Spin angular momentum transfer in magnetoresistive nanojunctions*, p. 2592).

[179] Z. Li and S. Zhang, *Magnetization dynamics with a spin-transfer torque*, Phys. Rev. B **68** (2003), no. 2, 024404.

[180] M. Misiorny and J. Barnaś, *Effects of intrinsic spin-relaxation in molecular magnets on current-induced magnetic switching*, Phys. Rev. B **77** (2008), no. 17, 172414.

[181] M. Misiorny and J. Barnaś, *Dynamics of current-induced magnetic switching of a single-molecule magnet*, IEEE Trans. Mag. **44** (2009), no. 11, 2523.

[182] J. Barnaś and A. Fert, *Magnetoresistance oscillations due to charging effects in double ferromagnetic tunnel junctions*, Phys. Rev. Lett. **80** (1998), no. 5, 1058.

[183] M. Misiorny and J. Barnaś, *Current-induced switching of a single magnetic molecule with an arbitrary orientation of the magnetic easy axis*, Solid State Sci. **11** (2009), no. 4, 772.

[184] F. Elste and C. Timm, *Cotunneling and nonequilibrium magnetization in magnetic molecular monolayers*, Phys. Rev. B **75** (2007), no. 19, 195341.

[185] M. Misiorny and J. Barnaś, *Current-induced magnet switching of an arbitrary oriented single-molecule magnet in the cotunneling regime*, J.Mag.Mag. Matter. (2009). (in press).

[186] G.D. Mahan, *Many-particle physics*, 2nd Ed., Physucs of solids and liquids, Plenum Press, New York, 1990.

[187] H. Bruus and K. Flensberg, *Many-body quantum theory in condesed matter physics*, Oxford Graduate Texts, Oxford University Press, 2004.

[188] C. Timm, *Tunneling through magnetic molecules with arbitrary angle between easy axis and magnetic field*, Phys. Rev. B **76** (2007), no. 1, 014421.

[189] J. Koch, M.E. Raikh, and F. von Oppen, *Pair tunneling through single molecules*, Phys. Rev. Lett. **96** (2006), no. 5, 56803.

[190] M. Turek and K. A. Matveev, *Cotunneling thermopower of single electron transistors*, Phys. Rev. B **65** (2002), no. 11, 115332.

[191] J. Koch, F. von Oppen, Y. Oreg, and E. Sela, *Thermopower of single-molecule devices*, Phys. Rev. B **70** (2004), no. 19, 195107.

[192] I. Weymann, *Spin-dependent transport in magnetic nanostructures with coulomb blockade*, Ph.D. Thesis, Poznań, 2005.

[193] I. Weymann and J. Barnaś, *Cotunneling through a quantum dot coupled to ferromagnetic leads with noncollinear magnetizations*, Eur. Phys. J. B **46** (2005), no. 2, 289.

[194] J. König, *Quantum fluctuations in the single electron transistor*, Ph.D. Thesis, 1999. published by Shaker, Aachen, 1999.

[195] F. Elste and C. Timm, *Transport through anisotropic magnetic molecules with partially ferromagnetic leads: Spin-charge conversion and negative differential conductance*, Phys. Rev. B **73** (2006), no. 23, 235305.

[196] M. Misiorny and J. Barnaś, *Switching of molecular magnets*, Phys. Stat. Sol. B **246** (2009), no. 4, 695.

[197] G. González and M. N. Leuenberger, *Berry-phase blockade in single-molecule magnets*, Phys. Rev. Lett. **98** (2007), no. 25, 256804.

[198] C. Timm, *Tunneling through molecules and quantum dots: Master-equation approaches*, Phys. Rev. B **77** (2008), no. 19, 195416.

[199] H. Schoeller and G. Schön, *Mesoscopic quantum transport: Resonant tunneling in the presence of a strong Coulomb interaction*, Phys. Rev. B **50** (1994), no. 24, 18436.

[200] J. König, J. Schmid, H. Schoeller, and G. Schön, *Resonant tunneling through ultrasmall quantum dots: Zero-bias anomalies, magnetic-field dependence, and boson-assisted transport*, Phys. Rev. B **54** (1996), no. 23, 16820.

[201] A. Thielmann, M.H. Hettler, J. König, and G. Schön, *Shot noise in tunneling transport through molecules and quantum dots*, Phys. Rev. B **68** (2003), no. 11, 115105.

[202] A. Thielmann, M.H. Hettler, J. König, and G. Schön, *Cotunneling current and shot noise in quantum dots*, Phys. Rev. Lett. **95** (2005), no. 14, 146806.

[203] I. Weymann, J. König, J. Martinek, J. Barnaś, and G. Schön, *Tunnel magnetoresistance of quantum dots coupled to ferromagnetic leads in the sequential and cotunneling regimes*, Phys. Rev. B **72** (2005), no. 11, 115334.

[204] J. König and J. Martinek, *Interaction-driven spin precession in quantum-dot spin valves*, Phys. Rev. Lett. **90** (2003), no. 16, 166602.

[205] I. Weymann and J. Barnaś, *Cotunneling through quantum dots coupled to magnetic leads: Zero-bias anomaly for noncollinear magnetic configurations*, Phys. Rev. B **75** (2007), no. 15, 155308.

[206] I. Weymann, *Effects of different geometries on the conductance, shot noise, and tunnel magnetoresistance of double quantum dots*, Phys. Rev. B **78** (2008), no. 4, 045310.

[207] Y.M. Blanter and M. Büttiker, *Shot noise in mesoscopic conductors*, Phys. Rep. **336** (2000), 1.

[208] J. Aghassi, *Electronic transport and noise in quantum dot systems*, Ph.D. Thesis, 2007.

[209] M. Julliere, *Tunneling between ferromagnetic films*, Phys. Lett. A **54** (1975), no. 3, 225.

[210] J. Barnaś and I. Weymann, *Spin-polarized transport through magnetic nanostructures*, J. Phys.: Condens. Matter **20** (2008), no. 43, 423202.

[211] I. Weymann and J. Barnaś, *Negative differential conductance and magnetoresistance oscillations due to spin accumulation in ferromagnetic double-island devices*, Phys. Rev. B **73** (2006), no. 3, 033409.

[212] A. Cottet, W. Belzig, and C. Bruder, *Positive cross correlations in a three-terminal quantum dot with ferromagnetic contacts*, Phys. Rev. Lett. **92** (2004), no. 20, 206801.

[213] E. Onac, F. Balestro, B. Trauzettel, C. F. Lodewijk, and L. P. Kouwenhoven, *Shot-noise detection in a carbon nanotube quantum dot*, Phys. Rev. Lett. **96** (2006), no. 2, 026803.

[214] Y. Zhang, L. DiCarlo, D.T. McClure, M. Yamamoto, S. Tarucha, C.M. Marcus, M.P. Hanson, and A.C. Gossard, *Noise correlations in a Coulomb-blockaded quantum dot*, Phys. Rev. Lett. **99** (2007), no. 3, 036603.

[215] W. Rudziński and J. Barnaś, *Tunnel magnetoresistance in ferromagnetic junctions: Tunneling through a single discrete leve*, Phys. Rev. B **64** (2001), no. 8, 085318.

[216] M. Wilczyński, R. Świrkowicz, W. Rudziński, J. Barnaś, and V. Dugaev, *Quantum dots attached to ferromagnetic leads: possibility of new spintronic devices*, J. Magn. Magn. Mater. **290** (2005), 209.

[217] F. M. Souza, J. C. Egues, and A. P. Jauho, *Quantum dot as a spin-current diode: A master-equation approach*, Phys. Rev. B **75** (2007), no. 16, 165303.

[218] C.A. Merchant and N. Marković, *Electrically tunable spin polarization in a carbon nanotube spin diode*, Phys. Rev. Lett. **100** (2008), no. 15, 156601.

[219] I. Weymann and J. Barnaś, *Spin diode based on a single-walled carbon nanotube*, Appl. Phys. Lett. **92** (2008), no. 10, 103127.

[220] J. Kondo, *Resistance minimum in dilute magnetic alloys*, Prog. Theor. Phys **32** (1964), no. 1, 37.

[221] W. Harrison, *Solid state thory*, MGraw-Hill Inc., 1970. (Polish trans. *Teoria ciała stałego*, PWN, 1976).

[222] G. Grüner and A. Zawadowski, *Magnetic impurities in non-magnetic metals*, Rep. Prog. Phys. **37** (1974), no. 12, 1497.

[223] N.W. Ashcroft and N.D. Mermin, *Solid state physics*, Thomson Lerning Inc., 1976. (Polish trans. *Fizyka ciała stałego*, PWN, 1986).

[224] R.M. White, *Quantum theory of magnetism. Magnetic properties of materials*, 3rd ed., Springer Series in Solid-State Sciences, Springer, 2007.

[225] A. C. Hewson, *The kondo problem to heavy fermions*, Cambridge University Press, 1997.

[226] L. Kouwenhoven and L. Glazman, *Revival of the Kondo effect*, Phys. World **14** (2001), 33.

[227] P.W. Anderson, *Localized magnetic states in metals*, Phys. Rev. **124** (1961), no. 1, 41.

[228] D. Goldhaber-Gordon, H. Shtrikman, D. Mahalu, D. Abusch-Magder, U. Meirav, and M.A. Kastner, *The Kondo effect in a single-electron transistor*, Nature (London) **391** (1998), no. 6663, 156.

[229] S.M. Cronenwett, T.H. Oosterkamp, and L.P. Kouwenhoven, *A tunable Kondo effect in quantum dots*, Science **281** (1998), no. 5376, 540.

[230] S. Sasaki, S. De Franceschi, J.M. Elzerman, W.G. Van der Wiel, M. Eto, S. Tarucha, and L.P. Kouwenhoven, *Kondo effect in an integer-spin quantum dot*, Nature (London) **405** (2000), no. 6788, 764.

[231] J. Nygård, D.H. Cobden, and P.E. Lindelof, *Kondo physics in carbon nanotubes*, Nature (London) **408** (2000), no. 6810, 342.

[232] J. Park, A.N. Pasupathy, J.I. Goldsmith, C. Chang, Y. Yaish, J.R. Petta, M. Rinkoski, J.P. Sethna, H.D. Abruña, P.L. McEuen, and D.C. Ralph, *Coulomb blockade and the Kondo effect in single-atom transistors*, Nature (London) **417** (2002), no. 6890, 722.

[233] W. Liang, M.P. Shores, M. Bockrath, J.R. Long, and H. Park, *Kondo resonance in a single-molecule transistor*, Nature (London) **417** (2002), no. 6890, 725.

[234] L.H. Yu and D. Natelson, *The Kondo effect in C_{60} single-molecule transistors*, Nano Lett. **4** (2004), no. 1, 79.

[235] A. N. Pasupathy, R. C. Bialczak, J. Martinek, J. E. Grose, L. A. K. Donev, P. L. McEuen, and D. C. Ralph, *The kondo effect in the presence of ferromagnetism*, Science **306** (2004), 86.

[236] A.F. Otte, M. Ternes, K. von Bergmann, S. Loth, H. Brune, C.P. Lutz, C.F. Hirjibehedin, and A.J. Heinrich, *The role of magnetic anisotropy in the Kondo effect*, Nat. Physics **4** (2008), no. 11, 847.

[237] M. Ternes, A.J. Heinrich, and W.-D. Schneider, *Spectroscopic manifestations of the kondo effect on single adatoms*, J. Phys.: Condens. Matter **21** (2009), no. 5, 053001.

[238] M. R. Wegewijs, C. Romeike, H. Schoeller, and W. Hofstetter, *Magneto-transport through single-molecule magnets: Kondo-peaks, zero-bias dips, molecular symmetry and Berry's phase*, New J. Phys. **9** (2007), 344.

[239] M.O. Scully and M.S. Zubairy, *Quantum optics*, Cambridge University Press, 1997.

[240] K. G. Wilson, *The renormalization group: Critical phenomena and the kondo problem*, Rev. Mod. Phys. **47** (1975), no. 4, 773S.

[241] R. Bulla, T.A. Costi, and T. Pruschke, *Numerical renormalization group method for quantum impurity systems*, Rev. Mod. Phys. **80** (2008), no. 2, 395.

[242] H. R. Krishna-Murthy, J. W. Wilkins, and K. G. Wilson, *Renormalization-group approach to the Anderson model of dilute magnetic alloys. I. Static properties for the symmetric case*, Phys. Rev. B **21** (1980), no. 3, 1003.

[243] H. R. Krishna-Murthy, J. W. Wilkins, and K. G. Wilson, *Renormalization-group approach to the Anderson model of dilute magnetic alloys. II. Static properties for the asymmetric case*, Phys. Rev. B **21** (1980), no. 3, 1044.

[244] R. Bulla, T. Pruschke, and A. C. Hewson, *Anderson impurity in pseudo-gap Fermi systems*, J. Phys.: Condens. Matter **9** (1997), no. 47, 10463.

[245] R. Bulla, *The numerical renormalization group method for correlated electrons*, Adv. Solid State Phys. **40** (2000), 169.

[246] S.R. White, *Density matrix formulation for quantum renormalization groups*, Phys. Rev. Lett. **69** (1992), no. 19, 2863.

[247] W. Hofstetter, *Generalized numerical renormalization group for dynamical quantities*, Phys. Rev. Lett. **85** (2000), no. 7, 1508.

[248] W. Hofstetter, *Renormalization group methods for quantum impurity systems*, Ph.D. Thesis, Augsburg, 2001.

[249] U. Schollwöck, *The density-matrix renormalization group*, Rev. Mod. Phys. **77** (2005), no. 1, 259.

[250] M. Sindel, *Numerical renormalization group studies of quantum impurity models in the strong coupling regime*, Ph.D. Thesis, München, 2004.

[251] M. Sindel, L. Borda, J. Martinek, R. Bulla, J. König, G. Schön, S. Maekawa, and J. von Delft, *Kondo quantum dot coupled to ferromagnetic leads: Numerical renormalization group study*, Phys. Rev. B **76** (2007), no. 4, 45321.

[252] L. I. Glazman and M. E. Raikh, *Resonant kondo transparency of a barrier with quasilocal impurity states*, JETP. Lett. **47** (1988), no. 8, 452.

[253] T. K. Ng and P. A. Lee, *On-site Coulomb repulsion and resonant tunneling*, Phys. Rev. Lett. **61** (1988), no. 15, 1768.

[254] M. S. Choi, D. Sánchez, and R. López, *Kondo effect in a quantum dot coupled to ferromagnetic leads: A numerical renormalization group analysis*, Phys. Rev. Lett. **92** (2004), no. 5, 56601.

[255] Ö. Legeza, C.P. Moca, A.I. Tóth, I. Weymann, and G. Zaránd, *Manual for the flexible DM-NRG code*, arXiv:0809.3143v1 (2008). (the code is available at http://www.phy.bme.hu/~dmnrg/).

[256] A.I. Tóth, CP Moca, Ö. Legeza, and G. Zaránd, *Density matrix numerical renormalization group for non-Abelian symmetries*, Phys. Rev. B **78** (2008), no. 24, 245109.

[257] T.A. Costi, A.C. Hewson, and V. Zlatić, *Transport coefficients of the anderson model via the numerical renormalization group*, J. Phys.: Condens. Matter **6** (1994), 2519.

[258] D.N. Zubarev, *Double-time Green functions in statistical physics*, Sov. Phys.–Usp. **3** (1960), 320.

[259] H. Haug and A.-P. Jauho, *Quantum kinetics in transport and optics of semiconductors*, Springer Series in Solid-State Sciences, Springer, 1998.

[260] R. Landauer, *Electrical resistance of disordered one-dimensional lattices*, Philos. Mag. **21** (1970), no. 172, 863.

[261] Y. Meir, N.S. Wingreen, and P.A. Lee, *Transport through a strongly interacting electron system: Theory of periodic conductance oscillations*, Phys. Rev. Lett. **66** (1991), no. 23, 3048.

[262] Y. Meir and N.S. Wingreen, *Landauer formula for the current through an interacting electron region*, Phys. Rev. Lett. **68** (1992), no. 16, 2512.

[263] M. Di Ventra, *Electrical transport in nanoscale systems*, Cambridge University Press, 2008.

[264] J. Martinek, Y. Utsumi, H. Imamura, J. Barnaś, S. Maekawa, J. König, and G. Schön, *Kondo effect in quantum dots coupled to ferromagnetic leads*, Phys. Rev. Lett. **91** (2003), no. 12, 127203.

[265] I. Tudosa, A.B. Stamm C.and Kashuba, F. King, H.C. Siegmann, G. Stöhr J.and Ju, B. Lu, and D. Weller, *The ultimate speed of magnetic switching in granular recording media*, Nature (London) **428** (2004), no. 6985, 831.

[266] A.V. Kimel, A. Kirilyuk, and T. Rasing, *Femtosecond opto-magnetism: ultrafast laser manipulation of magnetic materials*, Laser & Photon. Rev. **1** (2007), no. 3, 275.

[267] E. Beaurepaire, J.C. Merle, A. Daunois, and J.Y. Bigot, *Ultrafast spin dynamics in ferromagnetic nickel*, Phys. Rev. Lett. **76** (1996), no. 22, 4250.

[268] J. Hohlfeld, E. Matthias, R. Knorren, and K.H. Bennemann, *Nonequilibrium magnetization dynamics of nickel*, Phys. Rev. Lett. **78** (1997), no. 25, 4861.

[269] B. Koopmans, M. van Kampen, J.T. Kohlhepp, and W.J.M. de Jonge, *Ultrafast magneto-optics in nickel: magnetism or optics?*, Phys. Rev. Lett. **85** (2000), no. 4, 844.

[270] J. Hohlfeld, T. Gerrits, M. Bilderbeek, T. Rasing, H. Awano, and N. Ohta, *Fast magnetization reversal of GdFeCo induced by femtosecond laser pulses*, Phys. Rev. B **65** (2001), no. 1, 12413.

[271] B. Koopmans, M. van Kampen, and W.J.M. de Jonge, *Experimental access to femtosecond spin dynamics*, J. Phys.: Condens. Matter **15** (2003), no. 5, 723.

[272] A. Kirilyuk, A. Kimel, F. Hansteen, R. Pisarev, and T. Rasing, *Ultrafast all-optical control of the magnetization in magnetic dielectrics*, Fiz. Nizk. Temp. **32** (2006), no. 8-9, 985.

[273] A.V. Kimel, A. Kirilyuk, F. Hansteen, R.V. Pisarev, and T. Rasing, *Nonthermal optical control of magnetism and ultrafast laser-induced spin dynamics in solids*, J. Phy.: Condens. Matter **19** (2007), no. 4, 43201.

[274] V.V. Kruglyak, M.E. Portnoi, and R.J. Hickenc, *Use of the Faraday optical transformer for ultrafast magnetization reversal of nanomagnets*, J. Nanophoton. **1** (2007), 013502.

[275] L.P. Pitaevskii, *Electric forces in a transparent dispersive medium*, Sov. Phys. JETP **12** (1961), no. 5, 1008.

[276] P.S. Pershan, J.P. van der Ziel, and L.D. Malmstrom, *Theoretical discussion of the inverse Faraday effect, Raman scattering, and related phenomena*, Phys. Rev. **143** (1966), no. 2, 574.

[277] J.P. van der Ziel, P.S. Pershan, and L.D. Malmstrom, *Optically-induced magnetization resulting from the inverse Faraday effect*, Phys. Rev. Lett. **15** (1965), no. 5, 190.

[278] C.D. Stanciu, F. Hansteen, A.V. Kimel, A. Tsukamoto, A. Itoh, A. Kirilyuk, and T. Rasing, *Ultrafast interaction of the angular momentum of photons with spins in the metallic amorphous alloy GdFeCo*, Phys. Rev. Lett. **98** (2007), no. 20, 207401.

[279] A.V. Kimel, A. Kirilyuk, P. Usachev, R.V. Pisarev, A.M. Balbashov, and T. Rasing, *Ultrafast non-thermal control of magnetization by instantaneous photomagnetic pulses*, Nature (London) **435** (2005), no. 7042, 655.

[280] C.D. Stanciu, F. Hansteen, A.V. Kimel, A. Kirilyuk, A. Tsukamoto, A. Itoh, and T. Rasing, *All-optical magnetic recording with circularly polarized light*, Phys. Rev. Lett. **99** (2007), no. 4, 47601.

[281] F. Hansteen, A. Kimel, A. Kirilyuk, and T. Rasing, *Nonthermal ultrafast optical control of the magnetization in garnet films*, Phys. Rev. B **73** (2006), no. 1, 14421.

[282] Y.R. Shen and N. Bloembergen, *Interaction between light waves and spin waves*, Phys. Rev. **143** (1966), no. 2, 372.

[283] P.A. Fleury and R. Loudon, *Scattering of light by one- and two-magnon excitations*, Phys. Rev. **166** (1968), no. 2, 514.

[284] E.M. Lifshitz, L.D. Landau, and L.P. Pitaevskii, *Electrodynamics of continuous media*, 2nd Ed., Course of Theoretical Physics, vol. VIII, Pergamon Press, 1984.

[285] R. Hertel, *Theory of the inverse Faraday effect in metals*, J. Mag. Mag. Mater. **303** (2006), no. 1, 1.

[286] A.Y. Smirnov, *Direct mechanism of spin orientation by circularly polarized light*, Phys. Rev. B **60** (1999), no. 5, 3040.

[287] G.P. Zhang and W. Hübner, *Laser-induced ultrafast demagnetization in ferromagnetic metals*, Phys. Rev. Lett. **85** (2000), no. 14, 3025.

[288] S.R. Woodford, *Conservation of angular momentum and the inverse Faraday effect*, Phys. Rev. B **79** (2009), no. 21, 212412.

[289] M.I. Kurkin, N.B. Bakulina, and R.V. Pisarev, *Transient inverse Faraday effect and ultrafast optical switching of magnetization*, Phys. Rev. B **78** (2008), no. 13, 134430.

[290] P.S. Pershan, *Nonlinear optical properties of solids: energy considerations*, Phys. Rev. **130** (1963), no. 3, 919.

[291] L. Onsager, *Reciprocal relations in irreversible processes. I.*, Phys. Rev. **37** (1931), no. 4, 405.

[292] L. Onsager, *Reciprocal relations in irreversible processes. II.*, Phys. Rev. **38** (1931), no. 12, 2265.

[293] J. van Slageren, S. Vongtragool, A. Mukhin, B. Gorshunov, and M. Dressel, *Terahertz Faraday effect in single molecule magnets*, Phys. Rev. B **72** (2005), no. 2, 20401.

[294] M. Bal, J.R. Friedman, Y. Suzuki, K.M. Mertes, E.M. Rumberger, D.N. Hendrickson, Y. Myasoedov, H. Shtrikman, N. Avraham, and E. Zeldov, *Photon-induced magnetization reversal in the Fe_8 single-molecule magnet*, Phys. Rev. B **70** (2004), no. 10, 100408.

[295] M. Bal, J.R. Friedman, E.M. Rumberger, S. Shah, D.N. Hendrickson, N. Avraham, Y. Myasoedov, H. Shtrikman, and E. Zeldov, *Photon-induced magnetization changes in single-molecule magnets (invited)*, J. Appl. Phys. **99** (2006), no. 8, 08D103.

[296] L. Sorace, W. Wernsdorfer, C. Thirion, A.L. Barra, M. Pacchioni, D. Mailly, and B. Barbara, *Photon-assisted tunneling in a Fe_8 single-molecule magnet*, Phys. Rev. B **68** (2003), no. 22, 220407.

[297] K. Petukhov, S. Bahr, W. Wernsdorfer, A.L. Barra, and V. Mosser, *Magnetization dynamics in the single-molecule magnet Fe_8 under pulsed microwave irradiation*, Phys. Rev. B **75** (2007), no. 6, 064408.

[298] M. Bal, J.R. Friedman, M.T. Tuominen, E.M. Rumberger, and D.N. Hendrickson, *Measurement of magnetization dynamics in single-molecule magnets induced by pulsed millimeter-wave radiation*, J. Appl. Phys. **99** (2006), no. 8, 08D102.

[299] M. Bal, J.R. Friedman, Y. Suzuki, E.M. Rumberger, D.N. Hendrickson, N. Avraham, Y. Myasoedov, H. Shtrikman, and E. Zeldov, *Non-equilibrium magnetization dynamics in the Fe_8 single-molecule magnet induced by high-intensity microwave radiation*, Europhys. Lett. **71** (2005), no. 1, 110.

[300] J.H. Van Vleck, *Paramagnetic relaxation and the equilibrium of lattice oscillators*, Phys. Rev. **59** (1941), no. 9, 724.

[301] K.W.H. Stevens, *The theory of paramagnetic relaxation*, Rep. Prog. Phys. **30** (1967), 189.

[302] A. Abragam and B. Bleaney, *Electron paramagnetic resonance of transition ions*, Clarendon Press, Oxford, 1970.

[303] I. Chiorescu, W. Wernsdorfer, A. Müller, H. Bögge, and B. Barbara, *Butterfly hysteresis loop and dissipative spin reversal in the S=1/2, V_{15} molecular complex*, Phys. Rev. Lett. **84** (2000), no. 15, 3454.

[304] O. Waldmann, R. Koch, S. Schromm, P. Müller, I. Bernt, and R.W. Saalfrank, *Butterfly hysteresis loop at nonzero bias field in antiferromagnetic molecular rings: Cooling by adiabatic magnetization*, Phys. Rev. Lett. **89** (2002), no. 24, 246401.

[305] L. Chen, C.M. Ramsey, N.S. Dalal, T. Ren, F.A. Cotton, W. Wernsdorfer, and I. Chiorescu, *Phonon-bottleneck enhanced magnetic hysteresis in a molecular paddle wheel complex of Ru_2^{5+}*, Appl. Phys. Lett. **89** (2006), no. 25, 252502.

[306] G. De Loubens, D.A. Garanin, C.C. Beedle, D.N. Hendrickson, and A.D. Kent, *Magnetization relaxation in the single-molecule magnet Ni_4 under continuous microwave irradiation*, Europhys. Lett. **83** (2008), no. 3, 37006.

[307] A.K. Agyei and J.L. Birman, *On the linear magnetoelectric effect*, J. Phys.: Condens. Matter **2** (1990), no. 13, 3007.

[308] M. Fiebig, *Revival of the magnetoelectric effect*, J. Phys. D: Appl. Phys **38** (2005), no. 8, R123.

[309] J.D. Jackson, *Classical Electrodynamics*, 3rd Ed., John Wiley & Sons, 1999.

[310] R. Loudon, *The quantum theory of light*, 3rd Ed., Oxford University Press, 2000.

[311] G. Araki, *Quantum mechanics of circularly polarized photons. I. General theory.*, Prog. Theor. Phys. **1** (1946), no. 4, 125.

[312] R. Shankar, *Principles of quantum mechanics*, 2nd Ed., Springer, 2004.

[313] R. Eisberg and R. Resnick, *Quantum physics of atoms, molecules, solids, nuclei, and particles*, John Wiley & Sons, 1985.

Oświadczenie

Ja, niżej podpisany Maciej Misiorny, doktorant Wydziału Fizyki Uniwersytetu im. Adama Mickiewicza w Poznaniu oświadczam, że przedkładaną rozprawę doktorską pt. *'Charge and spin transport through magnetic molecules'* napisałem samodzielnie. Oznacza to, że przy pisaniu pracy, poza niezbędnymi konsultacjami, nie korzystałem z pomocy innych osób, a w szczególności nie zlecałem opracowania rozprawy lub jej istotnych części innym osobom, ani nie odpisywałem tej rozprawy lub jej istotnych części od innych osób.

Równocześnie wyrażam zgodę na to, że gdyby powyższe oświadczenie okazało się nieprawdziwe, decyzja o nadaniu mi stopnia naukowego doktora zostanie cofnięta.

Maciej Misiorny

Poznań, dnia 30 grudnia 2009 r.